Steam-Reheat Option for Supercritical-Water-Cooled Reactors

by

Eugene Saltanov

A Thesis Submitted in Partial Fulfillment
of the Requirements for the Degree of

Master of Applied Science

in

The Faculty of Energy Systems and Nuclear Science

Nuclear Engineering

University of Ontario Institute of Technology

December, 2010

Your file Votre référence
ISBN: 978-0-494-69929-4
Our file Notre référence
ISBN: 978-0-494-69929-4

CONTENTS

LIST OF TABLES

LIST OF FIGURES

ABSTRACT

SuperCritical-Water-cooled Reactors (SCWRs) are being developed as one of the Generation-IV nuclear-reactor concepts. Main objectives of the development are to increase thermal efficiency of a Nuclear Power Plant (NPP) and to decrease capital and operational costs. The first objective can be achieved by introducing nuclear steam reheat inside a reactor and utilizing regenerative feedwater heaters. The second objective can be achieved by designing a steam cycle that closely matches that of the mature supercritical fossil-fuelled power plants. The feasibility of these objectives is discussed. As a part of this discussion, heat-transfer calculations have been performed and analyzed for SuperCritical-Water (SCW) and SuperHeated-Steam (SHS) channels of the proposed reactor concept. In the calculations a uniform and three non-uniform Axial Heat Flux Profiles (AHFPs) were considered for six different fuels (UO_2, ThO_2, MOX, UC_2, UC, and UN) and at average and maximum channel power. Bulk-fluid, sheath, and fuel centerline temperatures as well as the Heat Transfer Coefficient (HTC) profiles were obtained along the fuel-channel length. The HTC values are within a range of 4.7 – 20 $kW/m^2 \cdot K$ and 9.7 – 10 $kW/m^2 \cdot K$ for the SCW and SHS channels respectively. The main conclusion is that while all the mentioned fuels may be used for the SHS channel, only UC_2, UC, or UN are suitable for a SCW channel, because their fuel centerline temperatures are at least 1000°C below melting point, while that of UO_2, ThO_2, and MOX may reach melting point.

ACKNOWLEDGEMENTS

Financial supports from the NSERC/NRCan/AECL Generation IV Energy Technologies Program and NSERC Discovery Grant are gratefully acknowledged.

I would like to acknowledge the work and thank for the contributions of Wargha Peiman, Amjad Farah, Krysten King, and Sarah Mokry.

Also, I owe thanks to Lisa Grande and Adam Caly for fruitful discussions, advices, and encouragement.

I am happy to thank my parents for moral and information support.

For reviewing and editing a portion of the thesis that was used in a technical report I gratefully thank Dr. Glenn Harvel.

Finally, I would like to specially acknowledge my supervisor Dr. Igor Pioro and thank him for his guidance, sharp editorial insights, and constructive criticism on the way of creation of this thesis.

DEFINITIONS

Below are the definitions of special terms and expressions used in the thesis and related to Supercritical Water-cooled nuclear Reactors (SCWRs).

Critical point (also called a *critical state*) is a point in which the distinction between the liquid and gas (or vapour) phases disappears, i.e., both phases have the same temperature, pressure and density. The *critical point* is, therefore, characterized by these phase state which have unique values for each pure substance.

Deteriorated Heat Transfer is characterized with lower values of the wall heat transfer coefficient compared to those at the normal heat transfer; and hence has higher values of wall temperature within some part of a test section or within the entire test section.

Improved Heat Transfer is characterized with higher values of the wall heat transfer coefficient compared to those at the normal heat transfer; and hence lower values of wall temperature within some part of a test section or within the entire test section.

Normal Heat Transfer can be characterized in general with wall heat transfer coefficients similar to those of subcritical convective heat transfer far from the critical or pseudocritical regions. Only normal heat transfer regime was considered in the thesis.

Pseudocritical point is a point at a pressure above the critical pressure and at a temperature above the critical temperature that corresponds to the maximum value of the specific heat for this particular pressure.

Supercritical fluid is a fluid at pressures and temperatures that are higher than the critical pressure and critical temperature.

Superheated steam is a steam at pressures below the critical pressure, but at temperatures above the critical temperature.

NOMENCLATURE

c_p	specific heat, J/kg·K
D	diameter, m
h	specific enthalpy, J/kg
htc	heat-transfer coefficient, W/m^2·K
k	thermal conductivity, W/m·K
k_{inf}	reactor multiplication constant for infinite lattice
K_{ir}	neutron flux irregularity coefficient
$\dot{m}$	mass-flow rate, kg/s
P	pressure, MPa
$\dot{Q}$	power or heat-transfer rate, W
R	radius, m
s	specific entropy, J/kg K
T	temperature, °C
x	steam content

Greek letters

α	thermal diffusivity, m^2/s
Δ	difference
π	steam-superheating-zone to boiling-zone power ratio
μ	dynamic viscosity, Pa·s

Non-dimensional Numbers

Nu	Nusselt number $\left(\frac{htc \cdot D_{hy}}{k}\right)$
$\overline{\mathbf{Pr}}$	Average Prandtl number $\left(\frac{\mu}{k} \cdot \frac{h_w - h_b}{T_w - T_b}\right)$

Pr Prandtl number $\left(\frac{\mu \cdot c_p}{k}\right)$

Re Reynolds number $\frac{4\dot{m}}{\mu \pi D_{hy}}$

Subscripts

b bulk-fluid
cr critical
e electrical
hy hydraulic
in inlet
main refers to main or primary steam directed to turbine
out outlet
reheat refers to secondary or superheated steam directed to turbine
th thermal
w wall
wt weight

Abbreviations and Acronyms

AECL Atomic Energy of Canada Limited
AHFP Axial Heat Flux Profile
BNPP Beloyarsk Nuclear Power Plant
BONUS BOiling NUclear Superheater
BORAX BOiling Reactor Experiment
BW Boling-Water (channel)
BWR Boiling Water Reactor
CANDU CANada Deuterium Uranium (reactor)
CANFLEX CANada FLEXible (fueling)
CCP Pump of Reactor Control System Cooling
CEP Condenser-Extraction Pump

CND	Condenser
CR-SCP	Channelized Reactor with water at SuperCritical Pressure
ESADE	Superheat Advance Demonstration Experiment
FEP	Feeding Electric Pump
FWP	Feedwater Pump
HHV	Higher-Heating Value
HP	High Pressure
HTC	Heat Transfer Coefficient
HTP	Heat-Transport Pump
HTR	Heater
HWR	Heavy Water Reactor
HX	Heat eXchanger
ID	Inside Diameter
IP	Intermediate Pressure (turbine)
KP-SKD	Channel Reactor of Supercritical Pressure (in Russian abbreviations)
LHV	Lower-Heating Value
LP	Low Pressure
LUEC	Levelized-Unit-Energy Cost
LWR	Light Water Reactors
Max.	Maximum
MCP	Main Circulation Pump
Min.	Minimum
MIT	Massachusetts Institute of Technology
MSR	Moisture Separator and Reheater
NIKIET	Russian abbreviation of RDIPE
NRC	National Resources Canada
NSERC	Natural Sciences and Engineering Research Council
NPP	Nuclear Power Plant
OD	Outside Diameter
O&M	Operating and Maintaining
PCh	Pressure Channel

PCP	Pump of Protective System Cooling
PT	Pressure Tube (reactor)
PV	Pressure Vessel (reactor)
PWR	Pressurized Water Reactor
RB	Reactor Building
RBMK	Russian Acronym for Channelized Reactor of High-Power
RDIPE	Research and Development Institute of Power Engineering (Moscow, Russia)
RFP	Reactor Feedwater Pump
SADE	Superheat Advance Demonstration Experiment
SC	SuperCritical
SCW	Supercritical Water
SCWR	Supercritical Water Reactor
SG	Steam Generator
SGHWR	Steam Generating Heavy Water Reactor
SHS	SuperHeated Steam (channel)
SS	Stainless Steel
T	Turbine
USAEC	United States Atomic Energy Commission
Z	Zirconium

CHAPTER 1

INTRODUCTION

One of the six Generation-IV nuclear reactor concepts[1] is a SuperCritical Water-cooled nuclear Reactor (SCWR), which is currently under development worldwide. An SCWR is a reactor that uses water at SuperCritical (SC) pressure as its coolant and generates SC "steam" at the reactor outlet. The main objectives for developing and utilizing SCWRs are: 1) To increase the thermal efficiency of Nuclear Power Plants (NPPs) from the current range of 33 – 35% to approximately 45 – 50% (based on gross-plant efficiency); 2) To decrease the capital and Operating and Maintaining (O&M) costs and, in doing so, decrease the unit-energy cost; and 3) Possibility for co-generation, including hydrogen generation (Naterer et al. 2009; Naidin et al. 2009b,c; Mokry et al. 2008).

The SCWR concepts (Pioro and Duffey 2007) follow two main types: (a) A large reactor Pressure Vessel (PV), analogous to conventional Light Water Reactors (LWRs); or (b) a channelized reactor in which individual Pressure Tubes (PTs) or Pressure Channels (PChs) carry high pressure, analogous to conventional Heavy Water Reactors (HWRs).

Within these two main classes (PV and PT) (Pioro and Duffey 2007), PT reactors are more flexible with respect to flow, flux and density changes than the PV reactors. A design whose basic element is a channel has an inherent advantage of greater safety than large vessel structures at supercritical pressures. In particular, the separation between moderator and coolant in a PT SCWR allows for significant enhancement in safety. Particularly, the moderator will serve as a back-up heat sink at normal and accident conditions and will reject heat through moderator-cooling system (Chow and Khartabil 2008). This design requires no operator action and has the potential to eliminate practically the possibility of core damage.

[1] The other five Generation IV systems are: gas-cooled fast reactor, very-high-temperature reactor, lead-cooled fast reactor, molten salt reactor, and sodium-cooled fast reactor.

There is a number of countries participating in the development of SCWRs of different designs. AECL and NIKIET (Duffey et al. 2008; Pioro and Duffey 2007) are currently developing concepts of PT SCWRs (for details, see Table 1.1).

Table 1.1. Major parameters of SCW-CANDU® and Channel Reactor with SuperCritical Pressure water (CR-SCP) (Pioro and Duffey 2007).

Parameters	Reactors	
	SCW CANDU*	**CR-SCP**
Developer	AECL	NIKIET
Country	Canada	Russia
Reactor Type	PT	
Reactor Spectrum	Thermal	
Coolant	Light water	
Moderator	Heavy water	
Thermal Power, MW_{th}	2540	1960
Electric Power, MW_e	1220	850
Thermal Efficiency, %	48	42
Pressure, MPa	25	25
Inlet Temperature, °C	350	270
Outlet Temperature, °C	625	545
Flowrate, kg/s	1320	922
Number of Fuel Channels	300	653
Number of Fuel Elements in Bundle	43	18
Length of Bundle String, m	6	–
Maximum Cladding Temperature, °C	850	700

* The data shown are for the no-reheat option.

SCWRs are considered as a conventional way for the ultimate development of water-cooled reactors, which are the vast majority of power nuclear reactors operating worldwide. This statement is based on the known history of the thermal power industry, which made a "revolutionary" step forward from the level of subcritical pressures (10 – 20 MPa) to the level of supercritical pressures (23.5 – 35 MPa) more than fifty years ago with the same major objective as that of SCWRs– to increase thermal efficiency of coal -fired thermal power plants by 10 – 15%.

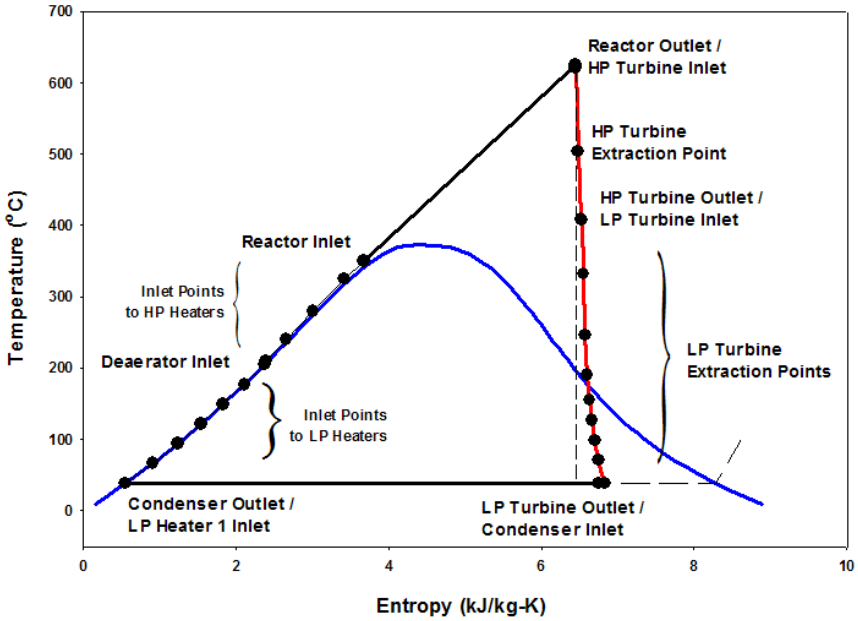

(a)

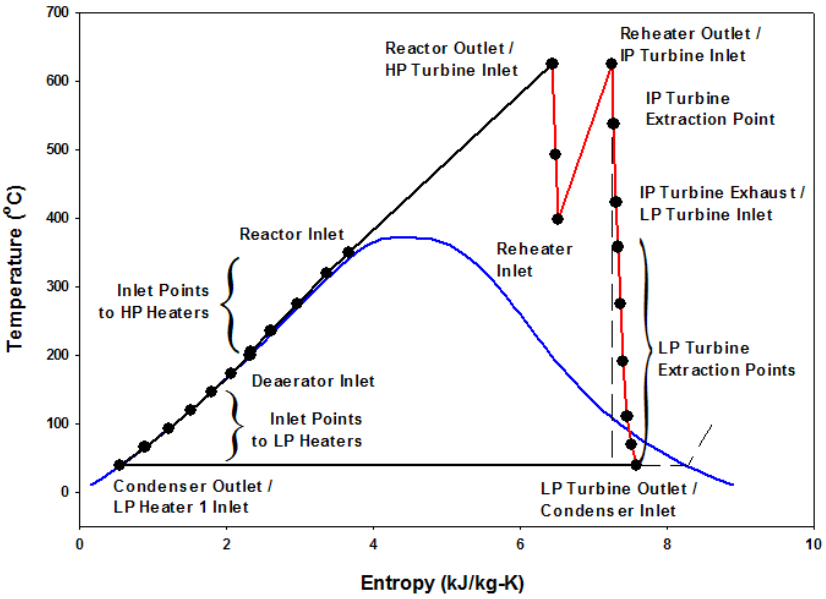

(b)

Figure 1.1. T-s diagram of no-reheat (a) and single-reheat (b) cycles (Pioro et al. 2010).

It is well-known that the thermal efficiency of the cycle can be increased by 2 – 4% with the implementation of steam reheat (T-s diagrams of no-reheat and single-reheat cycles are presented in Fig. 1.1). For that reason, currently, majority of the SC turbines are designed with a steam-reheat option. Furthermore, reheating steam reduces the amount of moisture in the last stages of the turbine. The increase in efficiency of the cycle with steam-reheat as compared to that of the

cycle with no-reheat is achieved due to extra heat added during steam-reheat stage (Pioro et al. 2010).

Therefore, it is important to summarize both the 50-year experience of the coal-fired thermal power industry and experience of implementing nuclear steam reheat at several experimental Boiling Water Reactors (BWRs) worldwide and utilize it in the context of developing SCWRs concepts with steam-reheat option. The general idea behind using this experience is to develop SCWRs, which are capable to operate successfully and efficiently with the proven SC technology, specifically the SC turbines from the thermal power industry.

Therefore, the main objectives of the thesis are:

1. To make a comprehensive literature review of operating experience of BWRs with nuclear steam reheat. No one has performed such a review before.
2. To develop a detailed thermal layout of a NPP with nuclear steam reheat at parameters that would be close to those in the proposed SCWR concept.
3. To perform and compare heat-transfer calculations of SHS and SCW channels with different fuels and at different power conditions.
4. Analyze the calculations and decide which fuel is suitable for the SHS and SCW conditions.

Chapter 2 of the thesis presents the literature review of operating experience of BWRs with nuclear steam. Review of supercritical thermal power plants is presented in Chapter 3. Chapter 4 is devoted to general consideration of thermal layouts for SCW NPPs. The developed detailed thermal layouts of SCW NPP with nuclear steam reheat are also presented in Chapter 4. Review of heat-transfer correlations for SCW and SHS conditions as well as the results of heat-transfer calculations are presented in Chapter 5. Conclusions are summarized in Chapter 6. Some ideas on future work are presented in Chapter 7.

CHAPTER 2

BOILING-WATER REACTORS WITH STEAM REHEAT

Major advancements in implementation of steam reheat inside the reactor core were made in the USA and Russia in 1960s – 1970s. No signs of any significant activity in this field in other countries were found. Three experimental reactors in the USA and two power reactors in Russia were developed, in which nuclear steam reheat was successfully implemented. It was realized that the next advancement in nuclear-reactor technology and improvement in thermal efficiency could be achieved by utilizing both coolant at supercritical parameters and subcritical superheated steam. However, at that time there were no reliable materials that could withstand high-temperature and high-pressure environment along with high neutron irradiation. Since the 1980's, the advancements in metallurgical technology has improved the reliability of materials to be used in supercritical-water environment, and recently the idea of SCWR was revived as as the ultimate development path for water cooling (Pioro and Duffey 2007). Further increase in thermal efficiency will be achieved by implementing nuclear steam reheat. Therefore, it is important to summarize known experience in nuclear steam reheat that was implemented in several BWRs.

2.1. USA Experience in Nuclear Steam Reheat

An active program for the development and demonstration of BWRs with nuclear steam reheat was implemented and directed by the United States Atomic Energy Commission (USAEC). Two general types of the reactors were demonstrated:

1. Reactors in which steam was generated and reheated in the same core (integral reheating design); and
2. Reactors which only used reheated steam that was supplied from another source (separate reheating design);

Under the USAEC program, the following reactors were constructed: Boiling Reactor Experiment V (BORAX–V, started operation in December of 1962), BOiling NUclear Superheater (BONUS, started operation in December of 1964), and Pathfinder (started operation in July of 1966). Main parameters of these reactors are listed in Tables 2.1 and 2.2 (Novick et al. 1965).

At the design stage of these reactors a certain number of problems arising with the implementation of steam reheat were realized and addressed. Among them were:

1. Fuel-element sheath performance and corrosion resistance at high temperatures;
2. Corrosion, erosion, and deposits on fuel-element surfaces due to ineffective steam separation prior to the reheating-zone inlet;
3. Maintenance of the desired power split in the evaporating and reheating zones during extended reactor operation;
4. Fission products carry-over in direct-cycle systems; And
5. Reactivity changes as a result of inadvertent flooding of the reheating zone.

In search of the solutions to these problems USAEC also instituted a number of programs to determine long-term integrity and behavior of the fuel-element sheath. Since May of 1959, the Superheat Advance Demonstration Experiment (SADE) and the subsequent Expanded SADE (ESADE) loops had been utilized to irradiate a total of 21 fuel elements in the Vallecitos BWR. Saturated steam at about 6.9 MPa from the Vallecitos BWR was supplied to the fuel-element section where it was superheated to temperatures of 418 – 480°C. The results of those irradiation tests combined with out-of-core corrosion tests led to the following conclusions (Novick et al. 1965):

1. Commercial 18-8 stainless steel (18-8 SS) was not satisfactory for fuel-sheath material in the SHS environment it was subjected to in the SADE and ESADE experiments;
2. Materials with higher nickel-alloy content, such as Inconel and Incoloy, appeared to perform satisfactorily as a sheath material in the SHS environment; And
3. Strain cycling coupled with environmental chemistry were significant in the failure rate

of sheath materials for reactors with steam reheat.

Additional information on design of these reactors constructed under the USAEC program can be found in USAEC reports 1959, 1961, and 1962 and in Ross (1961).

The major conclusion, which is based on the USA experience with nuclear steam reheat, is that the nuclear steam reheat is possible, and higher thermal efficiencies can be achieved, but this feature requires more complicated reactor-core design and better materials.

Table 2.1. Main general parameters of BWR NPPs with integral reheat design (Novick et al. 1965).

Parameters	BORAX–V		BONUS		Pathfinder	
	Evaporating zone	Reheating zone	Evaporating zone	Reheating zone	Evaporating zone	Reheating zone
Structural material (core)	A1(X8001)	SS	Zr–2	SS-248	Zr–2	SS
Fuel type	Rod	Plate	Rod	Rod	Rod	Annular
Fuel material	UO_2	UO_2– SS cermet	UO_2	UO_2	UO_2	UO_2–SS cermet
Fuel enrichment, %	4.95	93	2.4	3.25	2.2	93
Sheath material	SS-304	SS-304L	Zr–2	Inconel	Zr–2	SS-316L
Control rod shape	Cruciform and "T"	Cruciform and "T"	Cruciform	Slab	Cruciform	Round rod
Control rod material	Boral	Boral	1.0%$_{wt}$ ^{10}B in SS	1.0% $_{wt}$ ^{10}B in SS	2% $_{wt}$ ^{10}B in SS	2% $_{wt}$ ^{10}B in SS
Average power density, MW_{th}/m^3	42.5	40.5	33.6	11.5	45.2	46.5

Table 2.2. Main thermal parameters of BWR NPPs with integral reheat design (Novick et al. 1965).

Parameters	BORAX–V	BONUS	Pathfinder
Electric power, MW_e (gross)	3.5	17.5	66
Electric power, MW_e (net)	3.5	16.5	62.5
Thermal power, MW_{th}	20	50	200
Reheat loop to evaporating loop power ratio	0.21	0.35	0.22
Gross cycle thermal efficiency, %	–	35	33
Net cycle thermal efficiency, %	–	33	31
NPP steam cycle	Direct	Direct	Direct
Reheating-zone location	Central or Peripheral	Peripheral	Central
Nominal operating pressure, MPa	4.1	6.7	4.1

2.2. Russian Experience in Nuclear Steam Reheat

This section presents a unique compilation of materials that overviews all major aspects of operating experience of the first in the world industrial NPP with implemented nuclear steam reheat.

2.2.1. General information

Reactors with nuclear steam reheat were also developed in the former Soviet Union. Beloyarsk Nuclear Power Plant (BNPP) was the first NPP in the world where nuclear steam reheat was implemented. Two reactors (100 MW_e and 200 MW_e) were installed with identical steam parameters at the turbine inlet (P_{in} = 8.8 MPa and T_{in} = 500 – 510°C). The first reactor (Unit 1) was put into operation on April 26, 1964, and the second reactor (Unit 2) – on December 29, 1967. Both reactors have similar dimensions and design. However, the flow diagram and the core arrangement were significantly simplified in Unit 2, compared to that of Unit 1. Color schematics and simplified layouts of the BNPP Units 1 and 2 are shown in Figures 2.1 and 2.2.

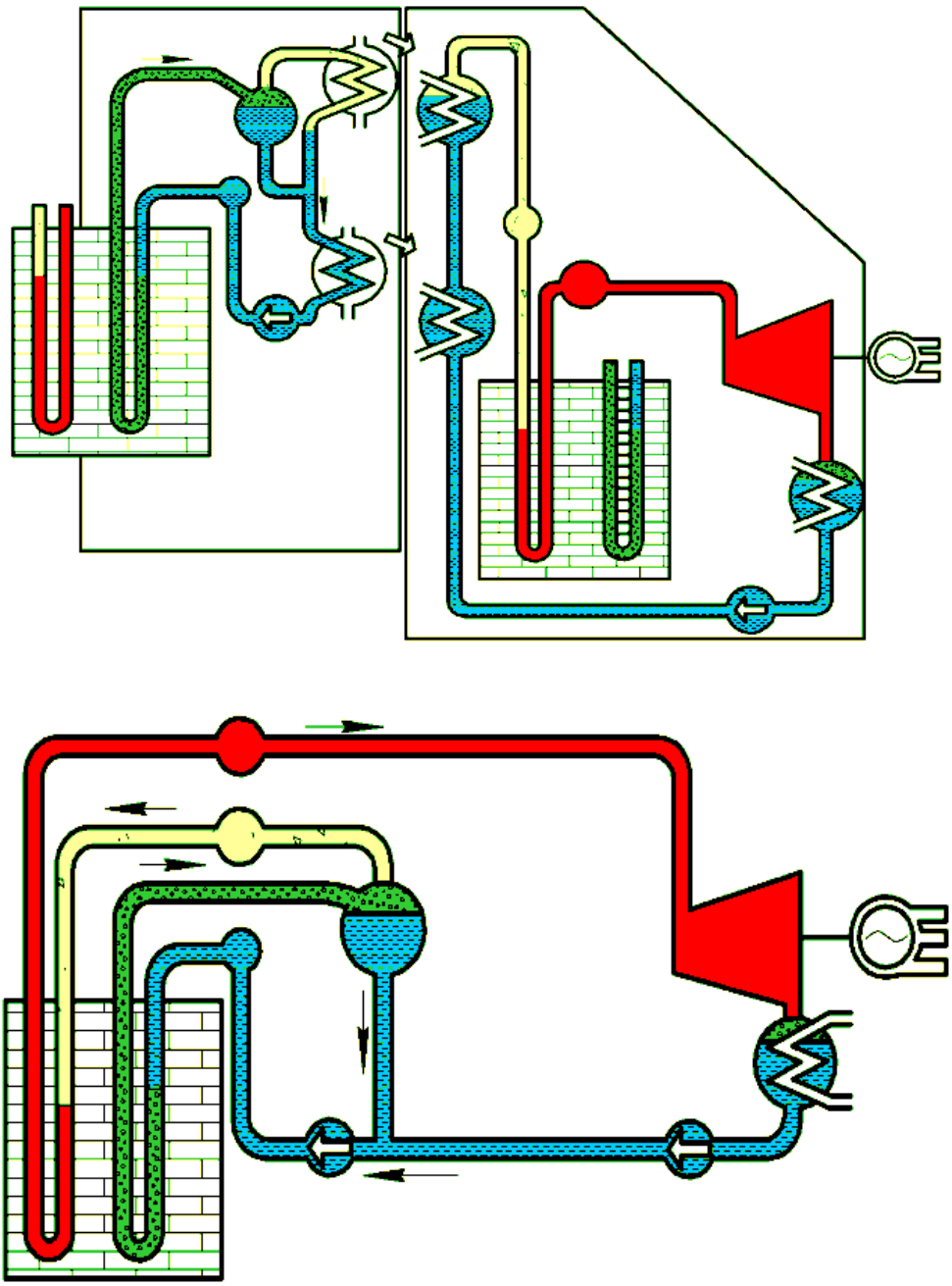

(a)

(b)

Figure 2.1. BNPP Unit 1 (a) and Unit 2 (b) general schematics of thermodynamic cycle (Yurmanov et al. 2009a):

– Reheated steam; **– Saturated steam;**

– Water-steam mixture; **– Water.**

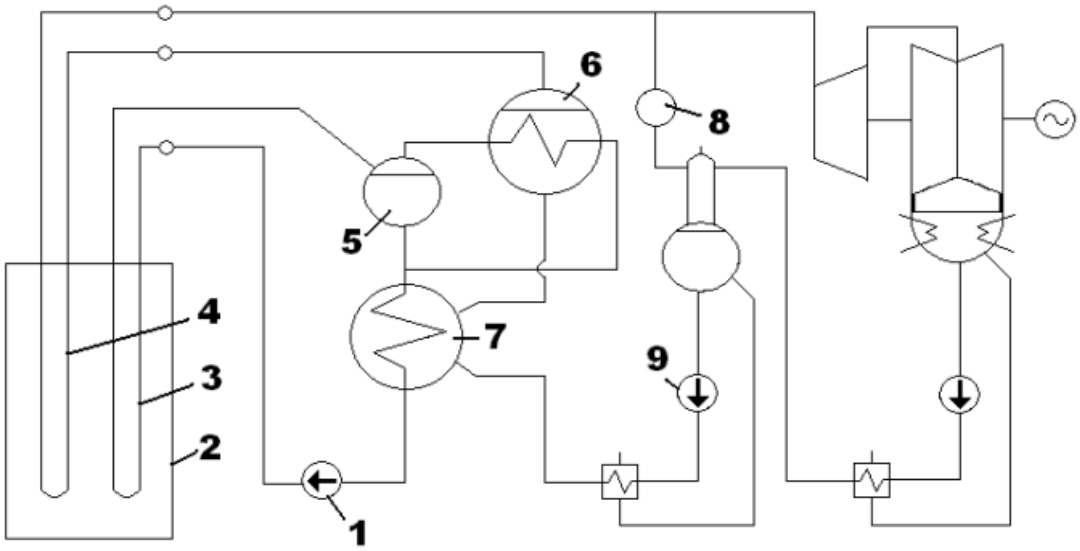

(a)

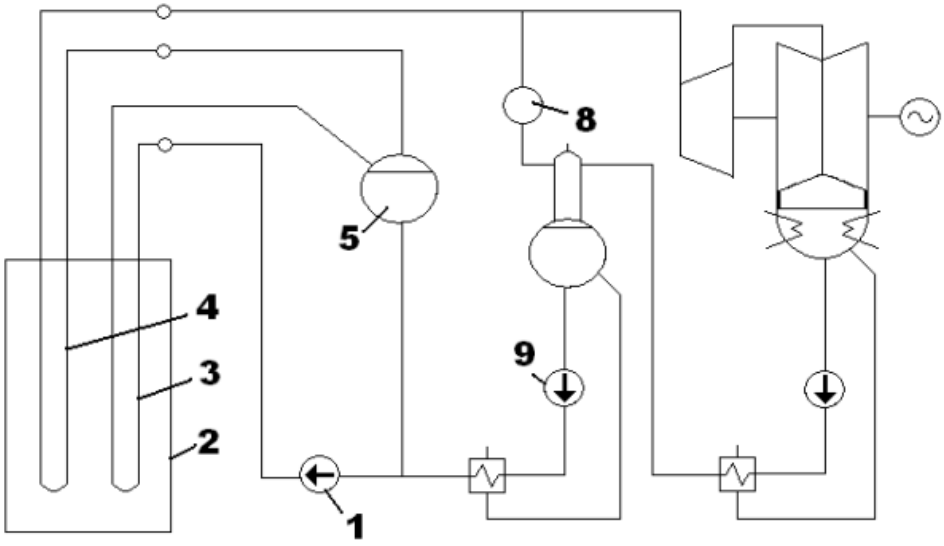

(b)

Figure 2.2. Simplified layout of BNPP Unit 1 (a) and Unit 2 (b) (Petrosyants 1969): 1 – circulation pump; 2 – reactor; 3 – Boiling Water (BW) channels; 4 – SHS channels; 5 – steam separator; 6 – Steam Generator (SG); 7 – economizer; 8 – bubbler; and 9 – Feed Water Pump (FWP).

Operation of BNPP has proved the feasibility of steam-reheat implementation on an industrial scale. Major results of the BNPP operation are listed below (Petrosyants 1969):

1. Reactor start-up from the cold state was realized without external heat sources. The reactor heat-up was carried out at 10% power until the water temperature in the separators reached 285 – 300°C at 8.8 MPa. Levels in the separators were formed during heat-up. Transition from water to steam cooling in the SHS channels did not cause significant reactivity changes.
2. The radial neutron flux flattening achieved was one of the best among operating reactors. The radial neutron flux irregularity coefficient, K_{ir}, for both units was 1.28 – 1.30, while the design values were: K_{ir} = 1.46 for Unit 1 and K_{ir} = 1.24 for Unit 2.
3. Radioactivity in the turbine and technological equipment of the plant is an important indicator for NPP. Radiation rates at the high-pressure cylinders were not higher than 10 μR/s and not higher than 8 μR/s at the low-pressure cylinders. Such low dose rates were attained by implementation of rod-fuel elements that eliminated the possibility of fission-fragment activity transported via the coolant loop. BNPP operation experience showed that radiation levels near Unit 1 equipment were significantly lower than that of other operating reactors, and releases of radioactive products into the atmosphere were 5 – 10 times lower than allowed by codes.

2.2.2. Cycle development

Reliability, simple design, and efficiency are the main criteria when choosing the flow diagram for both the fossil and nuclear power plants. Special requirements for impermeability and water regime are specified for NPPs. Additionally, the reasonable development of temperature regimes for fuel channels allows safe power increase for the given reactor size.

Several layouts of thermodynamic cycles for a NPP with a uranium-graphite reactor were considered for the BNPP. In the considered layouts (Figure 2.3) the coolant was either boiling water or superheated steam. Feasibility of the NPP designs was also taken into account (Dollezhal et al. 1958a).

Layout (a). A steam separator, steam generator (consisting of preheating, boiling and steam-superheating sections), and two circulation pumps are included in the primary coolant loop. Water and very high-pressure steam are the primary coolants. High- and intermediate-pressure steam is generated in the secondary loop and directed to the turbine.

Layout (b). Direct-cycle layout. Steam from a reactor flows directly to a turbine. The turbine does not require an intermediate-steam reheat.

Layout (c). Steam from a reactor flows directly to a turbine. In contrast to Layout (b), the turbine requires the intermediate-steam reheat. The reactor has three types of operating fuel channels: 1) water preheating, 2) evaporating-boiling, and 3) steam-superheating.

Layout (d). Direct-cycle layout. The evaporation and reheat are achieved inside a reactor. The turbine does not require the intermediate-steam reheat.

Layout (e). Direct-cycle layout. One or two intermediate-steam reheats are required.

Layout (f). Water circulates in the closed loop consisting of a reactor, steam separator, preheater, and circulation pump. Partial evaporation is achieved in the first group of channels. Steam exiting the steam separator is directed to the boiling section of the steam generator and condenses there. Condensate from the boiler is mixed with water from the separator. The cooled water is fed to a preheater and then directed to circulation pumps. The generated steam on the secondary side is superheated in the second group of channels and then directed to the turbine.

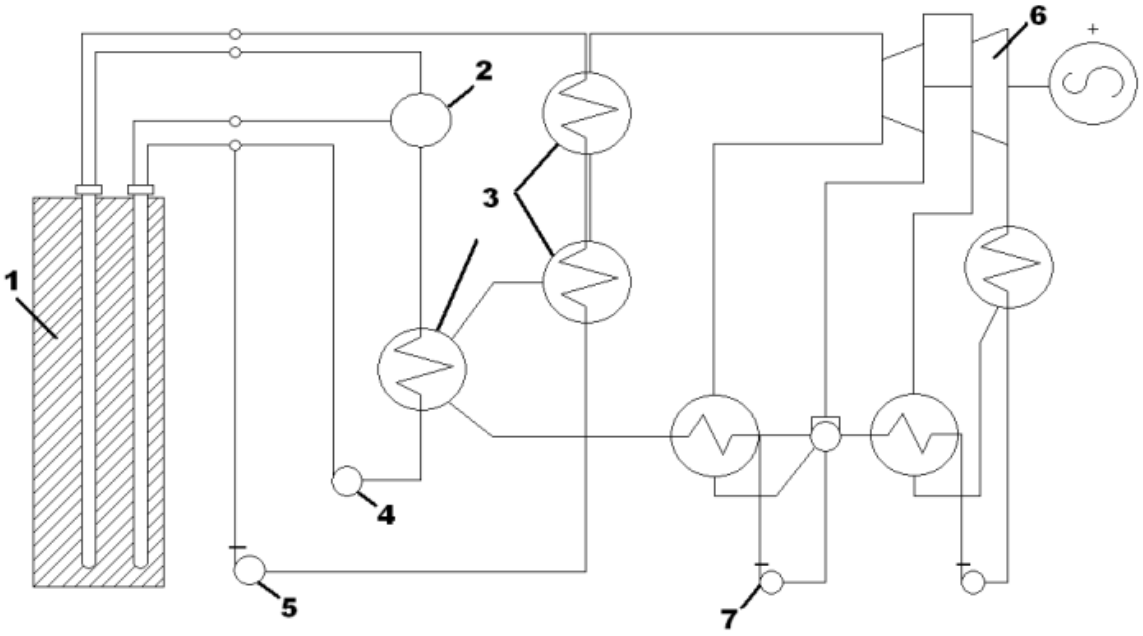

(a)

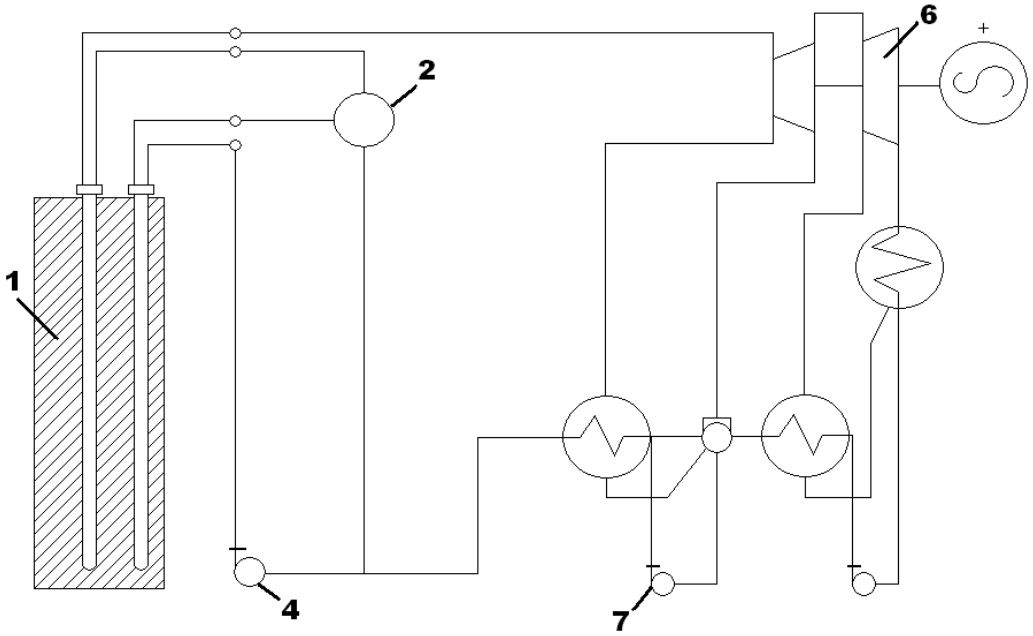

(b)

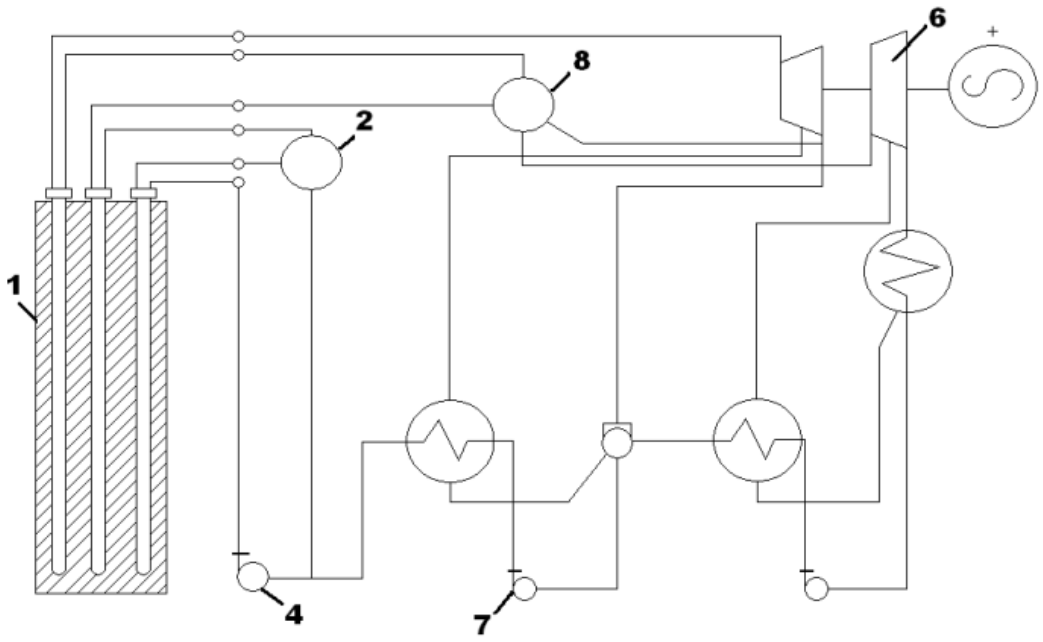

(c)

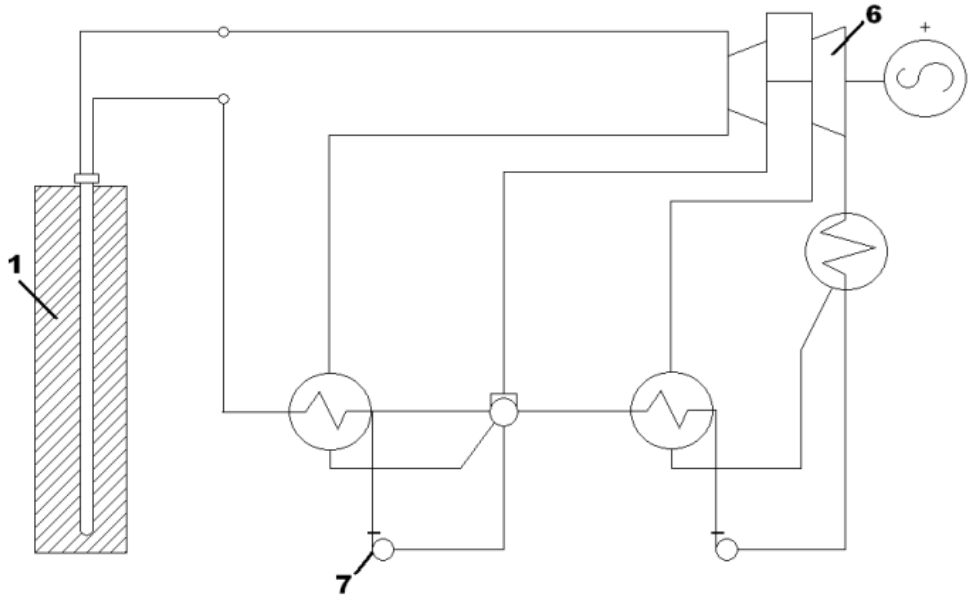

(d)

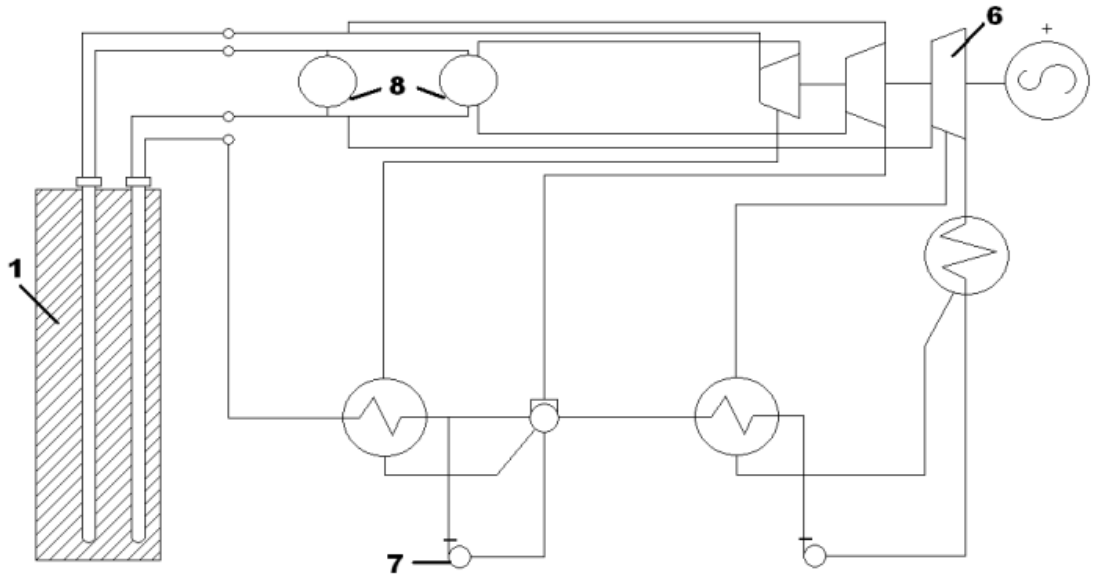

(e)

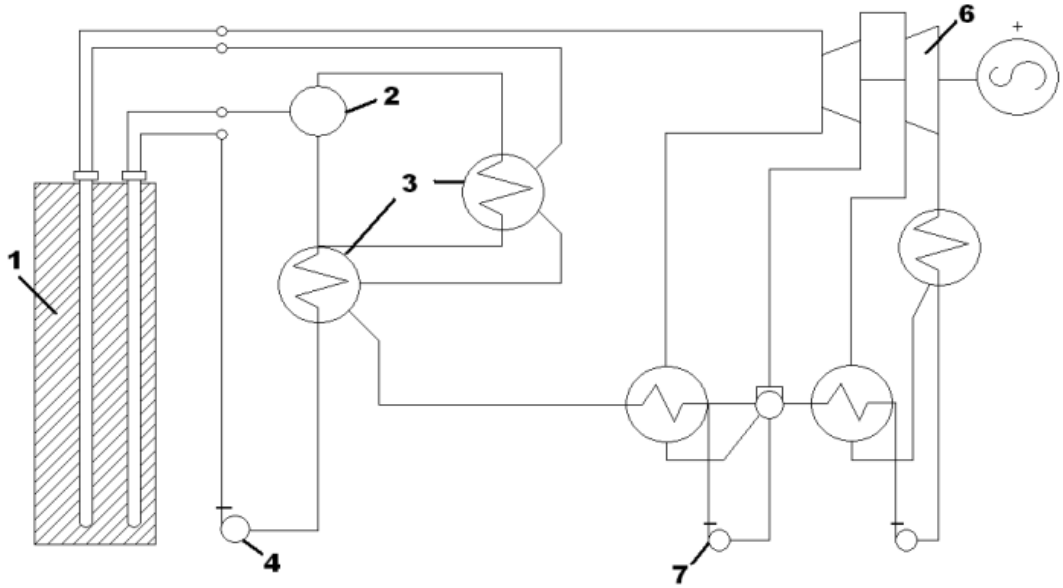

(f)

Figure 2.3. Possible layouts of NPPs with steam reheat (Dollezhal et al. 1958a): 1 – reactor; 2 – steam separator; 3 – SG; 4 – Main Circulation Pump (MCP); 5 – circulation pump; 6 – turbine with electrical generator; 7 – FWP; and 8 – intermediate-steam reheater.

Layouts (b–e) were not recommended due to unpredictable water-chemistry regimes at various locations throughout the thermodynamic cycle. Layout (a) with the secondary-steam reheat required high pressures and temperatures in the primary loop. Circulation pumps with different parameters (power and pressure) were used to feed common header upstream of the channels of the primary group. In this respect, Layout (a) was considerably more complex and expensive than Layout (f). Activation of SHS which could occur in Layout (f) wasn't considered to be posing any significant complications to the turbine operation, and hence remained a viable option (Dollezhal et al, 1958a).

From the considerations above, Layout (f) was chosen to be developed at the BNPP Unit 1. Surface-corrosion products in the secondary loop and salts in condenser coolant were trapped in the steam generator and removed from it during purging. Additionally, modern separators provided steam of high quality, which resulted in very low salt deposits in the turbine.

2.2.3. Beloyarsk NPP reactor design

The reactor was placed in a cylindrical concrete cavity, where the 3-m thick wall served as a part of the biological shield. A cooled ferro-concrete base of the reactor with six base jacks was implemented on the bottom of the cavity. The bottom bedplate attached to the bottom supporting ring was held by jacks. Cooling coils were placed on the bottom of the bedplate to provide its cooling.

The cylindrical graphite stack (3 m in diameter, 4.5 m in height) of the reactor was installed on the bottom bedplate. The stack was made of columns, assembled of hexagonal blocks (0.12 m width across corners) in the center and of sectors in the periphery. The central part of the stack was penetrated by vertical operating channels (long graphite cylinders containing inner thin steel tubes with fuel elements). The reactor core (7.2-m diameter and 6-m height) was surrounded with a 0.8-m thick graphite reflector. An additional 1-m thick graphite layer and an approx 0.5-m cast iron layer over the upper reflector formed the principal part of the biological shield. A 0.6-m thick graphite layer serving as the lower neutron shield was located below the lower

reflector.

The graphite stack (9.6-m overall diameter and 9.0-m height) was enclosed in a gas-tight cylindrical carbon-steel shell filled with nitrogen to prevent graphite deterioration. The outer graphite blocks were penetrated by steel uprights with horizontal lateral braces in several places along their height. The entire stack rested on the bottom bedplate. The graphite stack was covered on the top with a plate carrying standpipes with openings for the insertion of operating channels. The piping for feeding the coolant to the fuel bundles and for removing the coolant water from control rods was located between the standpipes. The piping of the operating channels and protective coating failure-detection system was also located between the standpipes. The plate rested on supports installed on the tank of the side water shield. The plate was connected with the graphite stack shell by means of a compensator, which allowed both for vertical elongations of the shell and horizontal elongations of the plate, which occurred during heating (Emelyanov et al. 1982).

The reactor had 1134 operating channels as shown in Figure 2.4 and contained 998 fuel channels, 6 automatic control rods, 78 channels for reactivity compensating rods, 16 shut-down rods, and 36 channels for ionization chambers and counters. The fuel channels were represented with 730 Boiling Water (BW) channels, also known as evaporating channels, and 268 SuperHeated Steam (SHSs) channels .

The main parameters of the BNPP reactors are listed in Table 2.3.

Table 2.3. Main parameters of BNPP reactors (Aleshchenkov et al. 1964; Dollezhal et al. 1969, 1971).

Parameters	BNPP Unit 1 (730 BWs & 268 SHSs)	BNPP Unit 2 (732 BWs & 266 SHSs)
Electrical power, MW_e	100	200
Number of K-100-90-type turbines	1	2
Inlet-steam pressure, MPa	8.5	7.3
Inlet-steam temperature, ºC	500	501
Gross thermal efficiency, %	36.5	36.6
Total metal content (top & bottom plates, vessel, biological shielding tank, etc.), t	1800	1800
Weight of separator drums, t	94	156
Weight of circulation loop, t	110	110
Weight of graphite stacking, t	810	810
Uranium load, t	67	50
Specific load, MW_{th}/t	4.3	11.2
Uranium enrichment, %	1.8	3.0
Specific electrical-energy production, MW_e·days/t	4000	10000
Square lattice pitch, mm	200	200
Core dimensions, m: Diameter Height	7.2 6	7.2 6

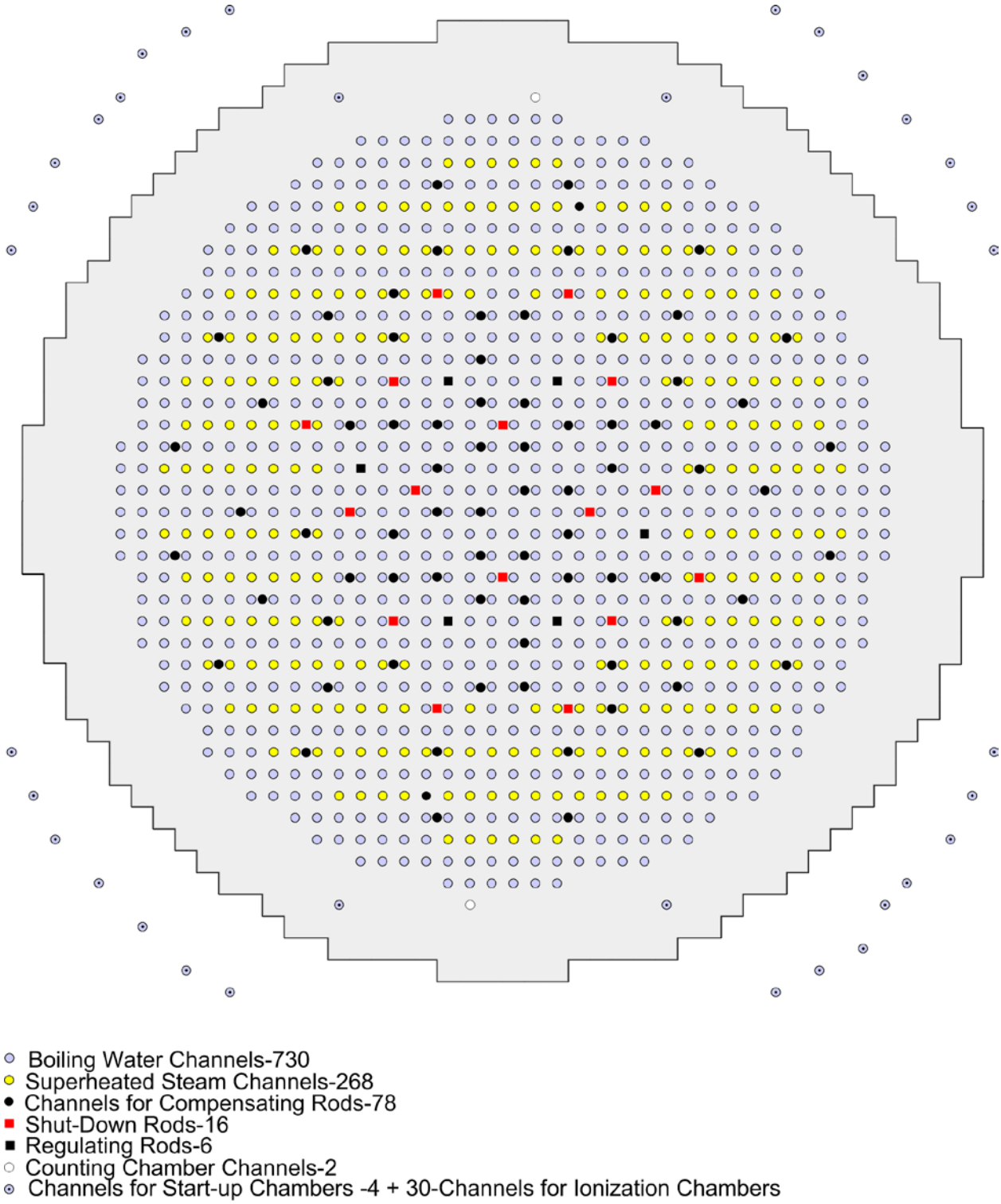

Figure 2.4. BNPP Unit 1 channels layout (Saltanov et al. 2010, this figure is based on the paper by Dollezhal et al. 1958b).

2.2.4. Physical parameters of Beloyarsk NPP reactors

General operating data of the BNPP Units 1 and 2 are listed in Table 2.4.

Table 2.4. General operating data of BNPP (Dollezhal et al. 1974b).

Unit	Parameters	Year of operation						
		1967	**1968**	**1969**	**1970**	**1971**	**1972**	**1973**
I	Utilization factor of installed power, %	49.5	61.6	75.4	81.3	83.3	69.0	73.4
	Utilization factor of calendar time, %	65	69.5	79.3	83.7	83.0	75.3	83.2
	Outlet steam *P*, MPa	7.5	7.9	8.2	8.6	8.6	7.8	7.8
	Outlet steam *T*, °C	439	486	497	511	505	505	498
	Gross efficiency, %	32.9	34.2	36.0	36.3	36.2	36.6	36.1
	Net efficiency, %	29.1	30.5	32.0	32.6	32.7	33.1	32.8
	Electric power for internal needs, %	11.5	10.8	9.5	8.1	7.6	7.6	7.6
II	Utilization factor of installed power, %	49.5	43.6	68.5	69.0	69.3	73.8	70.6
	Utilization factor of calendar time, %	65	79.7	88.8	82.5	84.1	90.9	86.2
	Outlet steam *P*, MPa	7.5	6.4	6.8	7.5	6.9	7.2	7.1
	Outlet steam *T*, °C	439	475	502	511	501	497	502
	Gross efficiency, %	32.9	34.4	35.6	37.4	37.2	36.8	36.0
	Net efficiency, %	29.1	31.6	32.9	34.2	34.2	33.6	32.6
	Electric power for internal needs, %	11.5	8.1	6.9	7.0	7.2	7.4	7.7

Flattening of the power distribution was achieved at the BNPP with physical profiling: appropriate distribution of control rods and fuel channels of different uranium enrichment (for fresh load) and profiling of burn-up fuel along the reactor radius. The reactor load consisted of SHS channels of 2% and 3% uranium enrichments (SHS-2 and SHS-3 respectively) and BW channels. The BW channels were located in rings in alternate locations with SHS-2 as shown in Figure 2.4. SHS-3 were located along the circumference and had lower pressure losses in the steam circuit (Dollezhal et al. 1964).

Neutronics calculations were made to choose optimal distribution of channels to achieve required power shape. Most of the calculations for the core-reactor physics were performed in the 2-group approximation. In accordance with the fuel-channels distribution the core was represented by four cylindrical regions with the radii: R_1 = 175 cm (234 fuel channels), R_2 = 268 cm (324 fuel channels), R_3 = 316 cm (220 fuel channels), and R_4 = 358 cm (220 fuel channels). The previous calculations and operating experience of large uranium-graphite reactors with relatively small neutron leakage showed that a simplified schematic could be used when neutron distribution in the reactor is determined by the multiplication characteristics of the reactor regions. The multiplications constants obtained for the 4 regions ($k_{inf,1}$ = 1.013, $k_{inf,2}$ = 1.021, $k_{inf,3}$ = 1.043, and $k_{inf,4}$ = 1.045) allowed flattening of the neutron distribution along the reactor radius with K_{ir} = 1.20 – 1.25. The increase in the multiplication constants values to the periphery of the reactor was attained by placing fuel channels with 3% uranium enrichment. Refueling schemes and, therefore, fuel burn-up at different regions were chosen such as to allow designed power flattening in the end of the campaign, with corresponding values of $k_{inf,i}$. Control rods insertion in the core maintained $k_{inf,i}$ values in the necessary limits during normal operation (Vikulov et al. 1971).

One of the requirements to be met when implementing nuclear steam reheat is to maintain a constant specified power ratio (π) of the steam-superheating zone to the boiling zone during the operating period. The SHS channel temperature up to 520°C at the BNPP was obtained by setting π = 0.41 at the optimum parameters of the thermodynamic cycle. The number of SHS channels was chosen to provide a π-value of 0.41 at the partial refueling scheme where the $K_{ir} \approx$ 1.25. The steady-state regime was characterized with small fluctuations of approximately 1% in

the π-value between the refuelings. Circular arrangement of SHS channels (Unit 1) had an advantage of small π-sensitivity to the changes in radial neutron flux distributions, while for central arrangement of SHS channels (Unit 2) π values were more sensitive (see Table 2.5).

Table 2.5. Steam-superheating-zone power to boiling-zone power ratio (π) dependence on neutron flux K_{eff} for BNPP Unit 2 (Vikulov et al. 1971).

π	0.408	0.429	0.452	0.494
K_{eff}	1.20	1.36	1.53	1.78

However, preference was given to the central arrangement of SHS channels, because this allowed attaining a higher π-value (around 12% higher) with the same number of SHS channels. Additionally, central arrangement of SHS channels provided better multiplication characteristics than BW channels. SHS channels were placed in the central region to increase average fuel burn-up by 10%. It should be noted, that during the initial operation period the burn-up rates were different for BW and SHS channels of fresh load, which led to an unbalance of power between superheating and boiling zones. Figure 2.5 shows the calculated dependence of π-values and power variations for different types of fuel channels on the power generated by the reactor (Vikulov et al. 1971).

Calculations were performed assuming $K_{ir} \approx 1.25$. A fast decrease in the superheating-zone power relative to that of the boiling zone in the initial period was accounted for by a lower power change in SHS channels due to slightly higher fuel conversion in the low enriched SHS-2. Practically achieved values of K_{ir} were approximately 1.4 for Unit 1 and 1.3 for Unit 2. Neutron balance in the core of the critical reactor in the beginning of the operation period is shown in Figure 2.6.

One of the features of the uranium-graphite reactors cooled with water is the possibility of reactivity change with water-content change in the reactor. Substitution of boiling water with steam in the operating channels leads to the rapid change of coolant average density. Failure of a fuel-element sheath is another possibility of water-content change that was considered while designing the BNPP reactors. The chosen core lattice with respect to reactivity change turned

out to be weakly dependent on water-content changes. It was explained by the compensation of effects of increased resonance neutrons captured by increased water content and an increase at the same time of non-productive neutrons absorption (Dollezhal et al. 1964). Normalized thermal-neutrons distribution along the operating channel cell was studied experimentally for the reactor lattice as shown in Figure 2.7. The normalized thermal-neutrons distributions along the reactor radius and height for both units are shown in Figures 2.8 and 2.9. The gradients indicate a significant disturbance in the normalized thermal-neutron flux near the outer edge of the reactor likely where the steam-reheat channels end affecting the power distribution. The results indicate a more stable distribution for the BNPP Unit 2.

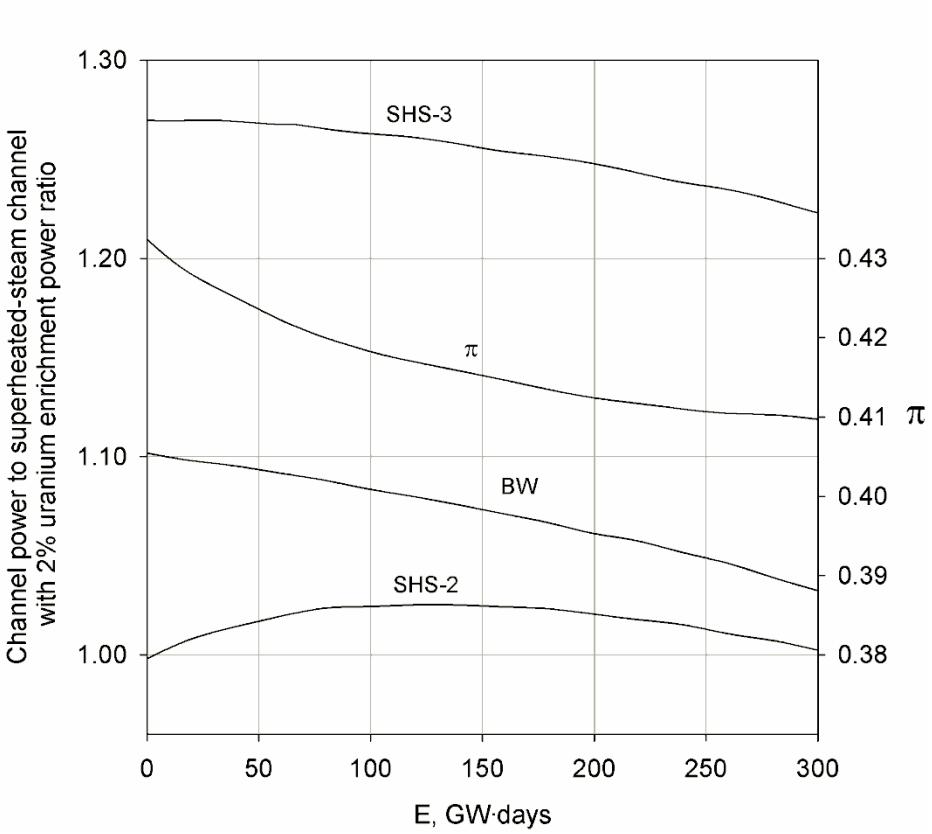

Figure 2.5. Channel power ratios and steam-superheating-zone to boiling-zone power ratio (π) dependence on burnup produced by BNPP Unit 2 during the first operating period (Vikulov et al. 1971): SHS-3 – superheated steam channel with 3% uranium enrichment and SHS-2 – superheated steam channel with 2% uranium enrichment.

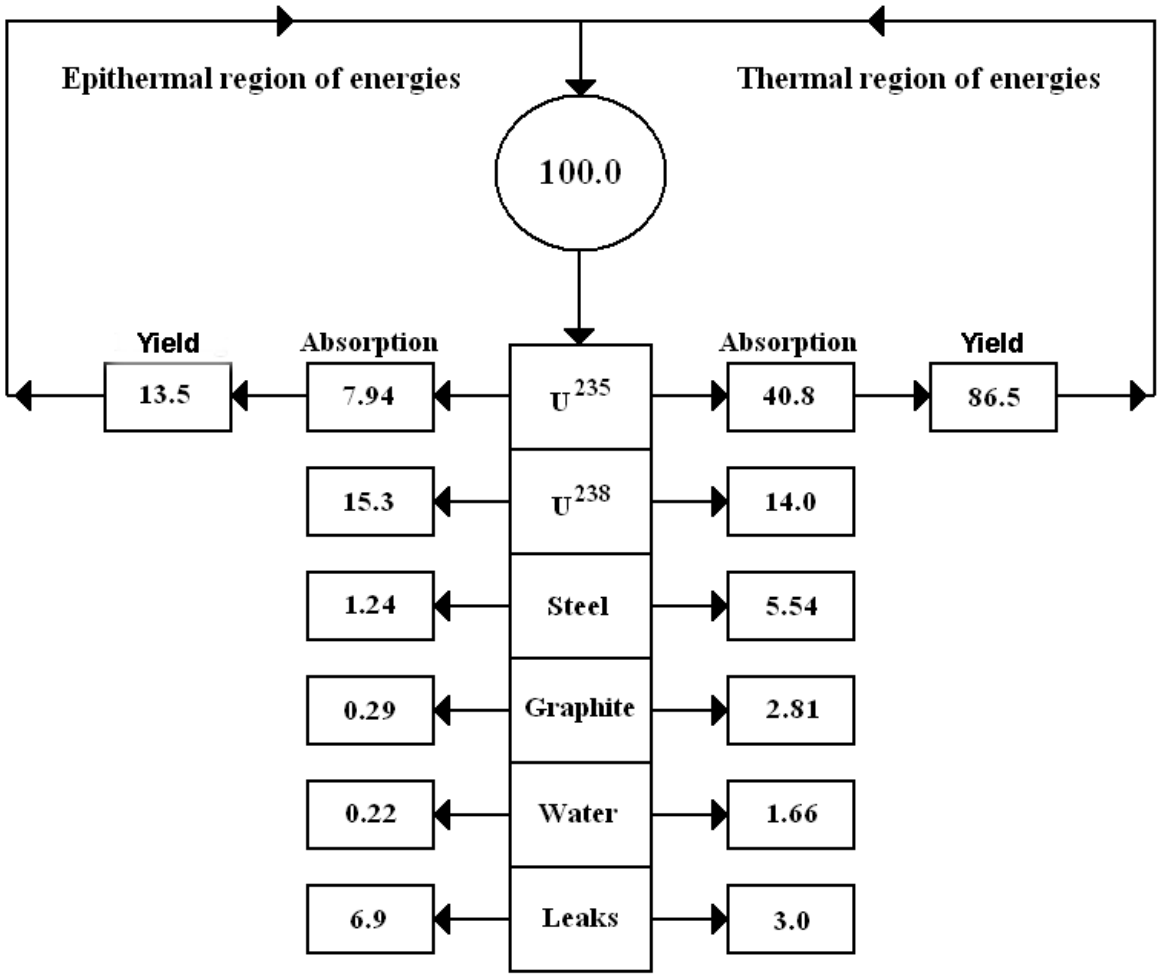

Figure 2.6. Neutron balance in a critical reactor (Dollezhal et al. 1958a).

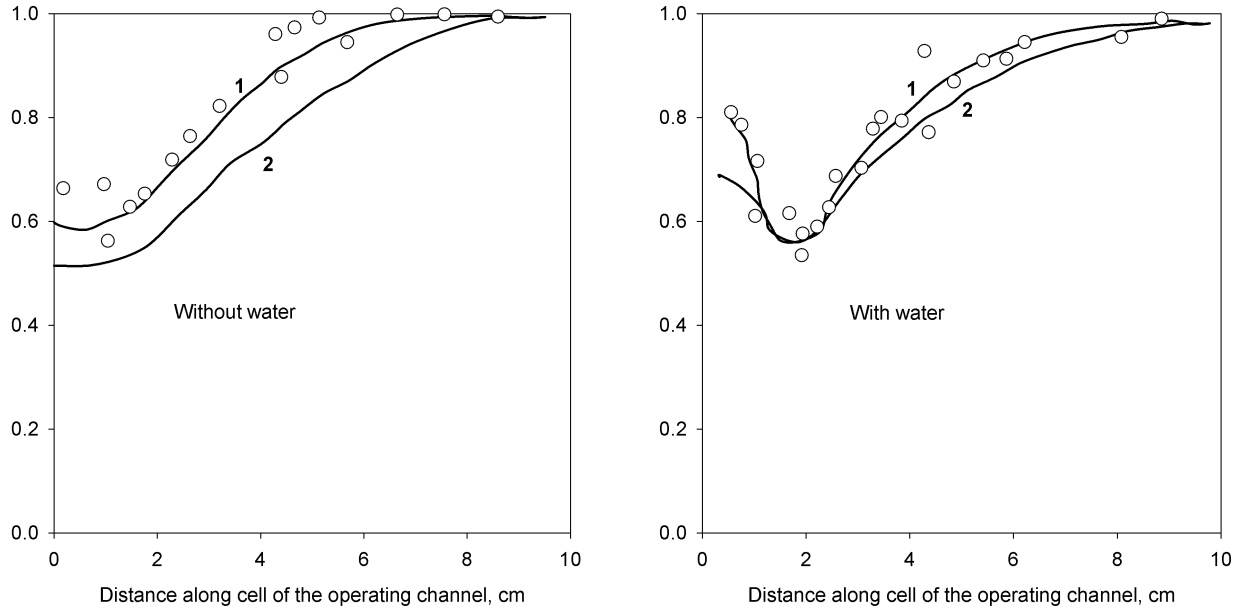

Figure 2.7. Normalized thermal-neutrons-density distribution along cell of the operating channel (Dollezhal et al. 1958b):1 – experimental curve and 2 – design curve.

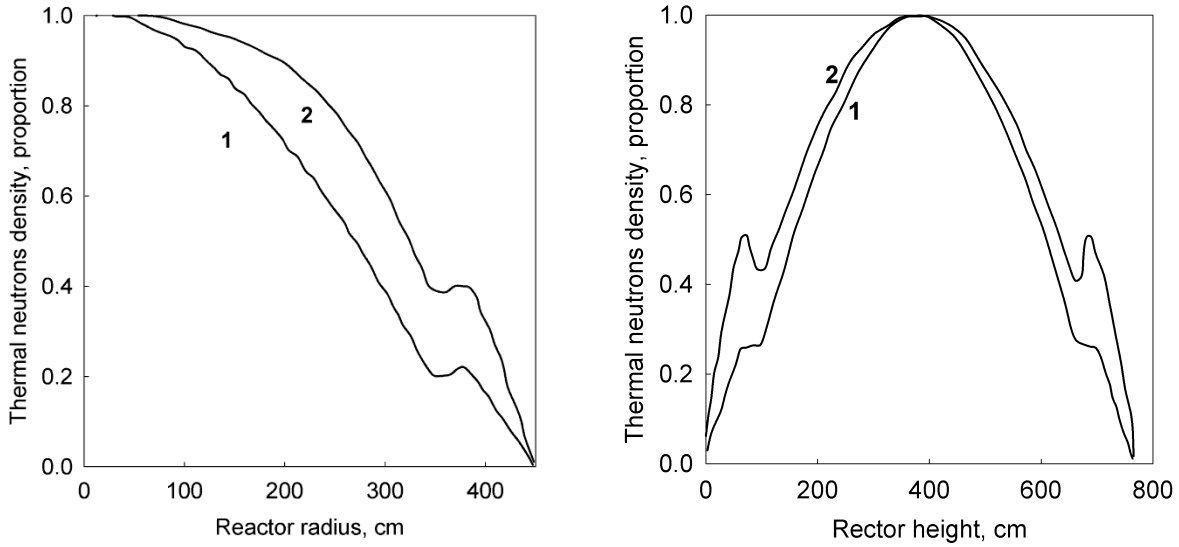

Figure 2.8. Normalized thermal-neutrons-density distribution along radius (a) and height (b) of the BNPP Unit 1 (Dollezhal et al. 1958a): 1 – beginning of the operating period and 2 – end of the operating period.

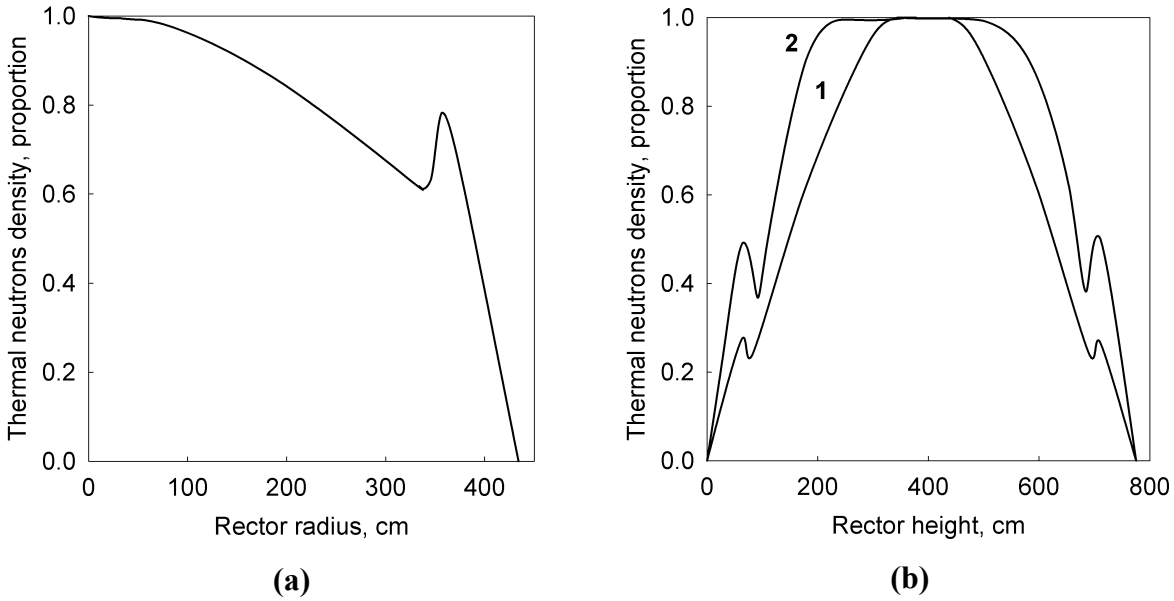

Figure 2.9. Normalized-thermal-neutron density distribution along radius (a) and height (b) of the BNPP Unit 2 (Dollezhal et al. 1964): 1 – beginning of the operating period and 2 – end of the operating period.

Distribution deformation near the end of operating period was explained by non-uniform fuel burn-up. The results proved the possibility of elementary diffusion-theory application for determining neutron distributions and showed the impact of the arrangement of the superheated-steam channels on power distribution.

2.2.5. Boiling-water channels

Fault-free operation of BW channels was achieved with reliable crisis-free cooling of bundles and avoiding interchannel and subchannel pulsations of the coolant-flow rate. The appropriate experiments were performed during design of the BNPP. As the result of increased power, the inner diameter of the fuel element was increased from 8.2 mm for Unit 1 to 10.8 mm for Unit 2. Note that an annular-fuel design is used and increasing the inner diameter results in thinner fuel and lower-centerline temperatures. Coolant is on the inside of the annular fuel and graphite is on the outside of the fuel as shown in Figure 2.11.

Experiments were performed at different pressures and equal heat flux, steam content and coolant mass fluxes and showed that wall temperature increases at the boiling crisis was higher

when coolant pressure was lowered. At the same time, with the lowered coolant pressure the critical steam content increased. The experiments on hydrodynamic stability showed that mass-flux pulsations within the region of high steam content did not introduce danger for the BNPP reactors, because nominal pressure in the evaporating loop was 8.8 MPa and steam content at the channels outlet was not higher than 35%. Wall-temperature oscillations were in the phase with the subchannel flow-rate pulsations. With the increased pressure both the amplitude of temperature oscillations and coolant flow rate decreased. The same effect occurred at the decreased heat flux and increased flow rate per channel. Wall-temperature oscillations were within the range of 65°C at 1000 kg/h flow rate and 30°C at 1500 kg/h flow rate at constant pressure of 4.9 MPa and 0.2 MW power (Dollezhal et al. 1964).

Fuel elements of larger inner diameter used at Unit 2 compared to that of Unit 1 allowed to lower heat flux and hydraulic resistance. With the equal outer diameter (20 mm), fuel elements inner diameter of the BWs at Unit 1 were 9.4×0.6 mm while that of Unit 2 – 12×0.6 mm. Diameter of the central tube for feeding the coolant was also increased. There were no other differences in the BWs construction used at BNPP Units 1 and 2. Uranium-molybdenum alloy with magnesium filler was used as fuel in the BWs. Parameters of the BWs are listed in Table 2.6.

Table 2.6. Parameters of BNPP boiling-water channels (Dollezhal et al. 1964).

Parameters	BNPP Unit 1	BNPP Unit 2
Channel power, kW	405	620
Flow rate per channel, t/h	2.400	4.2
Steam content at channel outlet, %	33.6	30.7
P_{in}, MPa	15.2	15.2
P_{out}, MPa	14.7	14.2
T_{in}, °C	300	303
T_{out}, °C	335	338
Max. heat flux, MW/m^2	0.58	0.72
Circulation rate, m/s	3.5	3.6
Max. T, °C: inner wall fuel	355 400	365 415

2.2.6. Superheated-steam channels

At the BNPP, SHS channels were operated at higher temperatures compared to those in the BW channels and, therefore, limited the choice of fuel composite and materials. The development of fuel elements for SHS channels underwent several stages. Preliminary tests on the manufacturing technology and performance of fuel elements of various designs were made. As the result, a tubular fuel element with a stainless-steel sheath and a uranium-dioxide fuel composite was chosen for further development (Samoylov et al. 1976). Fuel elements in the initial modification had a tubular design formed by two coaxial stainless-steel sheaths (9.4×0.6 mm and 20×0.3 mm, respectively). Thus, SHS channels with such fuel elements did not differ significantly from BW channels (Figure 2.10), consisting of 6 fuel elements arranged in a graphite collar with a central steam feeding tube. Steam entered the central tube and was superheated while passing along the fuel bundles.

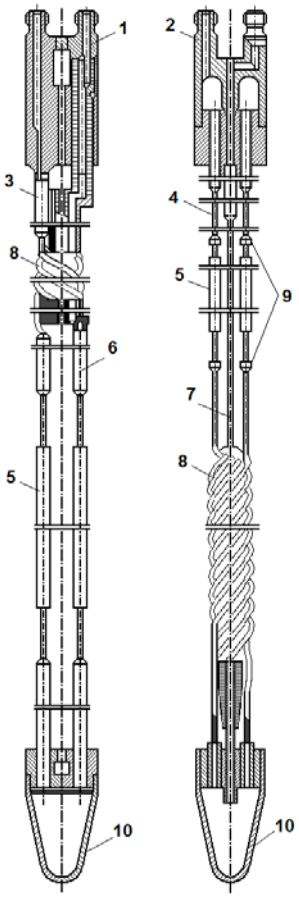

Figure 2.10. Principal design scheme of boiling-water and superheated-steam channels (Emelyanov et al. 1972b):
1 – head of boiling-water channel;
2 – head of superheated-steam channel;
3 – three downward-flow strings;
4 – six upward-flow strings;
5 – fuel bundle strings;
6 – three upward-flow strings;
7 – downward-flow strings;
8 – compensators;
9 – welded joints of tubes;
10 – tail.

Later, a U-shape desgin was developed. The central tube (9.4×0.6 mm) was replaced with an absorbing soft-control rod (12×0.6 mm). The decreased width of the active material decreased non-productive neutron absorption and allowed some power flattening. The steam was reheated first passing downward along three fuel bundles and then passing upwards along another three fuel bundles. Such construction reduced temperature conditions for SHS channels and allowed usage of simpler and cheaper materials. Also, reactor-graphite-stack temperature was lowered by 100°C at a channel power of 0.36 MW. This was achieved with the transfer of heat released in the graphite stack to the downward flow fuel elements that operated at intermediate temperatures (Dollezhal et al. 1964).

Efforts for further improvement of heat and physical parameters were made. They led to another modification of channels and fuel elements. One upward flowing fuel element was eliminated, inner fuel-element sheath was increased to the size of 16×0.7 mm, and outer-sheath size was increased to 23×0.3 mm. Physical and thermal parameters improved sharply after such a modification due to decreased matrix material in the fuel elements and increased flow cross-section. 6-elements channels were gradually replaced by 5-elements channels during refueling of the operating reactor. The reduction of one of the elements increases the steam velocity in the upward flowing fuel elements (Samoylov et al. 1976). Stainless steel was used as the outer-sheath material. Uranium-dioxide dispersed in matrix alloy was used as fuel elements in SHS channels. Improvements in the performance of various BNPP parameters are listed in Table 2.7.

Table 2.7. Average parameters of BNPP Unit 1 before and after installation of superheated-steam channels (Dollezhal et al. 1969).

Parameters	Before SHSs installation	After SHSs installation
Electrical power, MW_e	60–70	100–105
Steam P_{in}, MPa	5.9–6.3	7.8–8.3
Steam T_{in}, ºC	395–405	490–505
Exhaust steam P, kPa	9–11	3.4–4.0
Mass flowrate of water in 1st loop, kg/h	1400	2300–2400
P in separators, MPa	9.3–9.8	11.8–12.7
Gross thermal efficiency, %	29–32	35–36
Electrical power for internal needs, %	10–12	7–9

Cross sections of the U-shaped SHS channels are shown in Figure 2.11. SHS-channels parameters are listed in Table 2.8.

Table 2.8. Design parameters and operating conditions of superheated-steam channels (Dollezhal et al. 1964).

Parameters	BNPP Unit 1	BNPP Unit 2 (U-shaped channel with 6 fuel elements)	
		Downward-flow fuel elements	Upward-flow fuel elements
Max channel power, kW	368	767	
Min channel power, kW	202	548	
Steam mass-flow rate through max. power channel, kg/h	1900	3600	
Steam mass flow rate through channel operating at minimal power, kg/h	1040	2570	
Steam P_{in}/ P_{out}, MPa	10.8/9.81	12.9/12.3	12.2/10.8
Steam T_{in}/ T_{out}, °C	316/510	328/399	397/508
Max heat flux, MW/m^2	0.56	0.95	0.79
Max steam velocity, m/s	57	76	112
Max T, °C: cladding	530	426	531
fuel composite	550	482	565
graphite	725	735	735

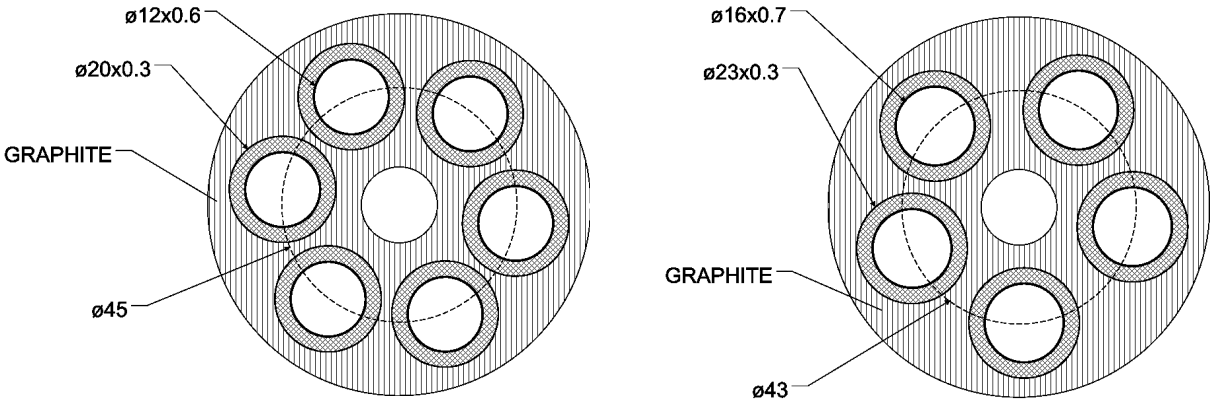

(a, initial variant) (b, modernized variant)

Figure 2.11. Cross section of BNPP superheated-steam reheat channel with 6 (a) and 5 (b) elements (dimensions in mm) (Dollezhal et al. 1974a).

Basic parameters of the BW and SHS channels of the BNPP are listed in Table 2.9.

Table 2.9. Basic parameters of fuel channels (Dollezhal et al. 1971; Emelyanov et al. 1972b).

Parameters	BNPP Unit 1		BNPP Unit 2	
	BW	SHS	BW	SHS
Dimensions of fuel elements inner sheath, mm	9.4×0.6	12×0.6	12×0.6	12×0.6
Dimensions of fuel elements outer sheath, mm	20×0.2	20×0.3	20×0.2	20×0.3
Number of fuel elements in channel, mm	6	6	6	6
Dimensions of central tube of channel, mm	18×1	–	20×1	–
Max channel power, kW	408	326	623	729
Main parameters of channels (P_{in}/T_{in}, MPa/°C)	13.2/300	10.8/315	14.2/300	12.7/335
Main parameters of channels (P_{out}/T_{out}, MPa/°C)	12.7/330	9.3/510	13.7/335	10.8/510
Weight of channel, kg	200	200	200	200

2.2.7. Mechanical strength of channels used in Beloyarsk NPP

The problem of providing necessary strength for the fuel channels was one of the problems to be resolved during designing BNPP reactors. Tubular compensators were used for compensation of thermal expansion of both downward-flow and upward-flow fuel bundles strings. Internal pressure stress and temperature stress were determined and analyzed for steady-state and transient conditions. Equivalent membrane stresses (defined from strength theory) caused by internal pressure were limited by 1/1.65 of yield stress. Local tensions exceeded yield stress in the individual zones where the fuel element tubes were connected to the heads and tails. Heads are detailed components with inlet and outlet hollows to allow coolant at different temperatures pass it (Emelyanov et al. 1972a). The temperature drop between the inlet and outlet of the heads was not significant for BW channels (30°C) and quite significant for SHS channels (up to 260°C). Under steady state conditions, significant temperature stresses could have been caused in the shell (∅34×1 mm), which connected head outlet connection to the channel cap. However, calculations showed that maximum stresses were only 12.5 kg/mm^2 in the shell and, therefore unlikely to exceed stress limits of the material. Maximum stress values during start-up and emergency shutdown of the BNPP reactors are listed in Table 2.10.

Table 2.10. Maximum stress in superheated-steam-channel head during transitional mode (Emelyanov et al. 1972a).

Mode	Element	Temperature change interval, °C	Stress, MPa
Heat up	Transition chamber	260–510	1.96
	Shell ∅34×1 mm	260–510	1.37
Emergency shutdown	Transition chamber	510–415	1.18
	Shell ∅34×1 mm	510–415	1.18

Additional tests on corrosion resistance of the stainless steel in contact with the water–steam mixture with oxygen and chlorine ions were performed (Emelyanov et al. 1972a). First,

compensators were put under displacement cyclic load at the highest working values (785 N/mm^2). Then the number of cycles was 6000. The cyclic load simulated the most damaged state of the compensators materials that would be in the end of channels operation period. Then water–steam mixture at P = 14.2 MPa and T = 340°C was passed through the channels compensators which were placed in an electrical furnace.

After holding the compensator for 144 h in the furnace, pressure in the compensators was decreased to 9.8 MPa, and temperature was decreased to 100±5°C. Simultaneously, water with 0.06 mg/l chlorides content was injected into the electrical furnace. Moisture was condensed at 95°C and evaporated at 105°C throughout the test. The moisture condensation-evaporation cycle was repeated 30 – 40 times during a 24-h period. The pressure was increased up to 14.2 MPa and temperature was increased up to 340 °C and the compensators were being held for another 144 h. Then the condensation-evaporation cycle was repeated and so on. Compensators were examined destructively after 144 – 1100 h under abovementioned conditions. The fracture pattern was identical for each case where a net of cracks was formed on the outer surface and cracks further developed into holes. More information on corrosion-mechanical and cyclic strength of the channel constructional elements may be found in the paper by Emelyanov et al. (1972a).

2.2.8. Hydrodynamic stability of the Beloyarsk NPP channels during reactors start-up

During start-up and nominal operating conditions it is necessary to provide reliable cooling of fuel bundles (crisis-free heat exchange and hydrodynamic stability). Experiments on set-up simulating Units 1 and 2 were performed for determining safe operating conditions for coolant flow rate with no pulsations during the start-up.

Both SHS and BW channels of the BNPP were filled with water in the initial state. During reactor start-up, the water in the SHS channels was to be discharged and transfer to cooling by steam was to be performed. Additionally, the units were preheated and started without external heat sources.

The coolant flow rate stability in the BW channels was studied for wide ranges of pressures, flow rates and powers (Smolin et al. 1965). Special attention was paid to determination of the pressure, flow rate, steam content and power. Different combinations of these parameters created conditions leading to pulsations. When occurred, flow rate pulsations took place when coolant reached saturation temperature at the outlet of the BWs. Pulsations were in the form of coolant flow rate periodical oscillations in peripheral tubes. Oscillations were phase-shifted in different tubes while the total flow rate was constant.

Two pulsation regions were determined as the result of the experiments: small steam content region (x = 0 – 15 %, 3 – 6 oscillations per min.) and high steam content region (x = 25 – 80%, 15 – 20 oscillations per min.). Flow rate pulsations in tubes were accompanied by wall tube temperature oscillations along its length with the frequency being equal to that of flow rate oscillations. Wall temperature oscillations in the top cross-sections of the heating zone within the small steam content region occurred with a shift to the smaller values in the surface or volumetric boiling zones and to both the smaller and higher values in the economizer zone. Wall temperature oscillations in the top cross-sections of the heating zone within the high steam content shifted only to the higher values causing boiling crisis (Smolin et al. 1965).

The curves distinguishing stability zones (above the curves) from pulsation zones (below the curves) for the BW and SHS channels of the BNPP Unit 2 are shown in Figure 2.12.

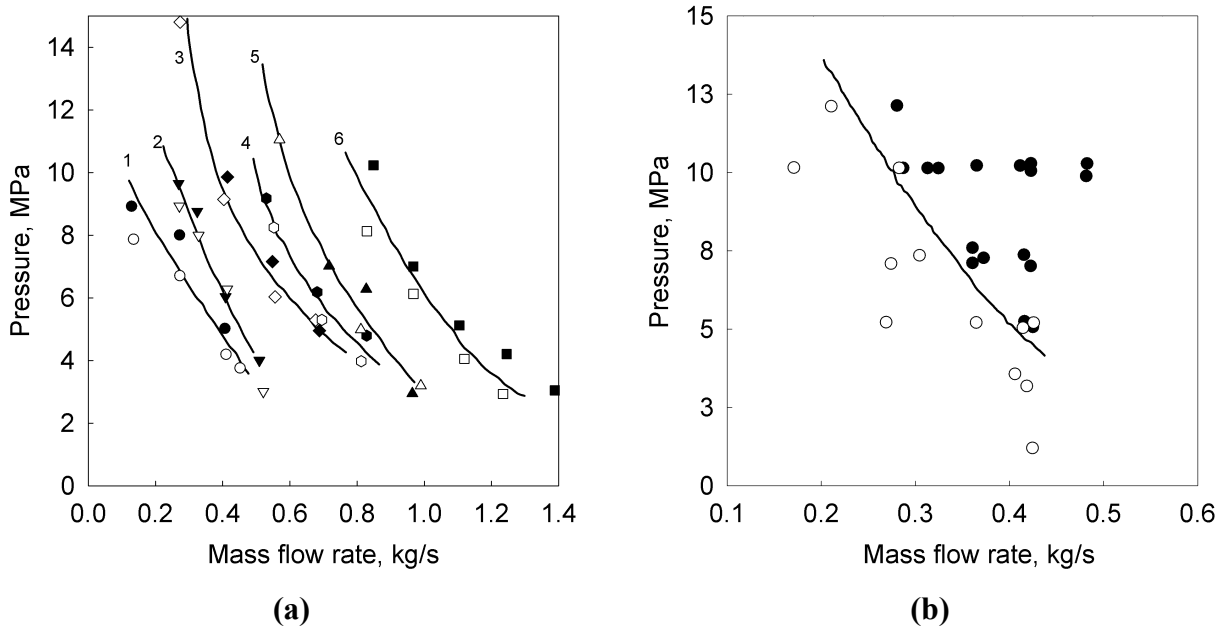

Figure 2.12. Ranges of hydrodynamic stability in BW (a) and SHS (b) channels of BNPP Unit 2 at different channel power (regions of channels stable operation are above curves, solid symbols) (Smolin et al. 1965): 1 – 50 kW; 2 – 100 kW; 3 – 200 kW; 4 – 300 kW; 5 – 400 kW; and 6 – 800 kW.

As seen in Figure 2.12 the range of stable operation of channels broadens with the increase in pressure or increase in flow rate. The stable operation range contracts with the increase in power. The operating conditions that provide stable flow rate and reliable cooling of the BW and SHS channels at the start-up and nominal operating conditions were chosen based on the performed research. The method of replacing water coolant by steam coolant in SHS channels using accumulated heat was accepted for experimental testing of start-up conditions on Unit 1. The method of gradual replacement of water in the SHS channels first by a water-steam mixture and then by steam was accepted for experimental tests of start-up regime on Unit 2 (Smolin et al. 1965). The experimentally obtained data are presented in Figures 2.13 – 2.15.

Both methods were elaborately tested and proved to provide reliable cooling of the BW and SHS channels during the start-up. They were adapted for the development of the BNPP start-up conditions.

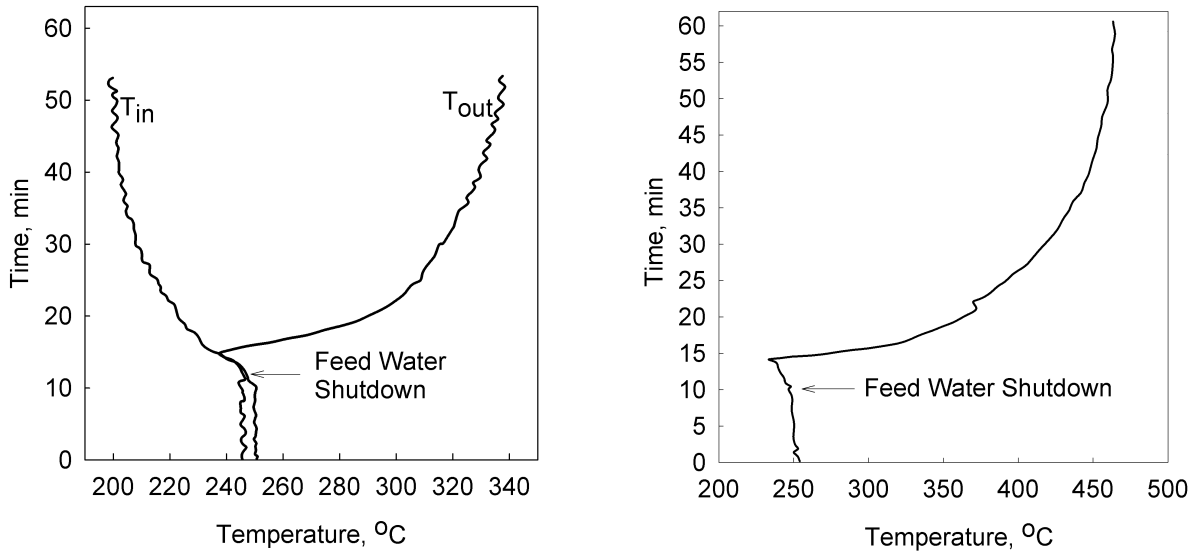

Figure 2.13. Temperature variations at BNPP Unit 1 SHS channels at transitional regime (Smolin et al. 1965): (a) – coolant inlet (T_{in}) and outlet temperatures (T_{out}) and (b) –sheath temperature.

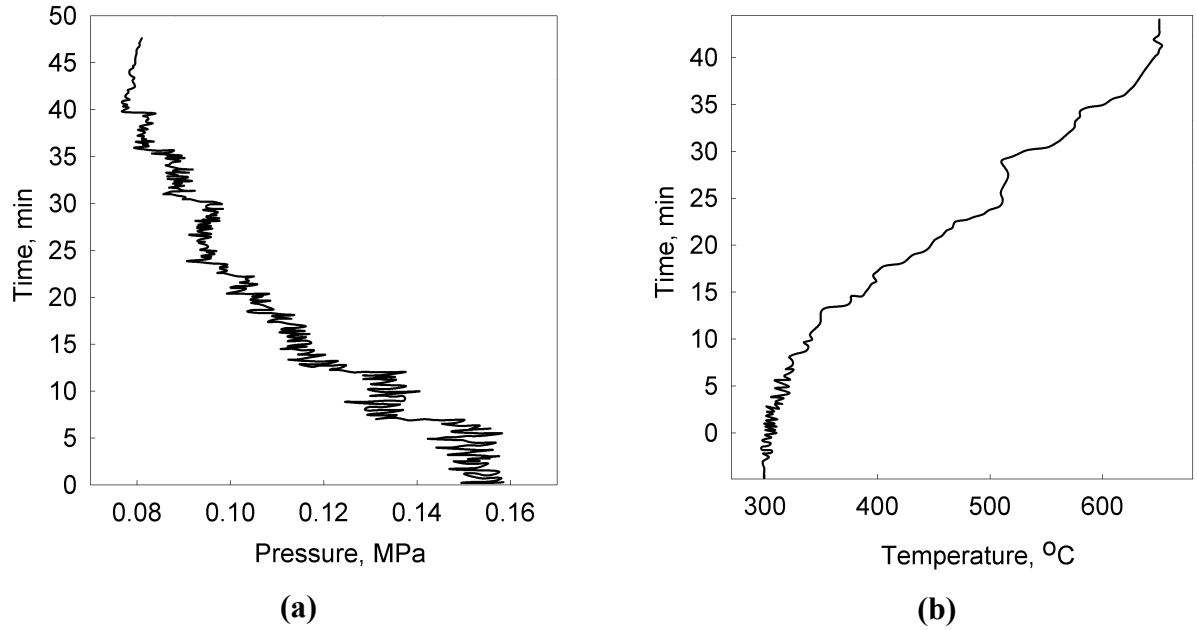

Figure 2.14. Variations of pressure drop (a) and sheath temperature (b) at BNPP Unit 2 during high-power start-up (Smolin et al. 1965).

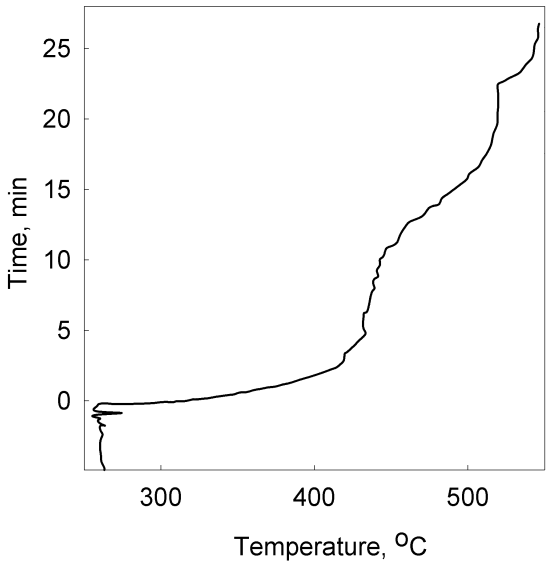

Figure 2.15. Sheath temperature variations during start-up with decreasing pressure at BNPP Unit 2 SHS channels (Smolin et al. 1965).

2.2.9. Start-up of Beloyarsk NPP reactors

The start-up testing of the Unit 1 and Unit 2 reactors of the BNPP are described in this section. During the Unit 1 start-up, both loops were filled with deaerated water, water circulation was established, air was removed, and the pressure was raised up to 10 MPa and 3 MPa in the primary and secondary loops, respectively (Aleshchenkov et al. 1971).

Equipment was heated up at 10 – 14% of reactor power. Average heat-up rate was kept at 30°C/h as measured at the separators. This value was chosen based on experience of drum boilers operation, though reactor equipment allowed significantly higher heat-up rate. No heat removal was provided during the heat-up to the 160°C coolant temperature at the reactor outlet. The water level was formed at 160°C in the bubbler and the excess heat started being released to the turbine condenser. When water temperature at the outlet of the SHS channels reached 230°C the heat-up was terminated. Total heat-up time was about 9 h.

At the next step, water was purged from SHS channels. The transient processes took place in the second loop while constant pressure and boiling-free cooling of BWs were provided in the

primary loop. Reactor power was rapidly reduced to ~2% of its nominal level and feedwater flow rate was reduced to provide water level in the SGs to purge SHS channels. Water-steam mixture from evaporators and steam from the steam loop were directed to the bubbler and then to the deaerator and the turbine condenser.

The purging of SHS channels started after the level in the SGs had been formed. The purging regime was monitored by the pressure drop between the reactor inlet and outlet steam headers and the coolant temperature at the outlet of each SHS channel. Additional steam discharge by increased pressure drop rate was achieved and thus the purging was accelerated by opening gate valves in front of the bubbler for 1 – 2 min. The pressure drop rate was chosen based upon the allowed temperature condition and was set to ~0.15 MPa/min. Overall time for the level formation in the evaporators was ~8 – 10 min, the time of purging ~6 – 10 min. The gate valves in front of bubblers were closed and reactor power was increased after the purging had finished. Thus, the pressure and the temperature in SHS channels were increase. After 2 hours the SHS channels purging had been finished and the reactor achieved a stable operation at 10% power level. The heating of steam pipes and the turbine was initiated and the turbine connection to the power line was prepared. Further power increase was made once the turbine had been connected to the power line.

The first loop was transferred to the boiling flow regime and the separators levels were formed at 35% reactor power and ~6 MPa pressure. During the transient to the boiling regime, the operating conditions of the MCPs were continuously monitored. Water temperature was maintained $5 - 6\,^{\circ}\mathrm{C}$ below the boiling margin for intake pipes of the main circulation pumps. Level formation in the separators was accompanied by smooth pressure change. It took about 3 h for the water to reach controlled level in the separators, the time being dependent only on the separator bleed lines throughput.

The specific features of a single-circuit flow diagram made the sequence of the BNPP Unit 2 start-up operations somewhat different. SHS channels purging and transition to boiling regime in the BW channels took place simultaneously. Filling of the circuits and equipment heat-up were the same as in Unit 1. The terminal heat-up parameters were higher ($P \approx 9.3$ MPa and $T \approx$

290°C). Two main circulation pumps were used to drive coolant circulation in the evaporating loop. After heat-up the reactor power was reduced to 2 – 3% of nominal level. SHS channels purging, and transition to boiling regime in the BW channels took place after the heat-up. The feedwater flow rate was considerably reduced, water was purged out of the separators, and the flow rate to the bubblers was increased to form levels in the separators. As a result, the water in the fuel channels and separators boiled causing the purging of water and water-steam mixture from SHS channels. The monitoring of the purging process was the same as at the Unit 1. After SHS channels purging had been completed, the reactor power was increased and steam flow into the bubbler was reduced at the reheated steam temperature rise rate of about 1°C/min with the pressure drop between the steam headers at least ~50 – 60 kPa. The automatic level control system was put into operation as soon as the water in the separators reached the rated level. The subsequent reactor power increase, turbine preparation, and connection of the turbine to the power line were the same as for Unit 1 (Aleshchenkov et al. 1971). Changes of the main parameters during Unit 2 start-up are shown in Figure 2.16.

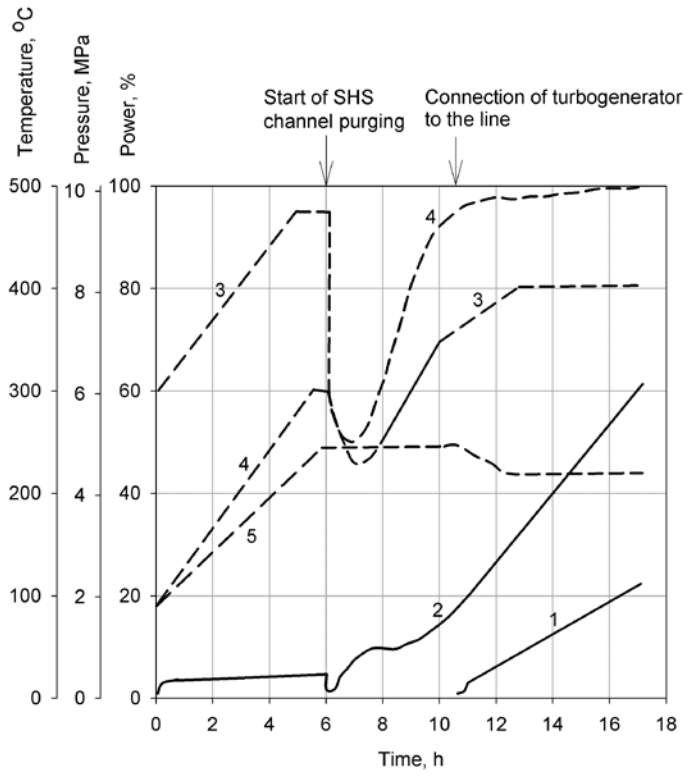

Figure 2.16. Variations of main parameters during start-up of BNPP Unit 2 (Aleshchenkov et al. 1971): 1 – turbine power; 2 – reactor power; 3 – steam pressure; 4 – coolant (water or steam) temperature at SHS channel outlet; and 5 – feedwater temperature.

2.2.10. Pumps

All pumps at the BNPP were high-speed type (3000 rpm). Serial high-power feeding pumps were used. Other pumps were special canned type, in which the motor spindle and pump spindle were revolved in a pumped medium and were separated from the motor stator by a thin hermetic nichrome plate. Bearing pairs of the pumps were lubricated and cooled by pumped water. The revolving details of bearings were made of advanced hard alloys and bearing bushes were made of special plastics. Some minor failures were observed in operation of MCP (Emelyanov et al. 1972b). Those were due to cracks in nichrome jacket, to malfunctioning of fan of the stator front parts, to pilot-valve distribution system imperfections, and to failures of the fasteners in the pump interior. Modernizations of some individual elements of the MCP and reconstruction of independent pump cooling loops improved optimal on-stream time between maintenance and repairing (16,000 h). As a result, the failure probability of the MCP was reduced to minimum. Operating experience of the MCP showed that serial pumps could be used instead of specially designed canned pumps under no fragment activity in the loops conditions that were achieved at BNPP. Basic characteristics of the pumps used at BNPP are listed in the Table 2.11.

Table 2.11. Basic characteristics of BNPP pumps (Emelyanov et al. 1972b).

Pump name	Unit	No. of pumps	Drive Power, kW	Pressure, MPa	Disharge, m^3/h	Pumped medium T, °C
MCP	1	3	520	0.98	650*	310
	1	1	520	0.98	650*	310
	2	4	750	1.53	650*	310
Feeding electric pump (FEP)	1	3	2000	15.45	270	160
	2	4	4000	17.60	500	160
Pump for reactor control system cooling	1	2	55	0.59	100	60
	2	2	65	0.68	125	60
Pump for protecting system cooling (PCP)	1	2	19.5	0.64	12	60
	2	2	19.5	0.64	12	60

* – Discharge is expressed in t/h.

2.2.11. Water regime

The experiments on effectiveness of water and steam radiolysis suppression by hydrogen in BW and SHS channels respectively were performed after 16 months of Unit 1 operation. Water and steam samples were taken at the drum-separator, MCPs, inlet and outlet of SHS channels. Ammonia dosing was terminated before the test for determination of the required amount of hydrogen that was necessary to suppress water and steam radiolysis that was partially caused by ammonia decomposition (Yurmanov et al. 2009b). Hydrogen concentration in saturated steam at the separator was found to be 45 – 88 nml/kg and in circulation water at the main circulation pump was found to be 2.75 – 12.8 nml/kg. Despite some hydrogen excess, oxygen concentration decreased from 2.28 mg/dm^3 to 0.1 mg/dm^3. Dissolved oxygen concentration in the circulating water at the main circulation pump did not exceed 0.01 – 0.03 mg/dm^3. At the next stage of experiments, steam radiolysis in SHS channels and the possibility of suppressing it by hydrogen concentration levels were studied. Hydrogen concentration was set to 1.2 – 6.2 nml/kg in steam and 1.2 – 1.8 nml/kg in circulating water. Oxygen concentration was below 0.15 mg/kg in steam and about 0.02 mg/dm^3 in the circulating water. The obtained results demonstrated effective suppression of water radiolysis.

Additional research was carried out at 60% reactor power. The results showed that the oxygen concentration was decreased to 0.03 mg/kg at the SHS channels outlet only at 45 nml/kg hydrogen concentration. The water-steam mixture at the turbine ejector consisted of hydrogen (62 – 65%) and oxygen (8 – 10%) at a hydrogen concentration of 40 – 45 nml/kg. The water-steam mixture was needed to be diluted with air to a non-explosive state, i.e. hydrogen volume fraction was to be decreased below 2 – 3% (Shitzman 1983).

The equipment for Unit 2 was made from the following constructional materials: stainless steel (5500 m^2, 900 m^2 of which were used for the core); carbon steel (5600 m^2); brass and cupronickel (14,000 m^2); stellite (4.8 m^2). The studies showed that radiolytic gases production rate was approximately 5 times lower than that of a BWR of the same power. Water radiolysis at

the BW channels of the BNPP Unit 1 was suppressed by ammonia dosing. This kept radiolityc oxygen content in water at several hundredths of a milligram per liter. Ammonia dosing wasn't used at Unit 2 due to the danger of corrosion of the condenser tubes and low-pressure heaters. Radiolytic fixation of oxygen in the steam that was bled to high-pressure heaters was achieved by hydrazine hydrate dosing. The operation norms and the actual quality of coolant at the BNPP Unit 2 are listed in the Tables 2.12 and 2.13. Additional information on water flow regime may be found in paper by Konovalova et al. (1971).

Table 2.12. Standards of water and steam quality for BNPP Unit 2 during operation (Konovalova et al. 1971).

Parameters	Feed water	Reactor circulating water	Reactor bleed water	Saturated and reheated steam	Turbine condensate
Water hardness (μg-equiv/kg)	≤3	≤15	–	–	3
Alkalinity (using mixed indication, excluding ammonia), (μg-equiv /kg)	–	–	≤50	–	–
Sodium, μg/kg	–	–	–	–	≤10
SiO^{2-}_3, μg/kg	≤30	–	≤1000	≤20	–
Chlorides, μg/kg	–	≤30*	–	–	–
Iron oxides, μg/kg	–	≤60	–	–	–
Copper content, μg/kg	≤5	–	–	–	≤5
Total corrosion products, μg/kg	–	–	≤500	–	≤5
Oxygen content, μg/kg	10	–	–	–	30
Oils content, μg/kg	300	–	–	–	–
pH	–	≥8.0	–	–	–

* During accident an increase of chlorides up to 150 μg/kg in reactor circulating water is tolerated during 20 h per 1000 h of reactor operation.

Table 2.13. Actual parameters of BNPP Unit 2 coolant quality during period of normal operation (Konovalova et al. 1971).

Parameters	Feed water	Reactor circulating water	Reactor bleed water	Saturated / Reheated steam	Turbine condensate
Water hardness, μg-eq./kg	<3	<3	3–6	– / –	3
SiO^{2-}_{3}, μg/kg	–	–	100–300	5–15 / 5–15	–
Chlorides, μg/kg	25	25	25	– / –	–
Iron oxides, μg/kg	20–60	20–60	30–60	20–30 / 20 –30	0
Copper, μg/kg	–	–	7–30	0.4 / –	0.8
Specific activity, Ci/l	–	–	10^{-5}	– / 10^{-7}	–
Oxygen, μg/kg	10–15	30	30	$(5–6)\cdot10^{3}$ / $(5–6)\cdot10^{3}$	40–50
Ammonia, mg/kg	1–25	0.6–1.4	0.6–1.4	0.8–2 / 0.8–2	1–2
pH	9.2–9.5	8–9	9–9.5	9–9.5 / 9–9.5	9–9.5

Comparison of data in Tables 5.12 and 5.13 shows that all indicators of coolant quality were in the range set by the water regime regulations during normal operating period.

In August 1972 (after 4.5 years of operation) neutral no-correction water was implemented at Unit 2 (Dollezhal 1974b). Operation in the new conditions revealed the following advantages over the ammonia treated state:

1. The cease of feedwater ammonia treatment led to the zero nitrate content in the reactor circulation water. This allowed an increase of the pH from 4.8 to the neutral level at the 300°C operating temperature.
2. Balance of the corrosion products content in the circulation water and chemical flushing of the BW channels showed that the rate of metallic oxide deposits formation on the fuel-bundles surfaces in the evaporating zone of the reactor was three times lower using no-correction water.
3. The Co-60 deposition rate outside the core was 7 – 10 times lower using no-correction

water.

4. Condensate purification experience using no-correction water allowed an increasing filter service cycle by 6 times.

2.2.12. Radiation conditions

Radiation conditions on the premises of the BNPP and at its immediate environs was found to be satisfactory. Radioactive emissions to the atmosphere were 5 – 10 times lower than allowed by codes. The turbines have not the radiation shielding, and maximum intensity was 1.0 – 1.5 and 2.0 – 5.0 μR/s at the high-pressure cylinder and 0.3 – 2.0 and 1.0 – 4.0 μR/s at the low-pressure cylinder for BNPP Unit 1 and 2 respectively. These values of intensities at the turbine were several times lower than those at other direct-cycle reactors. For example, the radiation intensity was about 100 μR/s at the turbines of SGHWR reactor in Winfrith (Dollezhal et al. 1969).

Steam activity at the turbine inlet was mainly caused by N-16 and its values were $2.5 \cdot 10^{-3}$ and $9 \cdot 10^{-3}$ Ci/kg for the BNPP Units 1 and 2 respectively. Coolant activity of the long-lived corrosion products was relatively acceptable: 10^{-8} Ci/kg at the evaporating loop and 10^{-9} Ci/kg at the reheat loop. Specific activities of the deposits on the water feeding tubes of the evaporating loop are presented in Table 2.14.

Radiation rates were 0.05 – 0.1 μR/s in the rooms where personnel worked constantly, and 0.3 – 12 μR/s in rooms occupied part-time. The dose rates during the reactor shut-down in the rooms not used by personnel and near the evaporating loop of Unit 1 were measured to be 25 – 200 μR/s, and were measured to be 15 – 20 μR/s near the steam superheating zone. The dose rates at those components were decreased by flushing and deactivation of the individual components of the equipment and deactivation of loops. Personnel were mainly exposed during maintenance work by the deposits of corrosion radioactive products on the surfaces of piping and equipment. The major data on radiation levels at the BNPP Units 1 and 2 are listed in Tables 2.15 – 2.17 and shown in Figures 2.17 – 2.22. Additional information on radioactive deposits build-up may be found in papers by Aleksandrova et al. (1968) and Veselkin et al. (1968).

Table 2.14. Activity of precipitations on tubing (water-supply channels) of evaporating loop of BNPP Unit 1 (Dollezhal et al. 1969).

Operational time, effective days	Specific activity, disintegrations/min·cm^2			
	Co-60, ×10^5	Mn-54, ×10^5	Co-58, ×10^5	Cr-51, ×10^5
80	1.7	0.38	0.32	2.7
120	2.2	0.56	0.39	3.1
160	3.6	1.2	0.420	6.1
300	6.2	1.5	0.65	5.0
460	9.0	1.6	0.68	4.1
780	16	1.6	0.62	5.2

Table 2.15. BNPP Unit 2 coolant activity, nCi/kg (Veselkin et al. 1971).

Sampling point	Co-60	Zn-65	Mn-54	Cr-51
Separator bleed water	100–300	400–800	4–30	30–300
Separator saturated steam	5–15	10-30	0.3–5	9–20
Direct steam	2–20	1–10	0.1–5	2–50
Steam condensate	0.3–5	0.4–3	0.2–1.5	0.5–6

Table 2.16. Deposits activity on surfaces of BNPP Unit 1 primary loop (Veselkin et al. 1968).

Isotope	Activity, Ci	Distribution along loop sections, %		
		Water	Steam-water	Steam
Co-60	14	30	68	1.9
Mn-54	3.2	44	54	1.8
Co-58	2.3	21	77	1.8
Cr-51	11	65	30	4.6

Table 2.17. Deposits activity on the surfaces of the BNPP Unit 1 second loop (Veselkin et al. 1968).

Isotope	Activity, mCi	Distribution along loop sections, %								
		Steam and LP water	HP water	Evaporators (water)	Saturated steam	Reheated steam	Turbine		LP heater (steam)	HP heater (steam)
							Stationary parts	Blades		
Co-60	29	8.0	20	25	3.8	34	6.3	0.1	0.08	2.7
Mn-54	26	4.5	8.3	41	7.2	33	3.3	0.06	0.04	2.6
Cr-51	140	5.1	2.8	5.4	0.7	17	65	1.0	0.06	3.0
Sb-124	45	4.0	2.8	12	0.4	43	29	0.5	0.1	3.2
Co-58	5	24	34	34	8	–	–	–	–	–

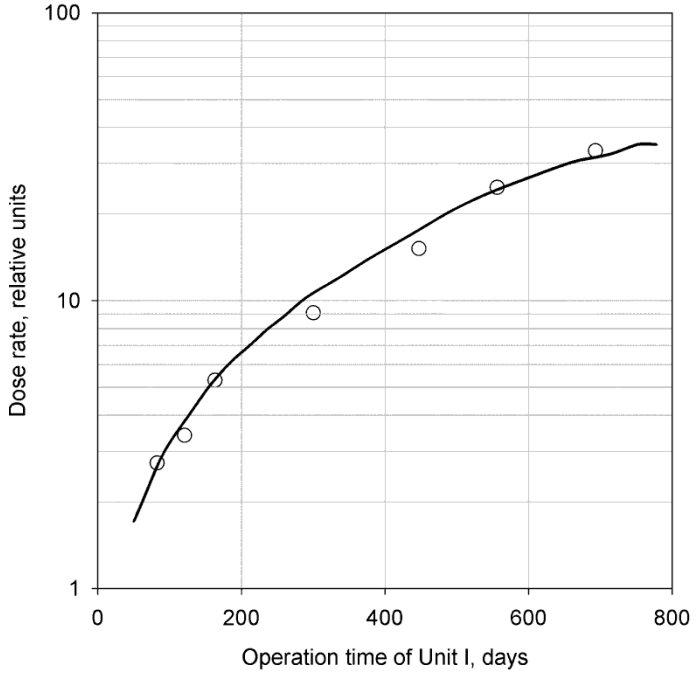

Figure 2.17. Dependence of dose date near boiling loop equipment of BNPP Unit 1 on its operation time (Dollezhal et al. 1969).

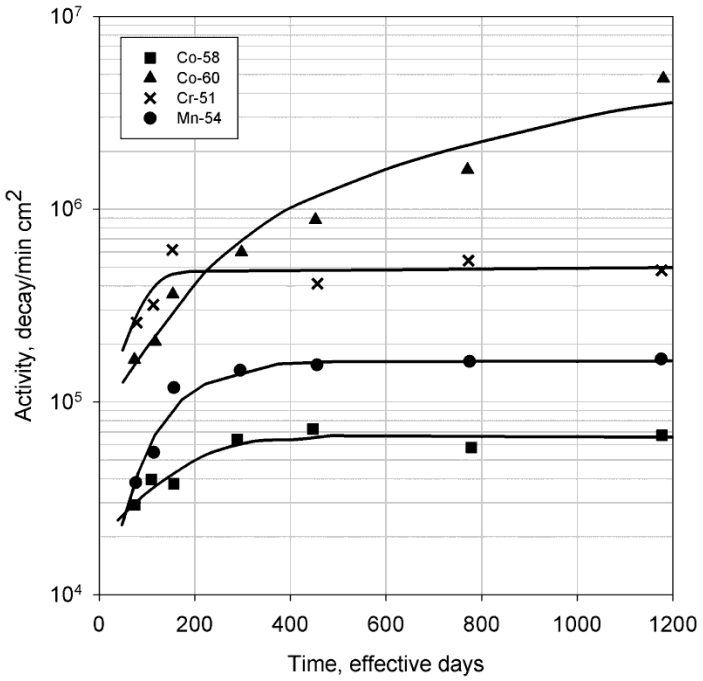

Figure 2.18. Activity dependence on operating time at BNPP Unit 1 boiling loop piping (Veselkin et al. 1971).

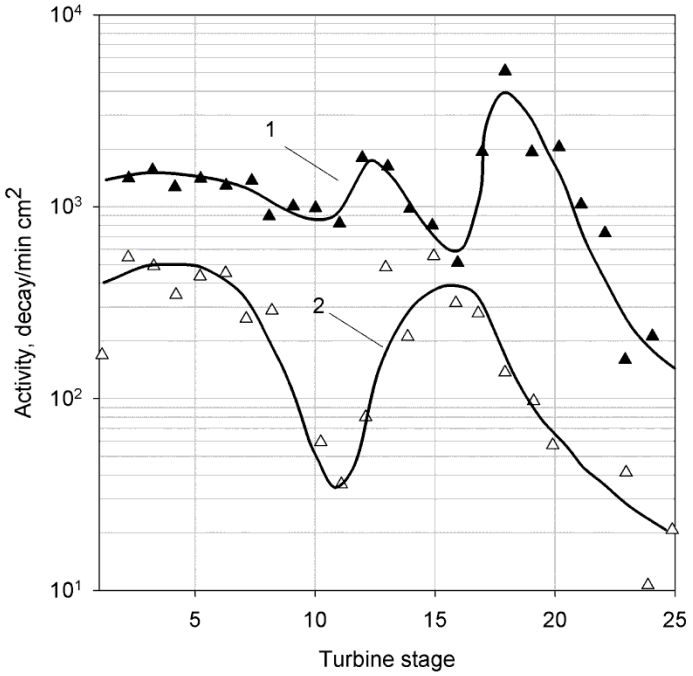

Figure 2.19. Specific activity of Co-60 deposits on turbine blades of BNPP Unit 1 (Veselkin et al. 1971): 1 – after 160 operating days and 2 – after 460 operating days.

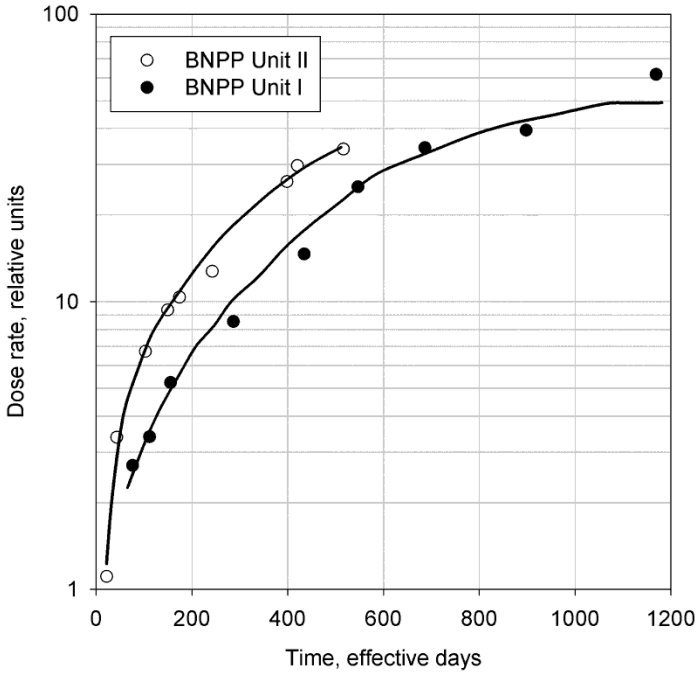

Figure 2.20. Relative change of dose rate (at shut-downs) near boiling loop equipment depending on operating time of unit (Veselkin et al. 1971).

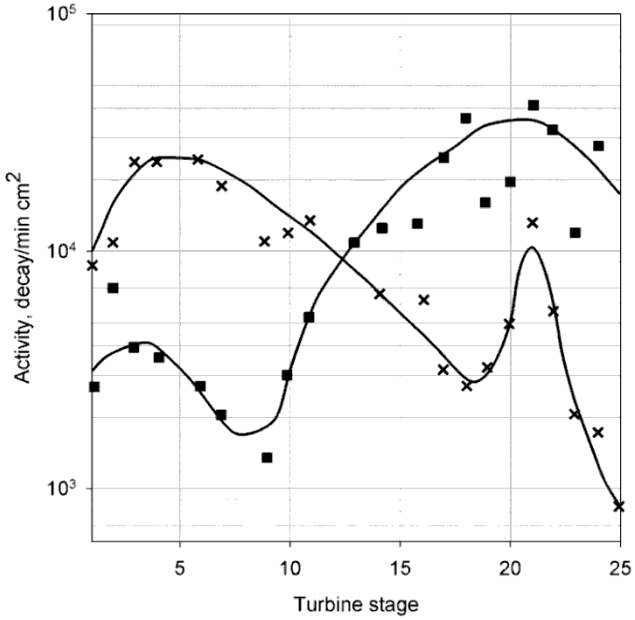

Figure 2.21. Cr-51 (■) and Zr-65 (×) activity distribution on BNPP Unit 2 turbine #2 blades after 294 effective days of operation (Veselkin et al. 1971).

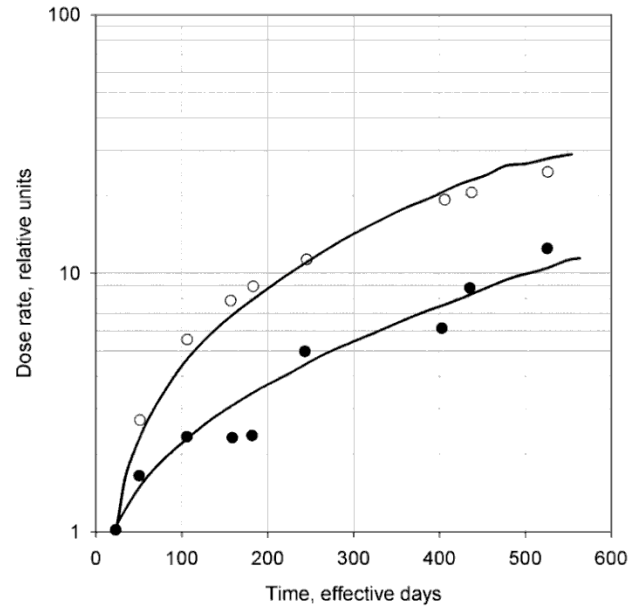

Figure 2.22. Relative dose rate variations near steam condensing and feeding loops of BNPP Unit 2 at start-up and shut-down regimes (Veselkin et al. 1971): ○ – equipment is filled with water from evaporating loop; ● – equipment is not filled with water from boiling loop.

2.2.13. Section-unit reactor with steam-reheat

The BNPP became the first in the world industrial NPP with a uranium-graphite power reactor. Examination of the main characteristics of the BNPP reactors (for example, see Table 2.8) shows that that performance of such type of reactors could be improved. BNPP used slightly enriched uranium and the calculations showed that increasing enrichment to 5% would increase fuel burn-up 4 − 10 times (up to 40,000 MW·days/t).

All channel reactors were constructed with traditional cylindrical shape of core. Therefore, power increase in such a reactor could be attained by increasing the number of working channels in the core and a proportional increase in diameter size. However, increase in power per reactor would then be limited by the maximum size of the reactor upper plate that could be built and withstand a high load. A way out of this situation was found in section-unit design of the channel reactor with a rectangular core. Such a shape would allow separating not only the core, but also reactor as a whole, into equal geometry sections. Then the reactor of a specified capacity can be constructed of the required number of sections. Each section would stay the same for reactors of different power outputs, and, consequently, core width and maximum size of the upper metalwork would stay the same too. Therefore, the power of a section-unit reactor power would not be limited by the size of the upper plate (Emelyanov et al. 1982).

Section-unit type reactors with coolant at supercritical fluid conditions (see Figure 2.23) was developed at NIKIET as an improvement to the existing RBMK (Russian acronym for Channelized Reactor of High-Power).

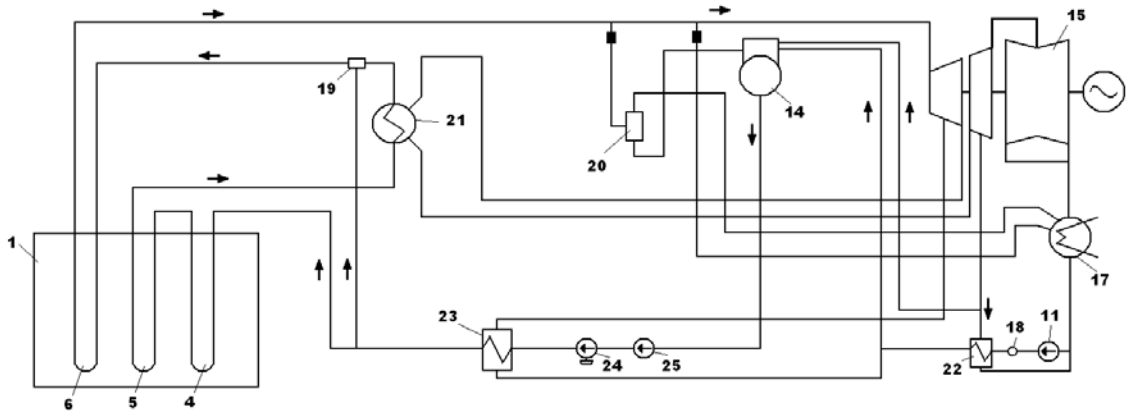

Figure 2.23. Schematic of NIKIET SCW NPP (Aleshchenkov et al. 1971): 1 – reactor; 4 – preheating channel; 5 – first SHS; 6 – second SHS; 11 – Condensate Extraction Pump (CEP); 14 – deaerator; 15 – turbo-generator; 17 – condenser; 18 – condenser purifier; 19 – mixer; 20 – start-up separator; 21 – intermediate steam reheater; 22 – low-pressure regenerative preheater; 23 – high-pressure regenerative preheater; 24 – feed turbo-pump; and 25 – booster pump.

Rod fuel bundles were inserted into Zirconium SHS (SHS-Z) channels (see Table 2.18, Figure 2.24.) on the core level. UO_2 fuel elements with steel sheath were designed. Fuel bundles were covered by a sheath to hold SHS-Z channel wall below 360°C (Grigoryants et al. 1979). Therefore, saturated steam entering the channel was split into two streams. About 25% of the steam flowed through the annular gap cooling the SHS-Z channel wall. Both streams mixed at the core exit. Steam mixture was at about 455°C. Tests with SHS-Z channels were performed in BNPP Unit 1 to check design decisions. SHS-Z channels were tested in 23 – 24 start-ups – shutdowns, including 11 emergency shutdowns of the reactor when the steam temperature change rate was 20 – 40°C/min during the first 3 minutes of an automatic control system operation, and 5°C/min after that. SHS-Z channel wall temperature reached 400 – 700°C and that of the fuel bundles sheath reached 650 – 740°C during start-up operation at a steam pressure of 2.45 – 4.9 MPa. Channels were operated about 140 h at high temperature conditions. Studies showed that fuel element seal failures were mainly due to short-duration overheating (Mikhan et al. 1988).

Table 2.18. Parameters of zirconium steam-reheat channels tested in BNPP (Mikhan et al. 1988).

Parameter	SHS-Z
Max channel power, kW	660
Steam mass flow rate, kg/h	3400
Number of fuel elements per assembly	6x2
Max. heat flux from fuel element, kW/m^2	7840
Fuel element maximum linear power, W/cm	246
Steam *P/T*, MPa/ºC: Channel inlet	9.8/310
Fuel-bundle inlet	9.1/340
Fuel-bundle outlet	8.5/545
Channel outlet	7.8/510
T_{max} (design), ºC: Fuel	1620
Cladding	635
Fuel bundle sheath	530
Zirconium channel wall	350
Uranium enrichment	10
Average channel burn-up rate, MW·day/kg	30

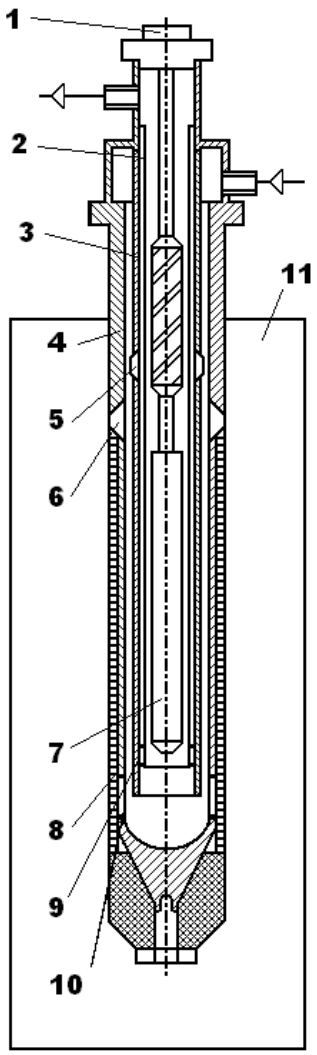

Figure 2.24. Principal scheme of SHS-Z (Mikhan et al. 1988):

1 – suspension rod;

2 – thermal screen;

3,4 – outer and inner tubes of bearing body;

5 – inner tube reducer;

6 – upper reducer of outer tube;

7 – fuel bundle;

8 – graphite sleeves;

9 – thermal screen and inner tube seal;

10 – lower reducer of outer tube; and

11 – reactor.

Additional information on SHS-Z-channel tests in BNPP Unit 1 may be found in the papers by Grigoryants et al. (1979) and by Mikhan et al. (1988).

2.3. Summary of Nuclear Steam-Reheat Experience

The operating experience of the reactors with nuclear steam reheat worldwide provides vital information on physical and engineering challenges associated with implementation of steam reheat in conceptual SCWRs. Three experimental reactors were designed and tested in the 1960s – 1970s in the USA. In the former Soviet Union, nuclear steam reheat was implemented at two units at the Beloyarsk NPP. Operating experience of the units showed a possibility of reliable and safe industrial application of nuclear steam reheat right up to outlet temperatures of 510 − 540°C after over a decade of operation. Thermal efficiency of the Beloyarsk NPP units was increased by 5% as the result of implementing nuclear steam-reheat. The introduction of nuclear steam reheat was economically justified in cases where the steam was superheated up to 500°C and higher with the use of stainless-steel-sheath fuel elements.

The experiments and operating experience obtained to date also indicate that further improvements in SHS channel design and in reactor design are possible.

CHAPTER 3

REVIEW OF SUPERCRITICAL THERMAL POWER PLANTS

The development work on supercritical Steam Generators (SGs) and turbines started in the USA in the early 1950s (Lee and Haller 1974). The first supercritical SG was put into operation at the Philo Plant of American Electric Power in 1957. The capacity of this unit was 120 MW with "steam" parameters of 31 MPa and 620/566/538ºC (main/reheat/reheat) (Retzlaff and Ruegger 1996). In the early sixties, another plant was built with ultra-supercritical parameters (pressure of 30 MPa, temperatures (primary and reheat) of 650ºC) (Smith 1999). The supercritical units built in the USA had thermal capacities from 400 to 1380 MW_{th}. Often the subcritical units for 1000 MW and higher were replaced with supercritical SGs in the USA (Ornatskiy et al. 1980). Major parameters of selected US supercritical turbines are listed in Table 3.1.

The implementation of supercritical power-plant "steam" generators in Russia (the former USSR) started with units having 300 MW_{th}. The first industrial SG operating at supercritical conditions in the former USSR was manufactured in 1961 for a coal-fired power plant (Ornatskiy et al. 1980). The next stage in further development of supercritical "steam" generators involved an increase in their thermal capacity to 500 MW and 800 MW. In 1966, the first 1000-MW ultra-supercritical plant started its operation in Kashira with a primary "steam" pressure of 30.6 MPa, and primary and reheat temperatures of 650 and 565ºC, respectively (Smith 1999). In modern designs of supercritical units, the thermal capacity was upgraded to 1200 MW_{th}. Major parameters of selected Russian SC turbines are listed in Tables 3.1 and 3.2. A detailed schematics of a thermal layout of a modern Russian SC thermal power plant is presented in Figures 3.1 and 3.2 (power plant efficiencies 43.6%, turbine power 660 MW_e, inlet pressure 28 MPa, main/reheat temperatures 600–620°C). More than 200 supercritical units were manufactured and put into operation in Russia over the last 25 years (Smith 1999).

Table 3.1. Major parameters of selected USA SC turbines (Ornatskiy et al. 1980).

	Parameters of Paradise Power Plant	**Parameters of Emos and Gevin Power Plants**
Steam Capacity, t/h (ton metric per hour)	3630	4438
Primary Pressure, MPa	24.2	27.3
Primary Temperature, °C	537	543
Secondary Steam Capacity, t/h	2430	3612
Secondary Pressure, MPa	3.65	4.7
Secondary Temperature, °C	537	538
Feedwater Temperature, °C	288	291
Turbine Thermal Efficiency, %	89	93

Table 3.2. Major parameters of selected Russian SC turbines (Ornatskiy et al. 1980).

Power, MW_e	Parameters	
300	Steam Capacity, t/h	950 – 1000
	Primary Pressure, MPa	25
	Primary Temperature, °C	545 – 585
	Secondary Pressure, MPa	3.5 – 3.9
	Feedwater Temperature, °C	260 – 265
	Turbine Thermal Efficiency, %	88 – 93
500	Steam Capacity, t/h	1650
	Primary Pressure, MPa	25
	Primary Temperature, °C	545
	Secondary Pressure, MPa	3.95
	Secondary Temperature, °C	545
	Feedwater Temperature, °C	277
	Thermal Efficiency, %	92
800	Steam Capacity, t/h	2650
	Primary Pressure, MPa	25
	Primary Temperature, °C	545
	Secondary Pressure, MPa	3.44
	Secondary Temperature, °C	545
	Feedwater Temperature, °C	275
	Turbine Thermal Efficiency, %	92 – 95

Table 3.3. Parameters of largest Russian SC turbines (Grigoryev and Zorin, 1982).

Parameters	K-1200-240	K-800-240	K-800-240*
Power, MW_e (max power)	1200 (1380)	800 (850)	800 (835)
Main Steam			
Pressure, MPa	23.5	23.5	23.5
Temperature, °C	540	540	560
Max Flow Rate Through HP Turbine, t/h	3950	2650	2500
Reheat Steam			
Pressure, MPa	3.5	3.2	3.4
Temperature, °C	540	540	565
No. of Steam Extractions	9	8	8
Outlet Pressure, kPa	3.6	3.4	2.9
Cooling Water			
Temperature, °C	12	12	12
Flow Rate, m^3/h	108,000	73,000	85,000
Feedwater Temperature, °C	274	274	270
Turbine Layout			
No. of Cylinders	5	5	6
No. of HP Cylinders	1	1	-
No. of IP Cylinders	2	2	-
No. of LP Cylinders	2	2	-
Turbine Mass and Dimensions			
Total Mass, t	1900	1300	1600
Total Length, m	48	40	40
Total Length with Electrical Generator, m	72	60	46
Average Diameter of HP Turbine, m	3.0	2.5	2.5
Turbine Specific Performance			
Specific Heat Rate, kJ/kW·h	7660	7720	7590

*Double-shaft turbine.

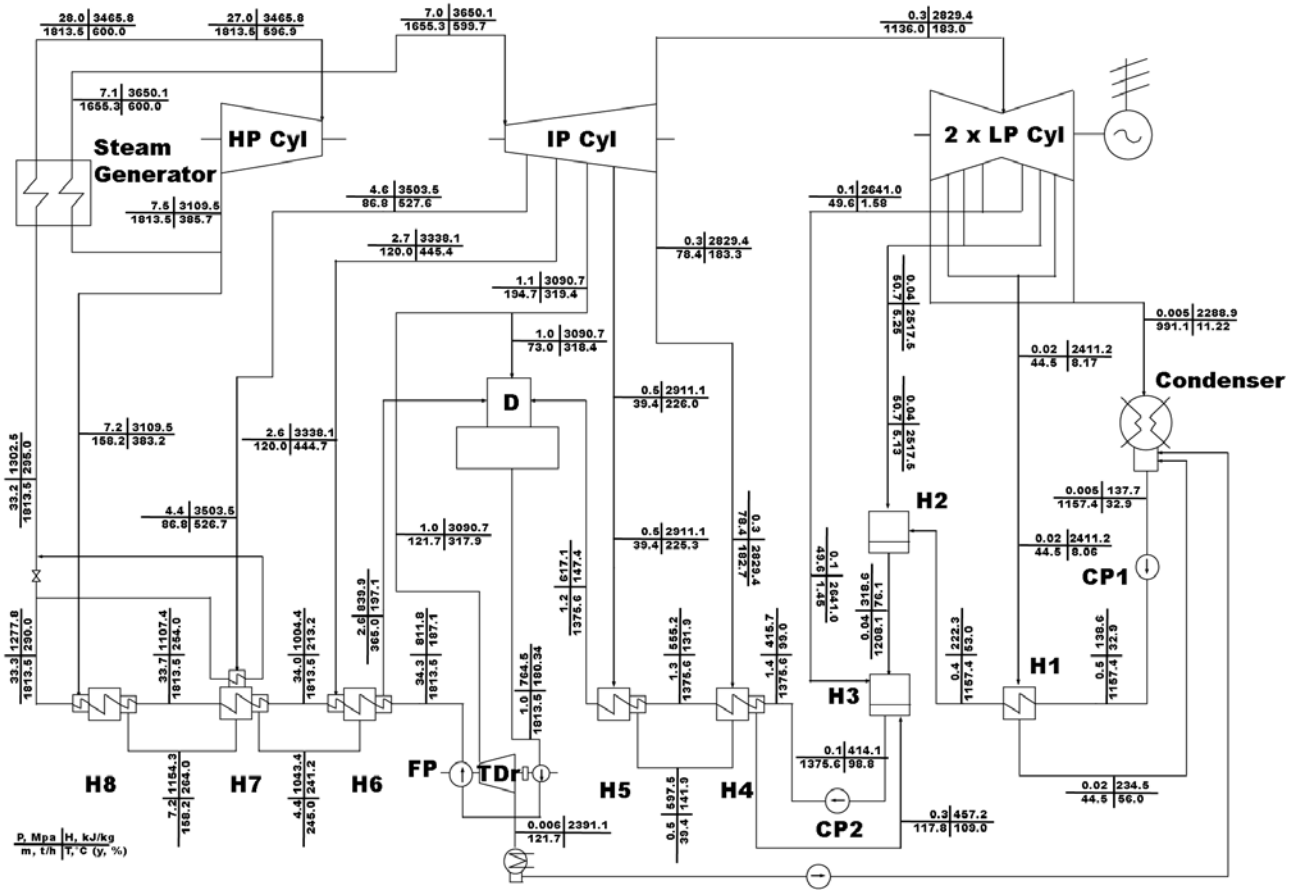

Figure 3.1. Single-reheat-cycle 660-MW$_e$ Tom-Usinsk thermal power plant (Russia) thermal layout (Kruglikov et al. 2009): Cyl – Cylinder; H – Heat exchanger (feedwater heater); CP – Circulation Pump; TDr – Turbine Drive; Cond P – Condensate Pump; GCHP – Gas Cooler of High Pressure; and GCLP – Gas Cooler of Low Pressure. 7.1 MPa reheat pressure.

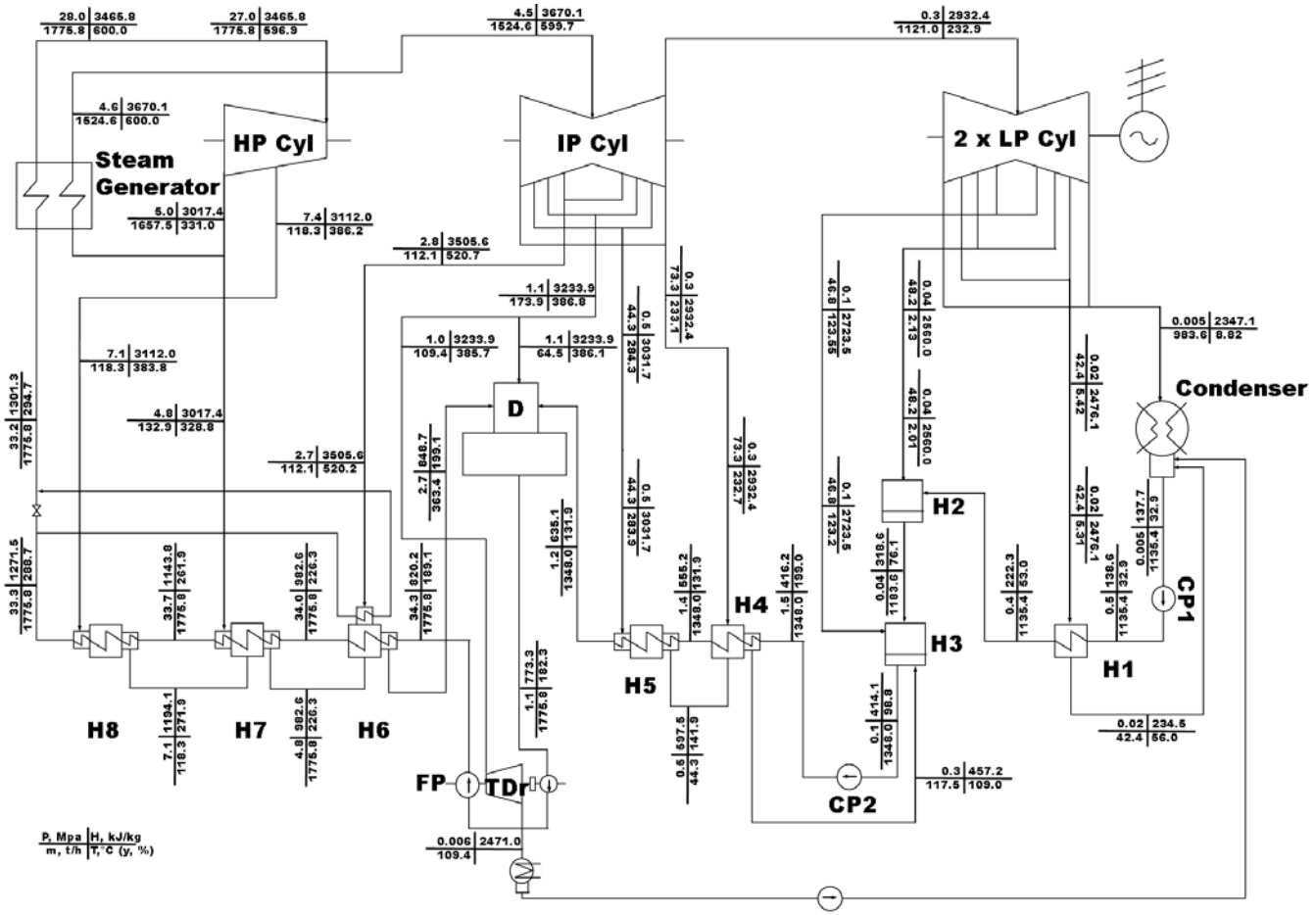

Figure 3.2. Single-reheat-cycle 660-MW$_e$ Tom-Usinsk thermal power plant (Russia) thermal layout (Kruglikov et al. 2009): Cyl – Cylinder; H – Heat exchanger (feedwater heater); CP – Circulation Pump; TDr – Turbine Drive; Cond P – Condensate Pump; GCHP – Gas Cooler of High Pressure; and GCLP – Gas Cooler of Low Pressure. 4.6 MPa reheat pressure.

In Japan, the first supercritical "steam" generator (600 MW) was commissioned in 1967 at the Anegasaki plant (Oka and Koshizuka 2002; Tsao and Gorzegno 1981). Nowadays, many power plants are equipped with supercritical SGs and turbines. Hitachi operating supercritical pressure "steam" turbines have the following average parameters: output – 350 (1 unit), 450 (2 units), 500 (3 units), 600 (11 units), 700 (4 units) and 1000 MW (4 units), pressure about 24.1 MPa (one unit 24.5 MPa), temperature (main/reheat) – 538/566ºC (the latest units 600/600ºC). Major parameters of selected Hitachi turbines are listed in Table 3.4.

Table 3.4. Major parameters of selected Hitachi SC turbines (Pioro and Duffey 2007).

First Year of Operation	Power Rating MW_e	Pressure MPa(g)	T_{main}/T_{reheat} °C
2011	495	24.1	566/566
2010	809	25.4	579/579
	790	26.8	600/600
2009	1000	25.0	600/620
	1000	25.5	566/566
	677	25.5	566/566
	600	24.1	600/620
2008	1000	24.9	600/600
	887	24.1	566/593
	887	24.1	566/593
	677	25.5	566/566
2007	1000	24.9	600/600
	870	25.3	566/593
2006	600	24.1	566/566
	600	24.1	566/566
2005	495	24.1	566/566
2004	700	24.1	538/566

First Year of Operation	Power Rating MW_e	Pressure MPa(g)	T_{main}/T_{reheat} °C
2003	1000	24.5	600/600
2002	700	25.0	600/600
1998	1000	24.5	600/600
1994	1000	24.1	538/566
1992	700	24.1	538/566
1991	600	24.1	538/566
1989	1000	24.1	538/566
	700	24.1	538/566
1985	600	24.1	538/566
1984	600	24.1	538/538
1983	700	24.1	538/538
	600	24.1	538/566
	600	24.1	538/566
	350	24.1	538/566
1981	500	24.1	538/538
1979	600	24.1	538/566
1977	1000	24.1	538/566
	600	24.1	538/566
	600	24.1	538/552/566*
1975	450	24.1	538/566
1974	500	24.1	538/566
	500	24.1	538/538
1973	600	24.1	538/552/566*
	450	24.1	538/566
1972	600	24.1	538/566
1971	600	24.1	538/566

*Double-reheat-cycle turbines.

The SC "steam"-turbine technology is experiencing continuous improvements. For example, Project Thermie-700 in Europe is developing a fossil-fueled "steam" generator-turbine unit for "steam" parameters of 35 MPa and 700°C with a target net-plant efficiency of 50 ~ 55%. It should be noted that this efficiency is expressed on a Lower-Heating Value (LHV), which, based on typical coal moisture contents is approximately equivalent to 47% – 52% on a HHV basis. The targeting implementation start date for the Thermie-700 is the early 2010s.

As one can see from the Tables 3.1 to 3.4, that 25 MPa and 600°C are common SC "steam" parameters in state-of-the-art fossil-fueled power plants (see Figure 3.1) and a few plants even operate at pressures as high as 35 MPa and at temperatures as high as 650°C. The capacity of SC turbines ranges from 300 MW_e to 1200 MW_e. The gross overall steam-cycle efficiency of SC fossil-fueled power plants typically ranges between 47% and 54% (i.e., net plant efficiencies between 38% and 43% on a Higher Heating Value (HHV) basis). With the current SC-turbine technology and the ongoing development, it is expected that the technologies required for the SCWR's steam parameters will be well proven when the Generation-IV SCWRs are market-ready.

The steam-cycle configuration of a SC cycle is very similar to a subcritical cycle in a modern fossil-fueled power plant. Steam is usually reheated once in a boiler after passing through the High-Pressure (HP) turbine, in order to achieve a higher efficiency. The regenerative feedwater-heating system consists of Low-Pressure (LP) and High-Pressure (HP) feedwater heaters (closed type) and a deaerator (mixing type). Usually, SC-"steam" cycles involve 8 to 10 stages of feedwater heating, while subcritical steam cycles typically involve 8 to 9 stages of feedwater heating.

While the modern SC turbines share many common merits, they also vary in many aspects, depending on the manufacturer preference. These differences can include turbine type (impulse or reaction), shaft combination (tandem or cross compound), cylinder arrangement, parameter choices (feedwater temperature, reheat pressure), etc. Individual manufacturers take different approaches in these areas based on their design

experiences. Some features (e.g., unit capacity, feedwater temperature, etc.) are flexible within certain ranges if required by customers.

Therefore, our analysis of SC-turbine data can be summarized as follows:

- Only very few double-reheat-cycle turbines were manufactured so far. The market demand for double-reheat turbines disappeared due to economic reasons after the first few units were built. The vast majority of the modern and upcoming SC turbines are single-reheat-cycle turbines.
- Major "steam" inlet parameters of these turbines are: the main or primary SC "steam" – P = 24 – 25 MPa and T = 540 –600°C; and the reheat or secondary subcritical-pressure steam – P = 3 – 7 MPa and T = 540 – 620°C.
- Usually, the main "steam" and reheat-steam temperatures are the same or very close in value (for example, 566/566°C; 600/600°C; 600/620°C).

These conclusions coincide with those made by Naidin et al. (2009a) and Pioro and Duffey (2007).

CHAPTER 4

THERMAL LAYOUTS FOR SCWRS: GENERAL CONSIDERATION

The SCWR concepts (Pioro and Duffey 2007) follow two main types: (a) A large reactor Pressure Vessel (PV), analogous to conventional Light Water Reactors (LWRs); or (b) a channelized reactor in which individual Pressure Tubes (PTs) or Pressure Channels (PChs) (see Figures 4.1 and 4.2) carry high pressure, analogous to conventional Heavy Water Reactors (HWRs).

A schematic of a typical channel is shown in Figure 4.3 with the SCWR fuel channel parameters listed in Table 4.1. A schematic of a typical PT type reactor core layout is shown in Figure 4.4.

Based on the review in the previous chapter on SC turbines it follows that for a SCWR to be matched with the modern SC turbines, the SCWR has to be operating on a single-reheat cycle with the following major parameters: (a) the SC water pressure of 25 MPa and temperature of 600– 625ºC at the reactor outlet and (b) the secondary subcritical - pressure steam – P = 3 – 5 MPa and T = 600 – 650°C at the reactor outlet. However, due to special safety requirements for nuclear reactors all possible options in terms of SC-water thermodynamic cycles have to be considered.

The following 3 cycles can be distinguished from the point of view of using different substance as a working fluid and as a coolant:

1. Direct cycle;
2. Indirect cycle; and
3. Dual cycle.

The last two cycles were actually introduced based on safety concerns. These cycles have less thermal efficiency compared to that of the direct cycle, but have increased safety in terms of an extra barrier between the reactor primary coolant, which may contain a certain level of radioactivity, and "clean" NPP equipment such as the turbine, feedwater heaters, circulation pumps, etc. In addition, the primary coolant may contain "unwanted" substances, which will deposit on turbine blades and other equipment (Duffey 2008).

A preliminary investigation of SCW NPP reheat options by Naidin et al. (2009a) revealed the following:

1. The no-reheat cycle offers a simplified SCW NPP layout, contributing to lower capital costs. However, the efficiency of this cycle is the lowest of all the considered configurations.
2. The single-reheat cycle has the advantage of higher thermal efficiency (compared to that of the no-reheat cycle) and reduced development costs due to a wide variety of single-reheat SC turbines manufactured by companies worldwide. The major disadvantage is an increased design complexity associated with the introduction of SHS channels to the reactor core.
3. While the double-reheat cycle has the highest thermal efficiency, it was deemed that the complicated nuclear-steam reheat configuration would significantly increase the design and construction costs of such a facility.

As such, configurations based on the no-reheat and single-reheat cycles were chosen for the analysis in the thesis.

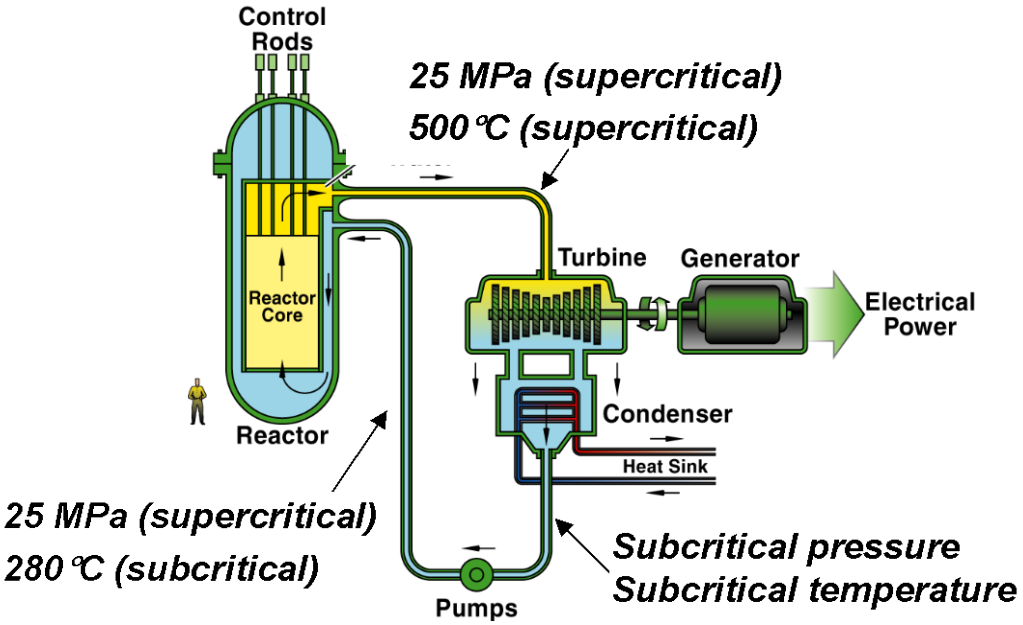

Figure 4.1. Schematic of US pressurized-vessel SCW nuclear reactor (courtesy of Professor J. Buongiorno (MIT)).

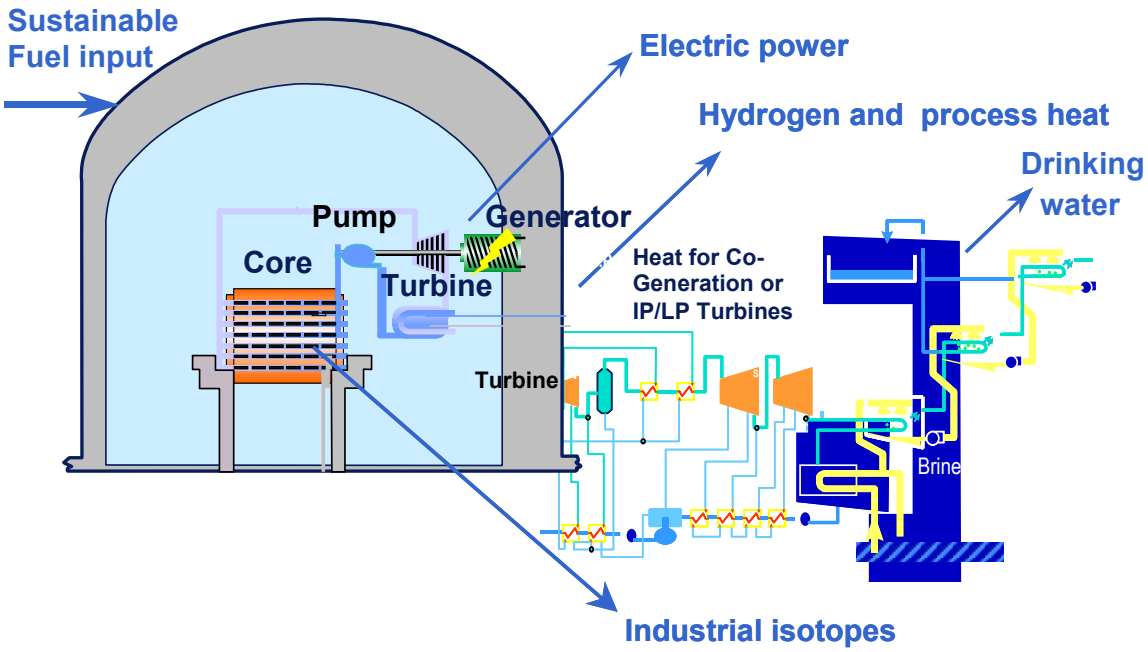

Figure 4.2. General scheme of pressure-channel SCW CANDU reactor (courtesy of Dr. R. Duffey (AECL)): IP – intermediate-pressure turbine and LP – low-pressure turbine.

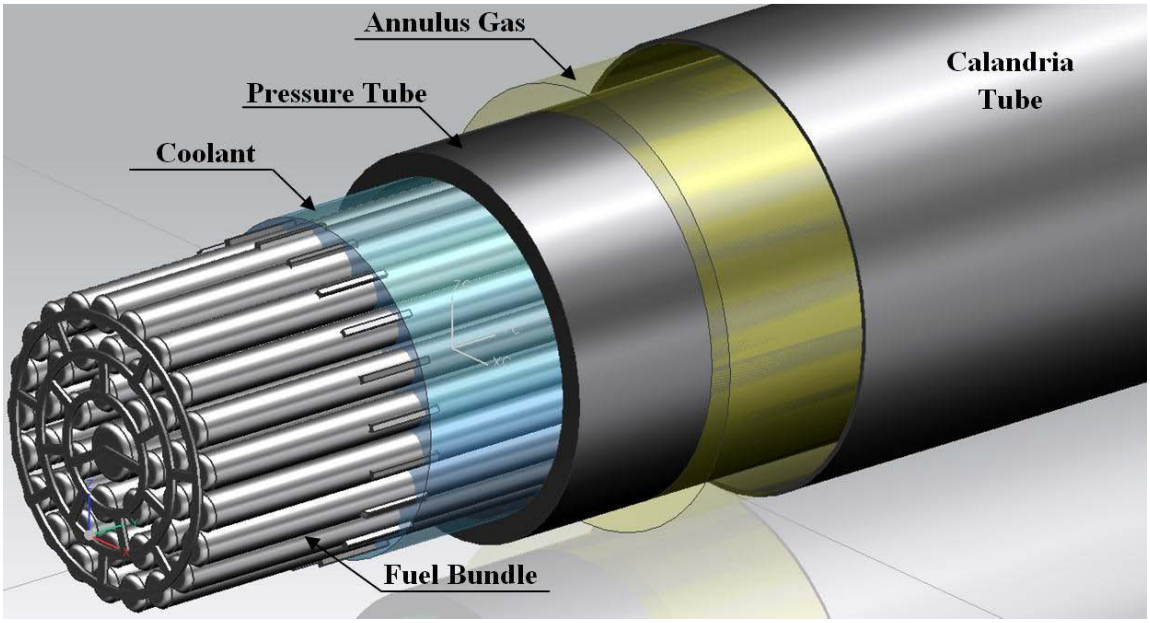

(a)

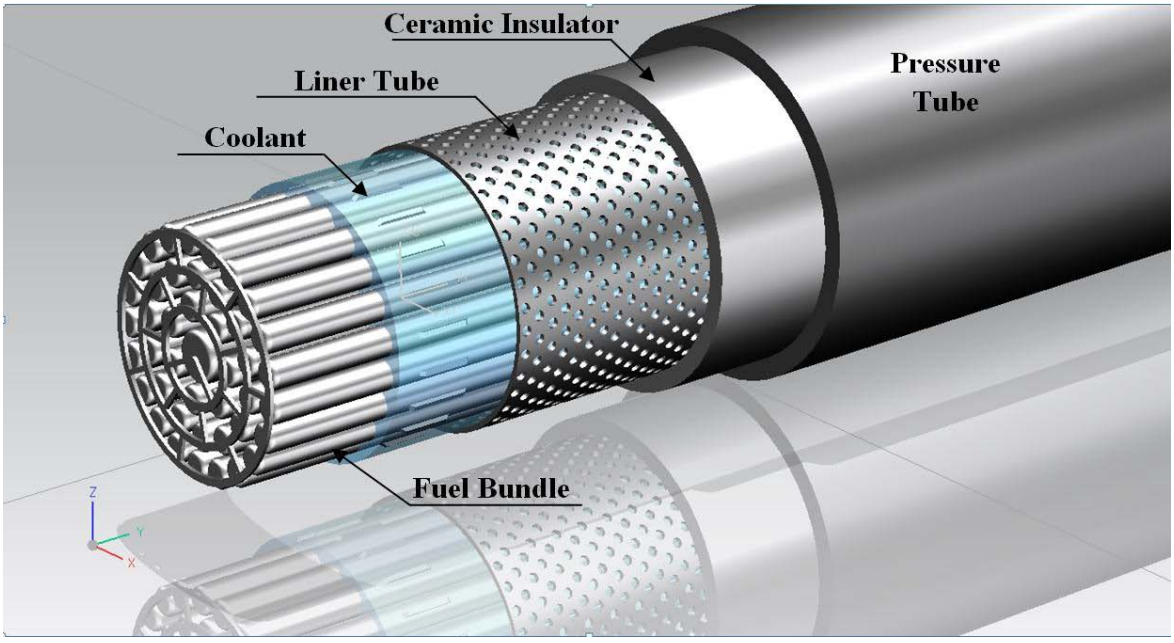

(b)

Figure 4.3. 3-D View of CANDU fuel channels: (a) CANDU-6 reactor (gas insulated) (shown for reference purposes) and (b) SCW CANDU reactor (AECL-design , ceramic insulated) (Saltanov et al. 2010, figure is based on the paper by Chow and Khartabil 2008)).

Table 4.1. Selected parameters of proposed SCWR fuel channels (Naidin et al. 2009a).

Parameters	Unit	Description / Value		
Max. cladding temperature (design value)	°C	850		
Max. fuel centerline temperature (industry accepted limit)	°C	1850		
Heated fuel-channel length	m	5.772		
Number of bundles / fuel channel	–	12		
Number of fuel rods per bundle	–	43		
Bundle type (Leung 2008)	–	CANFLEX	Variant-18	Variant-20
Number of heated fuel rods	–	43	42	42
Number of unheated fuel rods	–	–	1	1
Diameter of heated fuel rods (# of rods)	mm	11.5 (35) & 13.5 (8)	11.5	11.5
Diameter of unheated fuel rod	mm	–	18	20
Hydraulic-equivalent diameter of fuel channel	mm	7.52	7.98	7.83
Heated-equivalent diameter of fuel channel	mm	9.04	9.98	9.83
Heated area of fuel channel	m^2	9.26	8.76	8.76
Flow area of fuel channel	mm^2	3625	3788	3729
Pressure tube inner diameter	mm	103.45		
Average parameters of fuel channels in single-reheat (A) and no-reheat (C) cycles				
Heat flux in SCW channel (A&B[2] cycles)	kW/m^2	918	970	970
Heat flux in SHS channel (A&C cycle)	kW/m^2	594	628	628
Mass flux in SCW channel (A&B cycles)	kg/m^2s	1206	1154	1172
Mass flux in SHS channel (A&C cycle)	kg/m^2s	2759	2640	2682

[2] The layouts and discussion of different cycles (A, B, and C) are presented further in the text in sections 4.1 – 4.4.

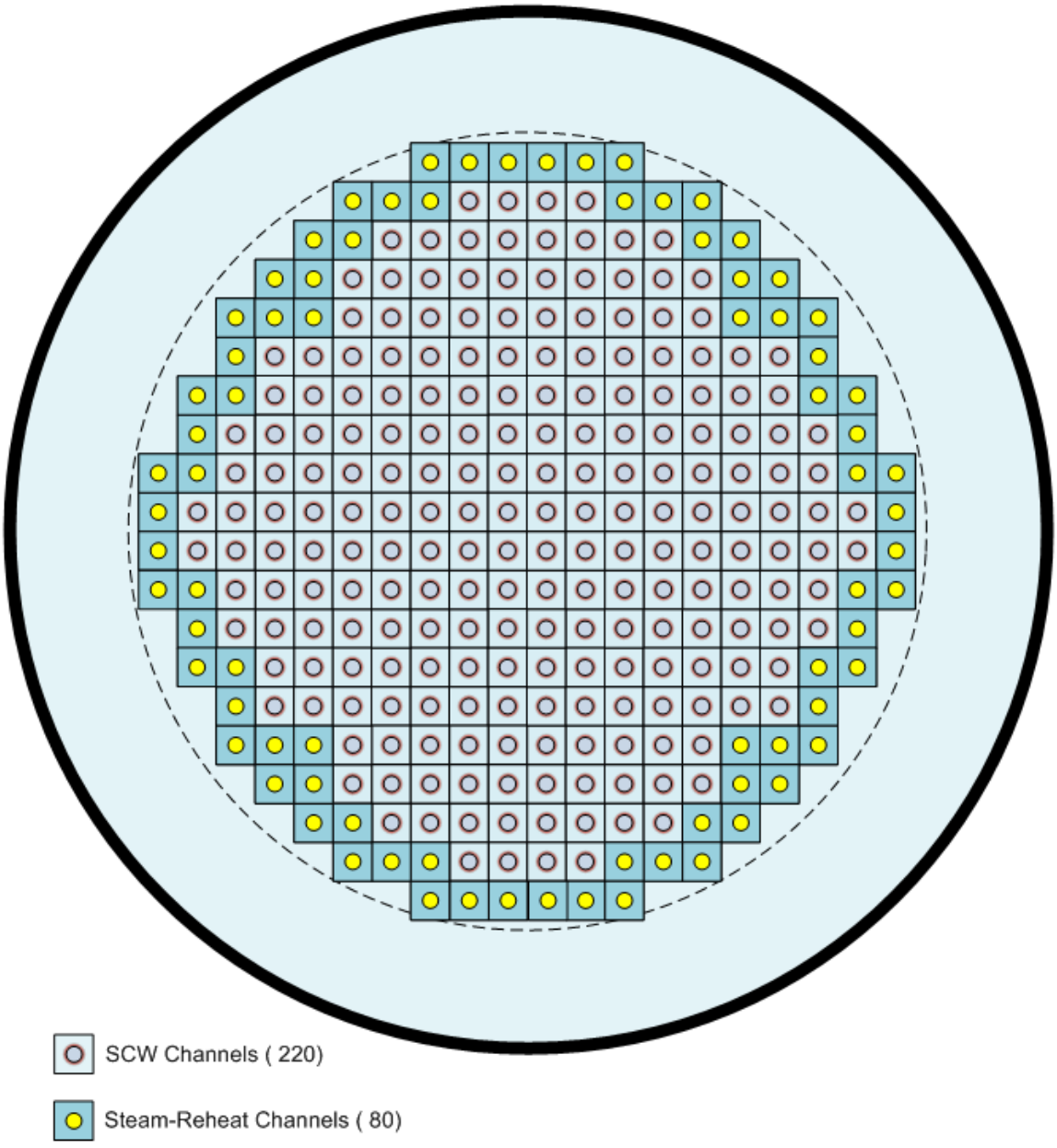

Figure 4.4. Possible channel layout of 1200-MW_e PT SCWR: OD – outside diameter and ID – inside diameter (Saltanov et al. 2010).

4.1. Single-Reheat Cycle

The proposed cycle layout for a SCW NPP with a single-reheat option is shown in Figure 4.5 (Cycle A). This cycle has the direct single-reheat regenerative configuration. As such, the SC "steam" exiting the reactor is expanded through a single-flow HP turbine.

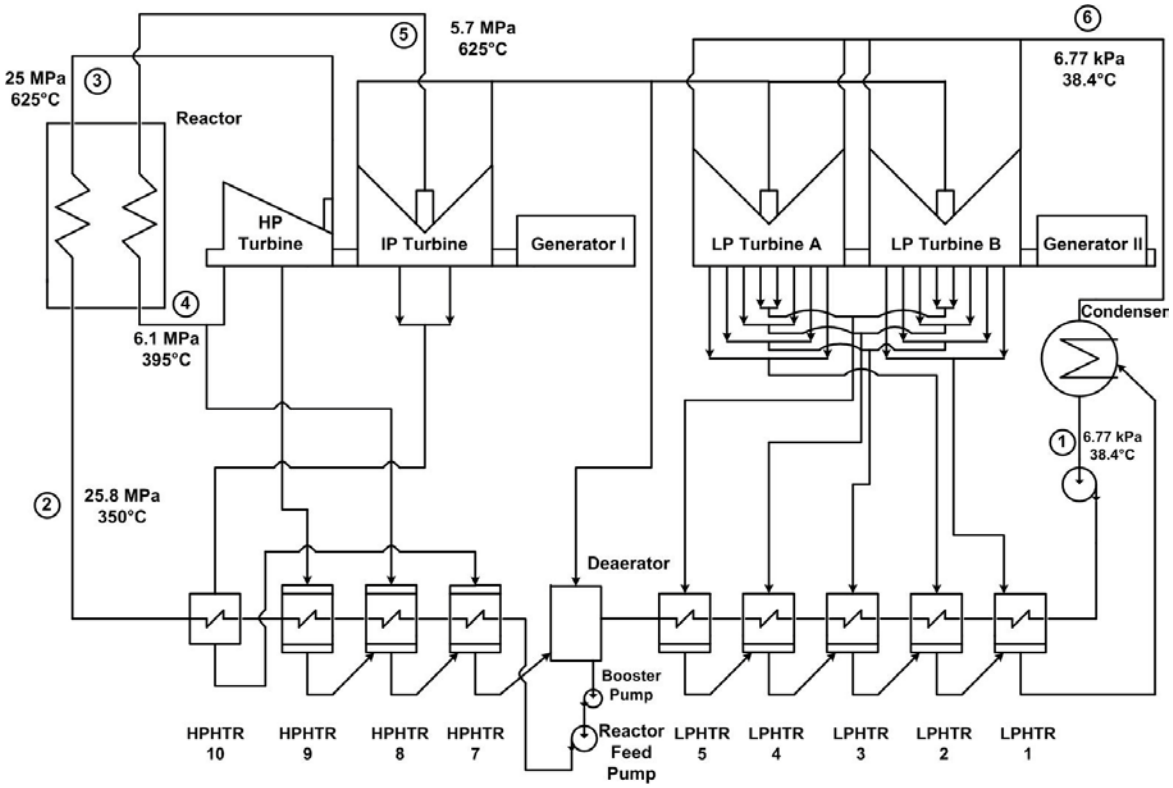

Figure 4.5. Direct single-steam-reheat Cycle A for SCW NPP based on Hitachi turbines (Naidin et al. 2009a).

As shown in Figure 4.4 (Cycle A), the steam is sent back to the reheater (SHS channels inside the reactor), where the temperature is raised to superheated conditions. Furthermore, the subcritical-pressure SHS is expanded in the IP turbine and transferred, through a cross-over pipe, to the LP turbines. Since the volume of the steam at the exhaust of the IP turbine is quite high, two LP turbines are being utilized. In Figure 4.4, the turbine-generator arrangement is a cross-compound: the HP and IP turbines are

located on the same shaft, while the LP turbines are located on a separate shaft (Naidin et al. 2009a).

4.2. Single-Reheat Cycle with MSR

Cycle B, shown in Figure 4.6, follows a slightly different arrangement. Actually, the Moisture Separator and Reheater (MSR) is used for a single-steam reheat instead of the reactor steam reheat. As such, the steam expanded in the HP turbine is sent to the IP turbine where it expands to saturated conditions (approximately 0.98 steam quality). Furthermore, the steam is passed through a MSR unit that contains one stage of moisture separation and two stages of reheat. From here, superheated steam exiting the MSR unit is sent to the inlet of the LP turbines where it is expanded to saturated conditions.

The steam is exhausted from the turbine to the condenser, suffering exhaust losses, which depend on the exhaust area and the steam velocity. The saturated steam undergoes a phase change and is condensed at a constant pressure and temperature by a cooling medium inside the condenser. The CEP is taking its suction from the condenser outlet. It pumps the condensate from the hotwell through a series of LP feedwater HeaTeRs (LP HTR 1 to 5 for Cycle A, LP HTR 1 to 4 for Cycle B) to the deaerator. The feedwater temperature differentials across the LP heaters are assumed to be approximately the same. The LP heaters are tube-in-shell, closed type heat exchangers. On the steam side, they contain condensing and subcooling zones (Naidin et al. 2009a).

The deaerator is an open-type feedwater heater, where the feedwater, extraction steam and drains of the HP heaters come into a direct contact. The feedwater is heated (at constant pressure) to the saturation temperature, and leaves the deaerator as saturated liquid. The Reactor Feedwater Pump (RFP) takes its suction from the deaerator and raises the feedwater pressure to the required value at the reactor inlet.

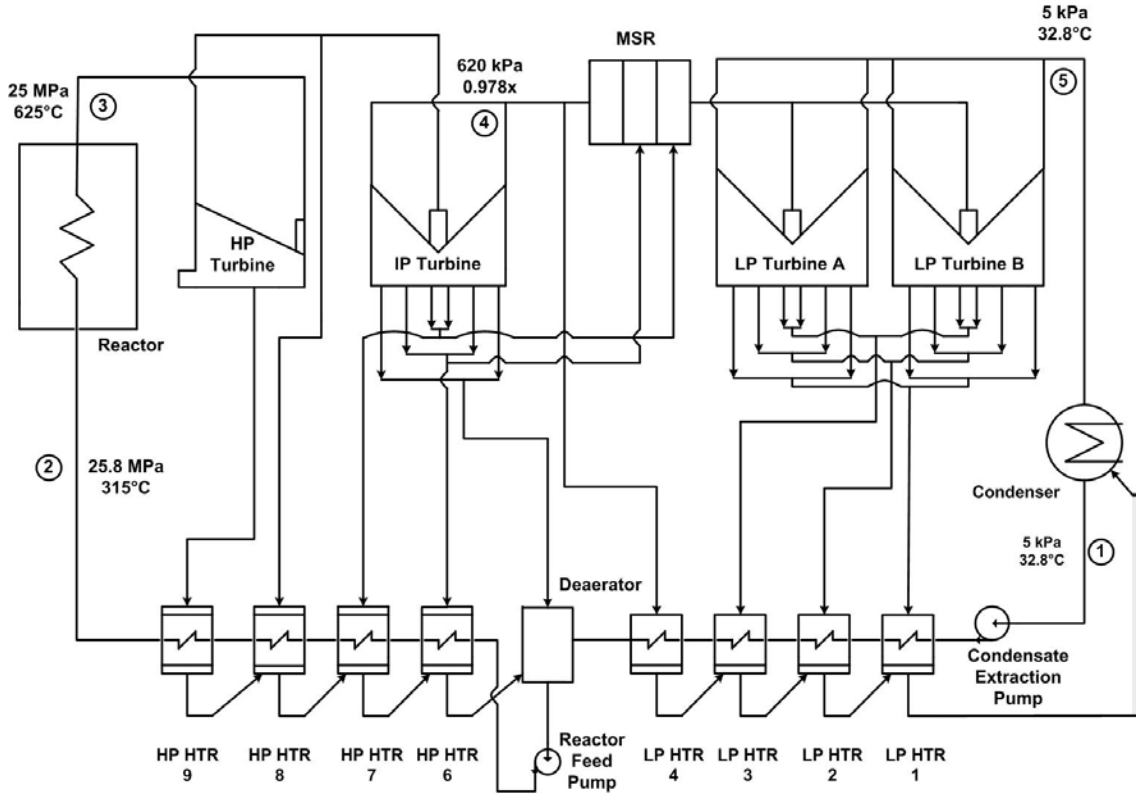

Figure 4.6. Single-reheat Cycle B with MSR for SCW NPP (Naidin et al. 2009a).

The feedwater is passed through 4 HP HTRs (6 to 9) in the case of Cycle B. The HP heaters are tube-in-shell, closed-type heat exchangers with de-superheating, condensing and subcooling zones.

4.3. No-Reheat Cycle

The single-reheat cycle introduces nuclear SHS channels, thus increasing the complexity of the reactor core design. Although preliminary results show that the thermal efficiency of the no-reheat cycle is approximately 2% lower than that of the single-reheat cycle, the less complex reactor-core configuration (all channels are cooled with SCW) might prove to be a major factor when selecting the most suitable design. In conclusion, it is worth

analyzing the possibility of a no-reheat SCW NPP Cycle C (see Figure 4.7) such as the one proposed in this section (Naidin et al. 2009a).

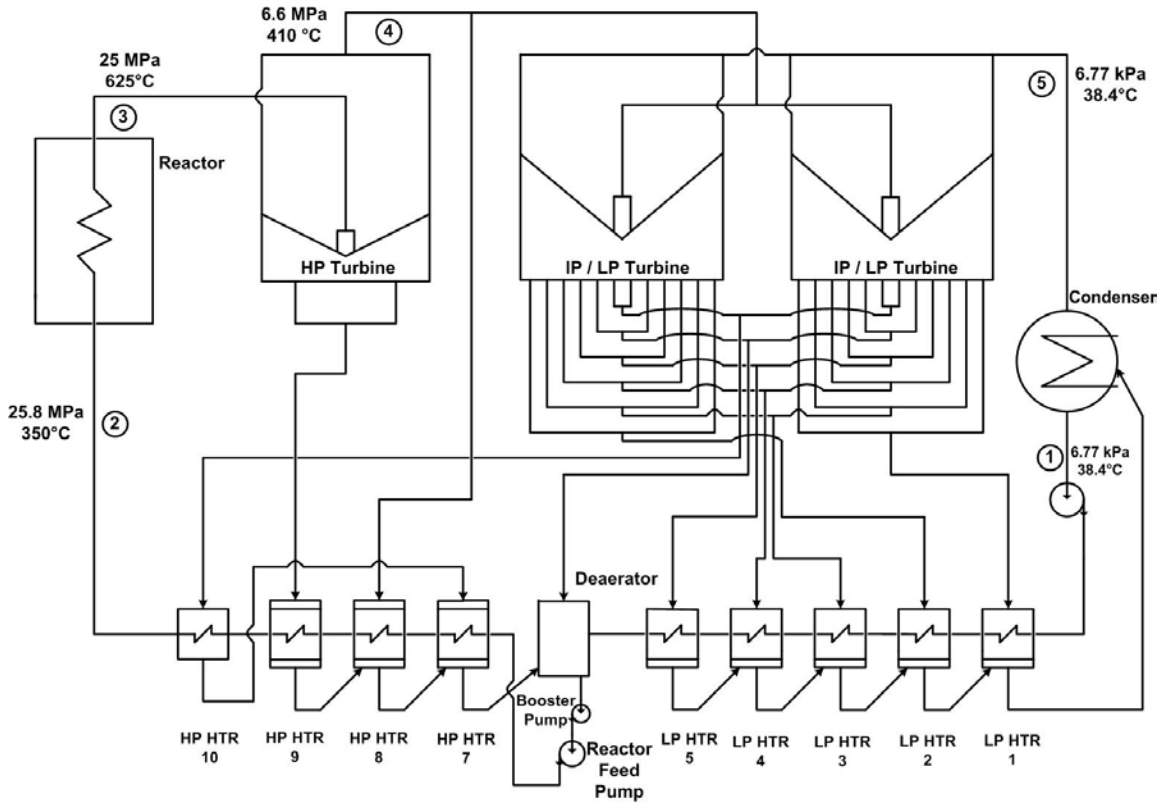

Figure 4.7. No-reheat Cycle C for SCW NPP (Naidin et al. 2009a).

The proposed no-reheat SCW NPP cycle consists of five LP HTRs, one deaerator, three HP HTRs and one topping de-superheater. The cycle has a direct, no-reheat, regenerative configuration. As such, the SC "steam" exiting the reactor is expanded through a double-flow HP turbine to superheated conditions. Since the volume of the steam at the exhaust of the HP turbine is quite high, two IP/LP turbines are being utilized. Furthermore, the steam is exhausted from the IP/LP turbine to the condenser. The saturated steam undergoes a phase change and is condensed at constant pressure and temperature by a cooling medium inside a condenser.

The CEP is taking its suction from the condenser hotwell. It pumps the condensate through a series of five LP HTRs (1 to 5) to the deaerator. The feedwater is heated at

constant pressure, and leaves the deaerator as saturated liquid. A RFP takes its suction from the deaerator and raises the feedwater pressure to the required value at the reactor inlet (25 MPa). Furthermore, the feedwater is passed through three HP HTRs (7 to 9) and a topping de-superheater (HP HTR 10).

4.4. Indirect Cycle

SCWR NPP indirect single-reheat-cycle arrangement is shown in Figure 4.8 (Naidin et al. 2009a). The SC "steam" from the reactor at a pressure of 25 MPa and temperature of 625^{o}C transfers the heat through a heat exchanger to the secondary loop. The SC "steam" from the secondary loop is expanded inside a single-flow HP turbine from the supercritical pressure of 25 MPa and temperature 550^{o}C (Point 3) to an intermediate pressure of 4.9 MPa and temperature of 300^{o}C (Point 4). The subcritical steam from HP turbine is sent to the second heat exchanger, where SC "steam" from the reactor at a pressure of 25 MPa and temperature of 625^{o}C raises the steam temperature in the secondary loop to superheated conditions through the heat exchanger. Then the superheated steam at a subcritical pressure of 4.5 MPa and temperature of 550^{o}C (Point 5) is expanded in the IP turbine and transferred through a cross-over pipe and expanded in the LP turbine to a pressure of 6.77 kPa and temperature of 38.4^{o}C (Point 6).

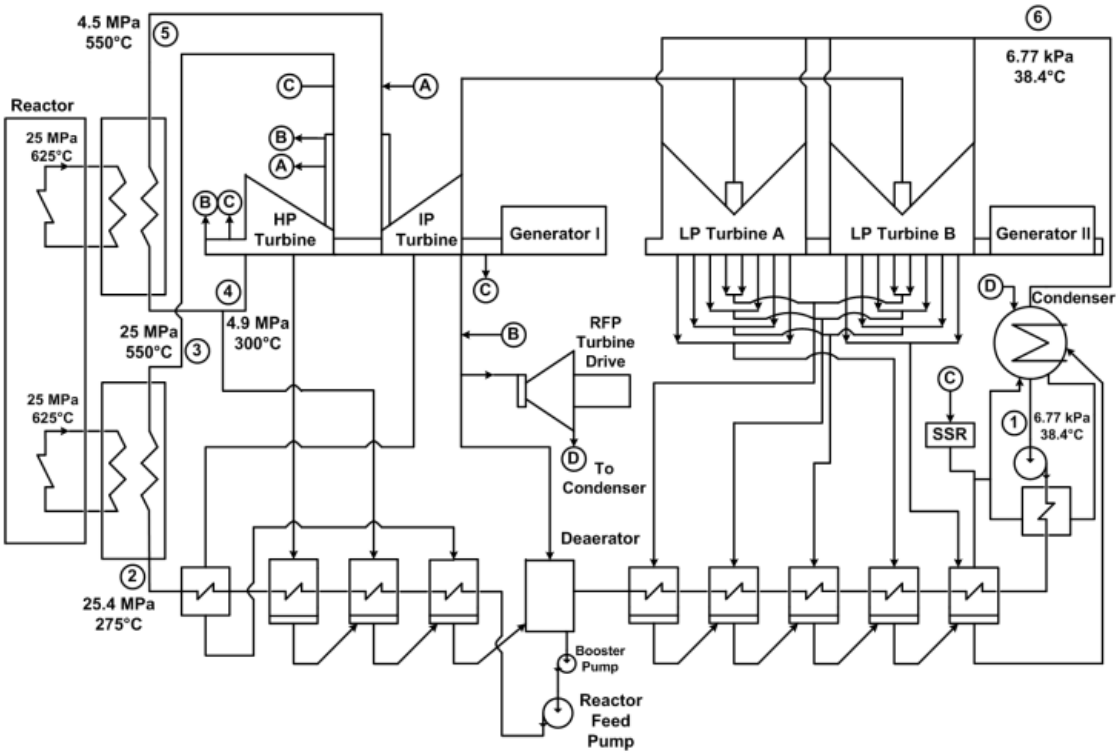

Figure 4.8. Indirect single-reheat cycle for SCW NPP (Naidin et al. 2009a).

Thermal efficiencies of all cycles are presented in Table 4.2 Selected parameters of the proposed Cycles A and C are presented in Table 4.3

Table 4.2. Thermal efficiency of SCW NPP cycles (Naidin et al. 2009a).

Cycle	Thermal Efficiency (%)
A	52
B	52
C	51

Table 4.3. Selected parameters of proposed SCW cycles (Naidin et al. 2009a).

Parameters	Unit	Description/Value	Description/Value
Cycle type	–	Single-Reheat (A)	No-Reheat (C)
Reactor spectrum	–	Thermal	
Fuel	–	UO_2 (ThO_2)	
Cladding material	–	Inconel or Stainless steel	
Reactor coolant	–	H_2O	
Moderator	–	D_2O	
Thermal Power Output	MW_{th}	2300	2340
Electrical Power Output	MW_e	1200	1200
Thermal Efficiency	%	52	51
SCW P_{in}	MPa	25.8	25.8
SCW P_{out} (estimated)	MPa	25	25
Inlet temperature of coolant (SCW)	°C	350	350
Outlet temperature of coolant (SCW)	°C	625	625
SHS P_{in}/P_{out}	MPa	6.1/5.7	–
SHS T_{in}/T_{out}	°C	400/625	–
Power thermal, SCW channels	MW_{th}	1870	2340
Power thermal, SHS channels	MW_{th}	430	–
Power thermal per SCW channel[3]	MW_{th}	8.5	8.5
Power thermal per SHS channel	MW_{th}	5.5	–
Number of fuel channels (total)	–	300	270
Number of SCW channels	–	220	270
Number of SHS channels	–	80	–
Total flow rate of SCW	kg/s	960	1190
Total flow rate of SHS	kg/s	780	–
Flow rate / SCW channel	kg/s	4.37	4.37
Flow rate / SHS channel	kg/s	10	–

[3] Presented in the table are *average* values of power per channel. In modeling heat-transfer along the SCW and SHS channels apart from the average, *maximum* channel power (+15%) was considered to account for neutron flux variations across core and due to uncertainty.

Concluding abovementioned results, the single-reheat cycle with heat regeneration and the corresponding arrangement appears to be the most advantageous as a basis for an SCW NPP.

4.5. Developed Detailed Thermal Layouts for NPPs Cooled with SCW

Unfortunately, schematics in Figures 4.5 – 4.8 are too general and have parameters only of the few elements of the cycles. Thus, a complete thermodynamic layout of a SCW NPP cannot be calculated based on these schematics. Therefore, the objective was to make a complete calculation of a SCW NPP thermodynamic layout. Figures 4.8 and 4.9 show recalculated schematics of a modern SC thermal power plant in Tom-Usinsk (Russia), based on the Figures 3.1 and 3.2. The layouts in Figures 4.8 and 4.9 are unique, because they contain full information on steam extraction from different stages of turbine and on the rest of the components of the layout. The characteristics of these layouts match the discussed above concept of the SCWR. Two variants are presented – for 600 MW_e output (two turbines should be used) and for 1200 MW_e output.

Recalculation was made based on mass flow and heat balance. Pressure drop along line was recalculated in proportion to the square of the ratio of the recalculated mass-flow rate to the reference mass-flow rate. This is valid assuming that differences in densities at the recalculated and reference temperatures are negligible. Rebalancing feedwater heaters and condenser required iterative search, since for these elements both mass and energy were to be conserved. Coolant at the deaerator and condenser outlets was assumed to be at saturated state.

It is important to mention, that heat-transfer calculations presented in the next section were made based on the parameters of generic SCW/SHS channels corresponding to the original AECL scheme, presented in Fig. 4.5. However, the detailed schematics presented below were developed after the heat-transfer calculations had been performed. Therefore, there is slight difference between the schematics in terms of inlet temperature to the SCW and SHS channels.

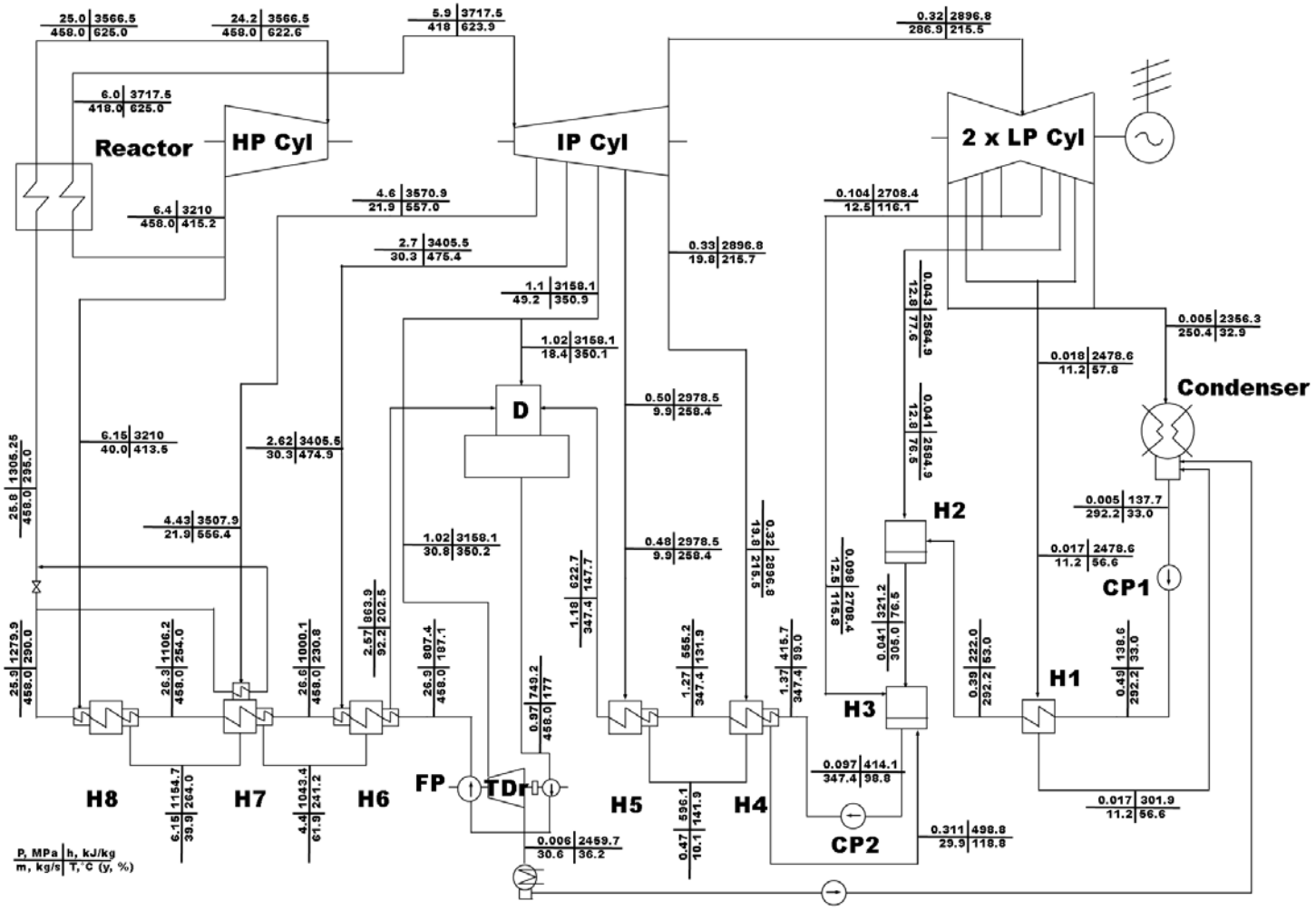

Figure 4.8. Thermal layout of 600-MW$_e$ single-reheat-cycle: Cyl – Cylinder; D – Deaerator; H – Heat exchanger (feedwater heater); FP - Feedwater pump; CP – Condenser Pump; and TDr – Turbine Drive;

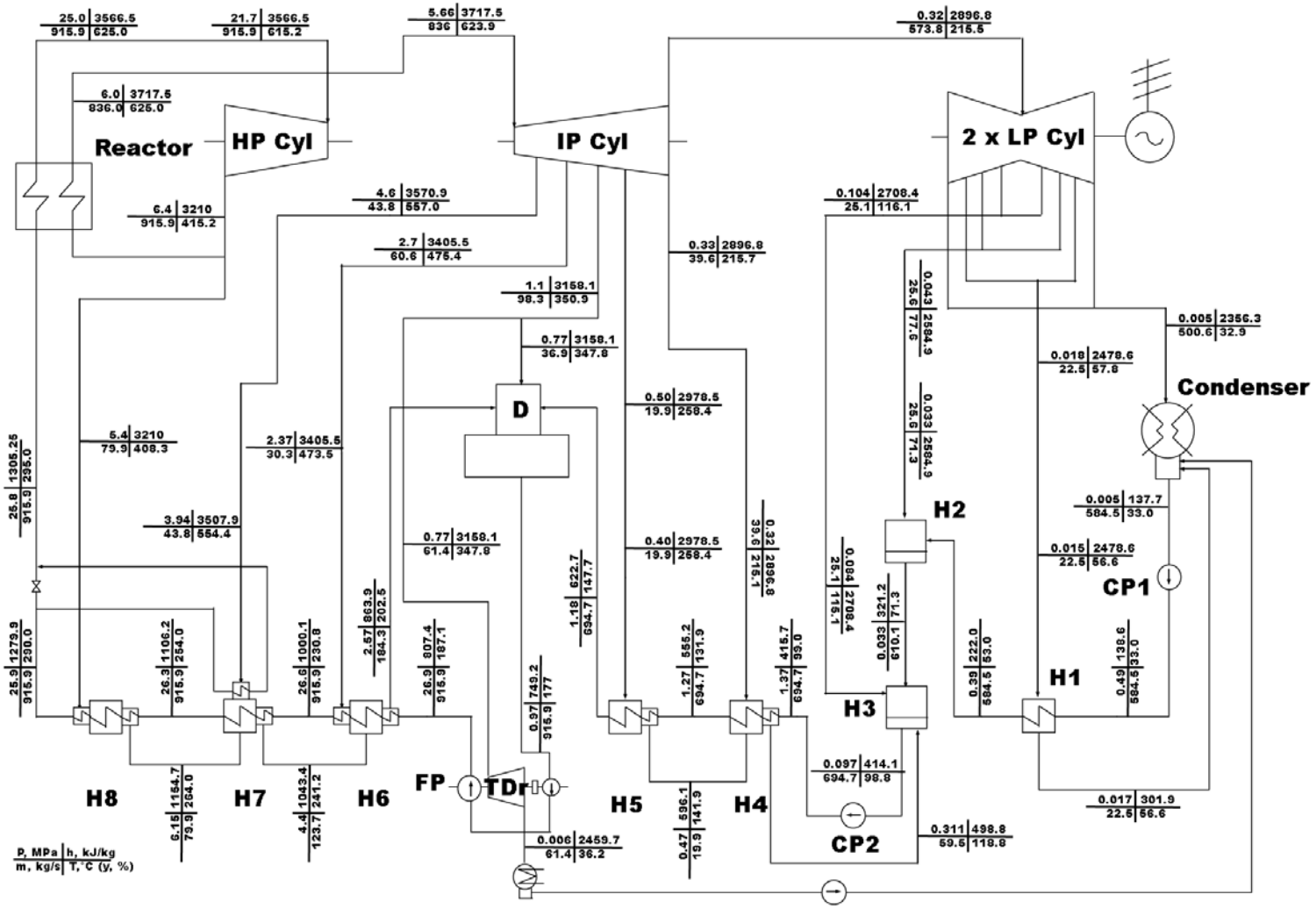

Figure 4.9. Thermal layout of 1200-MW$_e$ single-reheat-cycle: Cyl – Cylinder; D – Deaerator; H – Heat exchanger (feedwater heater); FP - Feedwater pump; CP – Condenser Pump; and TDr – Turbine Drive;

To conclude this chapter, the following advantages of the single-reheat cycle in application to SCW NPPs should be emphasized:

1. High thermal efficiency (45 – 50%), which is the current level for SC thermal power plants and close to the maximum thermal efficiency achieved in the power industry at combined-cycle power plants (up to 55%);
2. High reliability through proven state-of-the-art SC turbine technology;
3. Potential for co-generation of hydrogen; and
4. Reduced development costs based upon the wide variety of available SC turbines manufactured by companies worldwide.

However, the implementation of a single-reheat-cycle in SCW NPPs will require designing of the SHS channels and significant changes to the reactor-core design due to addition of these channels.

CHAPTER 5

HEAT-TRANSFER CALCULATIONS FOR GENERIC SUPERCTICIAL-WATER AND SUPERHEATED-STEAM CHANNELS

5.1. Overview of Relevant Correlations

At the current design stage of a generic SCW/SHS it is necessary to model coolant temperature distribution along the channel at steady-state at expected heat flux conditions and inlet coolant parameters. As the most basic approach, it is the bulk-fluid (or average in the cross-section) temperature is analyzed based on the heat-balance method. The next step is to determine temperatures of the sheath of the fuel element, as well as fuel centerline temperature. There are no exact analytical methods of prediction for temperature change across the coolant flowing in turbulent regime, and experimentally obtained heat-transfer correlations are used. Generally in such heat-transfer correlations, Nusselt number is correlated against the product of Reynolds number and Prandtl number, each raised to a certain power (so called Dittus-Boelter type). There are several heat-transfer correlations for the forced convection of a coolant in the supercritical and superheated-steam state. Below, the most recognized are discussed according to Pioro and Duffey (2007).

5.1.1. Correlations appropriate for SHS conditions

Due to the difficulty in dealing with the steep property variations, especially in turbulent flows and at high heat fluxes, satisfactory analytical methods have not yet been developed. Therefore, empirical generalized HTC correlations based on experimental data are used for HTC calculations for forced convective turbulent flows.

McAdams (1942) proposed to use the Dittus and Boelter (1930) equation in the following form for forced convective heat transfer in turbulent flows and subcritical pressures (this statement is based on the recent study by Winterton (1998)):

$$\mathbf{Nu_b} = C\,\mathbf{Re_b^{0.8}Pr_b^{\,n}}, \tag{5.1}$$

where C = 0.0243 and n = 0.4 for heating ($T_w > T_b$), and C = 0.0265 and n = 0.3 for cooling ($T_w < T_b$). This equation has been confirmed experimentally for the range of conditions: $0.7 \le \mathbf{Pr} \le 160$; $\mathbf{Re_b} \ge 10{,}000$.

For flows characterized with large property variations the following equation (Sieder and Tate 1936) is recommended:

$$\mathbf{Nu_b} = 0.027\mathbf{Re_b^{0.8}Pr^{1/3}}\left(\frac{\mu_b}{\mu_w}\right)^{0.14}, \tag{5.2}$$

where all properties are evaluated at T_b except μ_w, which is evaluated at T_w. This equation has been confirmed experimentally for the range of conditions: $0.7 \le \mathbf{Pr} \le 16{,}700$ and $\mathbf{Re_b} \ge 10{,}000$.

For superheated steam, a correlation was developed by Hadaller and Banerjee (1969):

$$\mathbf{Nu_f} = 0.0101\mathbf{Re_f^{0.877}Pr_f^{0.611}}\left(\frac{L_h}{D}\right)^{-0.033}, \tag{5.3}$$

where all properties are evaluated at the film temperature:

$$T_f = \frac{T_b + T_w}{2} \tag{5.4}$$

Gnielinski (1976) modified and improved a correlation developed by Petukhov and Kirillov (1958) for supercritical CO_2:

$$\mathbf{Nu_b} = \frac{\frac{\xi}{8}\left(\mathbf{Re_b} - 1000\right)\mathbf{Pr_b}}{1 + 12.7\sqrt{\frac{\xi}{8}}\left(\mathbf{Pr_b}^{2/3} - 1\right)}, \tag{5.5}$$

where friction factor ξ can be determined from an appropriate relation, such as Petukhov equation:

$$\xi = \frac{1}{(0.790 \ln \mathbf{Re_b} - 1.64)^2} \tag{5.6}$$

Gnielinski correlation (5.5) is valid for $.0.5 \leq \mathbf{Pr} \leq 2000$ and $3 \cdot 10^3 < \mathbf{Re_b} < 5 \cdot 10^6$.

5.1.2. Correlations appropriate for SCW conditions

Krasnoshchekov and Protopopov (1959, 1960) proposed (later, together with Petukhov (Petukhov et al. 1961)) the following correlation for forced convective heat transfer in water and carbon dioxide at supercritical pressures:

$$\mathbf{Nu} = \mathbf{Nu_0}\left(\frac{\mu_b}{\mu_w}\right)^{0.11}\left(\frac{k_b}{k_w}\right)^{-0.33}\left(\frac{\bar{c}_p}{c_{pb}}\right)^{0.35}, \tag{5.7}$$

where according to Petukhov and Kirillov (1958):

$$\mathbf{Nu_0} = \frac{\frac{\xi}{8}\,\mathbf{Re_b}\,\overline{\mathbf{Pr}}}{12.7\sqrt{\frac{\xi}{8}}\,(\overline{\mathbf{Pr}}^{\frac{2}{3}} - 1) + 1.07} \tag{5.8}$$

and

$$\xi = \frac{1}{(1.82\log_{10}\mathbf{Re_b} - 1.64)^2}\,. \tag{5.9}$$

In effect, the **Pr** and c_p were averaged over the ranges to account for the thermophysical properties variations. The majority of their data (85%) were generalized using Equation (5.7) and showed discrepancies within ±15%. Equation (5.7) is valid within the following ranges:

$2\cdot10^4 < \mathbf{Re_b} < 8.6\cdot10^5$, $0.85 < \overline{\mathbf{Pr}}_\mathbf{b} < 65$; $0.90 < \frac{\mu_b}{\mu_w} < 3.60$, $1.00 < \frac{k_b}{k_w} < 6.00$,

and $0.07 < \frac{\overline{c}_p}{c_{p,b}} < 4.50$.

Bishop et al. (1964) conducted experiments with supercritical water flowing upward inside tubes and annuli within the following range of flow and operating parameters: pressure 22.8 – 27.6 MPa, bulk-fluid temperature 282 – 527ºC, mass flux 651 – 3662 kg/m^{2}s and heat flux 0.31 – 3.46 MW/m^2. Their data for heat transfer in tubes were generalized using the following correlation, with a fit of ±15%:

$$\mathbf{Nu_x} = 0.0069\,\mathbf{Re_x^{0.9}}\,\overline{\mathbf{Pr}}_\mathbf{x}^{0.66}\left(\frac{\rho_w}{\rho_b}\right)_x^{0.43}\left(1 + 2.4\frac{D}{x}\right) \tag{5.10}$$

where x is the axial location along the heated length.

Swenson et al. (1965) investigated local forced-convection Heat Transfer Coefficients (HTCs) in supercritical water flowing inside smooth tubes. They found that, due to rapid changes in thermophysical properties of supercritical water near the pseudocritical point,

conventional correlations did not work well. They recommended the following correlation:

$$\mathbf{Nu_w} = 0.00459\,\mathbf{Re_w^{0.923}}\,\overline{\mathbf{Pr}}_{\mathbf{w}}^{0.613}\left(\frac{\rho_w}{\rho_b}\right)^{0.231} \tag{5.11}$$

Equation (5.11) was obtained within the following range: P = 22.8 – 41.4 MPa, G = 542 – 2150 kg/m^{2}s, T_w = 93 – 649ºC, and T_b = 75 – 576ºC; and re-produced the data to within ±15%. Also, this correlation predicted the data of carbon dioxide with good accuracy.

However, Swenson et al. assumed that thermal conductivity was a smoothly decreasing function of temperature near the critical and the pseudocritical points. According to their experimental data, the HTC in the pseudocritical region is strongly affected by heat flux. At low heat fluxes, the HTC had a sharp maximum near the pseudocritical temperature. At high heat fluxes, the HTC was much lower and did not have a sharp peak.

Krasnoshchekov et al. (1967) modified their original correlation for forced-convective heat transfer in water and carbon dioxide at supercritical pressures (see Equation (5.7)) to the following form:

$$\mathbf{Nu} = \mathbf{Nu_0}\left(\frac{\rho_w}{\rho_b}\right)^{0.3}\left(\frac{\bar{c}_p}{c_{pb}}\right)^{n}, \tag{5.12}$$

where $\mathbf{Nu}_0$ is defined in Equation (5.8). Exponent n is 0.4 at $\frac{T_w}{T_{pc}} \le 1$ or $\frac{T_b}{T_{pc}} \ge 1.2$; $n = n_1 = 0.22 + 0.18\frac{T_w}{T_{pc}}$ at $1 \le \frac{T_w}{T_{pc}} \le 2.5$; and $n = n_1 + (5 \cdot n_1 - 2)\left(1 - \frac{T_b}{T_{pc}}\right)$ at $1 \le \frac{T_b}{T_{pc}} \le 1.2$. Equation (5.12) is accurate within ±20% and is valid within the following range:

$8 \cdot 10^4 < \mathbf{Re}_b < 5 \cdot 10^5$, $0.85 < \overline{\mathbf{Pr}} < 65$, $0.09 < \frac{\rho_w}{\rho_b} < 1.0$, $0.02 < \frac{\overline{c}_p}{c_{p,b}} < 49.0$,

$0.9 < \frac{T_w}{T_{pc}} < 2.5$, $0.9 < \frac{T_w}{T_{pc}} < 2.5$ (q'' is in W/m^2) and $\frac{x}{D} \geq 15$.

Later, Krasnoshchekov et al. (1971) added to Equation (5.11) a correction factor for the tube entrance region in the form of

$$f\left(\frac{x}{D}\right) = 0.95 + 0.95\left(\frac{x}{D}\right)^{0.8} \tag{5.13}$$

Also, this correction factor can be used for a heated tube with abrupt inlet within $2 \leq \frac{x}{D} \leq 15$.

Jackson and Fewster (1975) modified the correlation of Krasnoshchekov et al. to employ a Dittus-Boelter type form for $\mathbf{Nu}_0$. Finally, they obtained a correlation similar to that of Bishop et al. (1964) without the effect of geometric parameters and with different values of constant and exponents:

$$\mathbf{Nu} = 0.0183\, \mathbf{Re_b}^{0.82}\, \overline{\mathbf{Pr}}^{0.5} \left(\frac{\rho_w}{\rho_b}\right)^{0.3} \tag{5.14}$$

Hence, it can be expected that Jackson and Fewster correlation will follow closely a trend predicted by Bishop et al. correlation (Equation (5.10)).

Dyadyakin and Popov (1977) performed experiments with a tight 7-rod bundle with helical fins cooled with supercritical water and they correlated their data for the local HTCs as:

$$\mathbf{Nu_x} = 0.021\,\mathbf{Re_x^{0.8}}\,\overline{\mathbf{Pr}}_{\mathbf{x}}^{0.7}\left(\frac{\rho_w}{\rho_b}\right)_x^{0.45}\left(\frac{\mu_b}{\mu_{in}}\right)_x^{0.2}\left(\frac{\rho_b}{\rho_{in}}\right)_x^{0.1}\left(1+2.5\frac{D_{hy}}{x}\right), \qquad (5.15)$$

where x is the axial location along the heated length in meters, and D_{hy} is the hydraulic-equivalent diameter in meters. This correlation fits the data (504 points) to within ±20%. The maximum deviation of the experimental data from the correlating curve corresponds to points with small temperature differences between the wall temperature and bulk temperature. Sixteen experimental points had deviations from the correlation within ±30%.

The latest SCW correlation developed by Mokry et al. (2009a) was obtained by analyzing a large set of experimental data obtained in Russia:

$$\mathbf{Nu_b} = 0.0061\,\mathbf{Re_b^{0.904}}\,\overline{\mathbf{Pr}}_{\mathbf{b}}^{0.684}\left(\frac{\rho_w}{\rho_b}\right)^{0.564} \qquad (5.16)$$

This correlation is valid within P = 22.8 – 29.4 MPa, q'' = 70 – 1250 kW/m^2, G = 200 – 1500 kg/m^{2}s and D_{hy} = 3 – 38 mm. The experimental dataset was obtained for supercritical water flowing upward in a 4-m-long vertical bare tube. The data was collected at pressures of about 24 MPa for several combinations of wall and bulk-fluid temperatures that were below, at, or above the pseudocritical temperature. The values for mass flux ranged from 200 – 1500 kg/m^{2}s, for heat flux up to 1250 kW/m^2 and inlet temperatures from 320 to 350°C. Mokry et al. (2009a) correlation has demonstrated a good fit for HTC values (±25%) and for wall temperatures (±15) for the analyzed dataset. A comparison done by Mokry et al. (2009b) showed that the Dittus-Boelter correlation significantly overestimates experimental HTC values within the pseudocritical range. The Bishop et al. and Jackson correlations tended also to deviate substantially from the experimental data within the pseudocritical range. The Swenson et al. (1965) correlation provided a better fit for the experimental data than the previous three correlations within some flow conditions, but did not follow up closely the experimental data within others.

Also, HTC and wall temperature values calculated with the FLUENT CFD code (Pioro et al. 2010, Vanyukova et al. 2009) might deviate significantly from the experimental data, for example, the *k*-*ε* model (wall function). However, the *k*-*ε* model (low-**Re** numbers) showed better fit within some flow conditions.

In a recent research on creating look-up tables for trans-critical heat transfer, Zahlan et al. (2010) analyzed a big number of correlations against a large set of date. They showed that the best agreement with the date in the supercritical water and superheated steam region had the correlation developed by Mokry et al. (2009) (see Tables 5.1 and 5.2).

Table 5.1. Overall weighted average and RMS errors within three supercritical sub-regions (Zahlan et al. 2010).

Correlation	Supercritical Region				Region	
	Liquid-Like		Gas-Like		Critical or Pseudocritical	
	Errors, %					
	Average	RMS	Average	RMS	Average	RMS
Bishop et al. (1965)	6.3	24.2	5.2	18.4	20.9	28.9
Swenson et al. (1965)	1.5	25.2	-15.9	20.4	5.1	23.0
Krasnochekov et al. (1967)	15.2	33.7	-33.6	35.8	25.2	61.6
Watts-Chou (1982)	4.0	25.0	-9.7	20.8	5.5	24.0
Chou (1982), Deter	5.5	23.1	5.7	22.2	16.5	28.4
Griem (1996)	1.7	23.2	4.1	22.8	2.7	31.1
Jackson (2002)	13.5	30.1	11.5	28.7	22.0	40.6
Mokry et al. (2009)	-3.9	**21.3**	-8.5	**16.5**	**-2.3**	**17.0**
Kuang et al. (2008)	-6.6	23.7	**2.9**	19.2	-9.0	24.1
Cheng et al. (2009)	**1.3**	25.6	**2.9**	28.8	14.9	90.6
Hadaller-Banerjee (1969)	7.6	30.5	10.7	20.5	-	-
Sieder-Tate (1936)	20.8	37.3	93.2	133.6	-	-
Dittus-Boelter (1930)	32.5	46.7	87.7	131.0	-	-
Gnielinski (1976)	42.5	57.6	106.3	153.3	-	-

In **bold** – the minimum values.

Table 5.2. Overall average and RMS error within subcritical region (Zahlan et al. 2010).

Correlation	Subcritical liquid		Superheated steam	
	Error, %			
	Average	RMS	Average	RMS
Sieder and Tate (1936)	27.6	37.4	83.8	137.8
Gnielinski (1976)	-4.3	**18.3**	80.3	130.2
Hadaller and Banerjee (1969)	27.3	35.9	19.1	34.4
Dittus-Boelter (1930)	10.4	22.5	75.3	127.3
Mokry et al. (2009)	**-1.1**	19.2	**-4.8**	**19.6**

In **bold** – the minimum values.

Therefore, Mokry et al. correlation was used to calculate temperature profiles along SCW and SHS channels. In the case of UO_2, usage of heat-transfer coefficient at average value may underestimate fuel centerline temperature by about 100°C. Therefore, the minimum value of heat-transfer coefficient was used (1.2 times lower than average) in order to have conservative results.

5.2. Generic Design of SCWR and Pressure Channels

It is envisaged that a generic SCWR will consist of 220 SCW channels and 80 SHS channels (Pioro and Duffey 2007). SHS channels are placed in the periphery of the core. SCW at a temperature of about 350ºC will enter the core and heated there up to temperature of about 625ºC. The HP turbine inlet pressure will be about 25 MPa. After expansion to the SHS state ($P \approx 6.1$MPa, $T \approx 350 - 400$ºC) it will be sent back to the reactor and superheated there to a temperature of about 625ºC and then sent to the IP section of the turbine. The detailed parameters of the single-reheat cycle for a generic SCWR are listed in Table 4.3. The cross section view of the generic SCWR is presented in Figure 4.4. Peiman et al. (2010) analyzed heat losses from such a configuration. Total heat loss for the 300 channels is predicted to be around 32.7 MW (about 1.4% of the reactor thermal power).

Table 5.3. Total Heat Losses per Fuel Channel and for 300 Fuel Channels (Peiman et al. 2010).

Fuel Channel	Ceramic-Insulated
Heat Loss/ SCW Channels, kW	105.2
Heat Loss/ SRH Channels, kW	112.3
# of SCW Channels	220
# of SRH Channels	80
Total Heat Loss (300 Channels), MW	32.7

Ceramic insulation was proposed for the fuel channel, while in conventional CANDU channels CO_2 is used as an insulator. The generic SCW channel consists of a liner tube, ceramic insulator, and PT. Inconel-718 is a potential candidate, which can be used as the material of choice for the PT. The minimum required thickness of PT at SCW conditions is approximately 7.6 mm. The main purpose of the liner tube, which is a perforated tube, is to protect the ceramic insulator during re-fuelling and operation with fuel bundles inside. The ceramic insulator, which is 70% porous and made of Yttria-Stabilized Zirconia (YSZ), should provide good thermal insulation (Peiman et al. 2010).

As mentioned above, water at the supercritical state will be used in the generic SCWR. All thermophysical parameters experience significant change near the pseudocritical point. Variations of some thermophysical properties of water along the SCW channel are plotted in the Figures 5.1 and 5.2 (values of the properties were calculated using NIST (2007) software).

The values of volumetric expansivity, Prandtl number, and specific heat experience 8 – 10 fold increase in the vicinity of the pseudocritical point. The values of viscosity, thermal conductivity and density drop 4 – 5 times in the vicinity of the pseudocritical point. For comparison, the graphs for the same properties are plotted along SHS channel in the same scale.

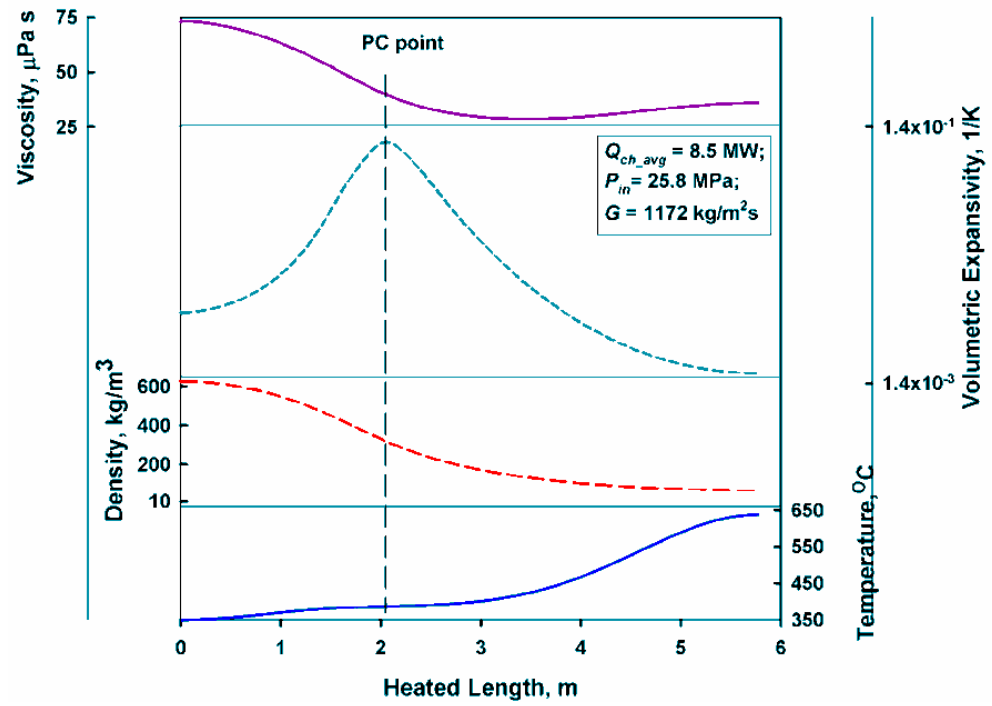

(a)

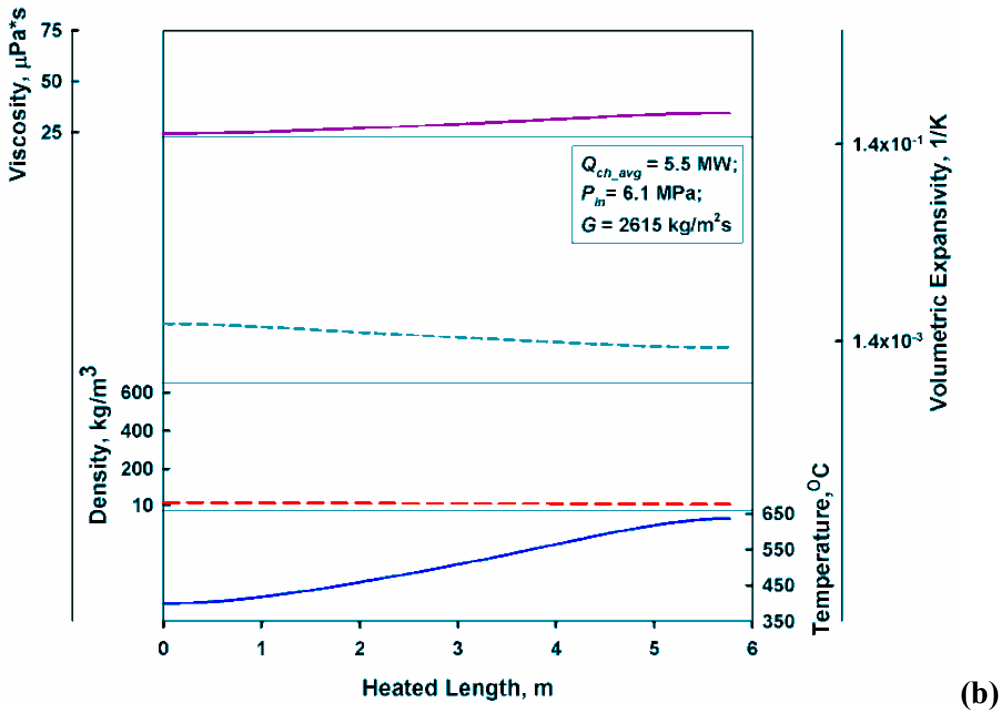

(b)

Figure 5.1. Variation of density, viscosity, and volumetric expansivity of water along SCW (a) and SHS (b) channels.

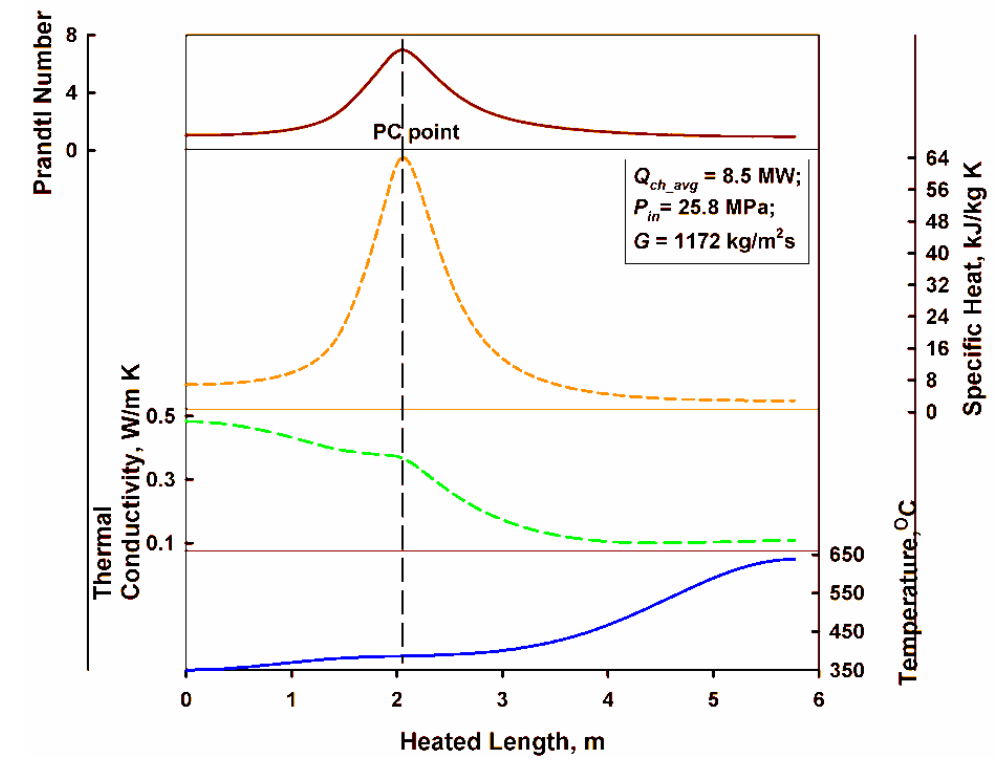

(a)

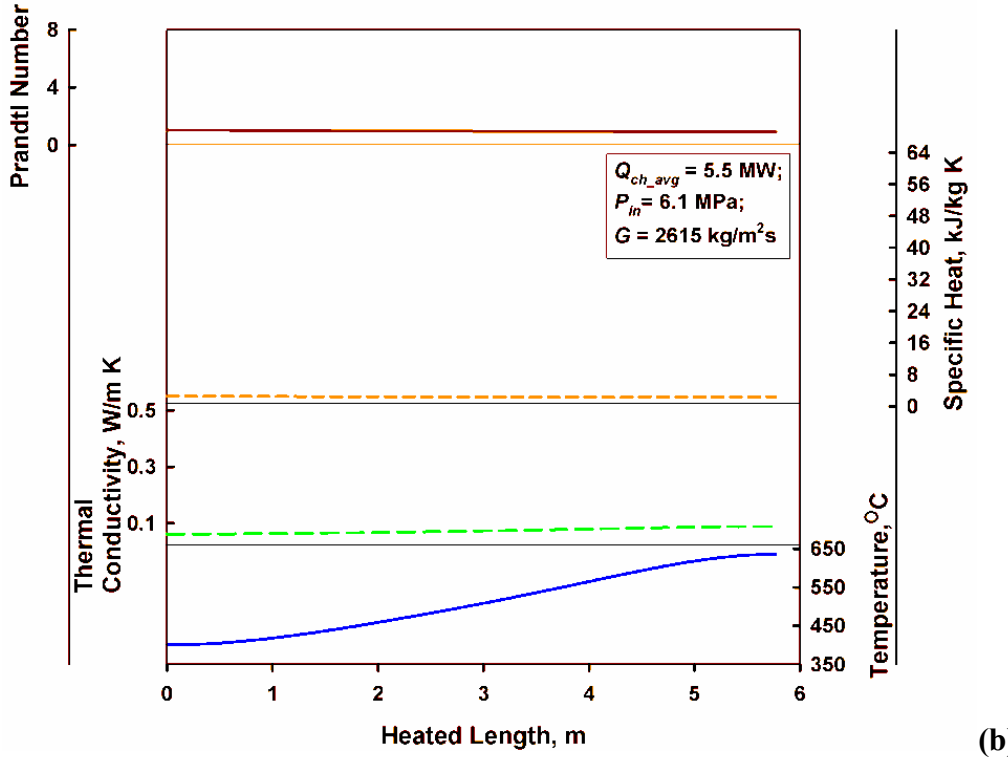

(b)

Figure 5.2. Variation of thermal conductivity, Prandtl number, and specific heat of water along SCW (a) and SHS (b) channels.

5.3. Heat-Transfer-Calculations Algorithm

Heat-transfer calculations were made for a channel with Variant-20 bundles. The model consists of two parts: (a) calculation of the hydraulic-equivalent diameter, D_{hy}, for the given geometry of the channel, and (b) calculation of bulk-fluid, fuel-element sheath, and fuel centerline temperatures along the cannel. In the model, steady-state operating conditions are assumed and one-dimensional heat transfer along heated length of the channel is evaluated.

In the part (a), the values of PT inner diameter, $D_{PT,i}$, outer diameter of the fuel-element sheath, $D_{SH,o}$, outer diameter of the central unheated control rod, D_{UH}, and number of fuel elements, N_{SH}, are the input parameters. Then area blocked by fuel elements, flow area, wetted perimeter, and D_{hy} are calculated (Equations 5.17 – 5.20):

$$A_{block} = \frac{\pi}{4}\left(N_{SH} D_{SH,o}^2 + D_{UH}^2\right) \tag{5.17}$$

$$A_{fl} = \frac{\pi}{4} D_{PT,i}^2 - A_{block} \tag{5.18}$$

$$p_{wet} = \pi(D_{PT,i} + N_{SH} D_{SH,o} + D_{UH}) \tag{5.19}$$

$$D_{hy} = \frac{4A_{fl}}{p_{wet}} = \frac{D_{PT,i}^2 - (N_{SH} D_{SH,o}^2 + D_{UH}^2)}{D_{PT,i} + N_{SH} D_{SH,o} + D_{UH}} \tag{5.20}$$

The calculated value of D_{hy} is equal to 7.83 mm for Variant-20 bundle.

In the part (b), first of all, the linear flux shape was set up. Four Axial Heat-Flux Profiles were considered: uniform, cosine-like, upstream-skewed, and downstream-skewed. The truncated cosine and upstream-skewed profiles were taken as proposed in the paper by Leung (2008). Downstream-skewed profile was obtained by symmetrical reflection of upstream-skewed profile with respect to longitudinal center of the channel. This idea was proposed by Allison et al. (2009). The AHFPs are plotted in Figure 5.3. These flux profiles were chosen based on the following ideas. Uniform profile is the easiest one to

be reproduced in the experimental set-up, therefore, calculated values could be verified by experimental. Moreover, if the even burn up is to be achieved in the reactor, then the flux shape is to be flattened, being close uniform profile. Cosine profile corresponds to theoretical solution to flux shape along finite cylindrical fuel element. Cosine-like profile of linear power density q' used at heat transfer calculations was taken from paper by Leung (2008), and is described as sum of two sinuses:

$$q' = 1.511 \cdot \sin\left(0.533 \cdot x + 0.04431\right) + 0.08373 \cdot \sin\left(1.589 \cdot x + 0.1137\right) \qquad (5.21)$$

Since it is virtually impossible to hold the same flux shape in all channels during all times, there are numerous other shapes. The one that covers all possible flux shapes is represented by downstream-skewed profile. Upstream-skewed profile is relevant to either the four-bundle-shift or two-bundle-shift refueling scheme in CANDU (Leung 2008).

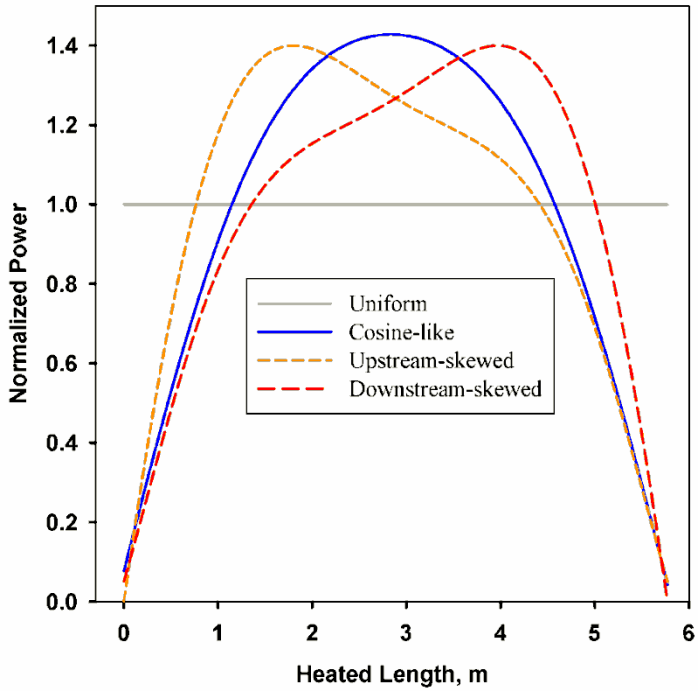

Figure 5.3. Various AHFPs used for heat-transfer calculations (based on Leung 2008).

After this the inlet values of temperature and inlet and outlet value of pressure are input. Linear pressure drop along the channel was assumed. Then iterative loop for calculation

of temperatures distribution was implemented. Channel length was sliced into elementary pieces, each 1 mm long. For piece i, value of specific enthalpy h_i was retrieved from NIST[4], specific enthalpy at the end of the piece, h_{i+1} was calculated from the heat balance on the piece, and T_{i+1} was retrieved from NIST:

$$h_i = f(T_i, P_i); \quad \dot{m}(h_{i+1} - h_i) = q'_{i+1} \Rightarrow h_{i+1} = \frac{q'_{i+1}}{\dot{m}} + h_i;$$
$$T_{i+1} = f(h_{i+1}, P_{i+1}) \Rightarrow h_{i+2} = f(T_{i+1}, P_{i+1}) \text{ and so on,}$$

where q' is linear power density.

Knowing bulk-fluid temperature allows calculating wall temperature. In the model, T_w was calculated from Mokry et al. correlation (see Equation (5.16)), where dimensionless groups were calculated from their definitions as follows:

$$\mathbf{Nu_b} = \frac{htc \cdot D_{hy}}{k}; \quad \mathbf{Re_b} = \frac{4\dot{m}}{\mu \cdot \pi D_{hy}}; \quad \overline{\mathbf{Pr}}_\mathbf{b} = \frac{\mu}{k} \cdot \underbrace{\frac{h_w - h_b}{T_w - T_b}}_{\bar{c}_p} \tag{5.22}$$

Mokry et al. correlation requires iteration be made to calculate T_w. Therefore, for the first piece of channel initial guess of T_w was made, HTC was calculated from Mokry et al. correlation, and corrected value of $T_{w,1}$ was calculated from Newton's cooling law:

$$q' = htc \cdot \pi D_{sh,od} N_{sh} \left(T_{w,1} - T_b\right) \Rightarrow T_{w,1} = \frac{q'}{htc \cdot \pi D_{sh,od} N_{sh}} + T_b$$

After that the value of $T_{w,1}$ is compared to T_w. If the absolute value of the difference between these values was higher than 0.1K, the value of $T_{w,1}$ was assigned to T_w. and another iteration was performed, starting from redetermination of heat-transfer coefficient

[4] This is a Fortran-based program which calculates various thermophysical parameters for different substances in gaseous and liquid phase, based on the given inputs. NIST may be called from different programs (Matlab, Excel, etc.) to calculate unknown parameter based on the two known.

from Mokry et al. correlation. Therefore, the iterations for the piece *I* were stopped after difference of wall temperatures T_w and $T_{w,1}$ became less than 0.1 K. For all the next pieces the initial guess of wall temperature was equal to: $T_{w,i+1} = T_{b,i+1} + (T_{w,i} - T_{b,i})$. This approach saved about 35,000 iterations for the channel. HTC profiles along SCW and SHS channels are plotted in Figures 5.4 and 5.5.

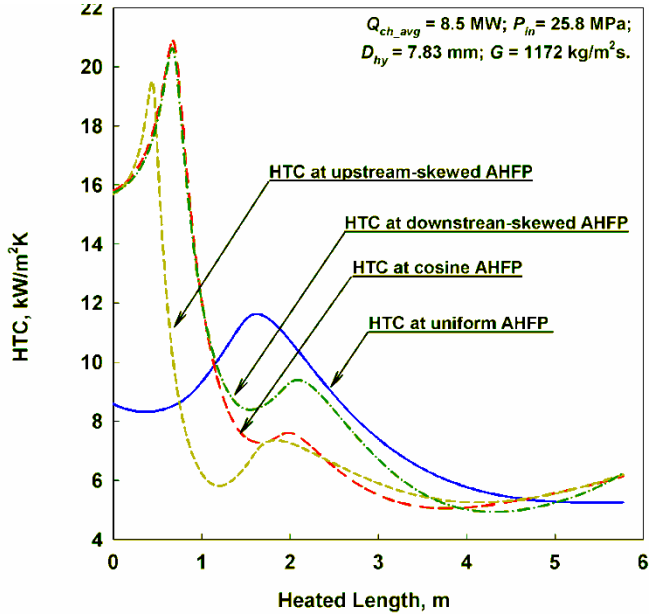

(a)

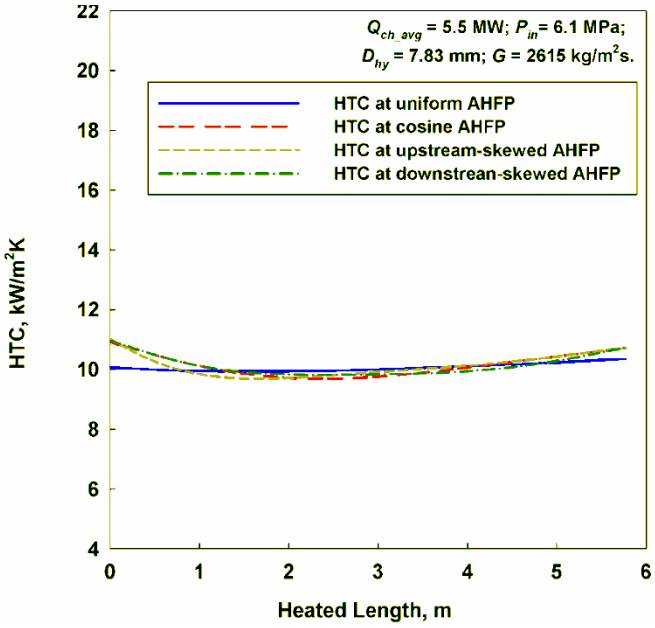

(b)

Figure 5.4. HTC profiles along SCW (a) and SHS (b) channels at average channel power.

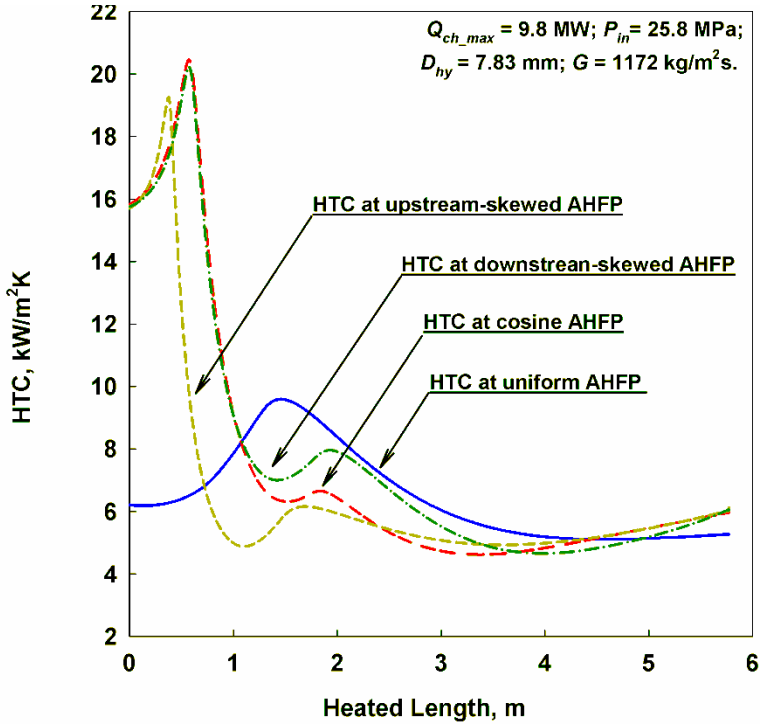

(a)

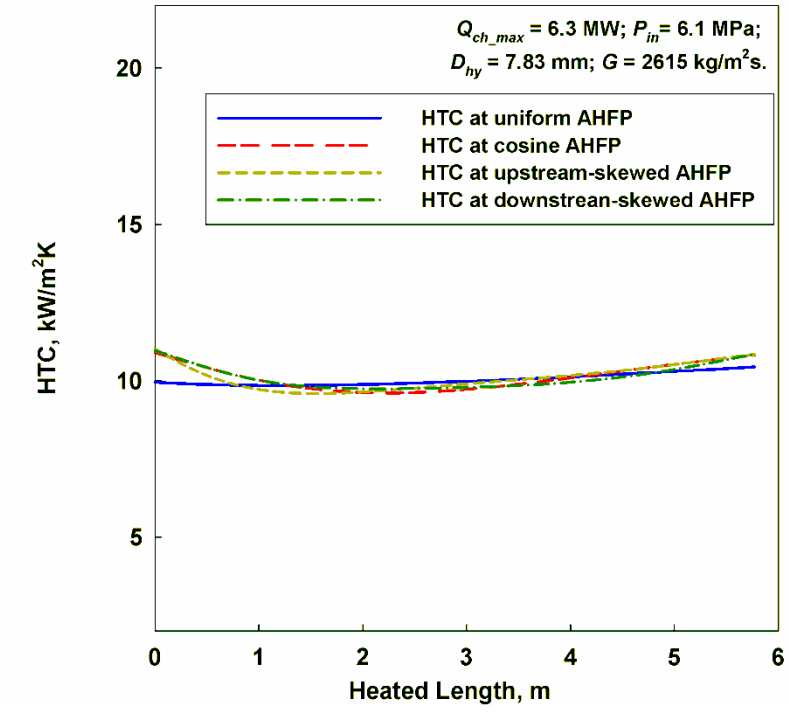

(b)

Figure 5.5. HTC profiles along SCW (a) and SHS (b) channels at maximum channel power.

After determining wall temperature, inner sheath temperature, $T_{sh,id}$, was determined from Fourier's law, assuming that the sheath material is Inconel-718:

$$q' = 2\pi k_{sh} N_{sh} \frac{T_{sh,id} - T_w}{\ln\left(\frac{D_{sh,od}}{D_{sh,id}}\right)} \Rightarrow T_{sh,id} = \frac{q'}{2\pi k_{sh} N_{sh}} \ln\left(\frac{D_{sh,od}}{D_{sh,id}}\right) + T_w ,$$

where $D_{sh,o}$ is outer diameter of sheath and $D_{sh,i}$ is inner diameter of sheath, the latter being equal to the fuel pellet diameter. Therefore, we assumed perfect contact between sheath and pellet. To substantiate this assumption, we refer to a paper by Chan et al. (1999), where heat-transfer coefficient between pellet and sheath is evaluated to be 65kW/m^{2}K at CANDU-6 channels operating conditions. It means that in case of SHS channel, at maximum power the maximum temperature drop between fuel pellet and sheath will be about 25ºC, which only slightly affects fuel centerline temperature. At SCW channel conditions, additionally sheath will be pressed to pellet at much higher pressure (about 25MPa. Thermal conductivity of sheath, k_{sh}, depends on temperature, according to Sweet et al. (1987), as:

$$k_{sh} = 11.45 + 1.156 \cdot 10^{-2} T + 7.72 \cdot 10^{-6} T^2 , \qquad (5.22)$$

where T is measured in ºC.

Fuel centerline temperature was calculated by calculating by dividing fuel pellet radius into 10,000 elements and calculating temperature increase across each successive ring towards the center. Solution to radial steady-state temperature distribution in a cylindrical configuration with uniform internal heat generation rate was used.

If volumetric heat generation rate is equal to q'''., then at inner surface of a cylindrical layer of radius r and elementary thickness Δr temperature would be:

$$T(r-\Delta r) = T(r) + \frac{q'''}{4k_f}(r^2 - (r-\Delta r)^2), \tag{5.23}$$

where k_f is thermal conductivity of fuel.

The model was programmed in MATLAB (2007) software. Flowchart of the program is included in Appendix A. The program was tested against a reference case of CANDU-6 fuel channel operating conditions (coolant specific heat is constant and equal to 5.5 kJ/kg·K, P = 10 MPa, T_{in} = 260ºC, $\dot{m}$ = 28 kg/s, k_{sh} = 14W/m·K, k_f = 2.4. W/m·K, average power equal to 5.5 MW). Test results are in Appendix B. The main conclusion from test un is that maximum relative error is of the order 10^{-5} and there are single cases when values of temperatures differ in the second decimal place. It shows convincingly that the programmed model is reliable and should produce reasonable results when use to calculate temperature profiles at the channel conditions of interest.

Different fuels where considered as the alternative to UO_2 due to its possible inadmissibly high temperature in a SCW channel[5]. Main thermal properties are presented in Table 5.4, and thermal conductivities of fuels considered are plotted in Figure 5.6.

Table 5.2. Selected properties of fuels (at 0.1 MPa, 1000°C) (Kirillov et al. 2007).

Fuel	Molecular mass, amu	Melting point,°C	ρ, kg/m^3	c_p, J/kg·K	k, W/m·K
UO_2	270	2850	10,630	320	3.10
ThO_2	264	3500	9,960	263	2.61
MOX	271	2750	10,767	324	2.88
UC_2	262	2550	13,000	240	15.7
UN	252	2850	13,987	250	22.9
UC	250	2365	13,010	260	28.8

[5] One of the reasons why search for an alternative to UO_2 to be used in the current CANDU-6 is not a question of principle is because the outlet temperature reached by coolant is 310°C, which is 15°C below the inlet temperature of the SCWR. The other reason is that UO_2 has negative temperature reactivity coefficient.

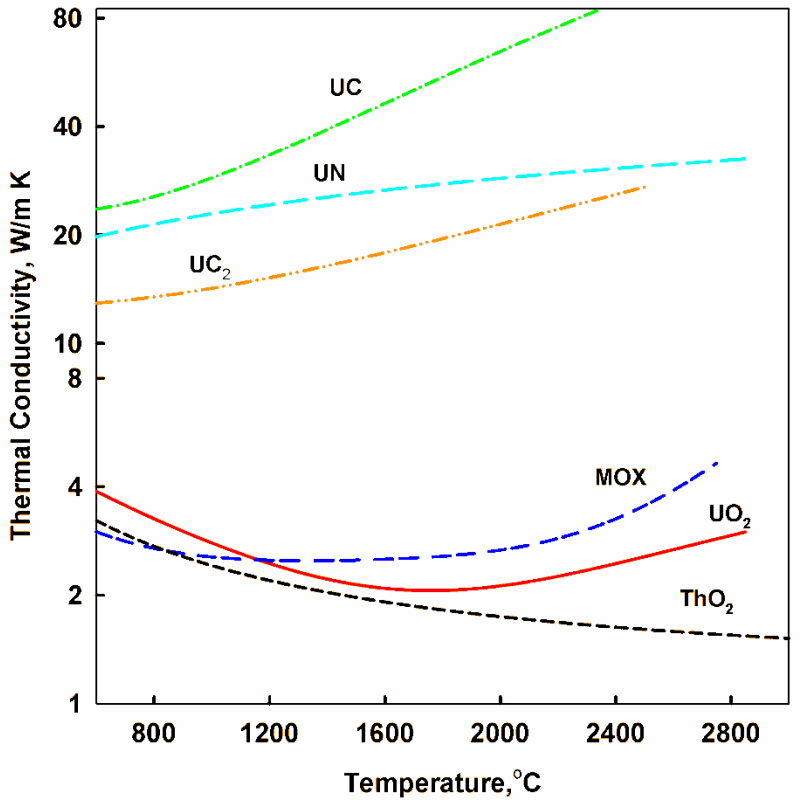

Figure 5.6. Thermal conductivities of nuclear fuels.

As it is seen from Figure 5.6, the fuels maybe distinguished into two groups according to their thermal conductivity *k* behaviour with temperature: for UO_2, ThO_2, and MOX, *k* is decreasing with temperature increase up to about 1650°C, while for UC_2, UC, and UN *k* is continuously increasing with the temperature.

5.4. Results of Heat-Transfer Calculations

Figures 5.7 – 5.30 represent bulk-fluid, fuel-element sheath, and fuel centerline temperature distributions along SCW and SHS channels at different AHFPs for UO_2, ThO_2, and UC. The graphs and numerical values for the rest three fuels are in the Appendix C. The graphs are arranged as follows: first temperature profiles along SCW and SHS channels are compared at average power, then – at maximum channel power.

For the uniform AHFP, there is an increase in HTC at about 1.5 m from the SCW channel inlet. Therefore, fuel centerline temperature decrease in that region and reaches the value that it had at the inlet only at a distance of about 3 m from the channel. In the case of SHS channel, the value of HTC stays almost constant, and one can observe almost linear increase in fuel centerline temperature.

In the case of the cosine-like AHFP, HTC drops sharply at a distance of 1 m from SCW channel inlet, and an accelerated increase in fuel centerline temperature is observes. Closer to the channel outlet HTC value recovers slightly and fuel temperature along with the decreased heat flux smoothly decreases. Along the SHS channel, HTC stays almost constant, and fuel temperature reaches maximum value at approximately channels center.

In the case of the upstream-skewed AHFP, maximum channel power is reached close to the channel inlet (for fuels with low thermal conductivity) and close to the channel outlet (for fuels with high thermal conductivity), and HTC value sharply drops at about 0.5 m from the inlet. Fuel temperature, therefore, increases to peak value at about 1.5 m from the inlet, then gradually drops due to improved heat transfer along next 3 meters and rapidly decreases along the last meter of the channel outlet. Similar behaviour is observed for the SHS channel.

In the case of the downstream-skewed AHFP, the fuel centerline temperature behaves in the opposite manner as compared to the upstream-skewed AHFP along SCW channel. Namely, though HTC drops at the inlet, fuel temperature reaches about 70% of peak value along the first meter of the channel and then gradually reaches its peak value. At the channel inlet, due to rapid drop in heat flux, fuel centerline temperature rapidly decreases to the values close of that of the coolant. Similar behaviour is observed for the SHS channel.

Numerical values of fuel centerline temperatures at 12 points for the fuels are presented in Appendix D at all AHFPs.

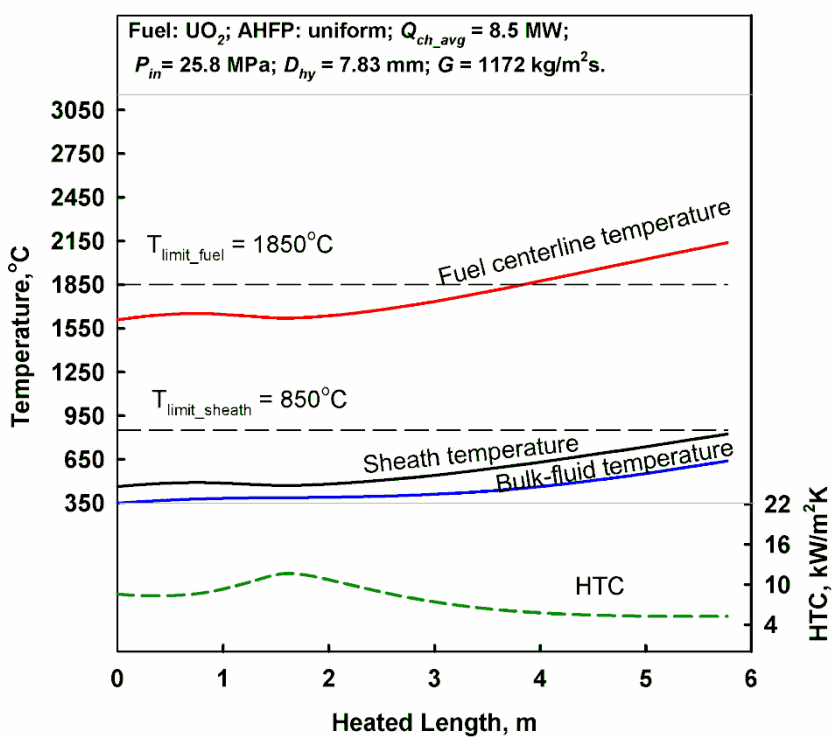

(a)

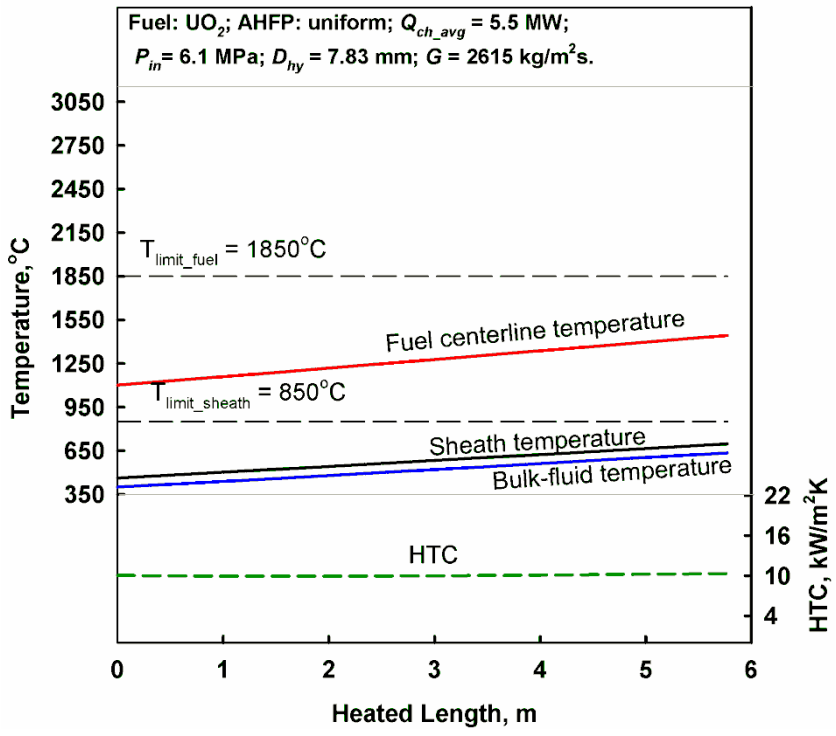

(b)

Figure 5.7. Temperature profiles at average power and uniform AHFP. (a) – SCW and (b) – SHS channels. Fuel: UO_2.

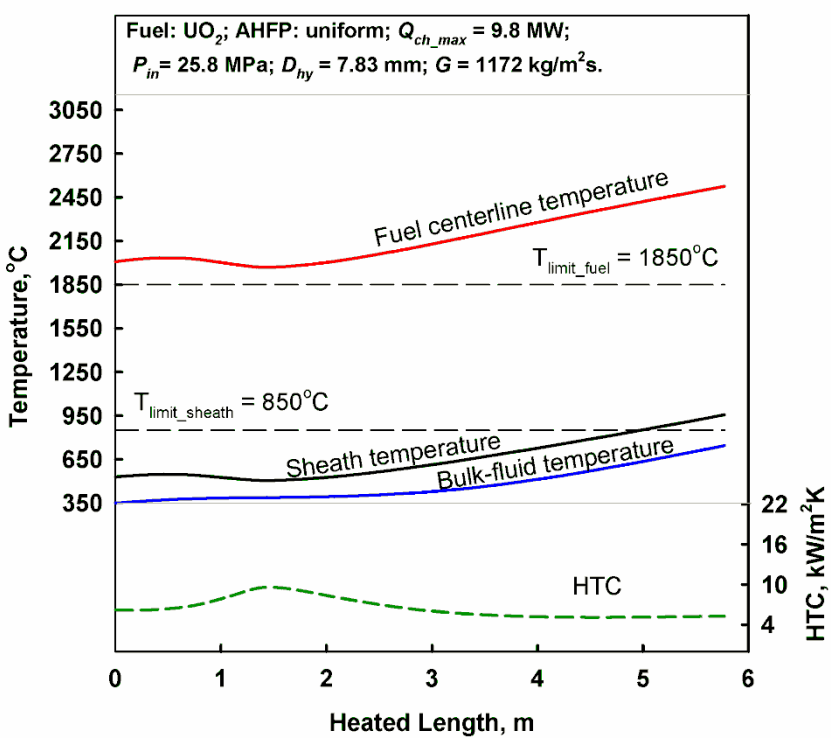

(a)

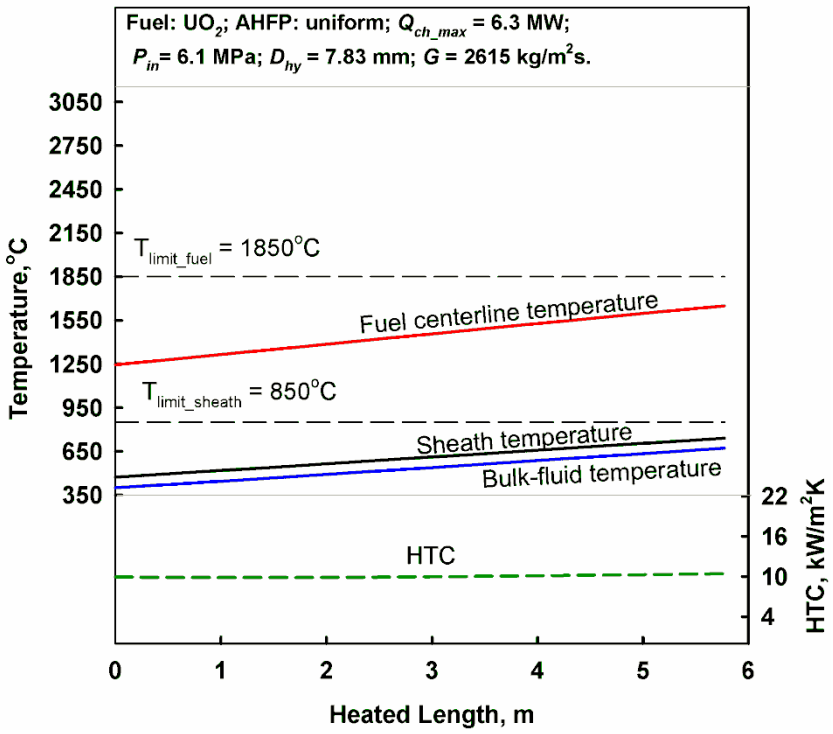

(b)

Figure 5.8. Temperature profiles at maximum power and uniform AHFP. (a) – SCW and (b) – SHS channels. Fuel: UO_2.

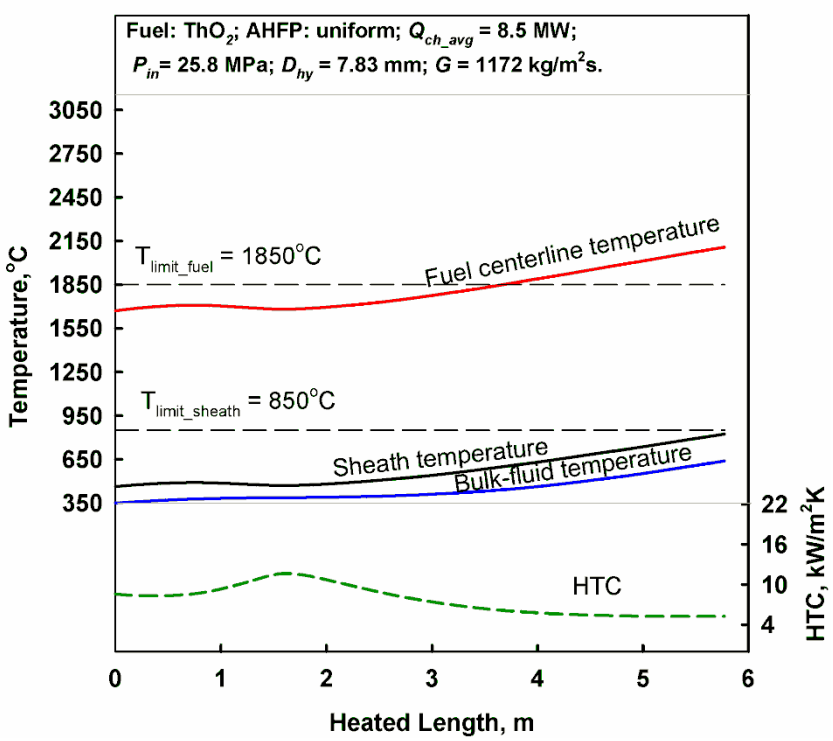

(a)

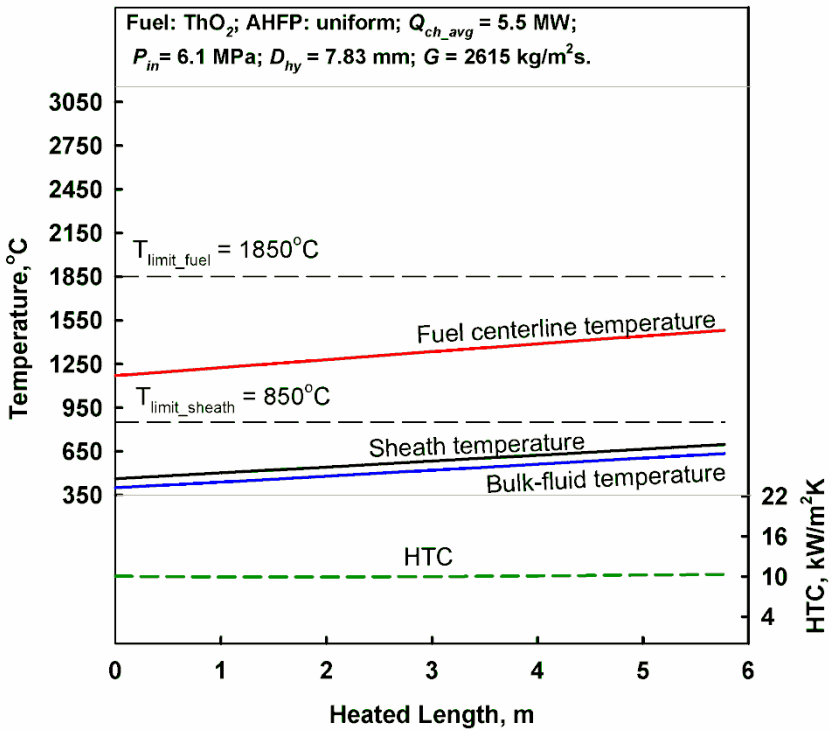

(b)

Figure 5.9. Temperature profiles at average power and uniform AHFP. (a) – SCW and (b) – SHS channels. Fuel: ThO_2.

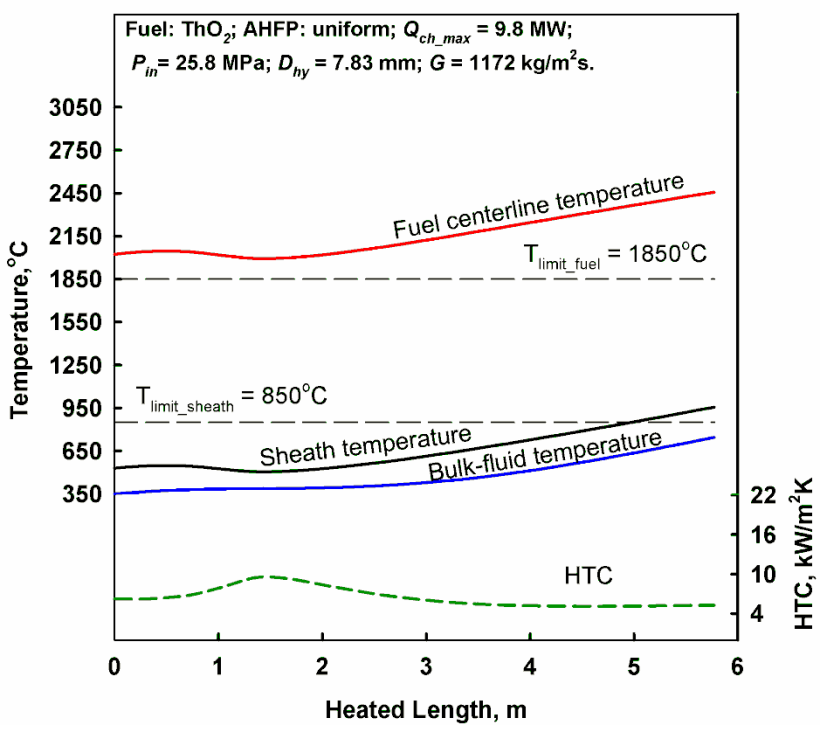

(a)

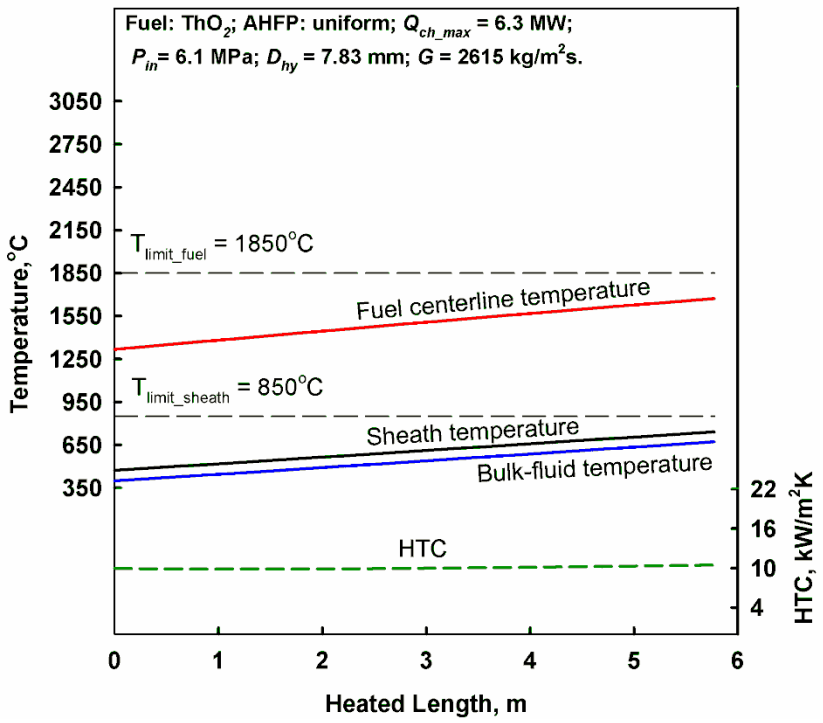

(b)

Figure 5.10. Temperature profiles at maximum power and uniform AHFP. (a) – SCW and (b) – SHS channels. Fuel: ThO_2.

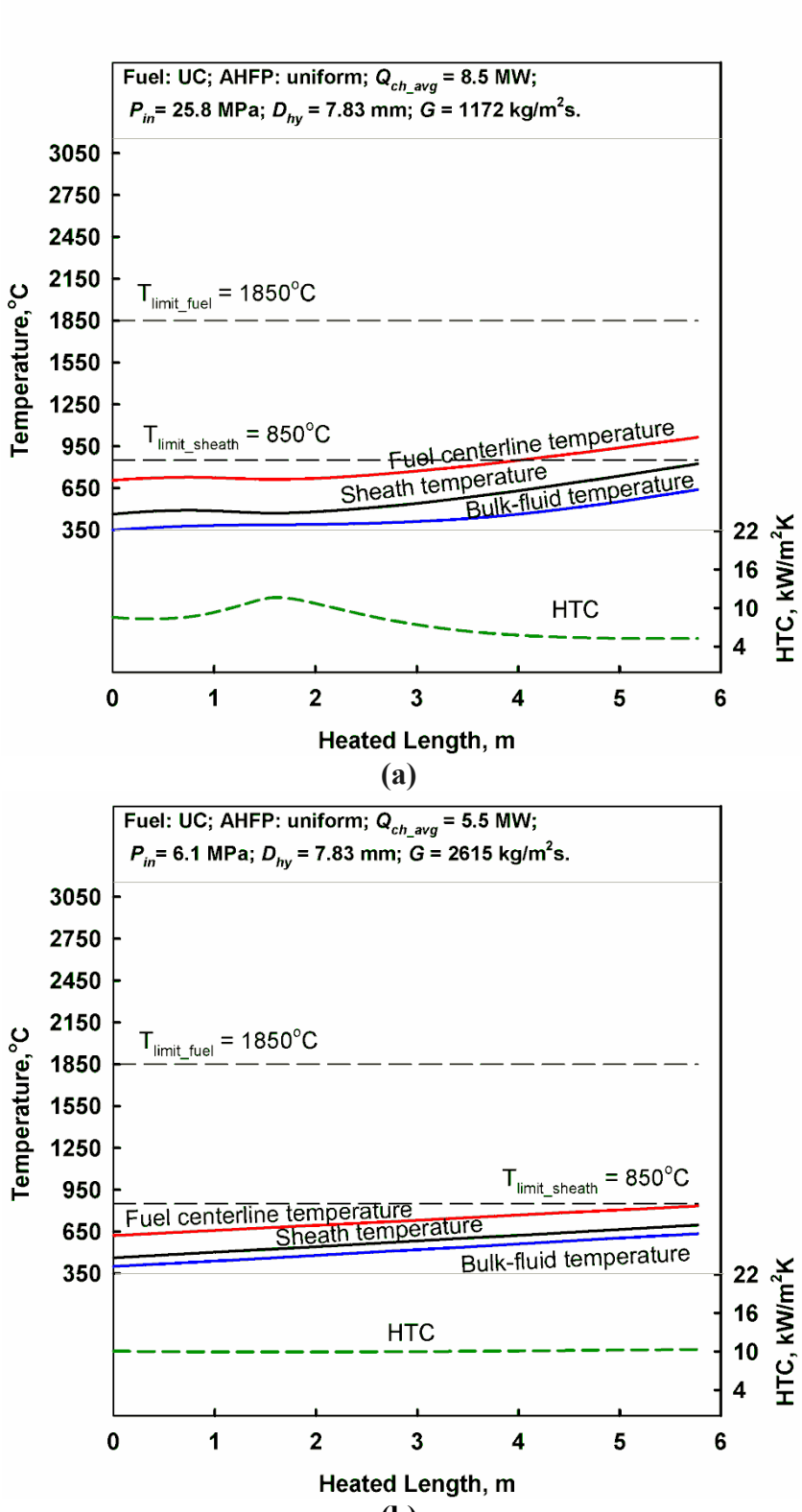

Figure 5.11. Temperature profiles at average power and uniform AHFP. (a) – SCW and (b) – SHS channels. Fuel: UC.

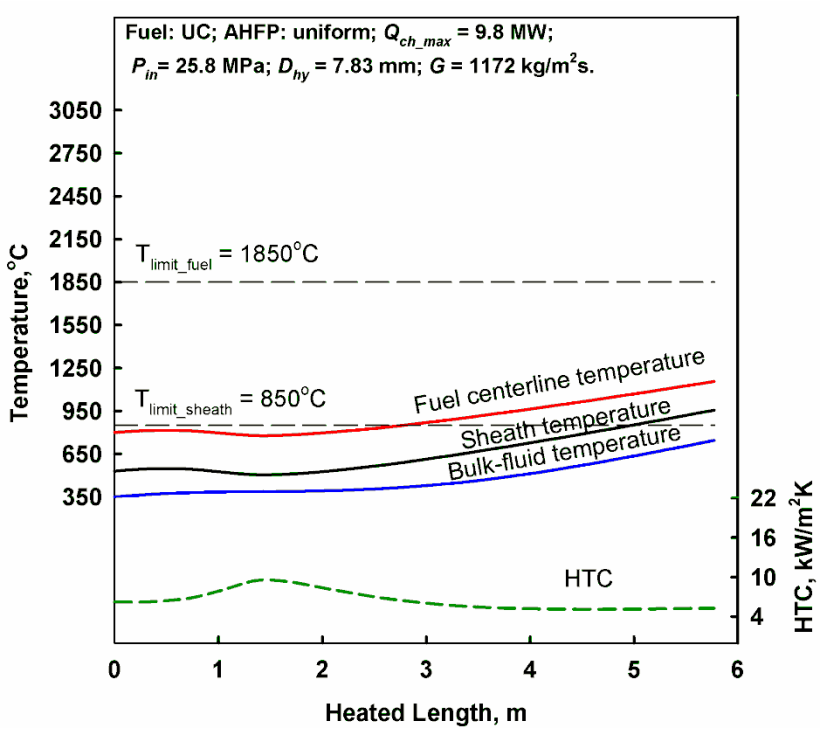

(a)

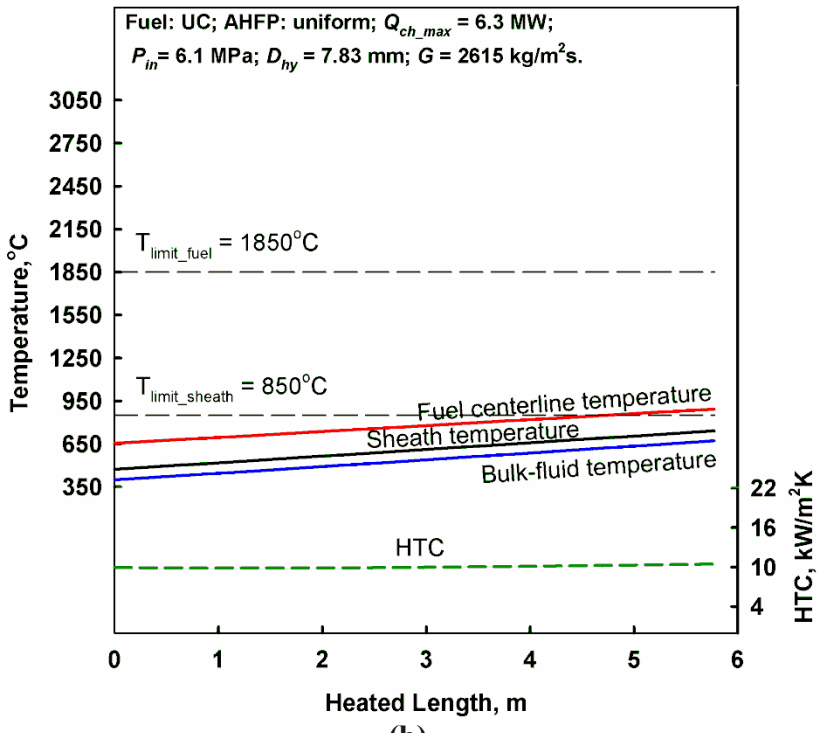

(b)

Figure 5.12. Temperature profiles at maximum power and uniform AHFP. (a) – SCW and (b) – SHS channels. Fuel: UC.

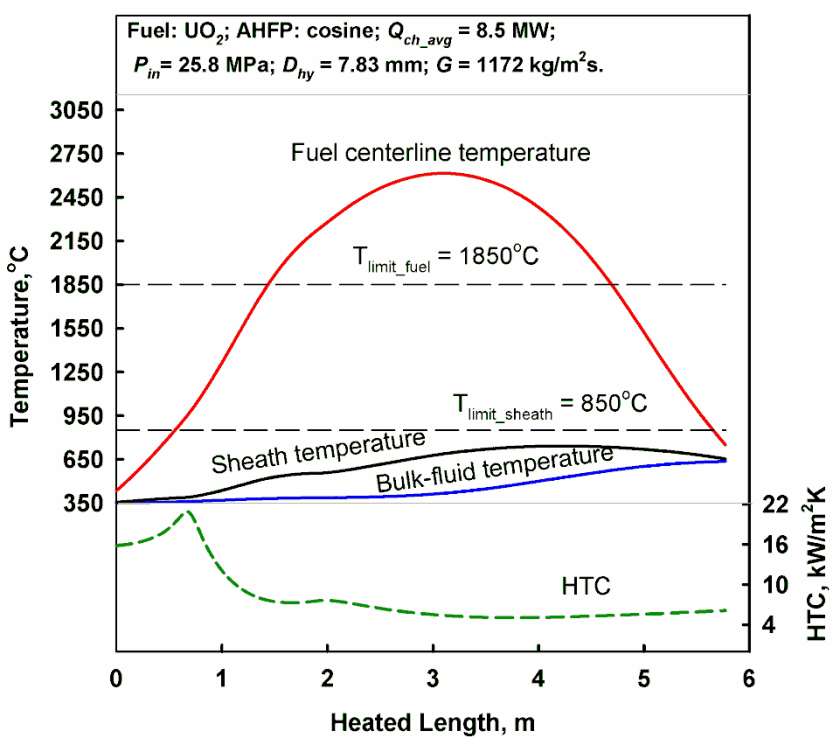

(a)

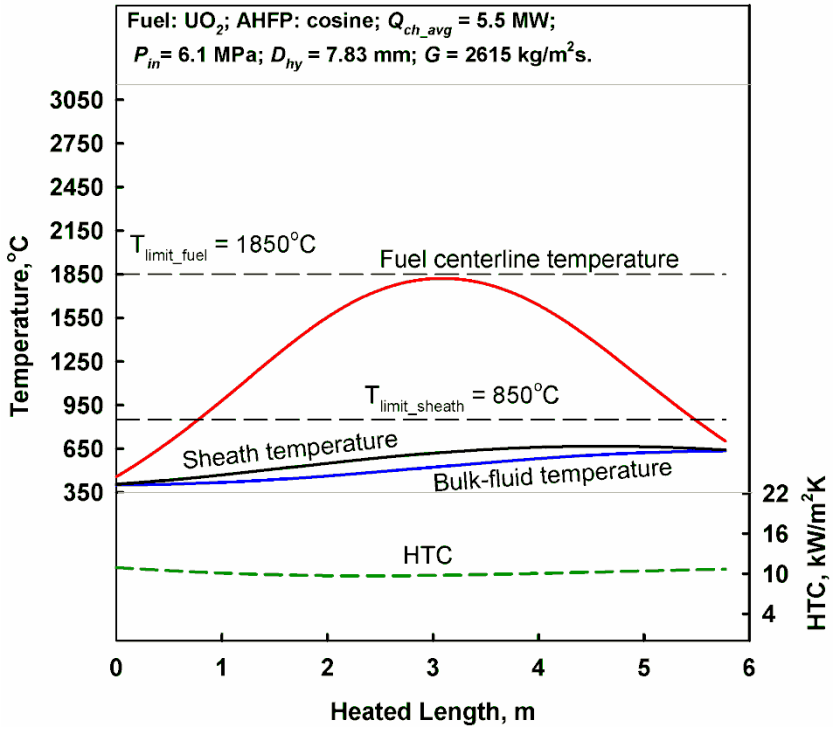

(b)

Figure 5.13. Temperature profiles at average power and cosine-like AHFP. (a) – SCW and (b) – SHS channels. Fuel: UO_2.

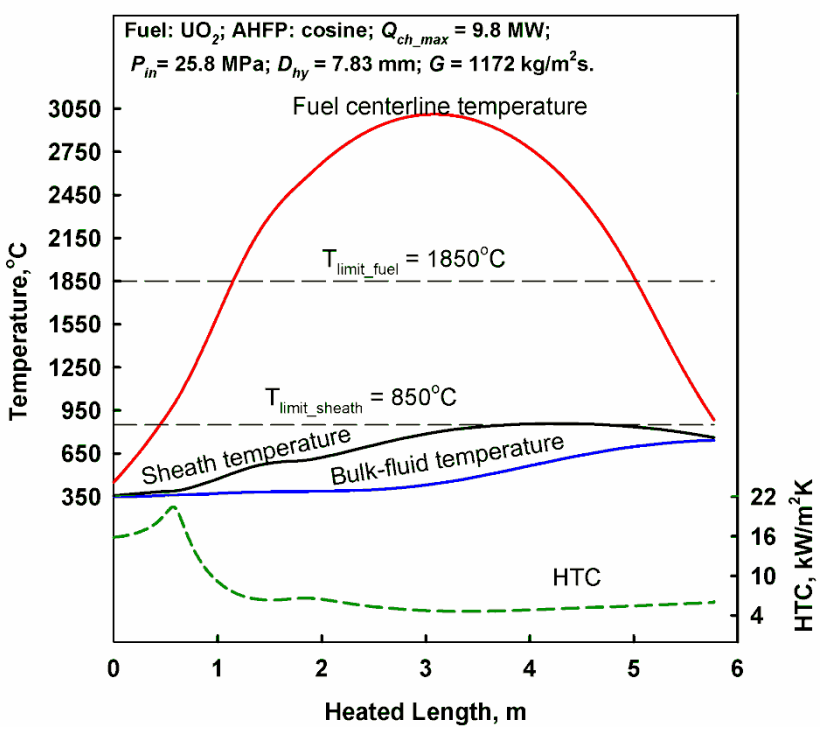

(a)

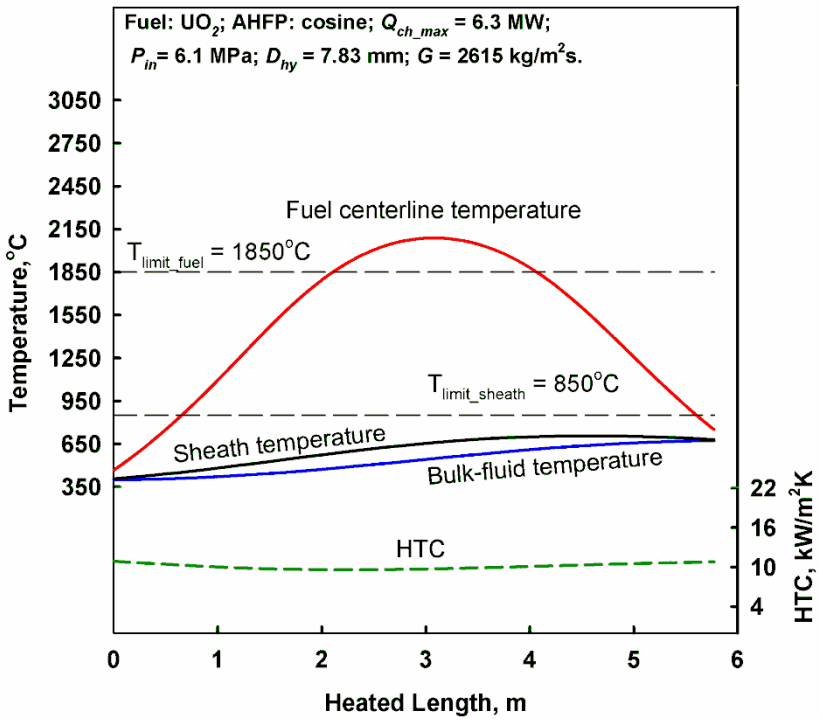

(b)

Figure 5.14. Temperature profiles at maximum power and cosine-like AHFP. (a) – SCW and (b) – SHS channels. Fuel: UO_2.

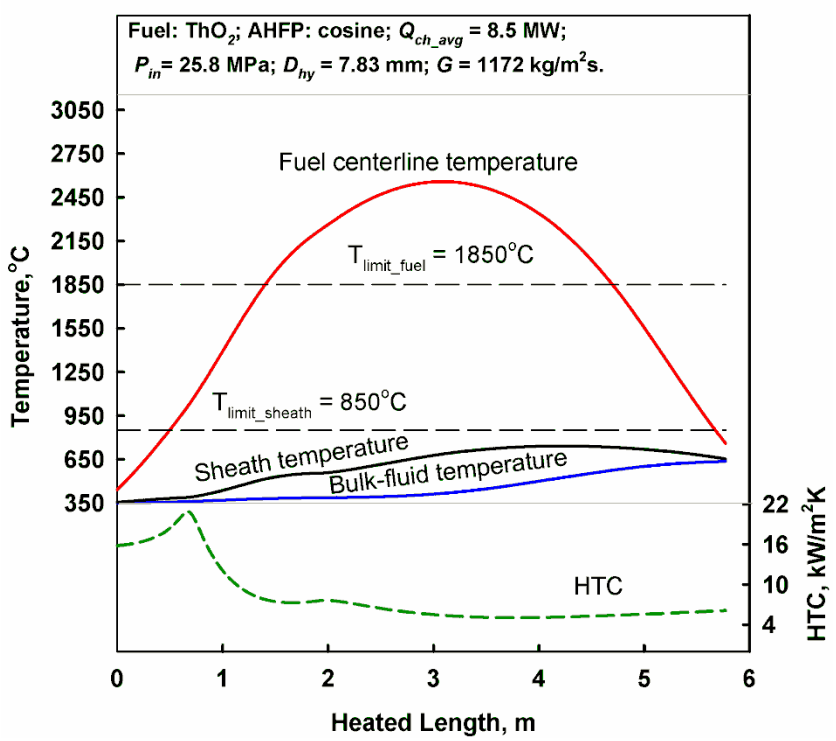

(a)

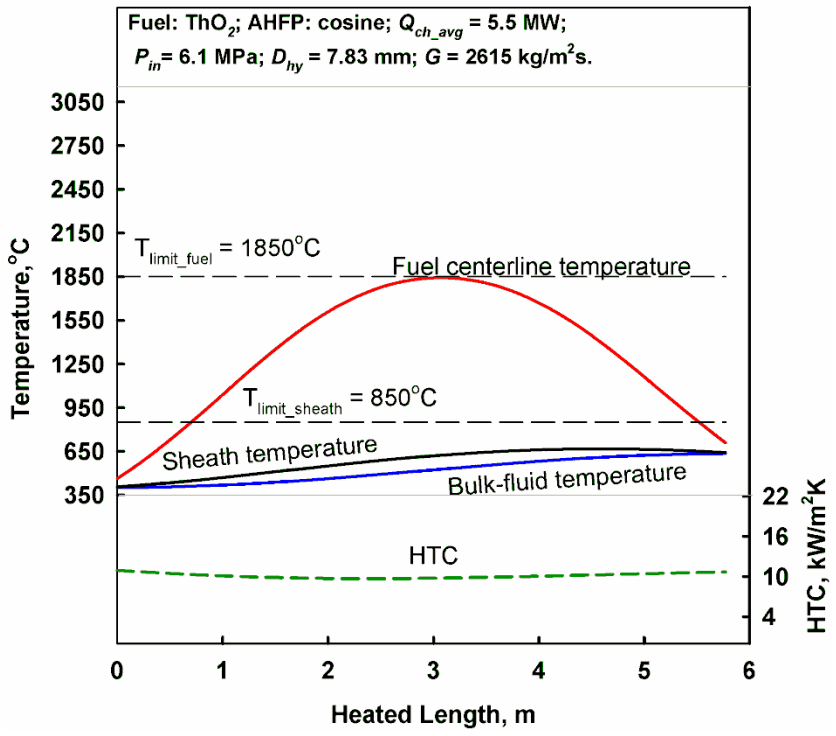

(b)

Figure 5.15. Temperature profiles at average power and cosine-like AHFP. (a) – SCW and (b) – SHS channels. Fuel: ThO_2.

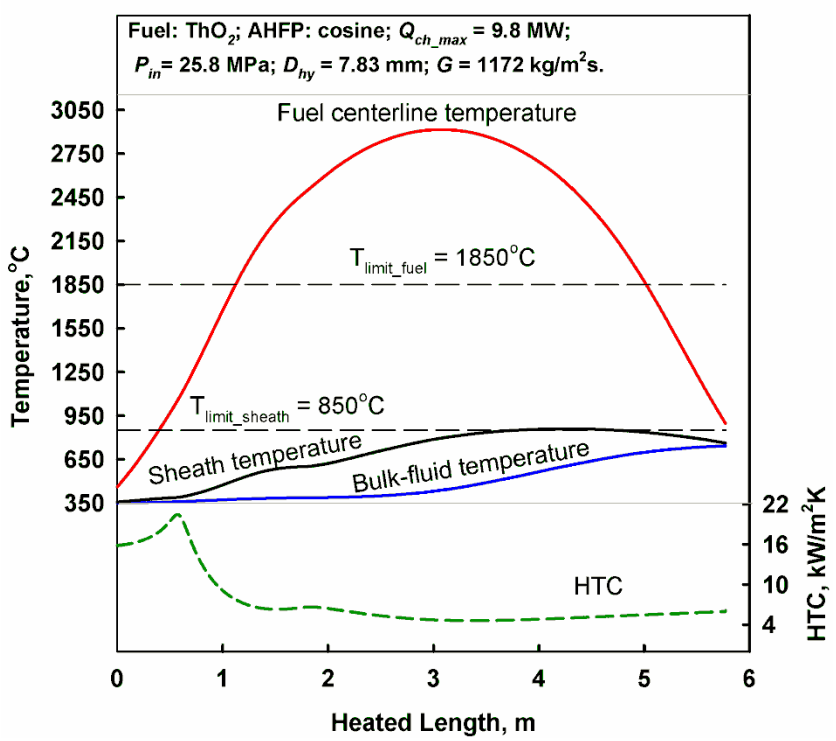

(a)

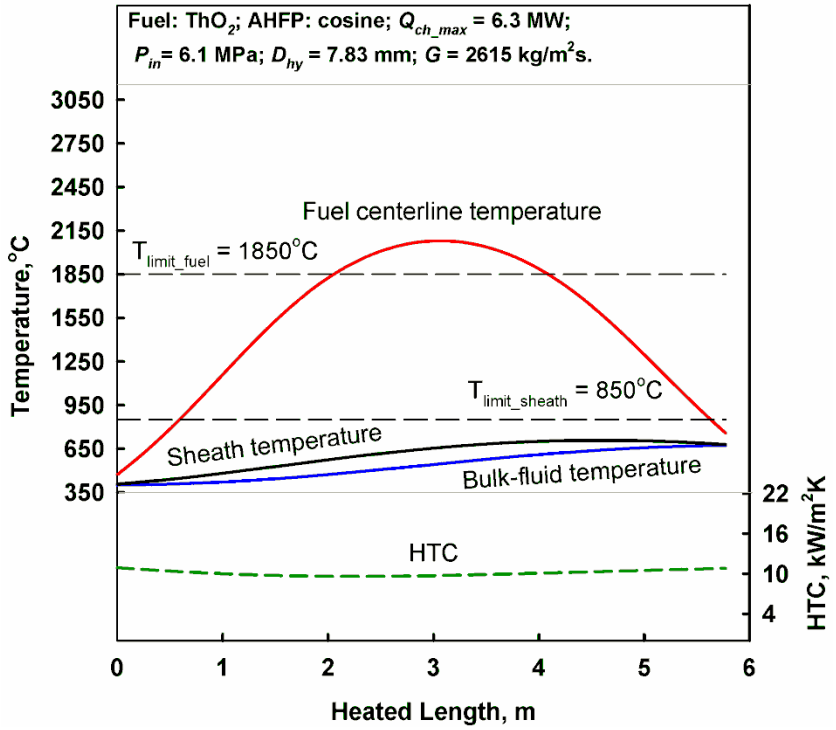

(b)

Figure 5.16. Temperature profiles at maximum power and cosine-like AHFP. (a) – SCW and (b) – SHS channels. Fuel: ThO_2.

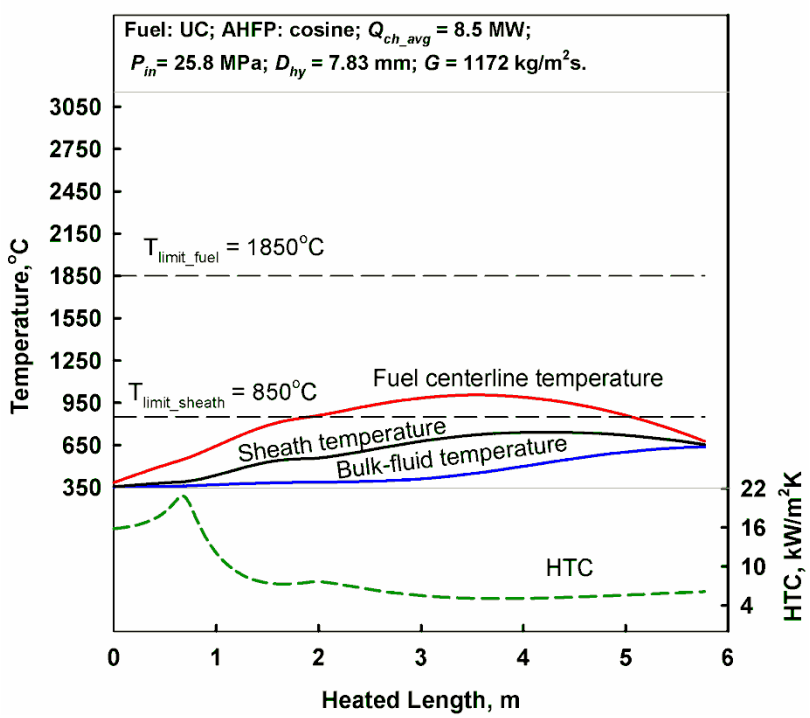

(a)

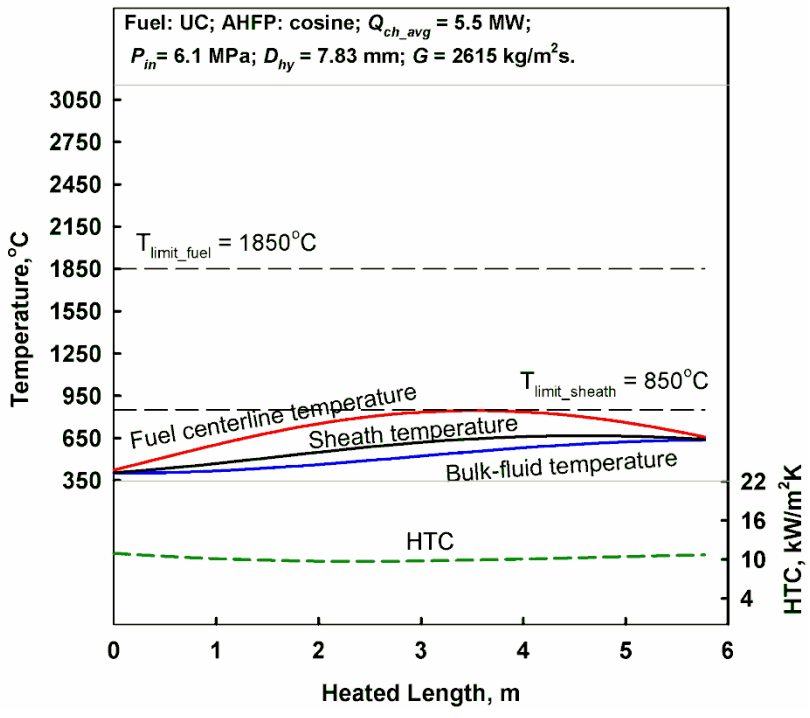

(b)

Figure 5.17. Temperature profiles at average power and cosine-like AHFP. (a) – SCW and (b) – SHS channels. Fuel: UC.

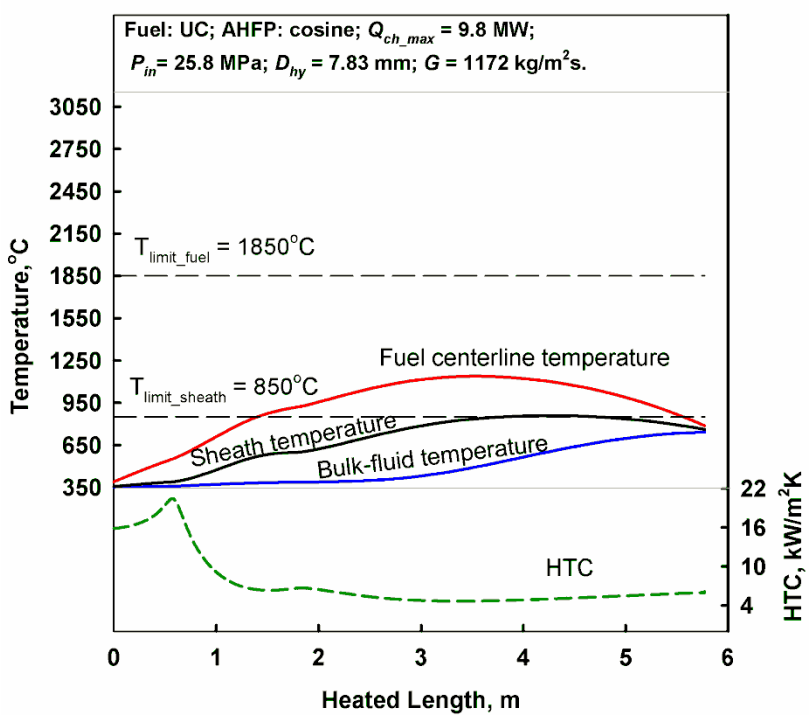

(a)

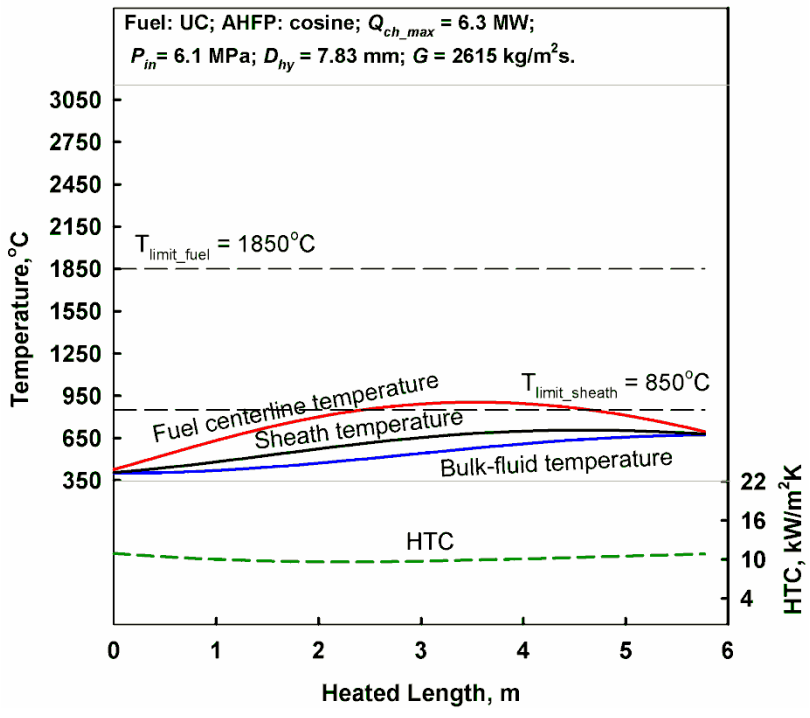

(b)

Figure 5.18. Temperature profiles at maximum power and cosine-like AHFP. (a) – SCW and (b) – SHS channels. Fuel: UC.

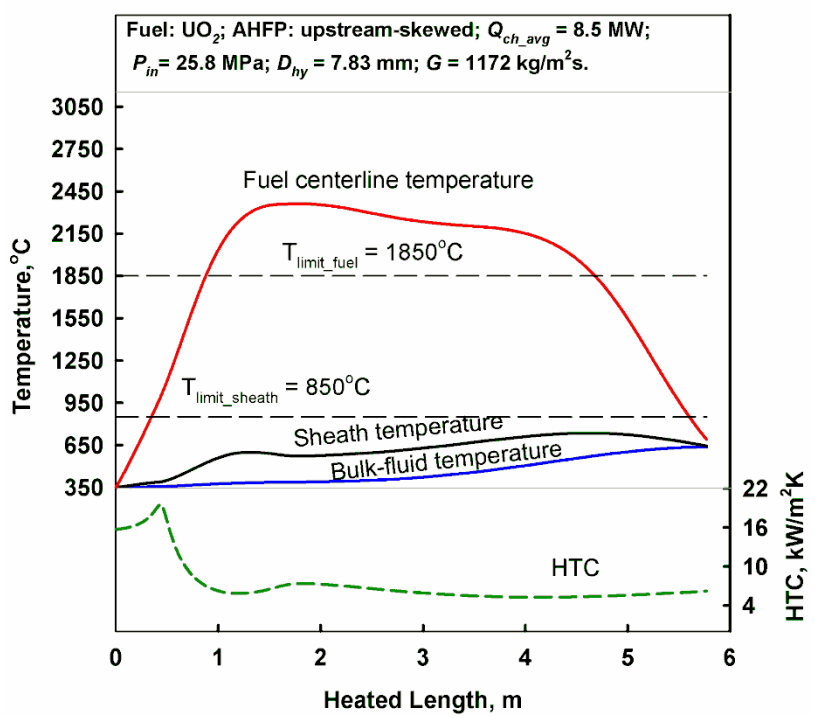

(a)

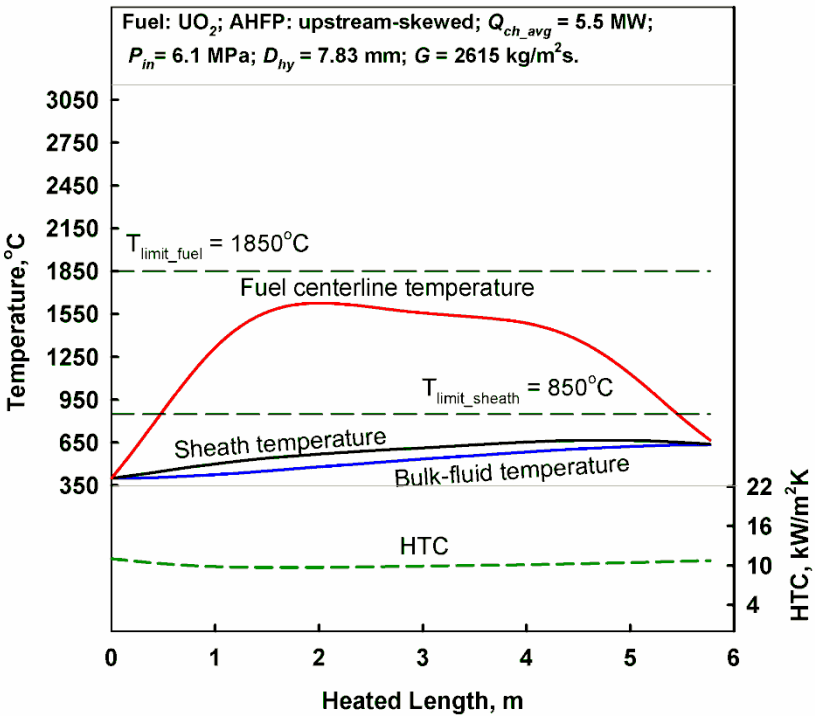

(b)

Figure 5.19. Temperature profiles at average power and upstream-skewed AHFP. (a) – SCW and (b) – SHS channels. Fuel: UO_2.

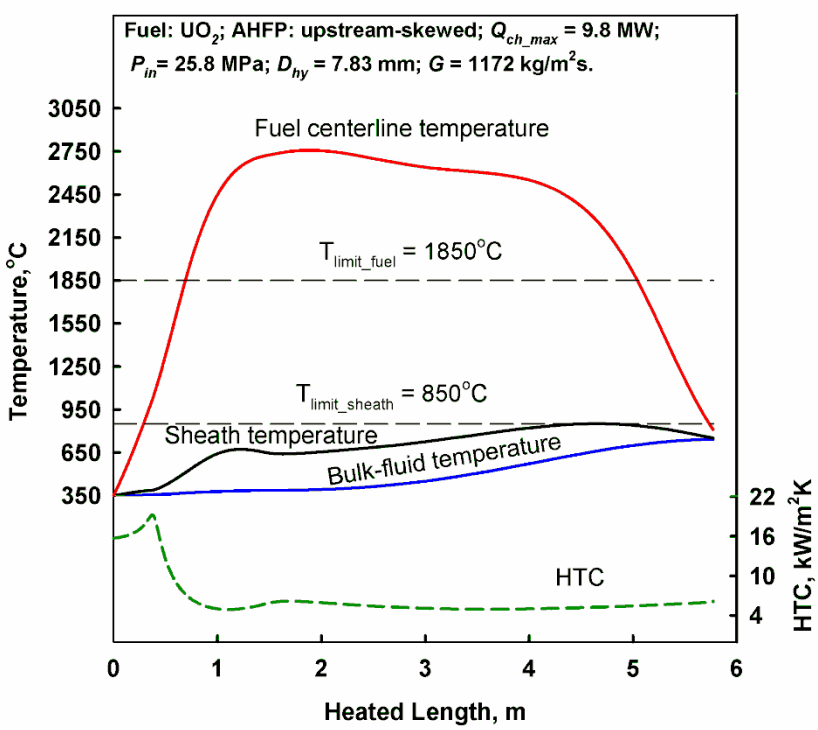

(a)

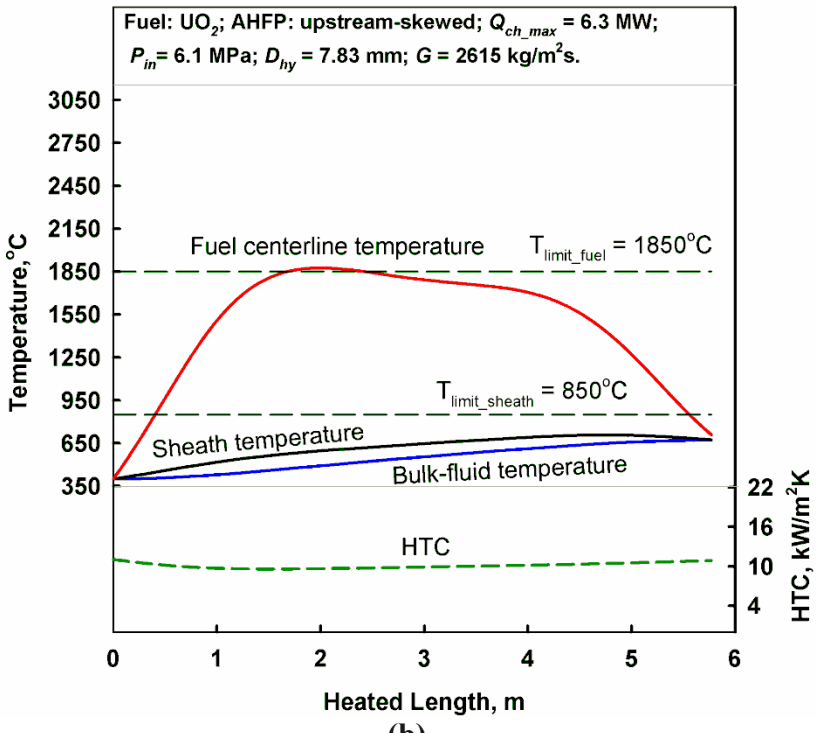

(b)

Figure 5.20. Temperature profiles at maximum power and upstream-skewed AHFP. (a) – SCW and (b) – SHS channels. Fuel: UO_2.

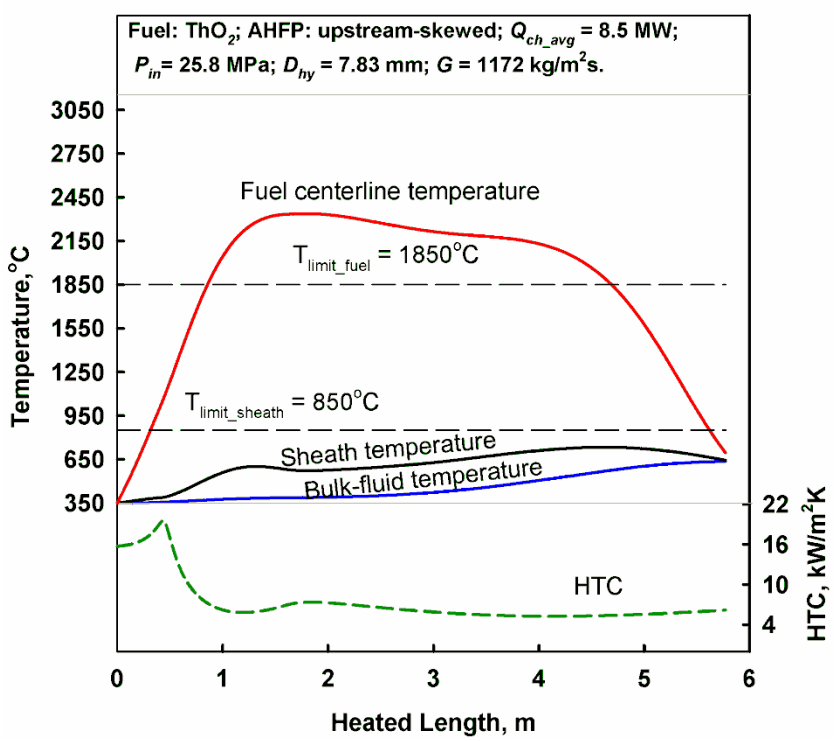

(a)

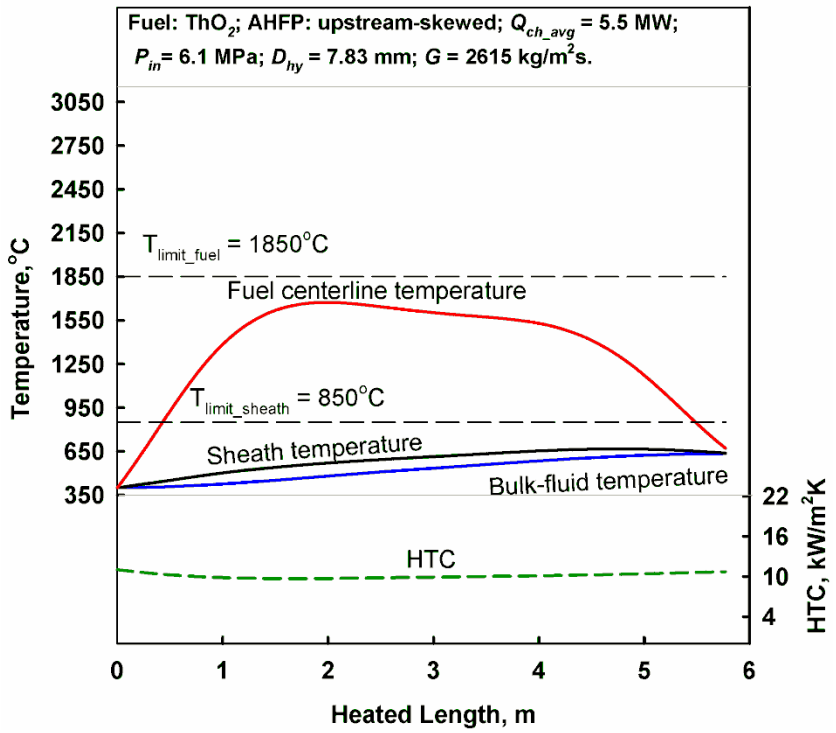

(b)

Figure 5.21. Temperature profiles at average power and upstream-skewed AHFP. (a) – SCW and (b) – SHS channels. Fuel: ThO_2.

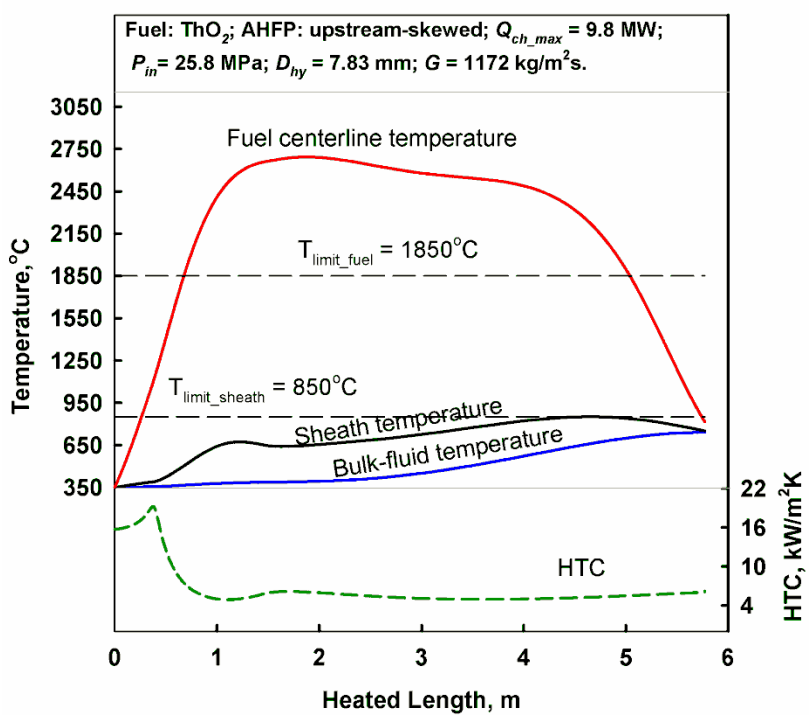

(a)

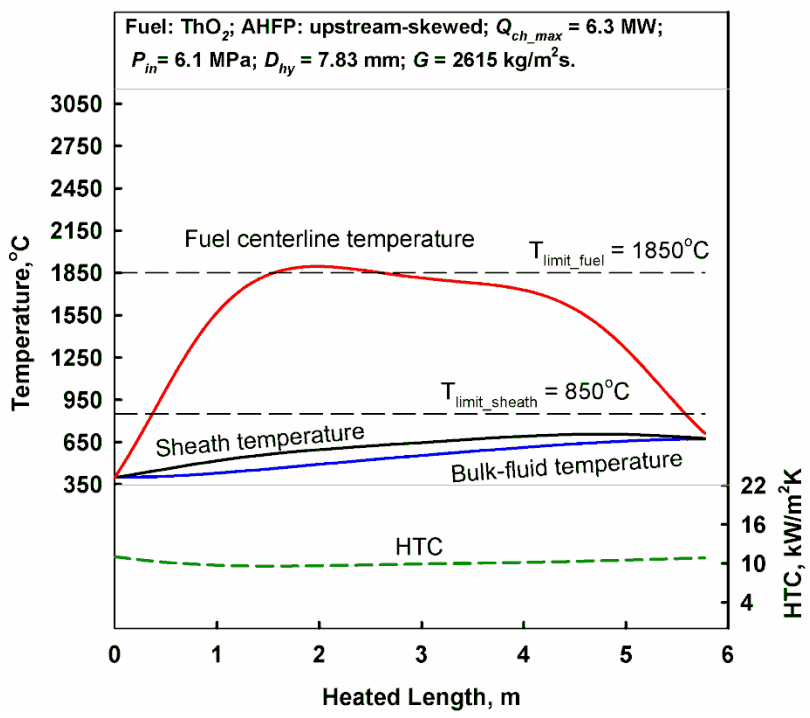

(b)

Figure 5.22. Temperature profiles at maximum power and upstream-skewed AHFP. (a) – SCW and (b) – SHS channels. Fuel: ThO_2.

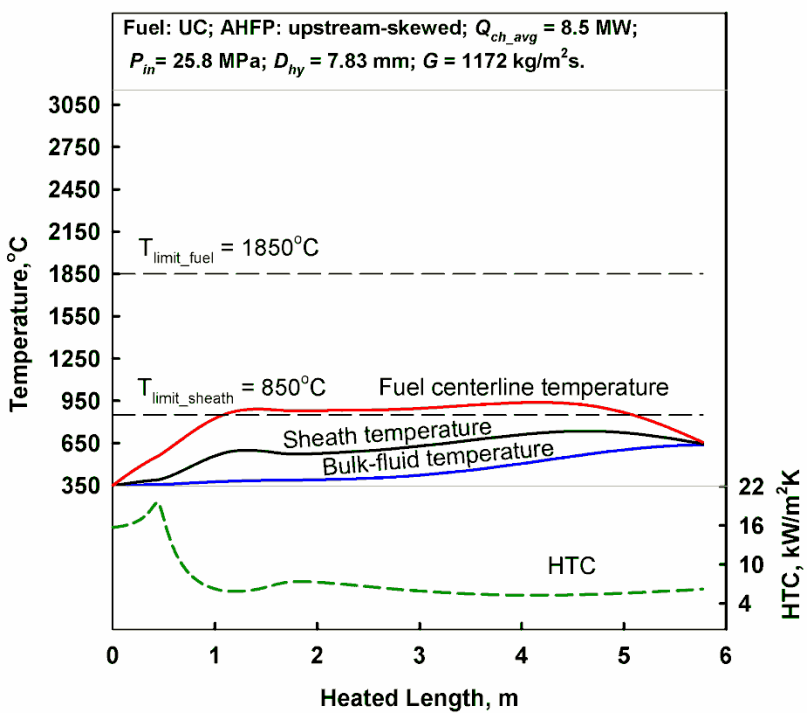

(a)

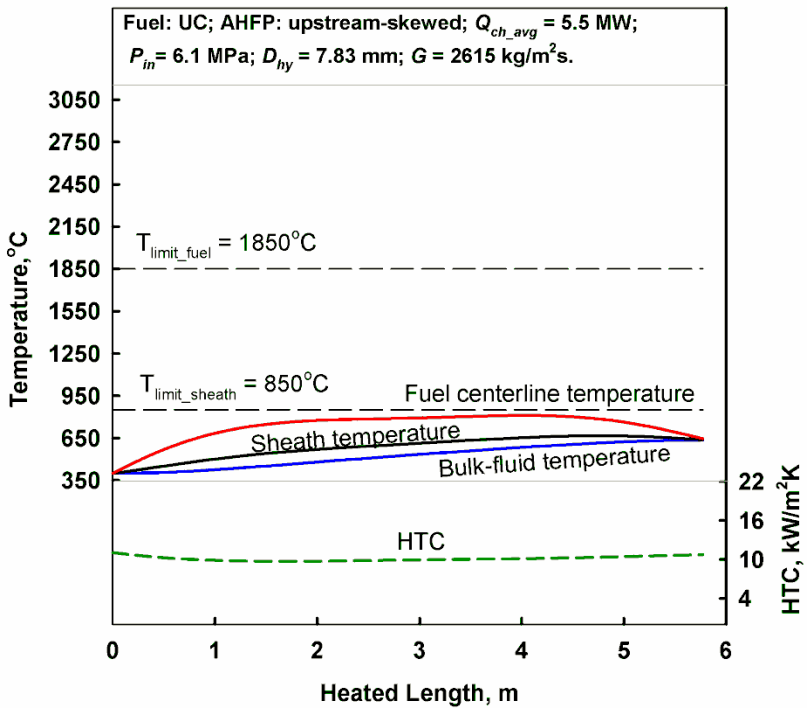

(b)

Figure 5.23. Temperature profiles at average power and upstream-skewed AHFP. (a) – SCW and (b) – SHS channels. Fuel: UC.

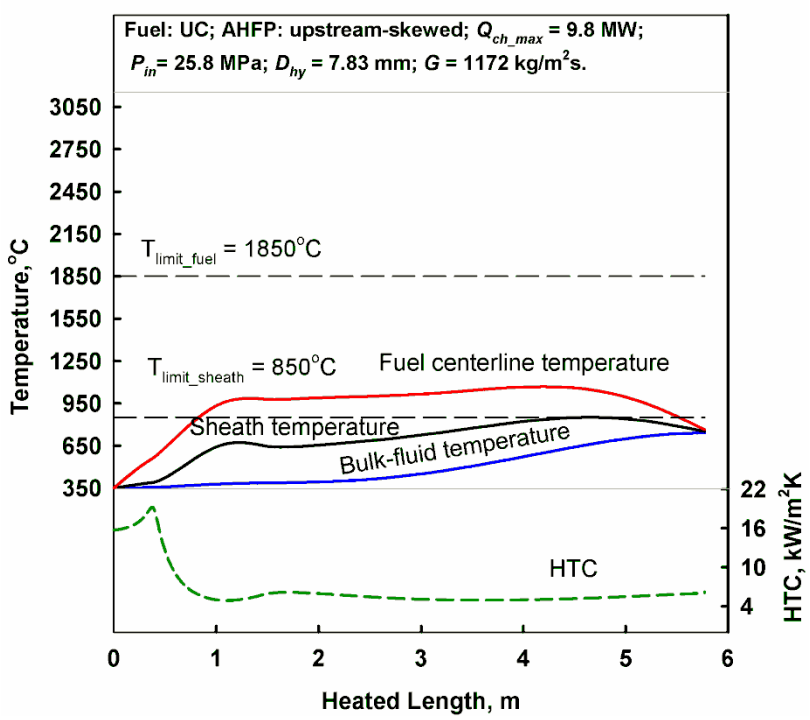

(a)

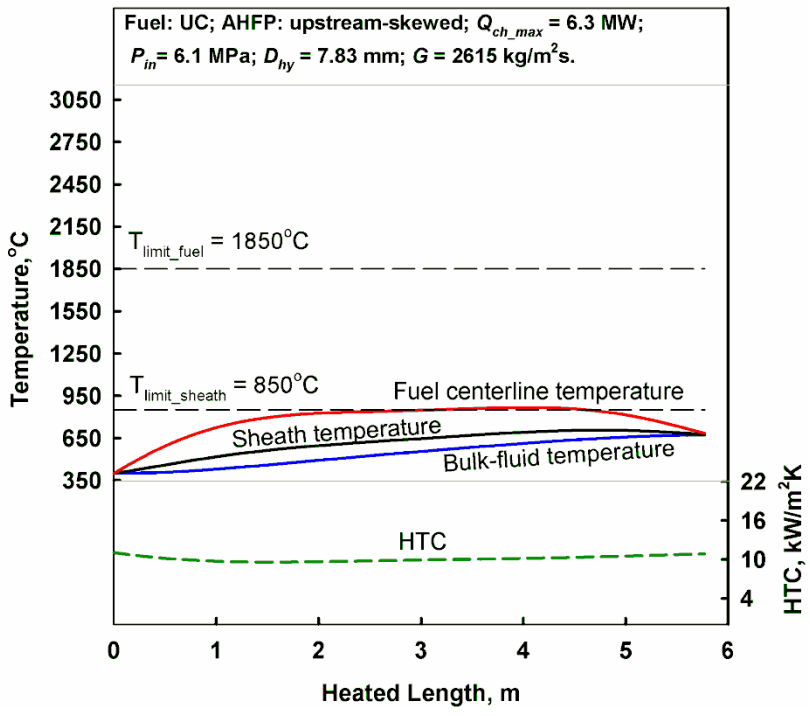

(b)

Figure 5.24. Temperature profiles at maximum power and upstream-skewed AHFP. (a) – SCW and (b) – SHS channels. Fuel: UC.

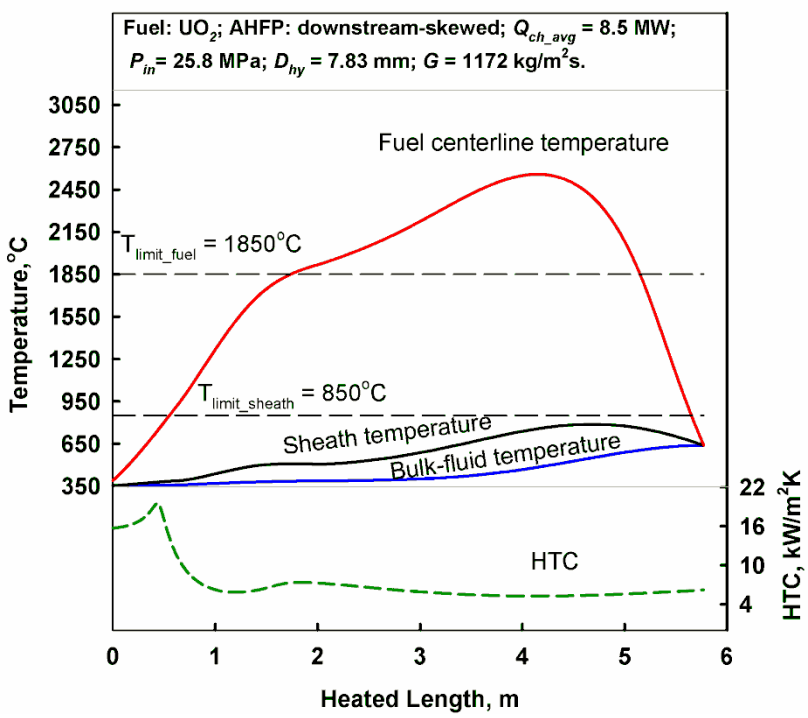

(a)

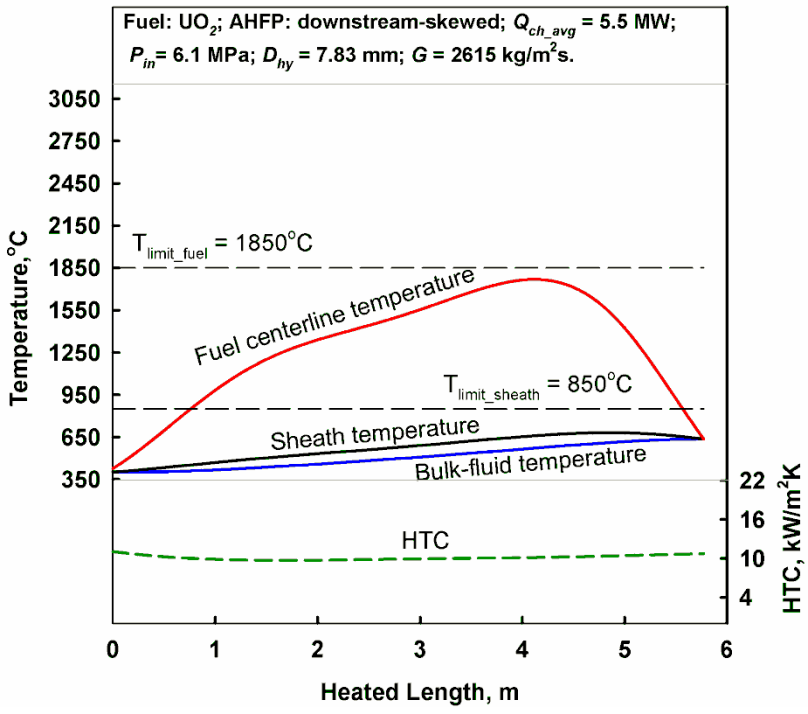

(b)

Figure 5.25. Temperature profiles at average power and downstream-skewed AHFP. (a) – SCW and (b) – SHS channels. Fuel: UO_2.

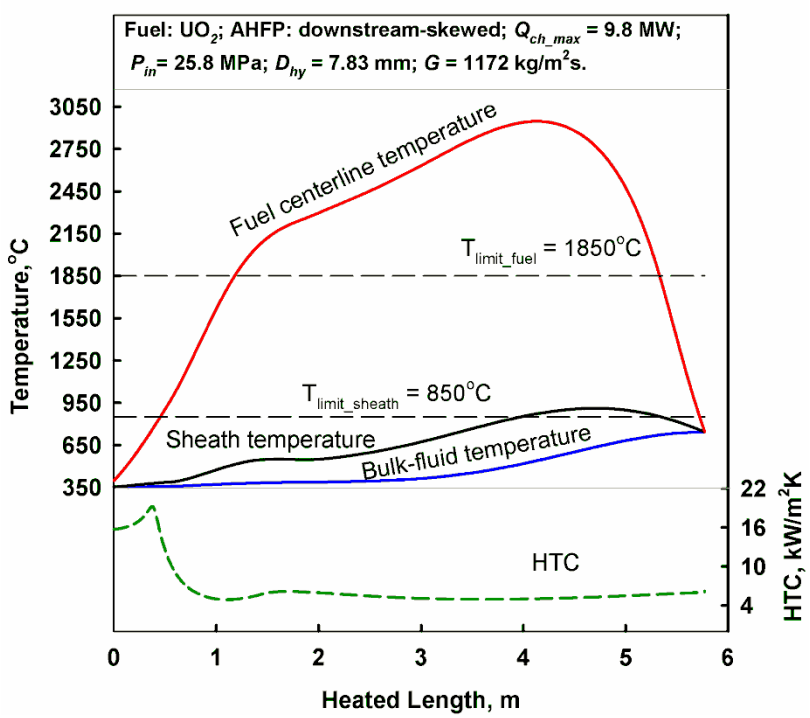

(a)

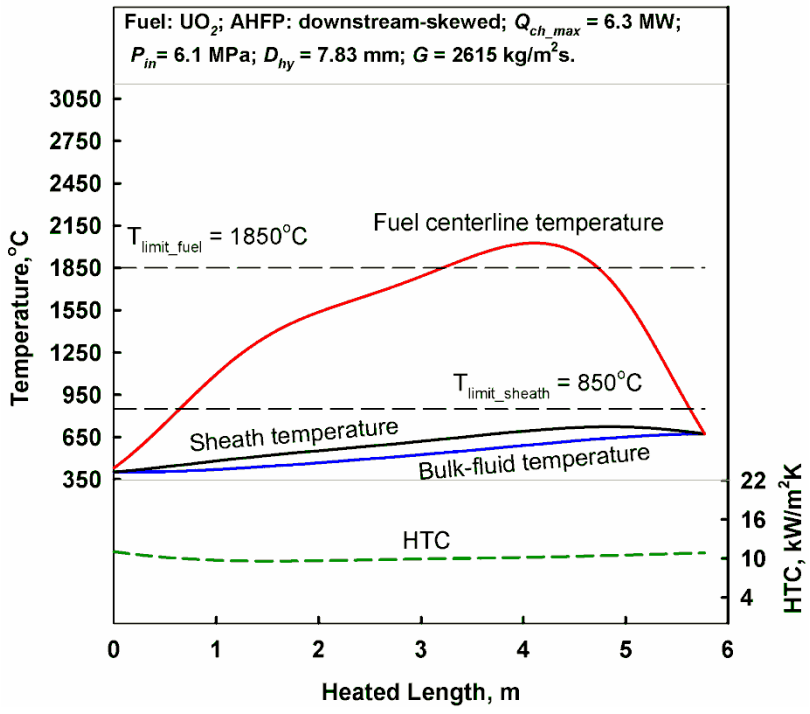

(b)

Figure 5.26. Temperature profiles at maximum power and downstream-skewed AHFP. (a) – SCW and (b) – SHS channels. Fuel: UO_2.

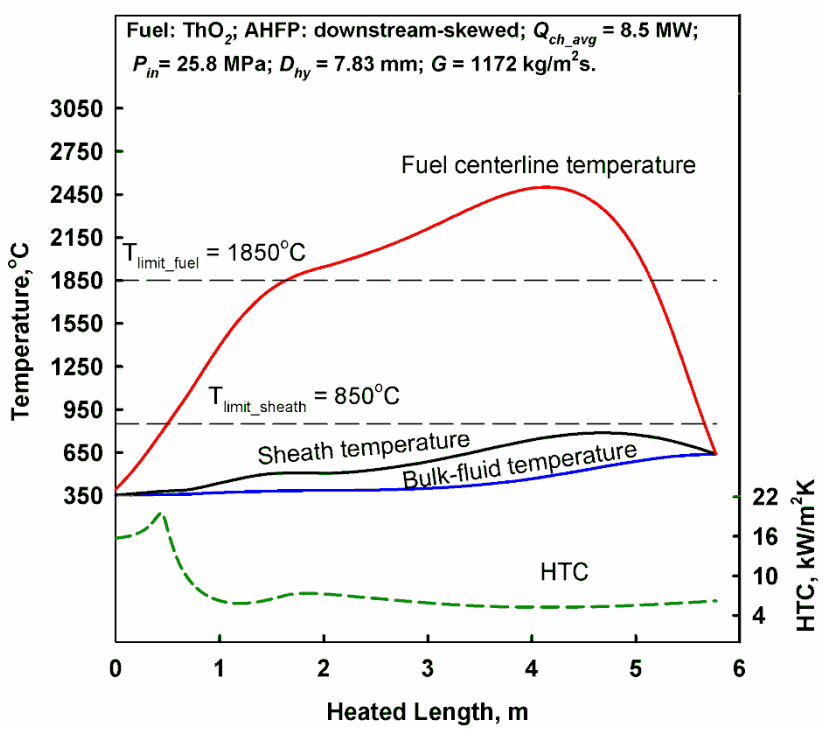

(a)

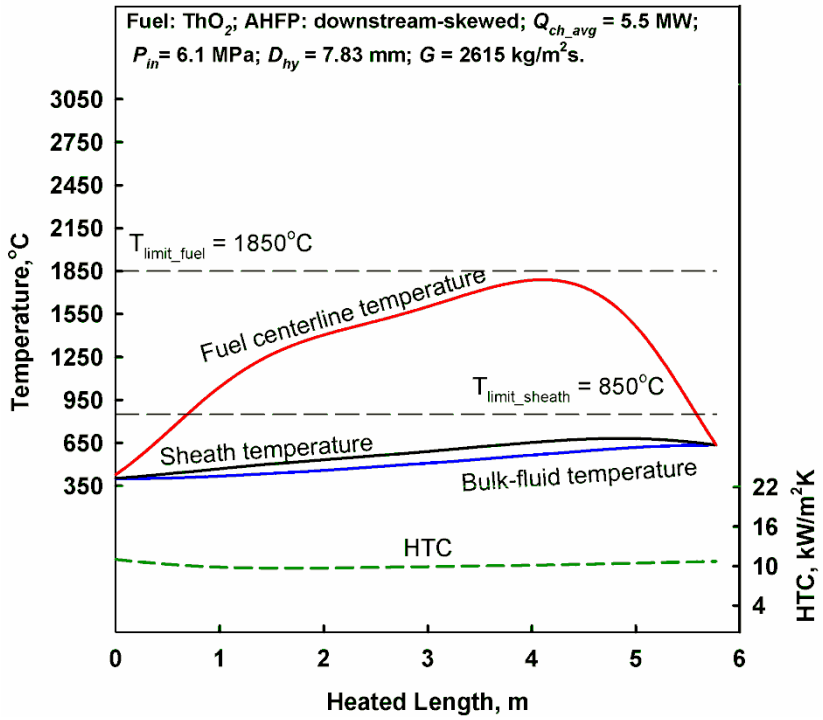

(b)

Figure 5.27. Temperature profiles at average power and downstream-skewed AHFP. (a) – SCW and (b) – SHS channels. Fuel: ThO_2.

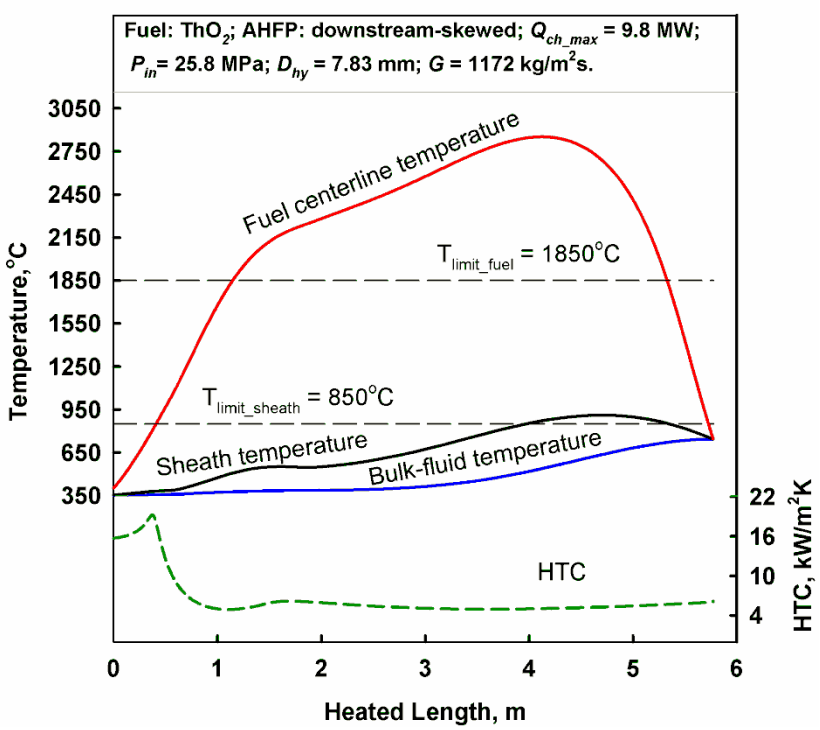

(a)

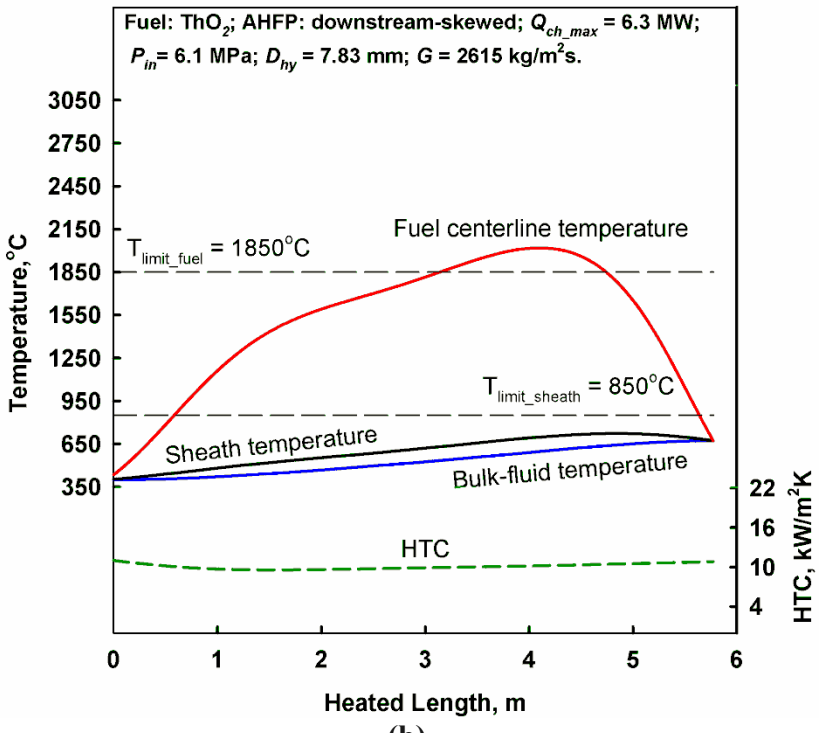

(b)

Figure 5.28. Temperature profiles at maximum power and downstream-skewed AHFP. (a) – SCW and (b) – SHS channels. Fuel: ThO_2.

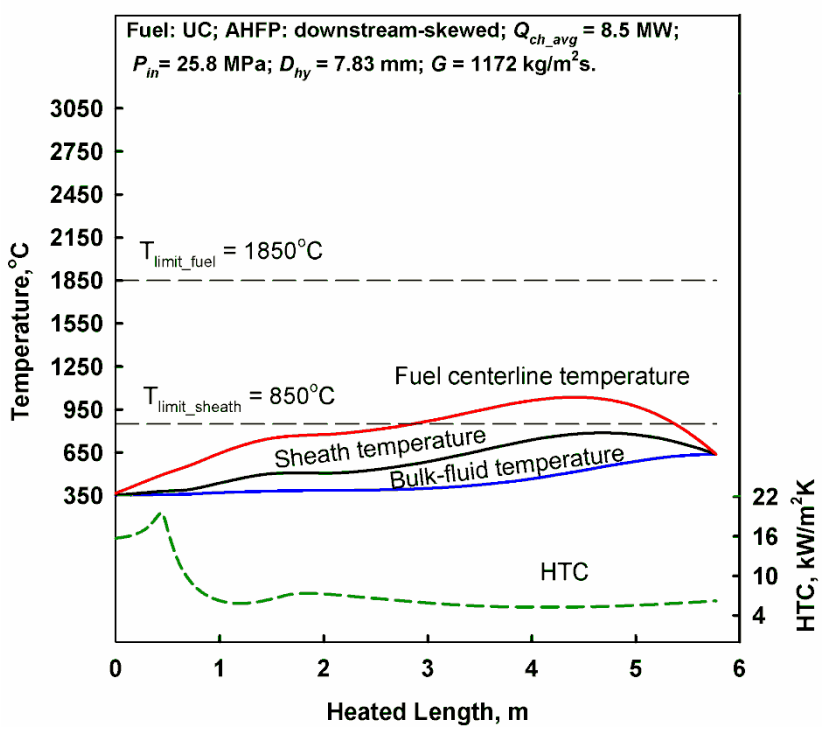

(a)

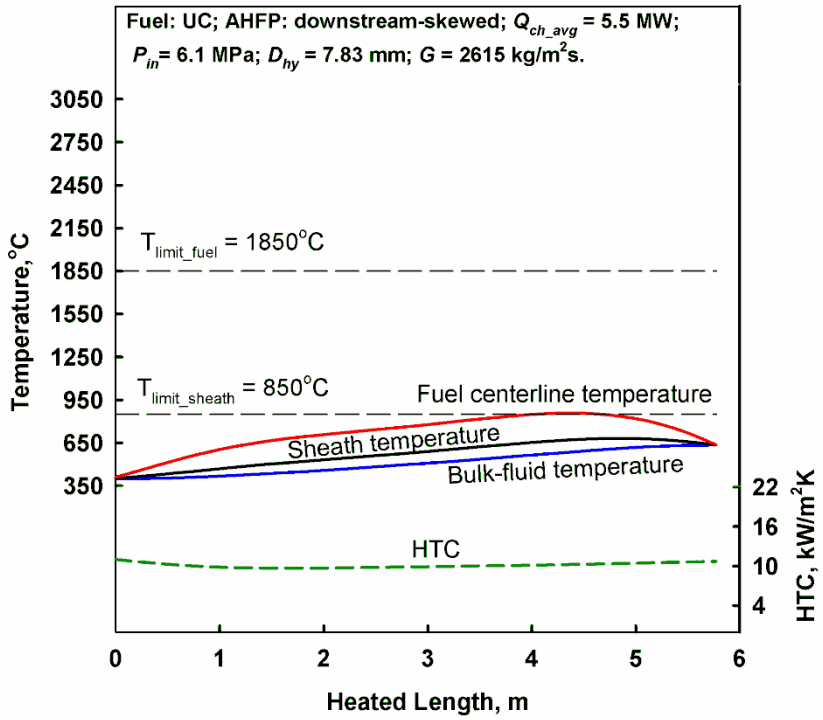

(b)

Figure 5.29. Temperature profiles at average power and downstream-skewed AHFP. (a) – SCW and (b) – SHS channels. Fuel: UC.

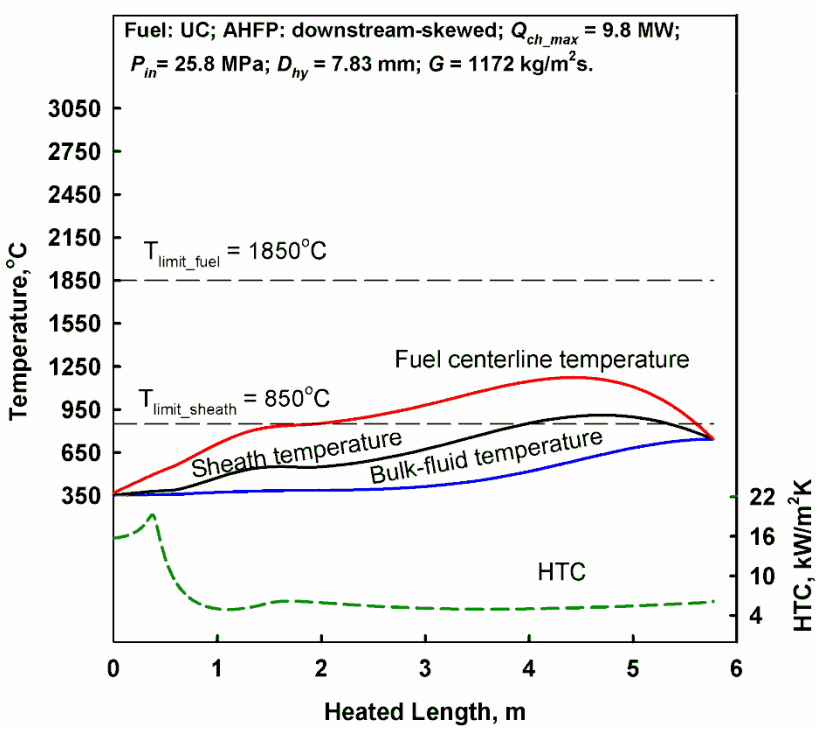

(a)

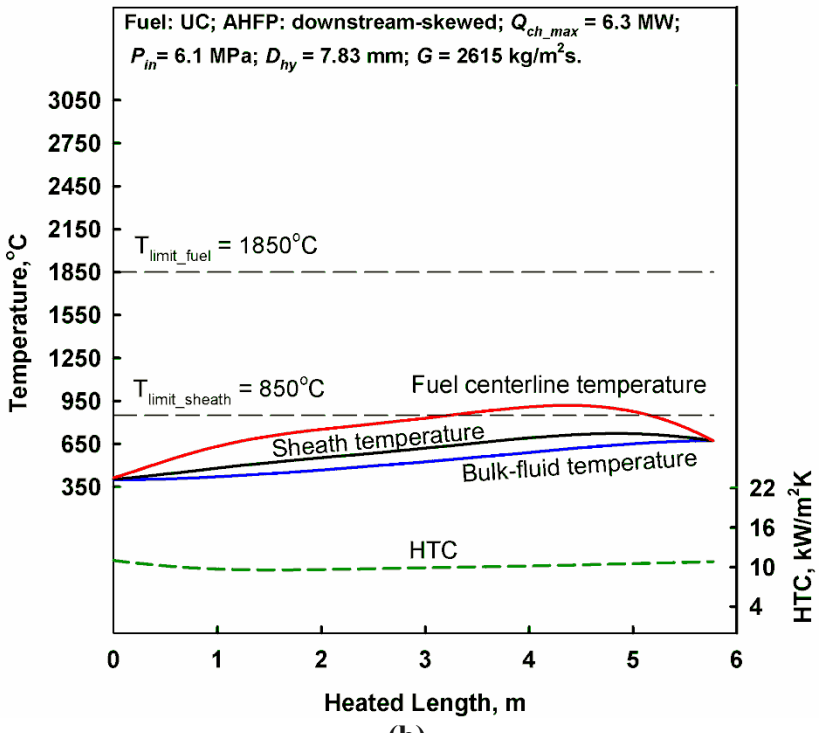

(b)

Figure 5.30. Temperature profiles at maximum power and downstream-skewed AHFP. (a) – SCW and (b) – SHS channels. Fuel: UC.

Thus, it may be seen from the Figures 5.7 to 5.30, that there is an accelerated rise in the temperatures closer to the inlet of the channel for the upstream-skewed AHFP, near the middle of the channel at cosine AHFP, and closer to the outlet of the channel for the downstream-skewed AHFP. In all cases the highest temperature is reached at uniform and downstream-skewed AHFP, the least stressed temperature conditions are achieved for the upstream-skewed AHFP.

Calculations showed that centerline temperature would exceed design limit for UO_2, ThO_2, and MOX (at maximum channel power) fuels when used in a SCW channel. Centerline temperature stays 600°C below the limit for fuels with significantly higher thermal conductivity than that of UO_2, namely, UC_2, UC, UN. For a SHS channel conditions, centerline temperatures of all fuels stay below the design limit. For UC and UN centerline temperature stays even below the design limit for sheath material at average channel power. Along SHS channel, maximum centerline temperature is reached by ThO_2. The peak values of fuel centerline temperatures at different AHFPs in SCW and SHS channel are presented in Tables 5.3 and 5.4 respectively.

Table 5.3. Peak values of fuel centerline temperatures (°C) in SCW channel at maximum power.

AHFP/Fuel	UO_2	ThO_2	MOX	UC_2	UN	UC
Uniform	**2525**	**2457**	**2128**	1280	1190	1157
Cosine-like	**2946**	**2843**	**2650**	1314	1183	1137
Upstream-skewed	**2712**	**2692**	**2251**	1203	1100	1068
Downstream-skewed	**3012**	**2916**	**2714**	1337	1215	1173

Temperature values in red are those exceeding the industry accepted limit for UO_2 of 1850°C

Table 5.4. Peak values of fuel centerline temperatures (°C) in SHS channel at maximum power.

AHFP/Fuel	UO_2	ThO_2	MOX	UC_2	UN	UC
Uniform	1650	1672	1325	974	909	894
Cosine-like	**2026**	**2020**	1562	1020	928	905
Upstream-skewed	**1875**	**1895**	1411	957	884	867
Downstream-skewed	**2089**	**2078**	1590	1027	941	918

Temperature values in red are those exceeding the industry accepted limit for UO_2 of 1850°C

It may noted from the table, that for the fuels with low thermal conductivities (UO_2, MOX, ThO_2), temperature drops by approximately 700 – 800°C at SHS conditions compared to SCW conditions, while for the fuels with higher thermal conductivities (UC_2, UC, UN) this drop is less and as about 250 – 300°C.

Also, the highest temperature is reached at downstream-skewed AHFP for all fuels.

As it may be seen from the tables, neither UO_2 nor ThO_2 may be used as fuel in SHS channels and MOX is also not a safe option. Therefore, an alternative fuel with higher thermal conductivity and appropriate swelling, corrosion-resistance, and mechanical strength should be considered to be used as fuel in SCW and SHS channels.

CHAPTER 6

CONCLUSIONS

Steam-reheat options were considered for a generic SCWR. The operating experience of several BWRs with nuclear steam reheat was reviewed. This unique experience provides vital information on physical and engineering challenges associated with implementation of steam reheat in conceptual SCWRs. Three experimental reactors were designed and tested in the 1960s – 1970s in the USA. In the former Soviet Union, nuclear steam reheat was implemented at two units at the Beloyarsk NPP. Operating experience of the units showed a possibility of reliable and safe industrial application of nuclear steam reheat right up to outlet temperatures of 510 − 540°C after over a decade of operation. Thermal efficiency of the Beloyarsk NPP units was increased by 5% as the result of implementing nuclear steam reheat. The introduction of nuclear steam reheat was economically justified in cases where the steam was superheated up to 500°C and higher with the use of stainless-steel-sheath fuel elements. The comprehensive review of the operating experience of the Beloyarsk NPP (first industrial BWR with steam reheat) was made as a unique compilation of various literature sources published during 1958 – 2009.

The experiments and operating experience obtained to date also indicate that further improvements in SHS channel design and in reactor design are possible.

Complete and detailed thermodynamic layouts for a single-reheat SCW NPP (600-MW_e and 1200-MW_e output) were developed.

Heat-transfer calculations were performed for SCW and SHS channels. Four different AHFPs and six different fuels were considered. Calculations were performed at average and maximum channel powers. The highest temperature is reached at the downstream-skewed AHFP for all fuels. Also, inner sheath temperature exceeds design limit of 750°C at maximum power along SCW channel.

UO_2, ThO_2 cannot be used and MOX is an unsafe at SHS conditions at maximum channel power, while UC_2, UN, and UC are more safe options. At SCW conditions both at average and maximum channel power and downstream-skewed AHFP, UO_2 might start to melt. Alternative fuels with higher thermal conductivity should be considered as a a potential option in SCW channels. Such an alternative fuel may be UC, which maximum temperature was calculated to be 1173°C. UC_2 and UN have slightly higher temperatures than that of UC, but still below the industry accepted limit and, therefore, as well may be used in SCW channels. However, the final choice of fuel must be also based on the assessment of other properties (gas release, cracking, swelling, and compatibility with SCW).

These together with the existing SC turbine technology, developed steam cycles, make steam-reheat implementation for a generic SCWR, one of the Generation-IV reactor concepts, a very promising and feasible option.

CHAPTER 7

FUTURE WORK

Future work on this topic may be devoted to the development of more complex heat-transfer models (based on a detailed three-dimensional problem of mass, momentum, and energy transfer inside the fuel channel). This would require investigation of approaches to model turbulence, complex geometry, writing and verification of a numerical algorithm, and, therefore, would require a significant effort. Also neutronics code may be developed to determine actual power shape along the channel. Another aspect of the thesis that may be further enhanced is the optimization of the developed thermodynamics layouts and calculation of temperature profiles along channels of such optimized layouts. Finally, fuels that are mentioned in the thesis should be assessed based on gas release, cracking, swelling, compatibility with SCW, etc.

REFERENCES

Aleksandrova, V.N., Veselkin, A.P., Levich, A.A., Lyutov, M.A., Sklyarov, V.P., Khandamirov, Yu. E., Shchapov, G.A., 1968. Research of the Long-Lived Isotopes Radiation in the Coolant of the Kurchatov's Beloyarsk Nuclear Power Plant, (In Russian) *Atomic Energy*, 24 (3), pp. 222–226.

Aleshchenkov, P.I., Zvereva, G.A., Kireev, G.A., Knyazeva, G.D., Kononov, V.I., Lunina, L.I., Mityaev, Yu.I., Nevskii, V.P., and Polyakov, V.K., 1971. Start-up and Operation of Channel-Type Uranium-Graphite Reactor with Tubular Fuel Elements and Nuclear Steam Reheating, *Atomic Energy* (Атомная Энергия, стр. 137–144), 30 (2), pp. 163–170.

Aleshchenkov, P.I., Mityaev, Yu.I., Knyazeva, G.D., Lunina, L.I., Zhirnov, A.D., and Shuvalov, V.M., 1964. The Kurchatov's Beloyarsk Nuclear Power Plant, (In Russian) *Atomic Energy*, 16 (6), pp. 489–496.

Allison, L., Villamere, B., Grande, L., Mikhael, S., Rodriguez-Prado, A. and Pioro, I., 2009. Thermal Design Options for SCWR Fuel Channel with Uranium Carbide and Uranium Di- Carbide Ceramic Fuels, Proc. ICONE-17, Brussels, Belgium, July 12-16, Paper #75975, 10 pages.

Baturov, B.B., Zvereva, G.A., Mityaev, Yu.I., and Mikhan, V.I., 1978. Nuclear Reheating of Steam, Results and Prospects at the Present Stage, *Atomic Energy* (Атомная Энергия, стр. 126–131), 44 (2), pp. 131–137.

Bishop, A.A., Sandberg, R.O. and Tong, L.S., 1964. Forced convection heat transfer to water at near-critical temperatures and super-critical pressures, Report WCAP-2056, Westinghouse Electric Corporation, Atomic Power Division, Pittsburgh, PA, USA, December, 85 pages.

Chan, P.K., Alavi, P., Chassie, G.G., Lau, J.H., Purdy, P.L., Rattan, D., Sejnoha, R., Tayal, M., Wong, B., and Xu, Z., 1999. An Update on the Design Verification of the CANFLEX Fuel Bundle, Proc. Of International conference on CANDU fuel, Niagara Falls, Ontario, Canada, September 26-30, pp. 114–123.

Chow, C.K., and Khartabil, H.F., 2008. Conceptual Fuel Channel Designs for CANDU – SCWR. *Nuclear Engineering and Technology*, Vol. 40, No. 1, pp. 1−8.

Dittus, F.W. and Boelter, L.M.K., 1930. Heat Transfer in Automobile Radiators of the Tubular Type, University of California, Berkeley, Publications in Engineering, Vol. 2, No. 13, pp. 443-461 (or Int. Communications in Heat and Mass Transfer, 1985, Vol. 12, pp. 3-22).

Dollezhal, N.A. and Emelyanov, I. Ya., 1976. Experience of High-Power Reactor Development in the USSR, (In Russian), *Atomic Energy*, 40 (2), pp. 117–125.

Dollezhal, N.A., Aleshchenkov, P.I., Baturov, B.B., Mityaev, Yu.I., 1974a. Some Results and Prospects of Nuclear Steam Reheat in Channel Reactors (Based on Operation Experience of the I.V. Kurchatov Nuclear Power Station at Belyi Yar), Proceedings of the Conference on NPP Operation Experience and Further Development of Nuclear Power Engineering, Dedicated to the 20th Anniversary of Nuclear Power Engineering, Obninsk, June 25–27, Vol. I, pp. 149–170.

Dollezhal, N.A., Malyshev, V.M., Shirokov, S.V., Emel'yanov, I.Ya., Saraev, Yu.P., Aleshchenkov, P.I., Mityaev, Yu.I., and Snitko, E.I., 1974b. Some Results of Operation of the I.V. Kurchatov Nuclear Power Station at Belyi Yar, *Atomic Energy* (Атомная Энергия, стр. 432–438), 36 (6), pp. 556–564.

Dollezhal, N.A., Aleshchenkov, P.I., Bulankov, Yu.V., and Knyazeva, G.D., 1971. Construction of Uranium-Graphite Channel-Type Reactors with Tubular Fuel Elements

and Nuclear-Reheated Steam, *Atomic Energy* (Атомная Энергия, стр. 149–155), 30 (2), pp. 177–182.

Dollezhal, I.Ya., Aleshchenkov, P.I., Evdokimov, Yu.V., Emel'yanov, I.Ya., Ivanov, B.G., Kochetkov, L.A., Minashin, M.E., Mityaev, Yu.I., Nevskiy, V.P., Shasharin, G.A., Sharapov, V.N., and Orlov, K.K., 1969. BNPP Operating Experience, (In Russian), *Atomic Energy*, 27 (5), pp. 379–386.

Dollezhal, N.A., Emel'yanov, I.Ya., Aleshchenkov, P.I., Zhirnov, A.D., Zvereva, G.A., Morgunov, N.G., Mityaev, Yu.I., Knyazeva, G.D., Kryukov, K.A., Smolin, V.N., Lunina, L.I., Kononov, V.I., and Petrov, V.A., 1964. Development of Power Reactors of BNPP-Type with Nuclear Steam Reheat, (In Russian), *Atomic Energy*, (11), pp. 335–344 (Report No. 309, 3rd International Conference on Peaceful Uses of Nuclear Energy, Geneva, 1964).

Dollezhal, N.A., Krasin, A.K., Aleshchenkov, P.I., Galanin, A.N., Grigoryants, A.N., Emel'anov, I.Ya., Kugushev, N.M., Minashin, M.E., Mityaev, Yu.I., Florinsky, B.V., and Sharapov, B.N., 1958a. Uranium-Graphite Reactor with Reheated High Pressure Steam, Proceedings of the 2nd International Conference on the Peaceful Uses of Atomic Energy, United Nations, Vol. 8, Session G-7, P/2139, pp. 398–414.

Dollezhal, N.A., Krasin, A.K., Aleshchenkov, P.I., Galanin, A.N., Grigoryants, A.N., Emel'anov, I.Ya., Kugushev, N.M., Minashin, M.E., Mityaev, Yu.I., Florinsky, B.V., and Sharapov, B.N., 1958b. Uranium-Graphite Reactor with Reheated High Pressure Steam, (in Russian), *Atomic Energy*, 5 (3), pp. 223–244.

Duffey, R.B., Pioro, I. Zhou, T., Zirn, U., Kuran, S., Khartabil, H. and Naidin, M., 2008. Supercritical Water-Cooled Nuclear Reactors (SCWRs): Current and Future Concepts – Steam-Cycle Options, Proceedings of the 16th International Conference on Nuclear Engineering (ICONE-16), Orlando, Florida, USA, May 11–15, Paper #48869, 9 pages.

Dyadyakin, B.V. and Popov, A.S., 1977. Heat transfer and thermal resistance of tight seven-rod bundle, cooled with water flow at supercritical pressures, (In Russian), Transactions of VTI (Труды ВТИ), No. 11, pp. 244–253.

Emelyanov, I.Ya., Shatskaya, O.A., Rivkin, E.Yu., and Nikolenko, N.Ya., 1972a. Strength Examination of BNPP Reactors' Fuel Channels Constructive Elements, (In Russian). *Atomic Energy*, 33 (3), pp. 729–733.

Emelyanov, I.Ya., Shasharin, G.A., Kyreev, G.A., Klemin, A.I., Polyakov, E.F., Strigulin, M.M., Shiverskiy, E.A., 1972b. Assessment of the Pumps Reliability of the Beloyarsk NPP from Operation Data, (In Russian). *Atomic Energy*, 33 (3), pp. 729–733.

Emelyanov, I.Ya. , Mikhan, V.I., Solonin, V.I., Demeshev, R.S., Rekshnya, N.F., 1982. *Nuclear Reactor Design*, (In Russian). *Energoizdat Publishing House*, Moscow, Russia, 400 pages.

Gnielinski, V., 1976. *Int. Chem. Eng.*, 16,.

Grigoryev, V.A. and Zorin, V.M., Editors, 1982. *Thermal and Nuclear Power Plants*, (In Russian), Energoatomizdat Publ. House, Moscow, Russia, p. 326.

Grigoryants, A.N., Baturov, B.B., Malyshev, V.M., Shirokov, S.V., and Mikhan, V.I., 1979. Tests on Zirconium SRCh in the First Unit at the Kurchatov Beloyarsk Nuclear Power Station, *Atomic Energy* (Атомная Энергия, стр. 55–56), 46 (1), pp. 58–60.

Hadaller, G. and Banerjee, S., 1969. Heat Transfer to Superheated Steam in Round Tubes, WDI-147.

Jackson, J.D. and Fewster, J., 1975. Forced convection data for supercritical pressure fluids, HTFS 21540.

Konovalova, O.T., Kosheleva, T.I., Gerasimov, V.V., Zhuravlev, L.S., and Shchapov, G.A., 1971. Water-Chemical Mode at the NPP with Channel Reactor and Nuclear Steam Reheat, (In Russian), *Atomic Energy*, 30 (2), pp. 155–158.

Krasnoshchekov, E.A. and Protopopov, V.S., 1959. Heat transfer at supercritical region in flow of carbon dioxide and water in tubes, (In Russian), Thermal Engineering (Теплоэнергетика, стр. 26–30), No. 12, pp. 26–30.

Krasnoshchekov, E.A. and Protopopov, V.S., 1960. About heat transfer in flow of carbon dioxide and water at supercritical region of state parameters, (In Russian), Thermal Engineering (Теплоэнергетика, стр. 94), No. 10, p. 94.

Krasnoshchekov, E.A., Protopopov, V.S., Van, F. and Kuraeva, I.V., 1967. Experimental investigation of heat transfer for carbon dioxide in the supercritical region, Proceedings of the 2nd All-Soviet Union Conference on Heat and Mass Transfer, Minsk, Belarus', May, 1964, Published as Rand Report R-451-PR, Edited by C. Gazley, Jr., J.P. Hartnett and E.R.C. Ecker, Vol. 1, pp. 26–35.

Kruglikov, P.A., Smolkin, Yu.V. and Sokolov, K.V., 2009. Development of Engineering Solutions for Thermal Scheme of Power Unit of Thermal Power Plant with Supercritical Parameters of Steam, (In Russian), Proc. of Int. Workshop "Supercritical Water and Steam in Nuclear Power Engineering: Problems and Solutions", Moscow, Russia, October 22–23, 6 pages.

Lee, R.A. and Haller, K.H., 1974. Supercritical water heat transfer developments and applications, Proceedings of the 5th International Heat Transfer Conference, Tokyo, Japan, September 3–7, Vol. IV, Paper No. B7.7, pp. 335–339.

Leung, L.K., 2008. Effect of CANDU Bundle-Geometry Variation on Dryout Power. *Proceedings of the 16th International Conference on Nuclear Engineering* (pp. 1- 8). Orlando, Florida: ICONE-16. Paper #48827.

MATLAB version 7.4, R2007a, computer software, The MathWorks, Inc., Natick, Massachusetts, USA.

McAdams, W.H., 1942. Heat Transmission, 2nd edition, McGraw-Hill, New York, NY, USA, 459 pages.

Mikhan, V.I., Glazkov, O.M., Zvereva, G.A., Mihaylov, V.I., Stobetskaya, G.N., Mityaev, Yu.I., Yarmolenko, O.A., Kozhevnikov, Yu.N., Evdokimov, Yu.V., Sheynkman, A.G., Zakharov, V.G., Postnikov, V.N., Gladkov, N.G., and Saraev, O.M., 1988. Reactor Testing of Zirconium Steam-Reheat Channels with Rod Fuel Elements in Reactors of the First Stage of BNPP, (In Russian), BNPP Operating Experience: Information Materials (in 4 volumes), USSR Academy of Sciences, Ural Branch. 4.3. Fuel Assemblies and Constructional Materials. Heat Transfer Equipment of the Nuclear Power Units, 207 pages.

Mokry, S., Gospodinov, Ye., Pioro, I. and Kirillov, P., 2009a. Supercritical Water Heat-Transfer Correlation for Vertical Bare Tubes, Proceedings of the 17th International Conference on Nuclear Engineering (ICONE-17), Brussels, Belgium, July 12-16, Paper#76010, 8 pages.

Mokry, S., Farah, A., King, K., Gupta, S., Pioro, I. and Kirillov, P., 2009b. Development of a Supercritical Water Heat-Transfer Correlation for Vertical Bare Tubes, Proc. Int. Conf. "Nuclear Energy for New Europe", Bled, Slovenia, Sep. 14-17, Paper #210, 14 pages.

Mokry, S., Naidin, M., Baig, F., Gospodinov, Ye., Zirn, U., Bakan, K., Pioro, I. and Naterer, G., 2008. Conceptual Thermal-Design Options for Pressure-Channel SCWRs, Proceedings of the 16th International Conference on Nuclear Engineering (ICONE-16), Orlando, FL, USA, May 11–15, Paper #48313.

Naidin, M., Mokry, S., Pioro, I., Duffey, R., and Zirn, U., 2009a. SCW NPPs: Layouts and Thermodynamic Cycles, International Conference "Nuclear Energy for New Europe", Bled, Slovenia, Sep. 14-17, Paper #704, 12 pages.

Naidin, M., Mokry, S., Baig, F., Gospodinov, Ye., Zirn, U., Pioro, I. and Naterer, G., 2009b. Thermal-Design Options for Pressure-Channel SCWRs with Co-Generation of Hydrogen, J. of Engineering for Gas Turbines and Power, Vol. 131, January, 8 pages.

Naidin, M., Mokry, S., Monichan, R., Chophla, K., Pioro, I., Naterer, G. and Gabriel, K. 2009c. Thermodynamic Analysis of SCW NPP Cycles with Thermo-Chemical Co-Generation of Hydrogen, Proceedings of the International Conference on Hydrogen Production-2009 (ICH2P-09), University of Ontario Institute of Technology, Oshawa, Ontario, Canada, Paper No. ICH2P-GP163, 14 pages.

Naterer, G., Suppiah, S., Lewis, M., Pioro, I. et al., 2009. Recent Canadian Advances in Nuclear-Based Hydrogen Production and the Thermochemical Cu-Cl Cycle, Int. J. of Hydrogen Energy (IJHE), Vol. 34, pp. 2901-2917.

NIST Reference Fluid Thermodynamic and Transport Properties—REFPROP, 2007. NIST Standard Reference Database 23 (on CD: Executable with Source plus Supplemental Fluids in ZIP File), Version 8.0, E.W. Lemmon, M.O. McLinden and M.L. Huber, National Institute of

Novick, M., Rice, R.E., Graham, C.B., Imhoff, D.H., and West, J.M., 1965. Developments in Nuclear Reheat, Proceedings of the 3rd International Conference on Peaceful Uses of Nuclear Energy, Geneva 1964, Vol. 6, pp. 225–233.

Oka, Yo. and Koshizuka, S., 2002. Status and prospects of high temperature (supercritical-pressure) light water cooled reactor research and development, Proceedings of the 13th Pacific Basin Nuclear Conference, Shenzhen City, China, October 21–25.

Ornatskiy, A.P., Dashkiev, Yu.G. and Perkov, V.G., 1980. *Supercritical Steam Generators*, (In Russian), Vyshcha Shkola Publ. House, Kiev, Ukraine, 287 pages.

Peiman, W., Gabriel, K., and Pioro, I., 2010. Heat-loss Calculations For Pressure-channel SCWRS, Proc. 2nd Canada-China Joint Workshop on Supercritical Water-Cooled Reactors (CCSC-2010), Toronto, Ontario, Canada: Canadian Nuclear Society, April 25-28

Petrosyants, A.M., 1969. Power Reactors for Nuclear Power Plants (from the First in the World to the 2-GW Electrical Power NPP) , (In Russian). *Atomic Energy*, 27 (4), pp. 263–274.

Petukhov, B.S. and Kirillov, 1958. About heat transfer at turbulent fluid flow in tubes, (In Russian), Thermal Engineering (Теплоэнергетика, стр. 63–68), (4), pp. 63–68.

Pioro, I., Mokry, S., Peiman, W., Grande, L. and Saltanov, Eu., 2010. Supercritical Water-Cooled Nuclear Reactors: NPP Layouts and Thermal Design Options of Pressure Channels, Proceedings of the 17th Pacific Basin Nuclear Conference (PBNC-2010), Cancun, Mexico, October 24-30, 31 pages.

Pioro, I.L. and Duffey, R.B., 2007. *Heat Transfer and Hydraulic Resistance at Supercritical Pressures in Power Engineering Applications*, ASME Press, New York, NY, USA, 334 pages.

Retzlaff, K.M. and Ruegger, W.A., 1996. Steam turbines for ultrasupercritical power plants, GER-3945A, General Electric Company, Schenectady, NY, USA, 13 pages.

Ross, W.B., 1961. Pathfinder Atomic Power Plant, Superheater Temperature Evaluation Routine, An IBM-704 Computer Program. United States Atomic Energy Commission, Office of Technical Information, Oak Ridge, TN, 49 pages.

Saltanov, Eu., Peiman, W., Farah, A., King, K., Naidin, M. and Pioro, I., 2010. Steam-Reheat Options for Pressure-Tube SCWRs, Proceedings of the 18th International Conference On Nuclear Engineering (ICONE-18), Xi'an, China, May 17-21, Paper 29972, 12 pages.

Samoilov, A.G., Pozdnyakova, A.V., and Volkov, V.S., 1976. Steam-Reheating Fuel Elements of the Reactors in the I.V. Kurchatov Beloyarsk Nuclear Power Station, *Atomic Energy* (Атомная Энергия, стр. 371-377), 40 (5), pp. 451–457.

Shitzman, M.E., 1983. *Neutral-Oxygen Water Regime at Supercritical-Pressure Power Units*, (in Russian), Energoatomizdat Publishing House, Moscow, Russia.

Sieder, E.N. and Tate, G.E., 1936, *Ind. Eng. Chem.*, 28 (1429).

Smith, D., 1999. Ultra-supercritical CHP: Getting more competitive, *Modern Power Systems*, January, pp. 21–32.

Smolin, V.N., Polyakov, V.K., Esikov, V.I., and Shuyinov, Yu.N., 1965. Test Stand Study of the Start-up Modes of the Kurchatov's Beloyarsk Nuclear Power Plant, (In Russian). *Atomic Energy*, 19 (3), pp. 261–269.

Swenson, H.S., Carver, J.R. and Kakarala, C.R., 1965. Heat transfer to supercritical water in smooth-bore tubes, Journal of Heat Transfer, Transactions of the ASME, Series C, 87 (4), pp. 477–484.

Tsao, D. and Gorzegno, W.P., 1981. Variable-pressure once-through steam generators—experience and development, Proceedings of the American Power Conference, Vol. 43, pp. 287–293.

USAEC Report ACNP-5910, 1959. Allis-Chalmers Manufacturing Co., Pathfinder Atomic Power Plant, Final Safeguards Report, May.

USAEC Report (MaANL-6302), 1961. Design and Hazards Summary Report—Boiling Reactor Experiment V (Borax-V), Argonne National Laboratory.

USAEC Report PRWRA-GNEC 5, 1962. General Nuclear Engineering Corp., BONUS, Final Hazards Summary Report, February.

Vanyukova, G.V., Kuznetsov, Yu.N., Loninov, A.Ya., Papandin, M.V., Smirnov, V.P. and Pioro, I.L., 2009. Application of CFD-Code to Calculations of Heat Transfer in a Fuel Bundle of SCW Pressure-Channel Reactor, Proc. 4th Int. Symp. on Supercritical Water-Cooled Reactors, Heidelberg, Germany, March 8-11, Paper No. 28, 9 pages.

Veselkin, A.P., Beskrestnov, N.V., Sklyarov, V.P., Khandamirov, Yu.E., and Yashnikov, A.I., 1971. Radiation Safety Aspects in Designing and Operating Channel-Type Power Reactors, (In Russian), *Atomic Energy*, 30 (2), pp. 144–149.

Veselkin, A.P., Lyutov, M.A., Khandamirov, Yu.E., 1968. Radioactive Deposits on the Surfaces of the Kurchatov's Beloyarsk Nuclear Power Plant, (In Russian), *Atomic Energy*, 24 (3), pp. 219–222.

Vikulov, V.K., Mityaev, Yu.I., Shuvalov, V.M. , 1971. Some Issues on Beloyarsk NPP Reactor Physics, (In Russian), *Atomic Energy*, 30 (2), pp. 132–137.

Winterton, R.H.S., 1998. Where did the Dittus and Boelter equation come from? International Journal of Heat and Mass Transfer, 41 (4–5), pp. 809–810.

Yurmanov, V.A., Belous, V. N., Vasina, V. N., and Yurmanov, E.V., 2009a. Chemistry and Corrosion Issues in Supercritical Water Reactors, Proceedings of the IAEA International Conference on Opportunities and Challenges for Water Cooled Reactors in the 21st Century, Vienna, Austria, October 26−30.

Yurmanov, V.A., Vasina, V. N., Yurmanov, E.V and Belous, V. N., 2009b. Water Regime Features and Corrosion Protection Issues in NPP with Reactors at Supercritical Parameters", (In Russian), Proceedings of the IAEA International Conference on Opportunities and Challenges for Water Cooled Reactors in the 21st Century, Vienna, Austria, October 26−30.

Zahlan, H., Groeneveld, D. and Tavoularis, S., 2010. Look-Up Table for Trans-Critical Heat Transfer, Proc. 2nd Canada-China Joint Workshop on Supercritical Water-Cooled Reactors (CCSC-2010), Toronto, Ontario, Canada: Canadian Nuclear Society, April 25-28

APPENDIX A

FLOWCHART OF THE MATLAB PROGRAM FOR HEAT-TRANSFER CALCULATIONS

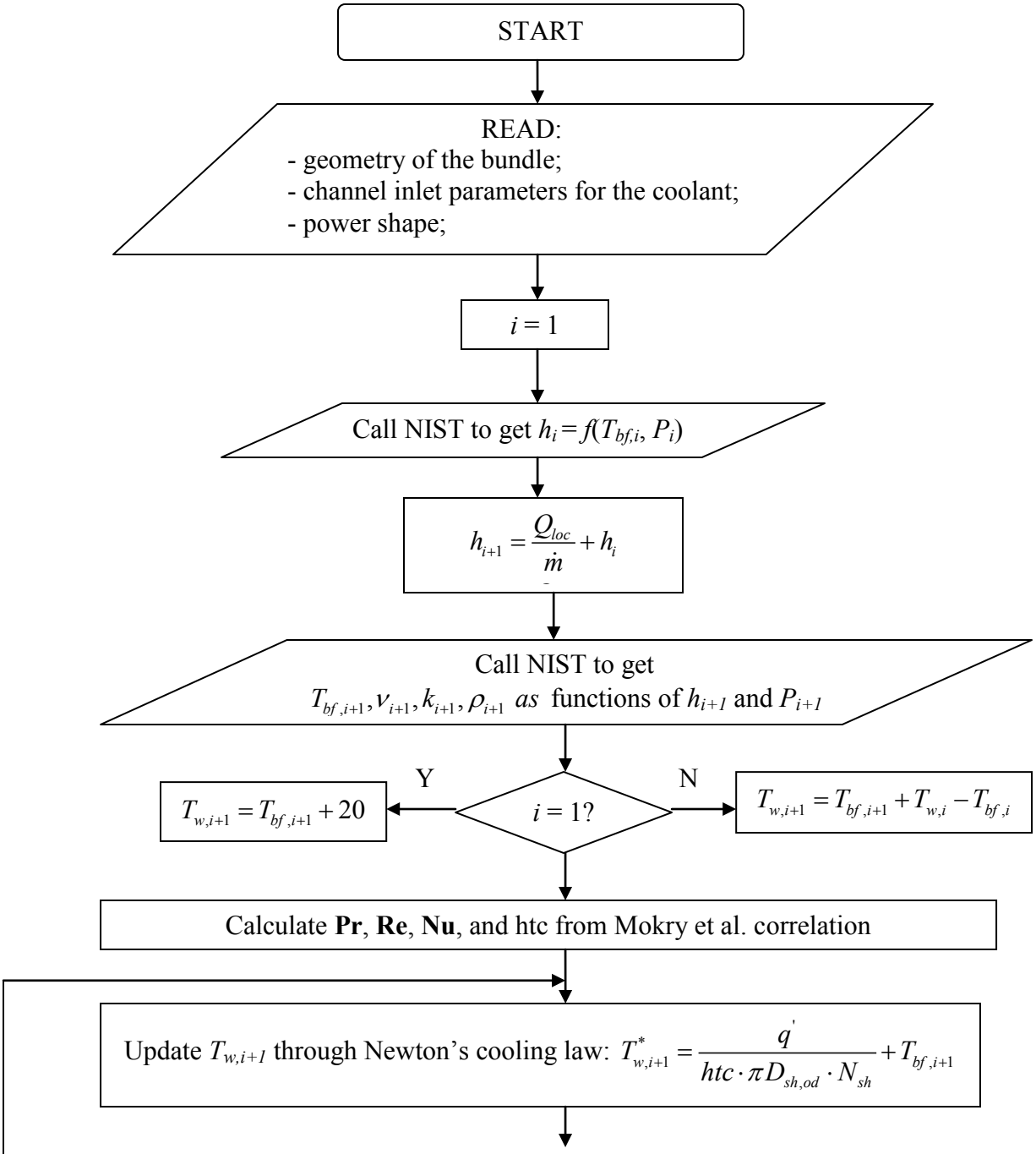

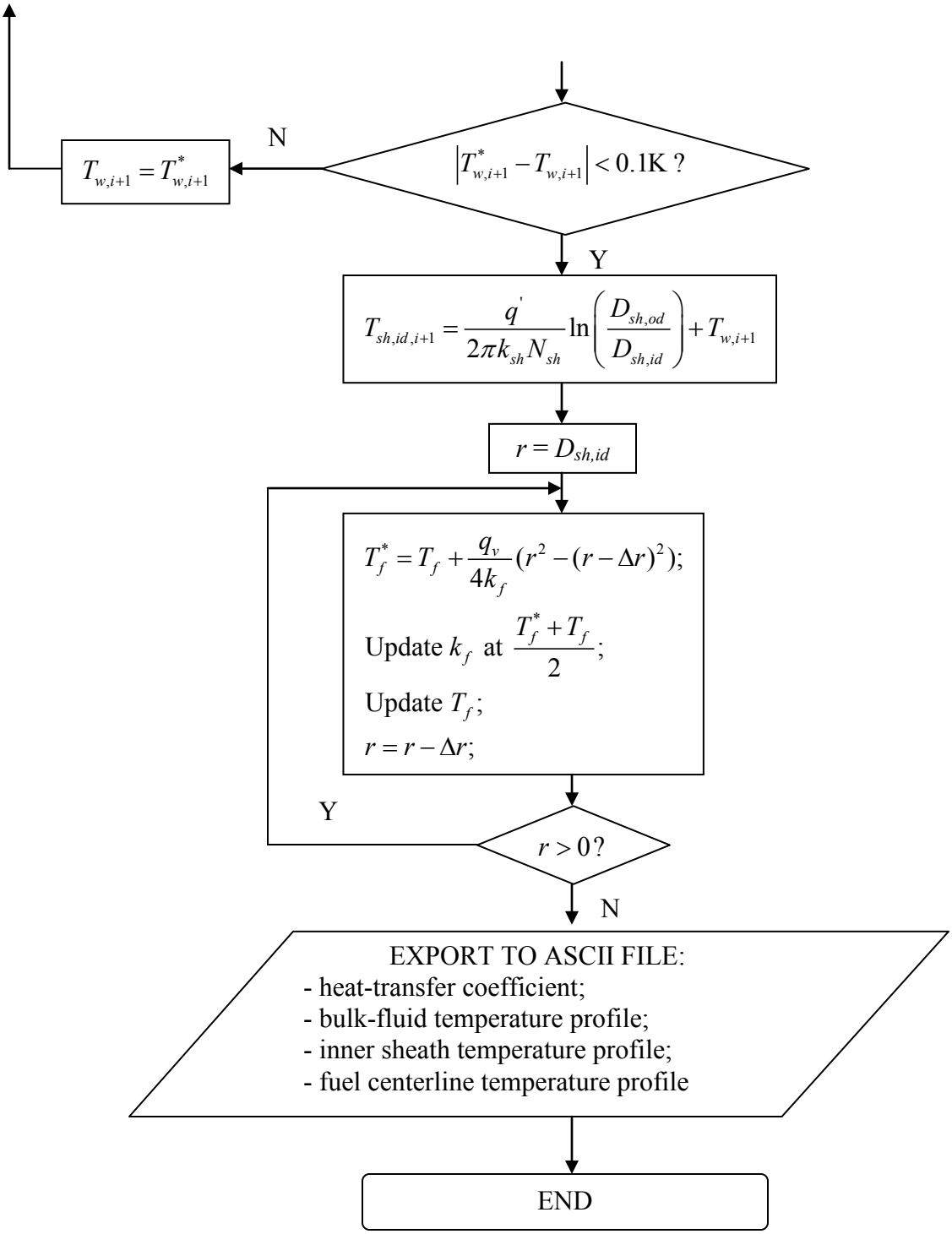
$\left|T^*_{w,i+1} - T_{w,i+1}\right| < 0.1\text{K}$?
N
$T_{w,i+1} = T^*_{w,i+1}$
Y
$T_{sh,id,i+1} = \frac{q'}{2\pi k_{sh} N_{sh}} \ln\left(\frac{D_{sh,od}}{D_{sh,id}}\right) + T_{w,i+1}$
$r = D_{sh,id}$
$T^*_f = T_f + \frac{q_v}{4k_f}(r^2 - (r - \Delta r)^2)$;
Update k_f at $\frac{T^*_f + T_f}{2}$;
Update T_f;
$r = r - \Delta r$;
Y
$r > 0$?
N
EXPORT TO ASCII FILE:
- heat-transfer coefficient;
- bulk-fluid temperature profile;
- inner sheath temperature profile;
- fuel centerline temperature profile
END

APPENDIX B

TEST RUN OF MATLAB PROGRAM AND COMPARISON WITH ANALYTICAL RESULTS

Figure B.1 shows temperature profiles for a reference case of CANDU-6 channel average operating conditions (coolant c_p = 5.5 kJ/kg·K, k = 0.573 W/m·K, $\mu = 9.27 \cdot 10^{-5}$ Pa·s, P = 10 MPa, T_{in} = 260ºC, $\dot{m}$ = 28 kg/s, k_{sh} = 14W/m·K, k_f = 2.4. W/m·K, average power equal to 5.5 MW, variant-20 bundle). Table B.1 shows comparison of analytical values and those calculated by the program written in Matlab (the values calculated in the program are highlighted with blue color).

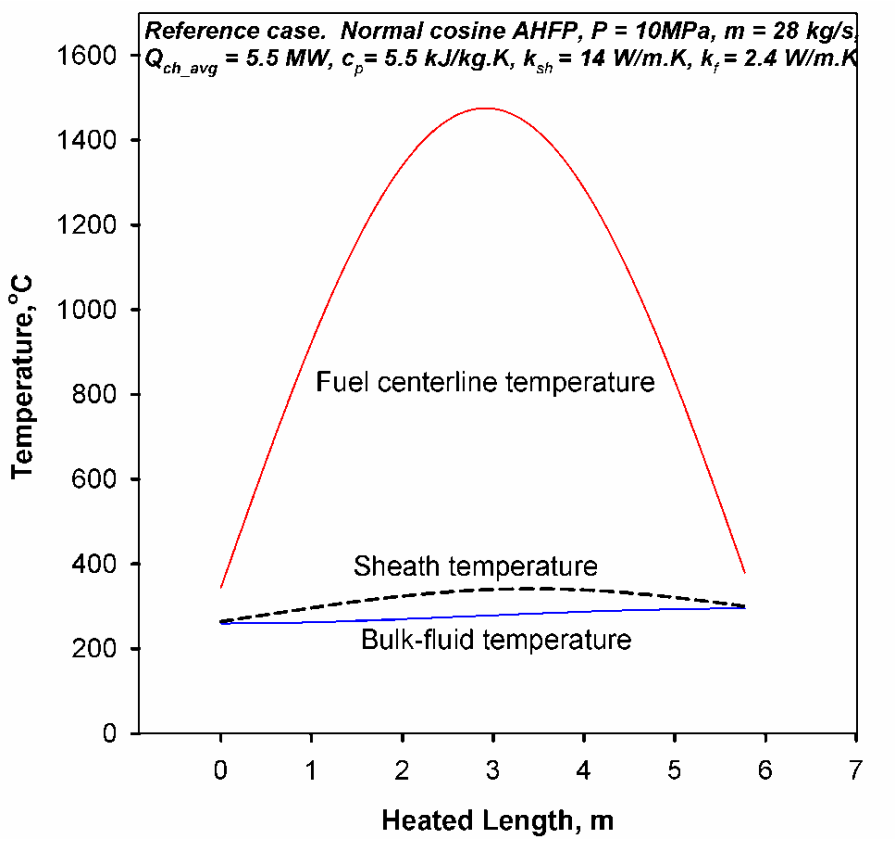

Figure B.1. Temperature profiles along channel in the reference case.

Table B.1. Comparison of analytical and calculated with Matlab values of temperatures.

x, m	T_{bf},°C	T_{bf},°C	Error	T_{sh},°C	T_{sh},°C	Error	T_{fuel},°C	T_{fuel},°C	Error
0	260	260	1.78E–07	264	264	1.15E–06	344	344	1.53E–06
0.481	260	260	3.78E–05	280	280	1.27E–06	633	633	2.29E–06
0.962	260	260	8.44E–06	295	295	9.96E–07	903	903	2.48E–06
1.443	262	262	1.17E–05	310	310	1.14E–06	1137	1137	2.58E–06
1.924	265	265	1.41E–05	323	323	1.16E–06	1317	1317	2.64E–06
2.405	269	269	1.53E–05	333	333	8.32E–07	1433	1433	2.63E–06
2.886	273	273	1.57E–05	339	339	9.84E–07	1475	1475	2.60E–06
3.367	277	277	1.50E–05	341	341	9.83E–07	1442	1442	2.59E–06
3.848	282	282	1.33E–05	340	340	8.17E–07	1335	1335	2.61E–06
4.329	286	286	1.07E–05	335	335	8.30E–07	1161	1161	2.46E–06
4.810	290	290	7.50E–06	326	326	9.68E–07	933	933	2.42E–06
5.291	293	293	3.88E–06	314	314	8.88E–07	667	667	2.21E–06
5.772	296	296	1.08E–07	300	300	1.08E–07	380	380	1.60E–06

As one can, maximum relative error is of the order 10^{-5} and there are single cases when values of temperatures differ in the second decimal place. It shows convincingly that the programmed model is reliable and should produce reasonable results when use to calculate temperature profiles at the channel conditions of interest.

APPENDIX C

TEMPERATURE PROFILES ALONG SUPERCRITICAL-WATER AND SUPERHEATED-STEAM CHANNELS WITH MOX, UC2, AND UN FUELS

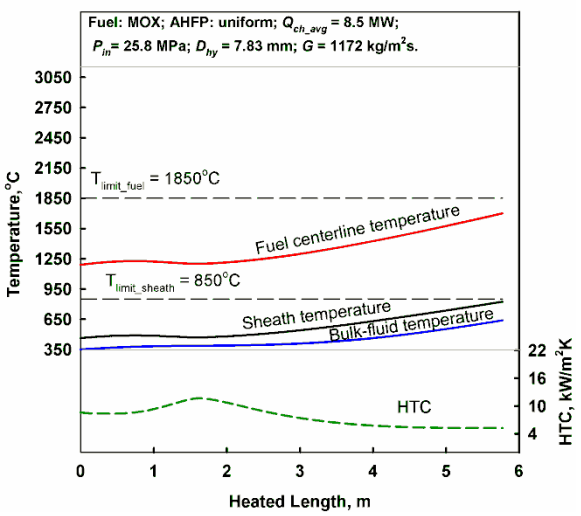

(a)

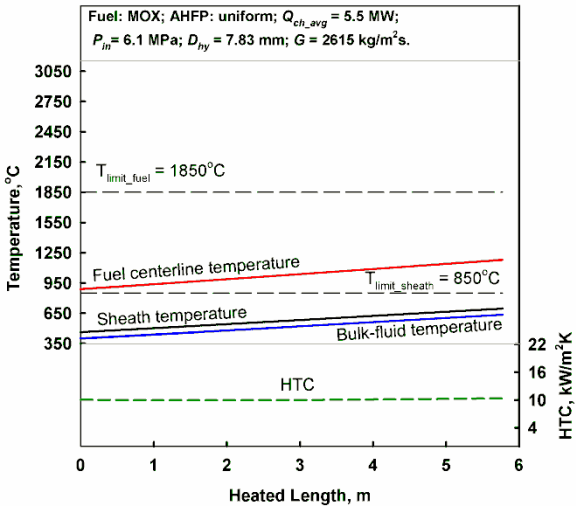

(b)

Figure C.1. Temperature profiles at average power and uniform AHFP. (a) – SCW and (b) – SHS channels. Fuel: MOX.

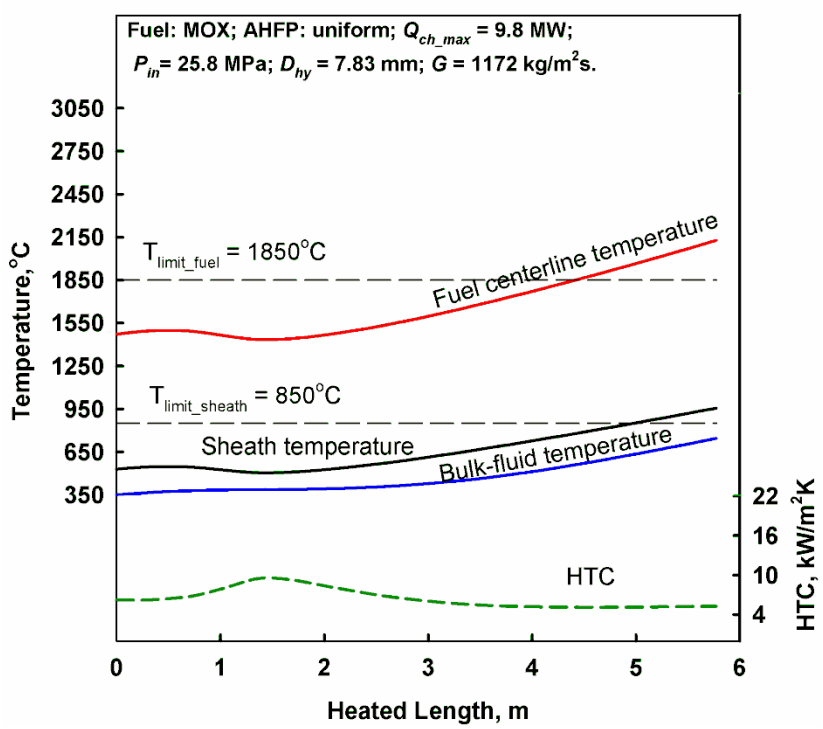

(a)

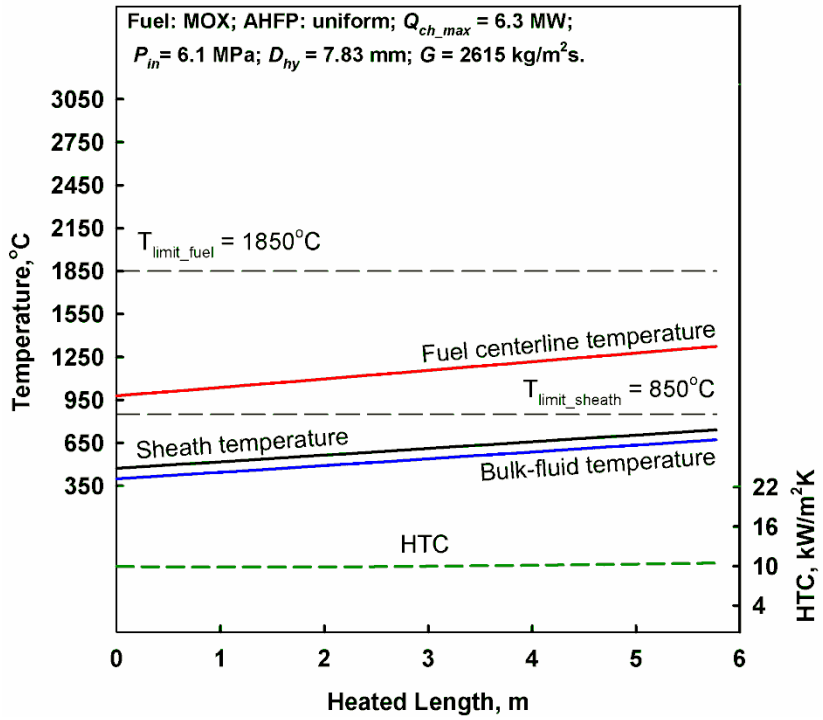

(b)

Figure C.2. Temperature profiles at maximum power and uniform AHFP. (a) – SCW and (b) – SHS channels. Fuel: MOX.

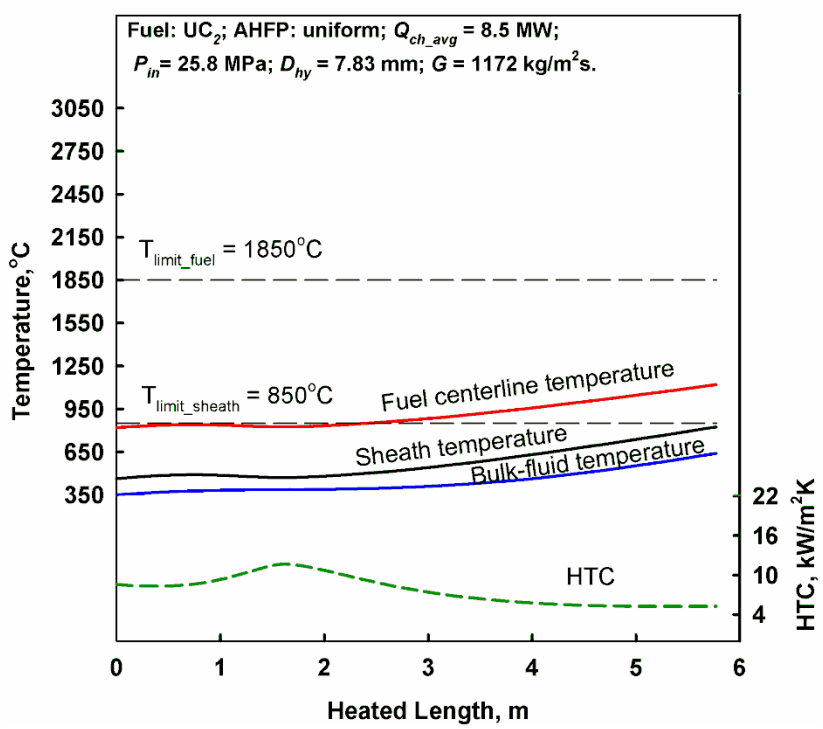

(a)

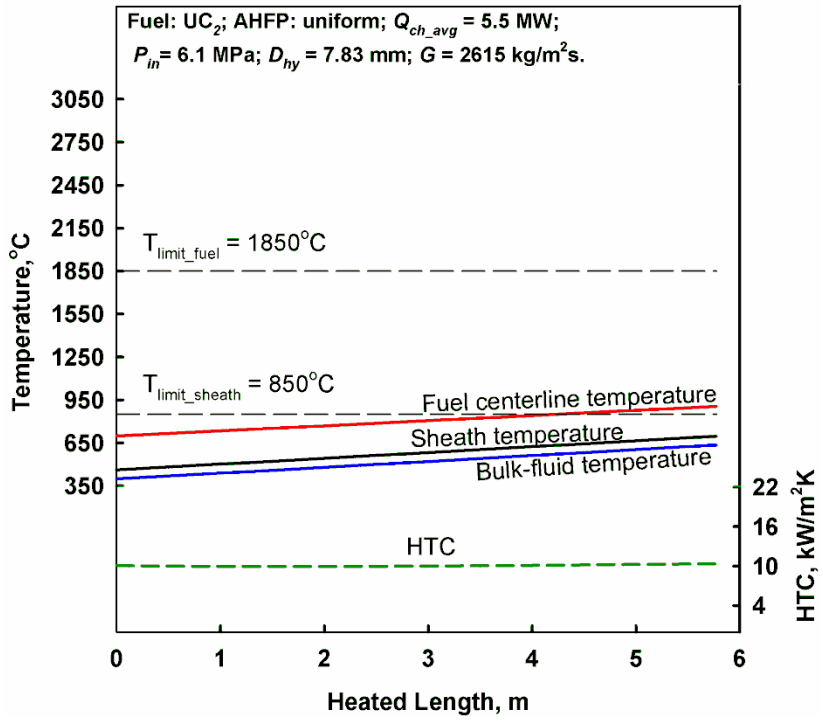

(b)

Figure C.3. Temperature profiles at average power and uniform AHFP. (a) – SCW and (b) – SHS channels. Fuel: UC_2.

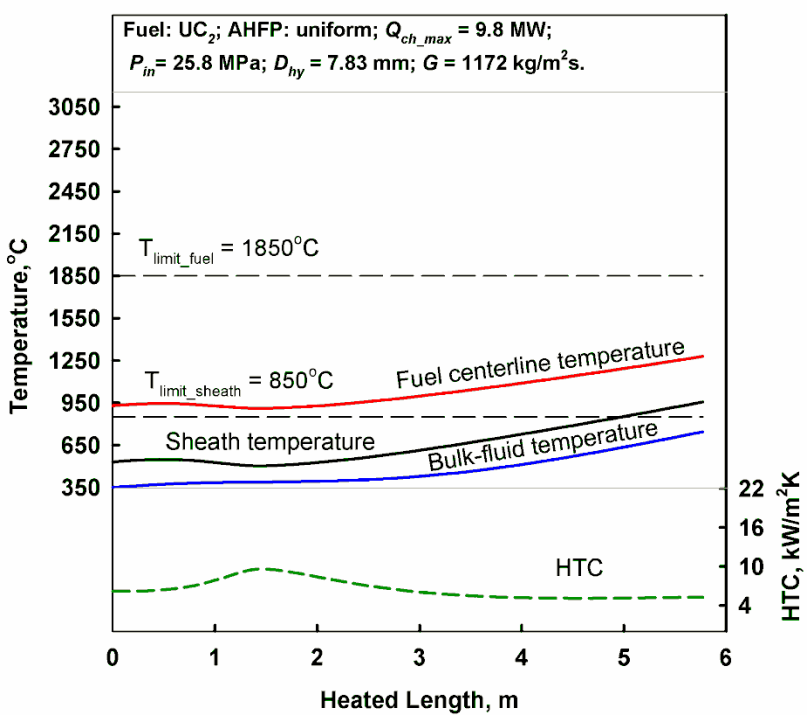

(a)

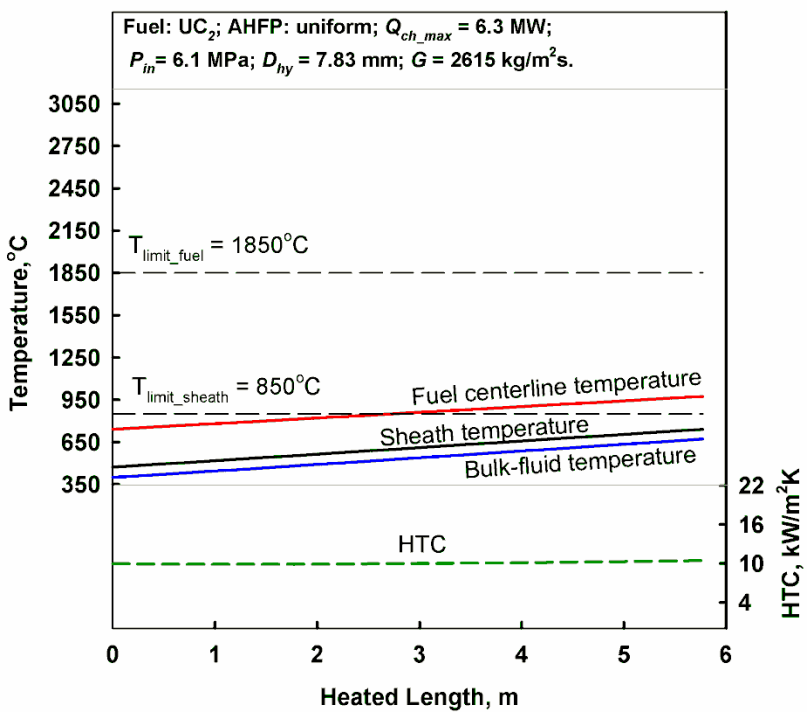

(b)

Figure C.4. Temperature profiles at maximum power and uniform AHFP. (a) – SCW and (b) – SHS channels. Fuel: UC_2.

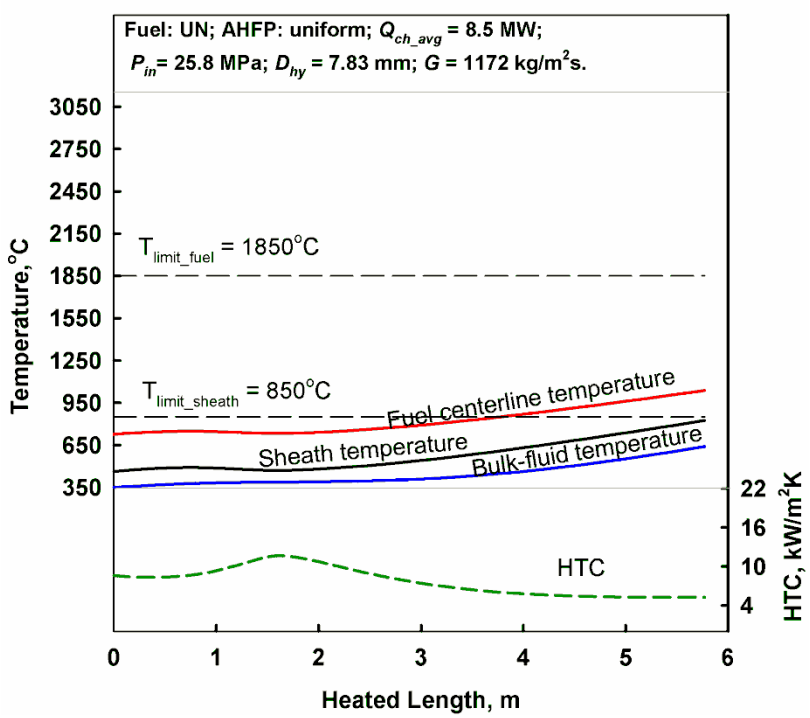

(a)

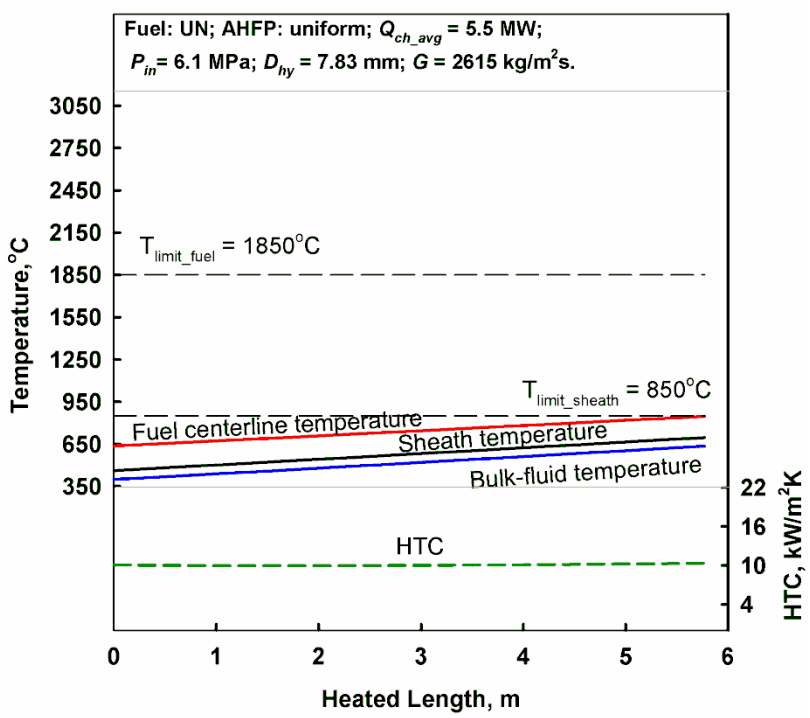

(b)

Figure C.5. Temperature profiles at average power and uniform AHFP. (a) – SCW and (b) – SHS channels. Fuel: UN.

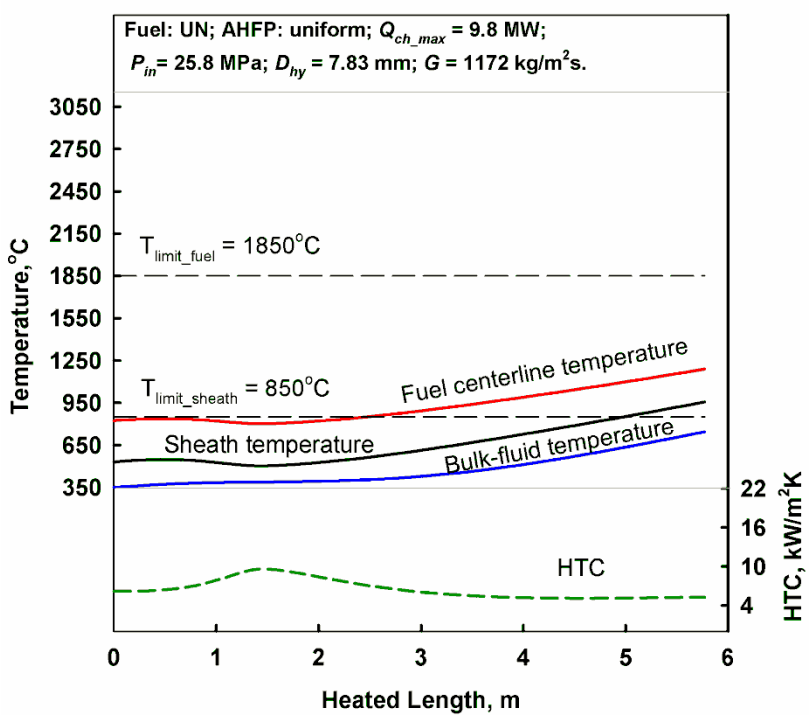

(a)

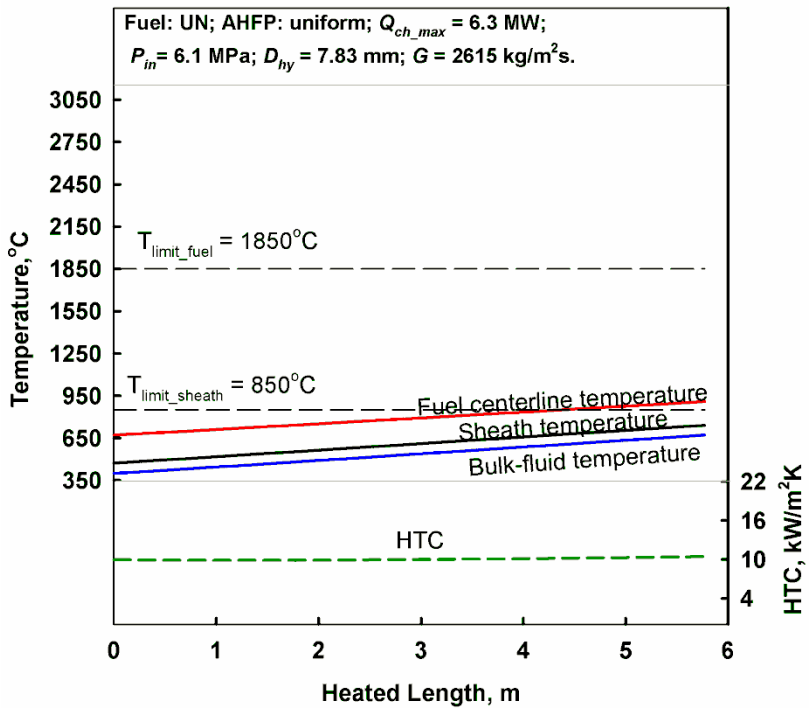

(b)

Figure C.6. Temperature profiles at maximum power and uniform AHFP. (a) – SCW and (b) – SHS channels. Fuel: UN.

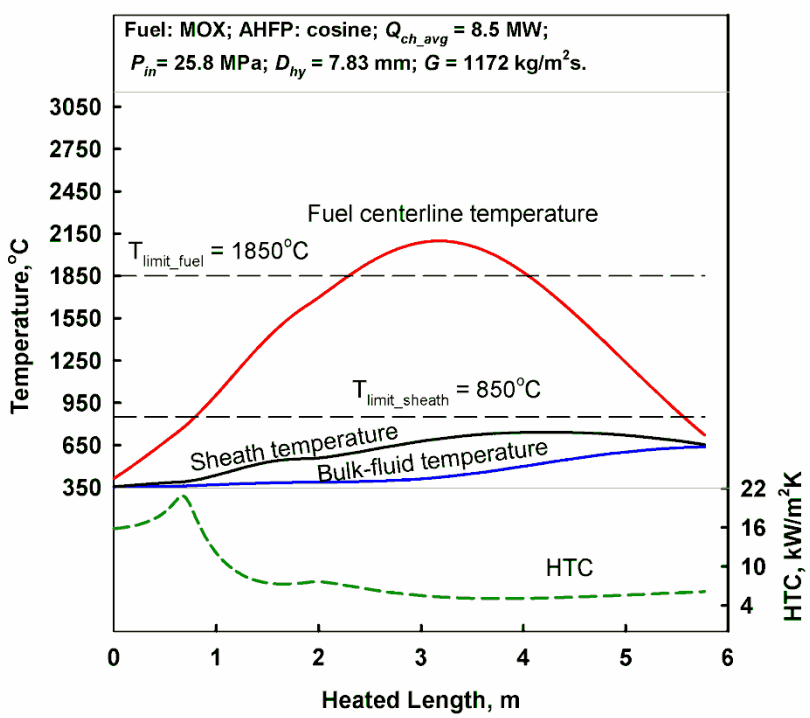

(a)

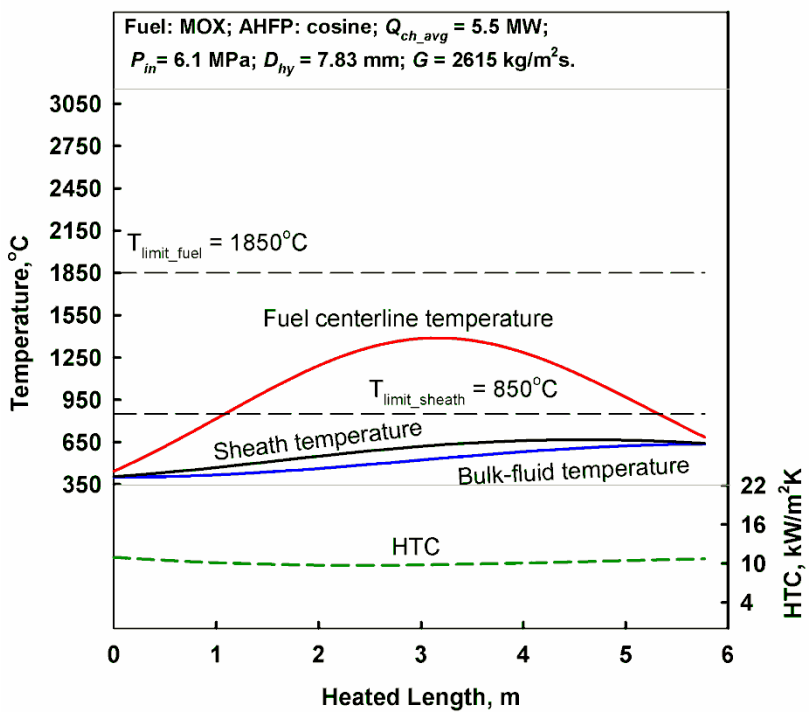

(b)

Figure C.7. Temperature profiles at average power and cosine AHFP. (a) – SCW and (b) – SHS channels. Fuel: MOX.

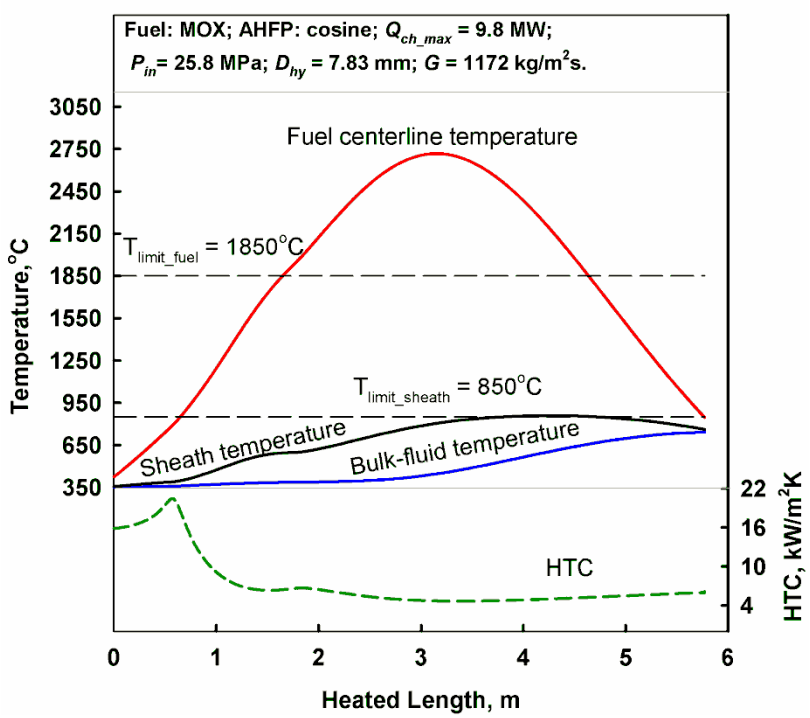

(a)

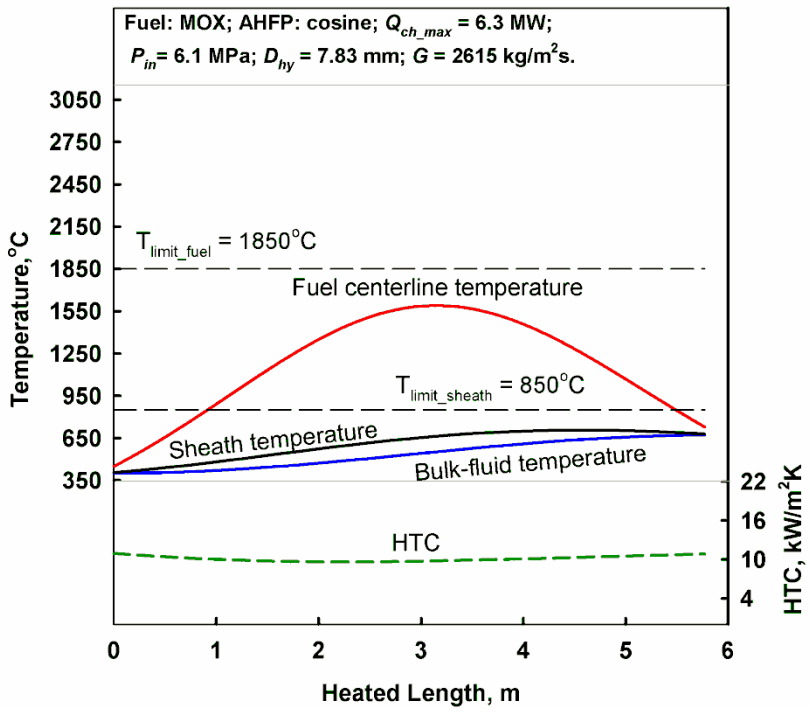

(b)

Figure C.8. Temperature profiles at maximum power and cosine AHFP. (a) – SCW and (b) – SHS channels. Fuel: MOX.

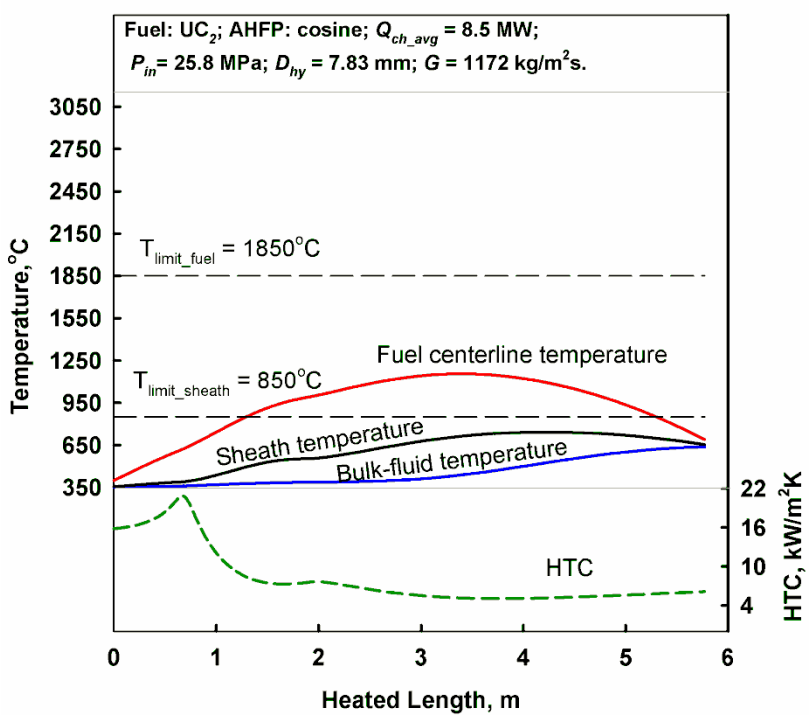

(a)

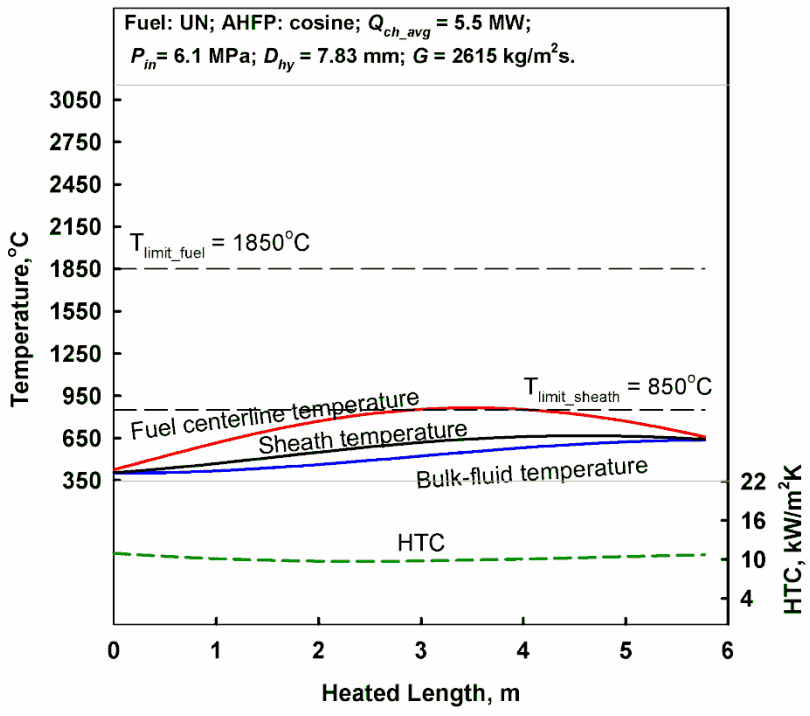

(b)

Figure C.9. Temperature profiles at average power and cosine AHFP. (a) – SCW and (b) – SHS channels. Fuel: UC_2.

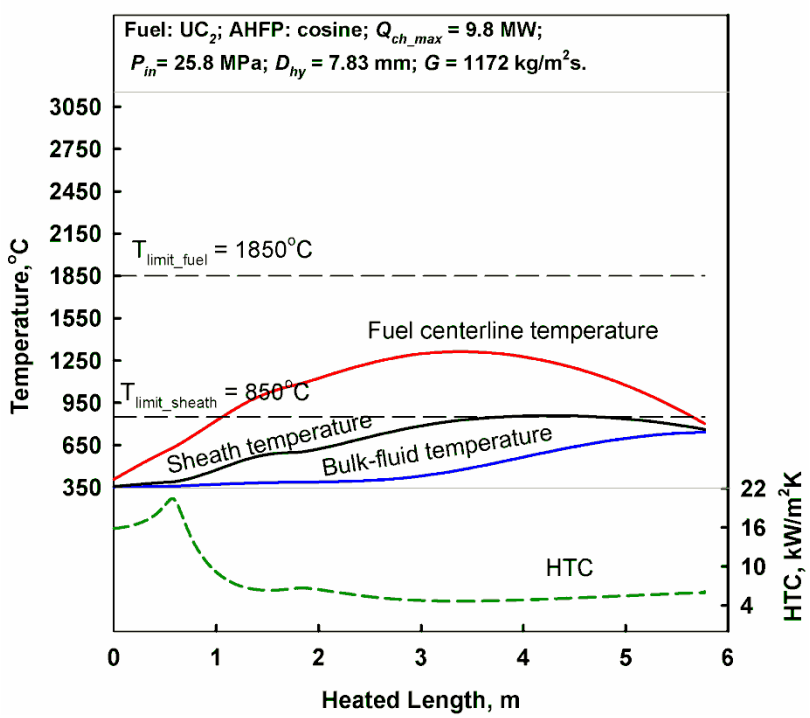

(a)

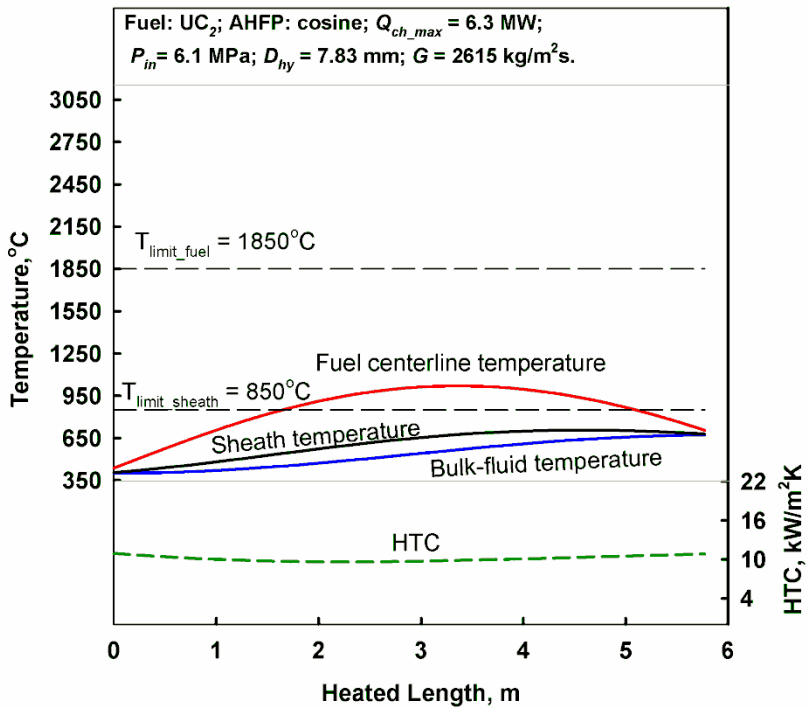

(b)

Figure C.10. Temperature profiles at maximum power and cosine AHFP. (a) – SCW and (b) – SHS channels. Fuel: UC_2.

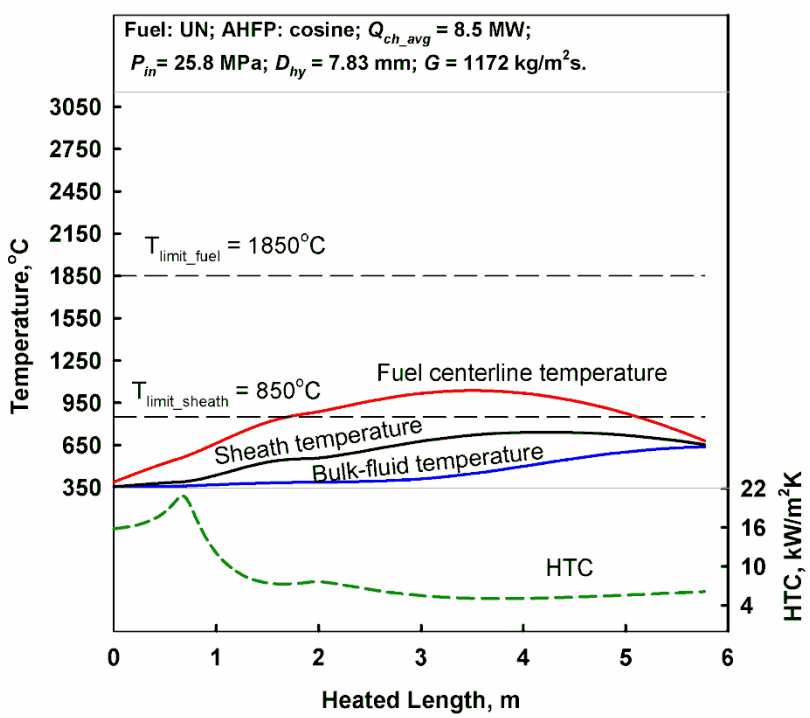

(a)

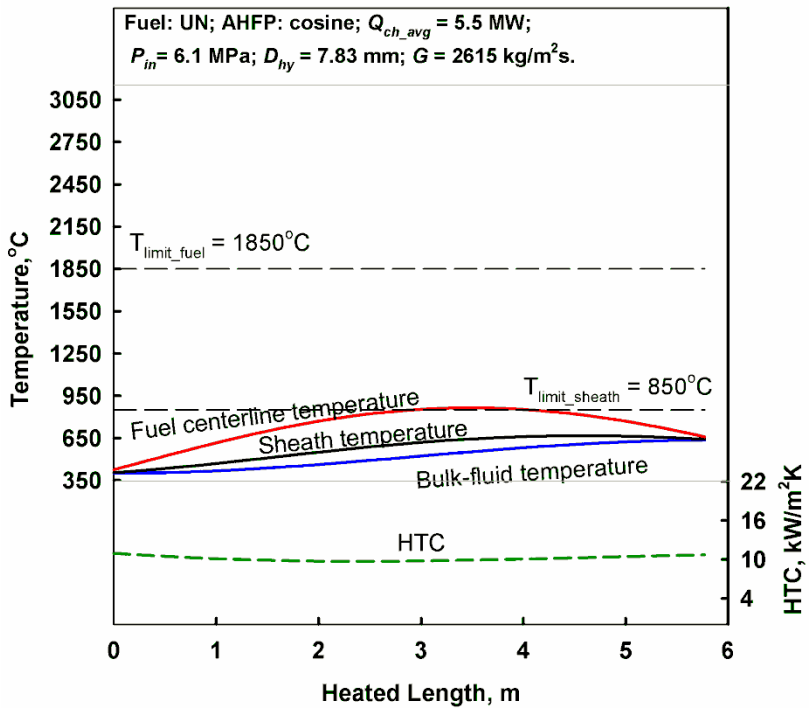

(b)

Figure C.11. Temperature profiles at average power and cosine AHFP. (a) – SCW and (b) – SHS channels. Fuel: UN.

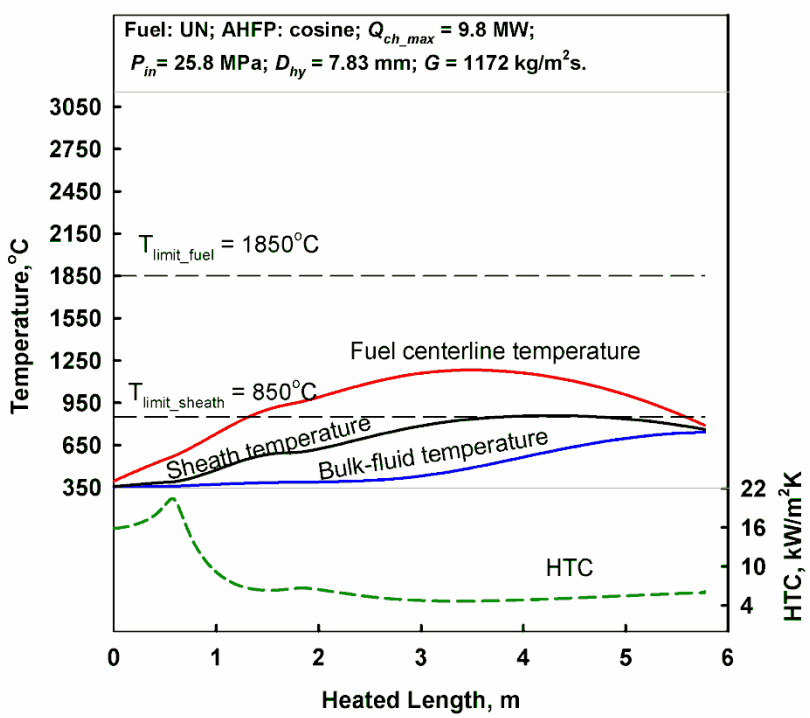

(a)

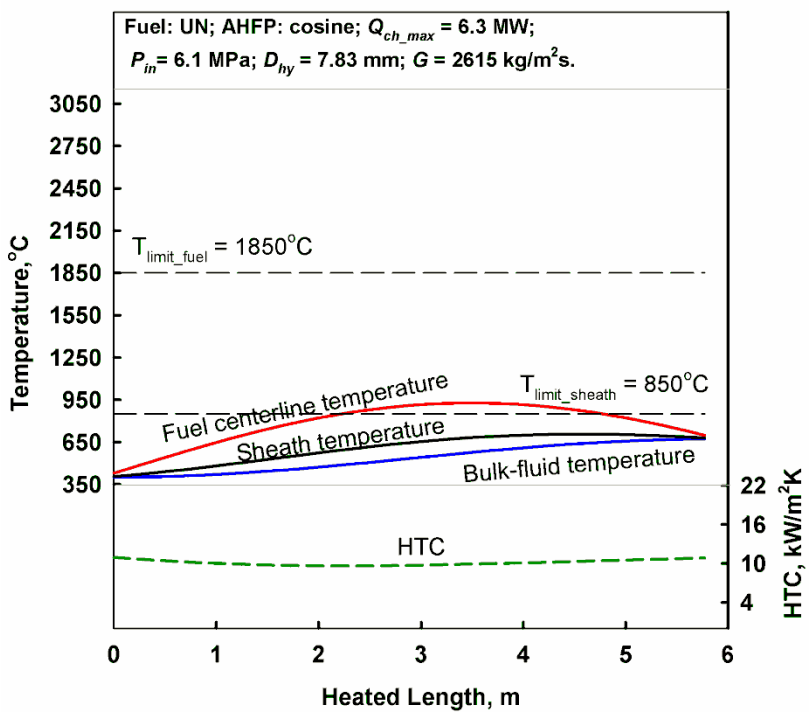

(b)

Figure C.12. Temperature profiles at maximum power and cosine AHFP. (a) – SCW and (b) – SHS channels. Fuel: UN.

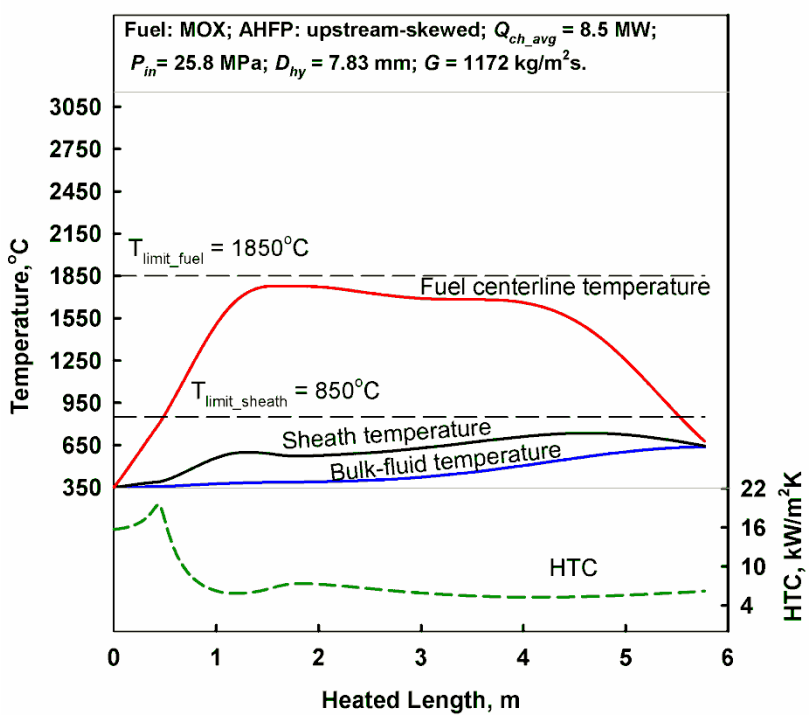

(a)

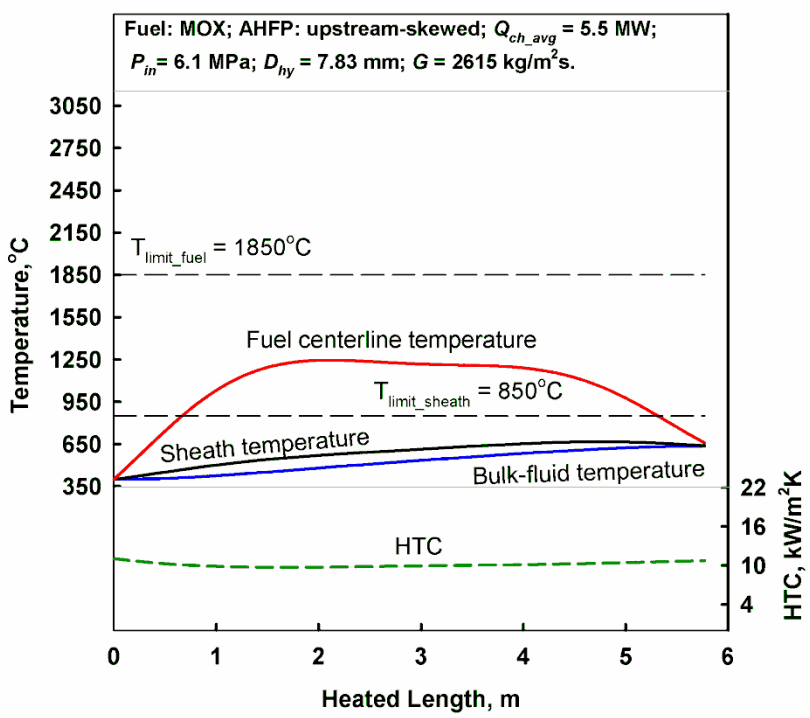

(b)

Figure C.13. Temperature profiles at average power and upstream-skewed AHFP. (a) – SCW and (b) – SHS channels. Fuel: MOX.

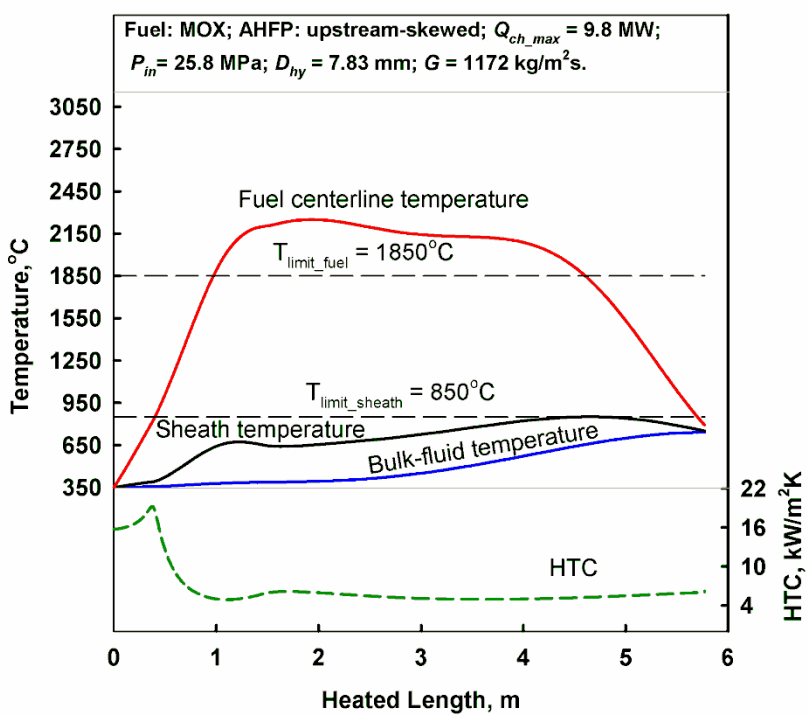

(a)

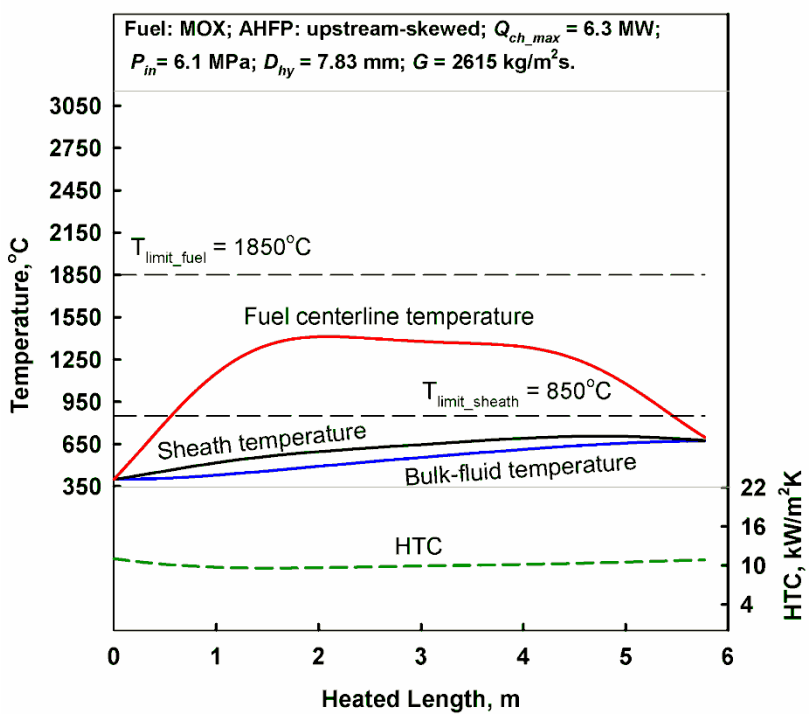

(b)

Figure C.14. Temperature profiles at maximum power and upstream-skewed AHFP. (a) – SCW and (b) – SHS channels. Fuel: MOX.

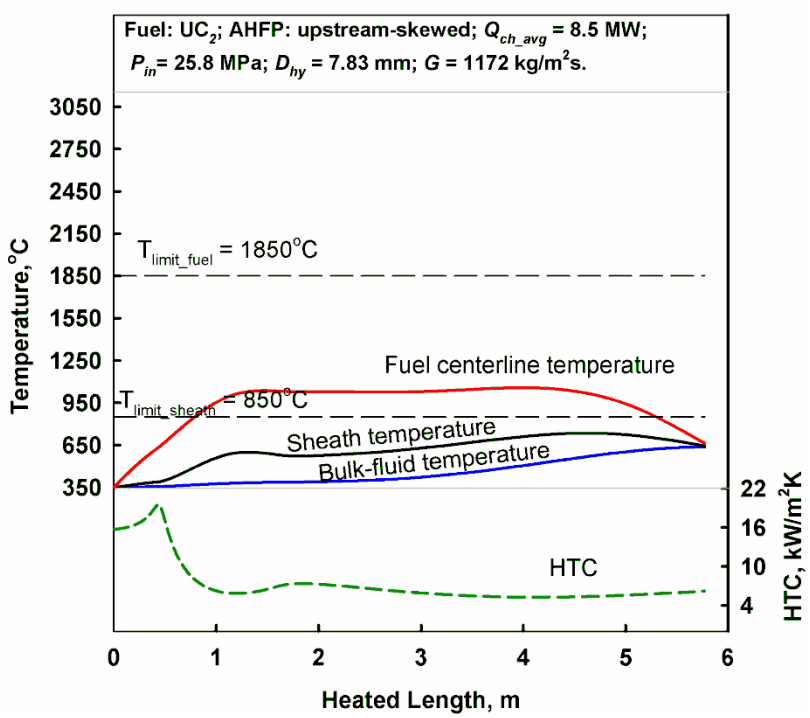

(a)

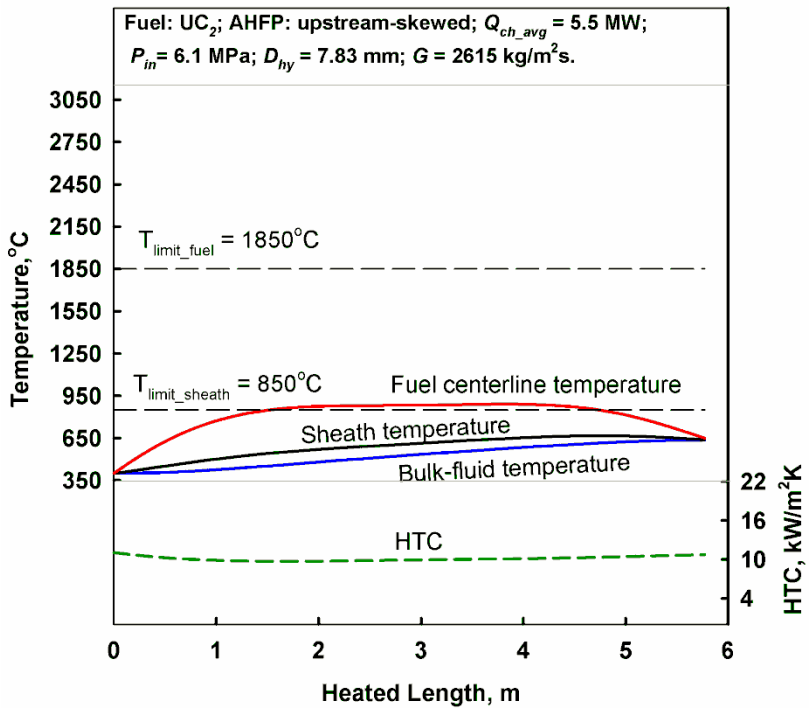

(b)

Figure C.15. Temperature profiles at average power and upstream-skewed AHFP. (a) – SCW and (b) – SHS channels. Fuel: UC_2.

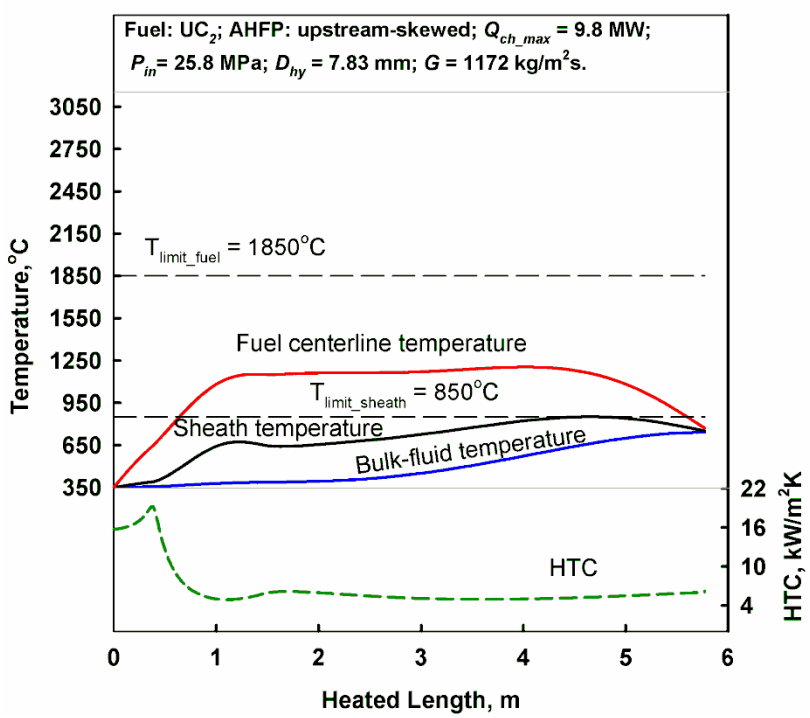

(a)

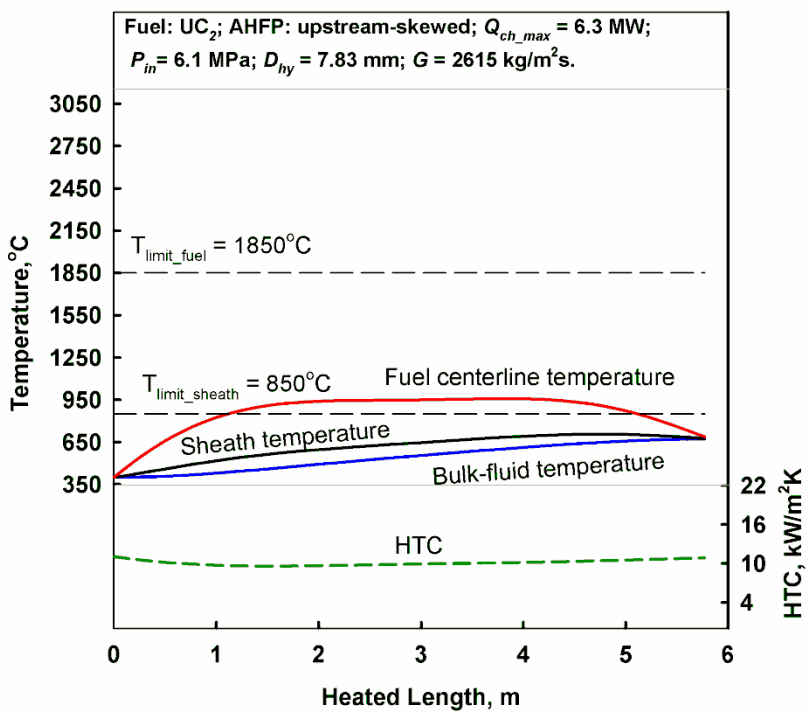

(b)

Figure C.16. Temperature profiles at maximum power and upstream-skewed AHFP. (a) – SCW and (b) – SHS channels. Fuel: UC_2.

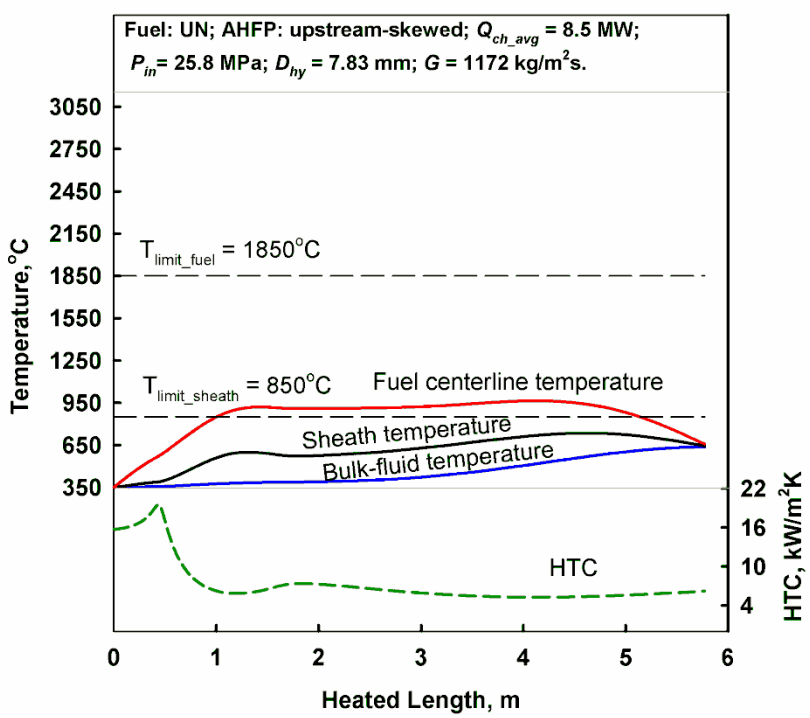

(a)

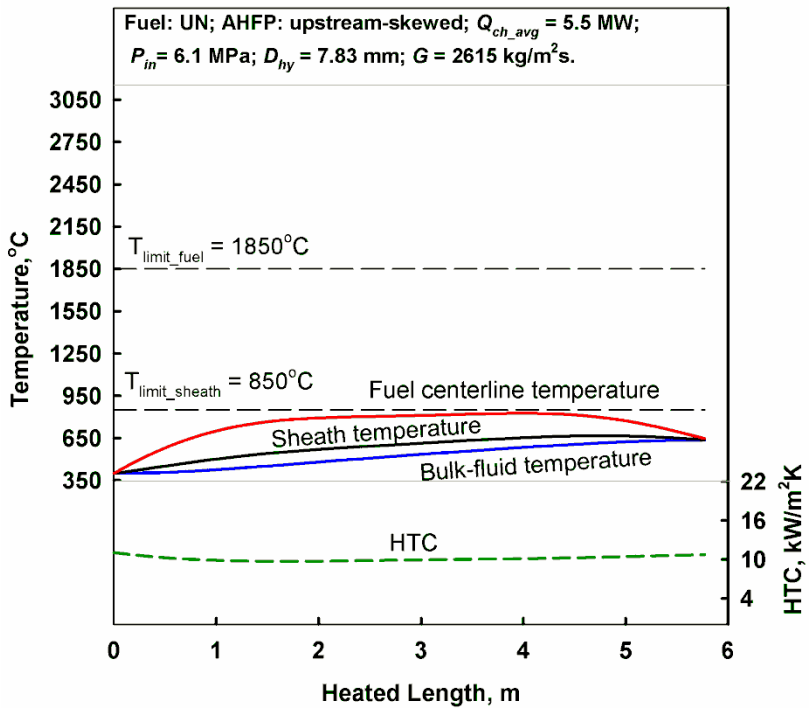

(b)

Figure C.17. Temperature profiles at average power and upstream-skewed AHFP. (a) – SCW and (b) – SHS channels. Fuel: UN.

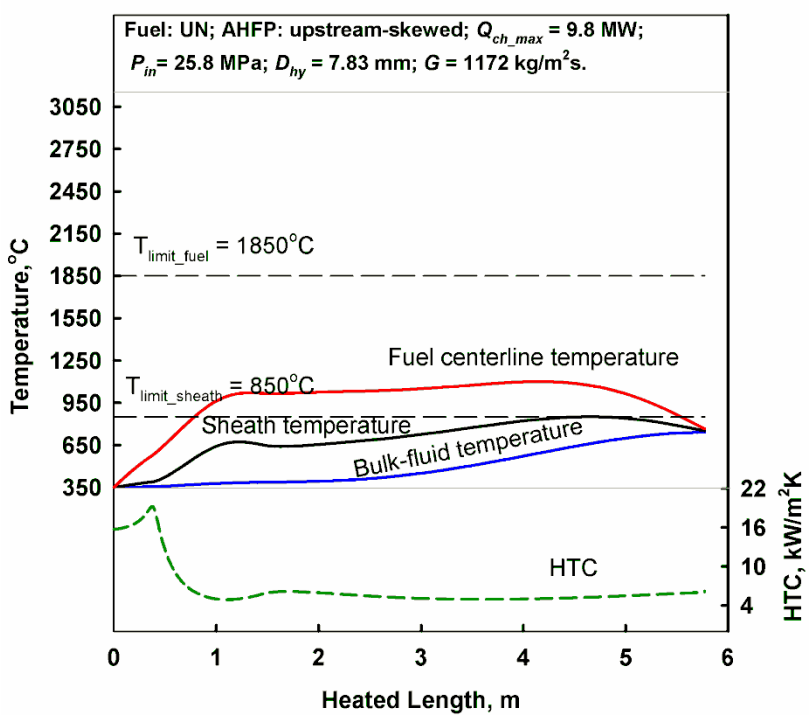

(a)

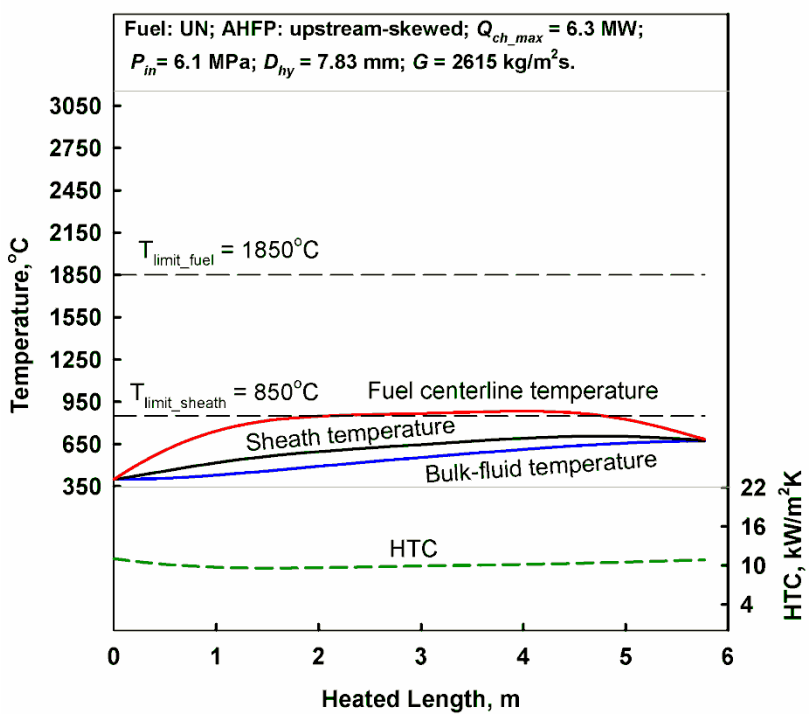

(b)

Figure C.18. Temperature profiles at maximum power and upstream-skewed AHFP. (a) – SCW and (b) – SHS channels. Fuel: UN.

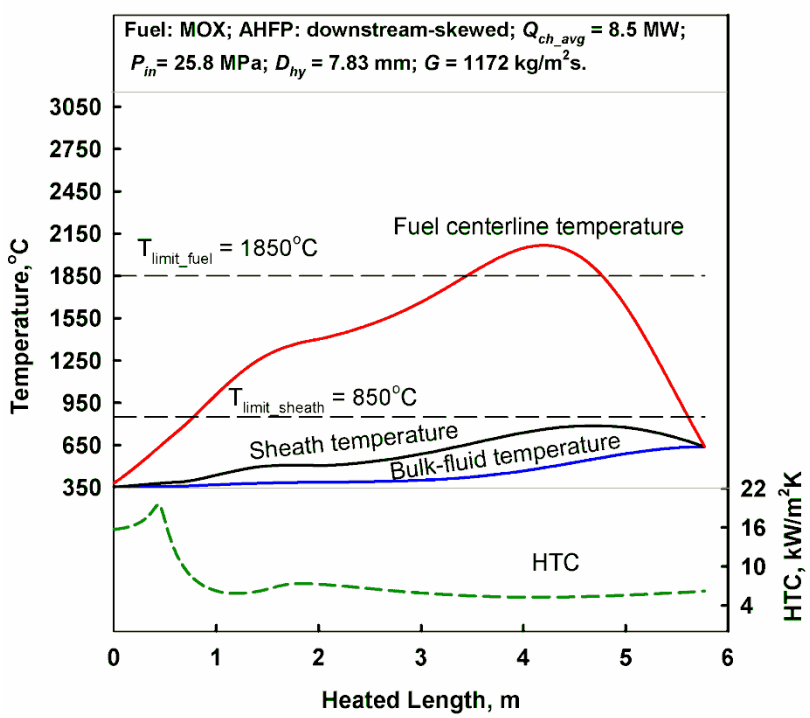

(a)

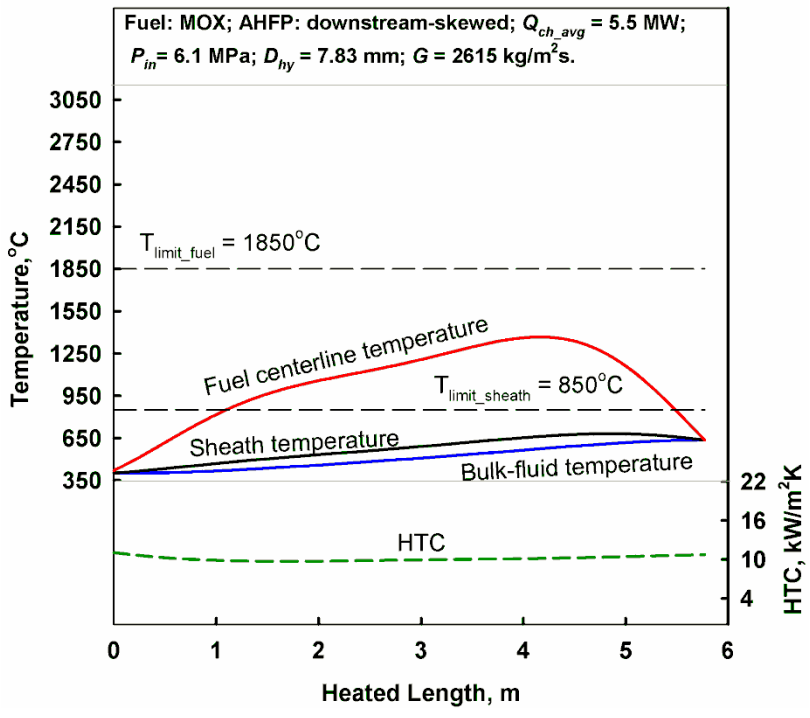

(b)

Figure C.19. Temperature profiles at average power and downstream-skewed AHFP. (a) – SCW and (b) – SHS channels. Fuel: MOX.

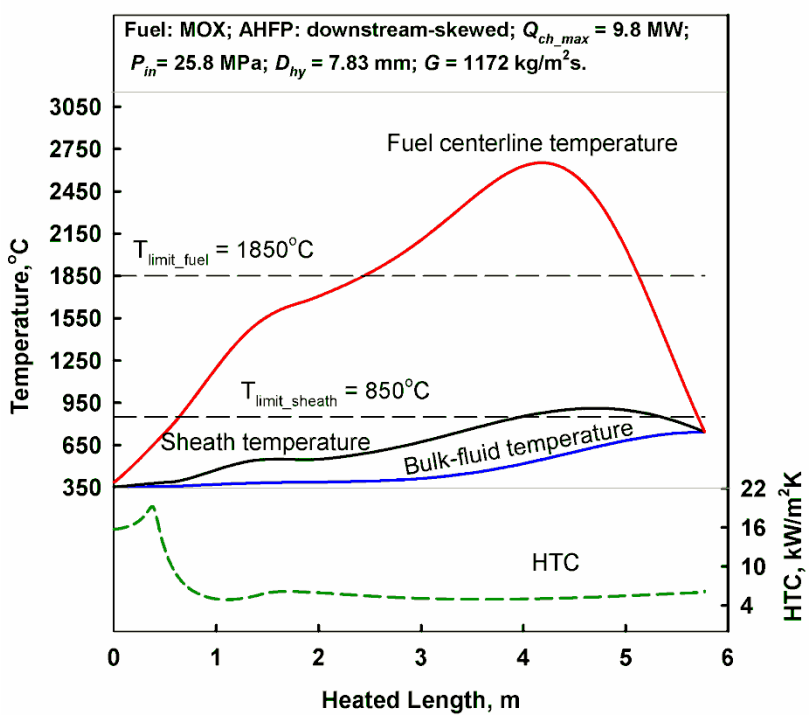

(a)

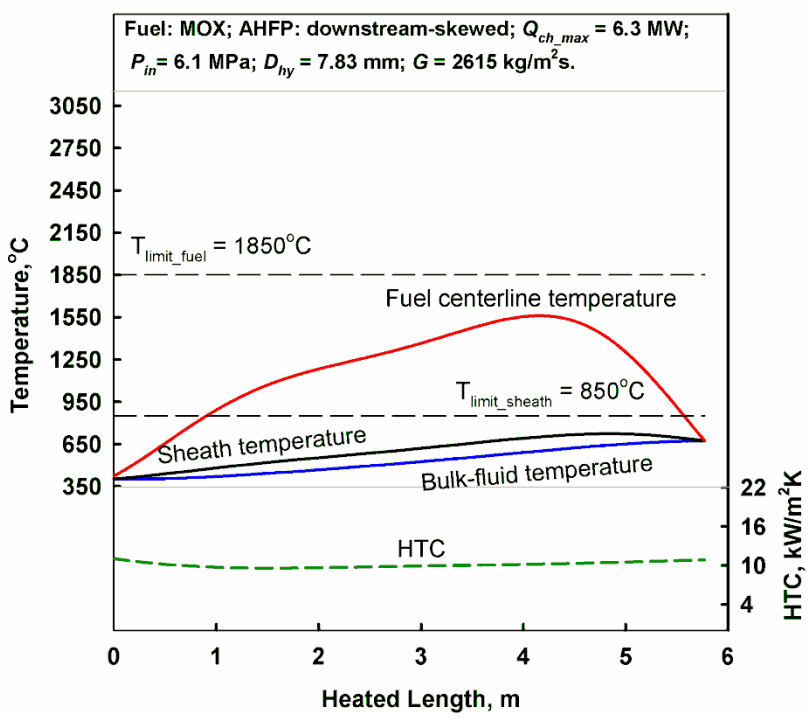

(b)

Figure C.20. Temperature profiles at maximum power and downstream-skewed AHFP. (a) – SCW and (b) – SHS channels. Fuel: MOX.

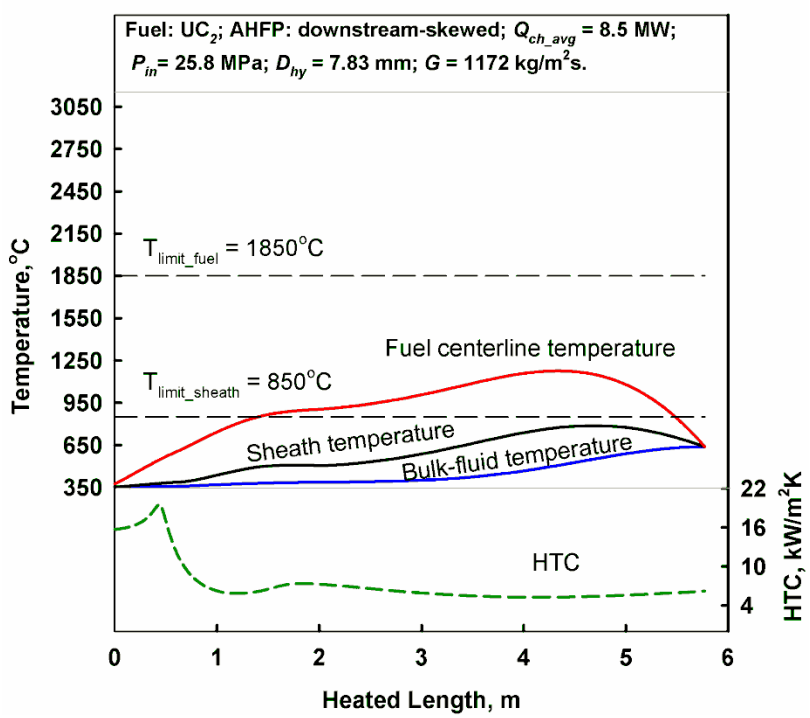

(a)

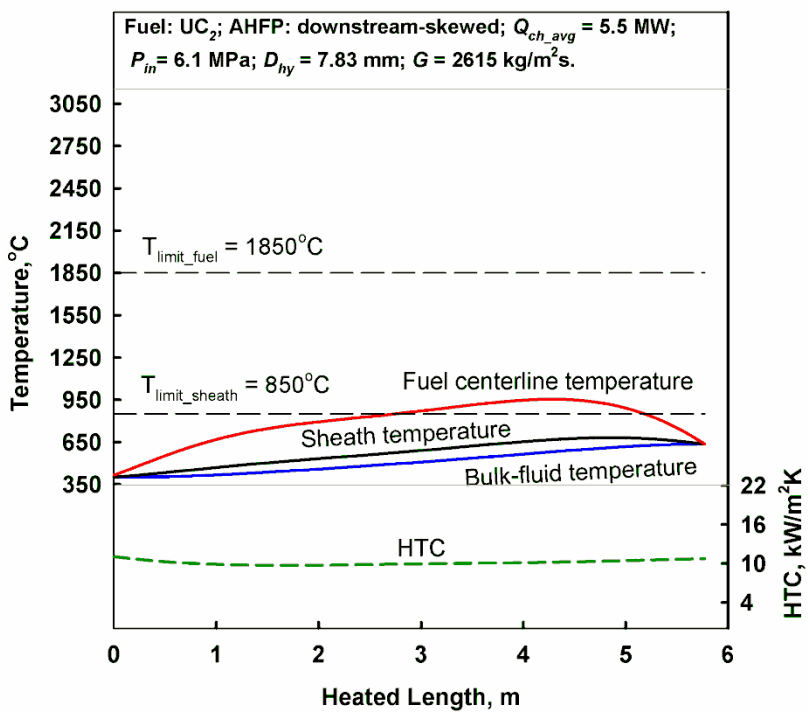

(b)

Figure C.21. Temperature profiles at average power and downstream-skewed AHFP. (a) – SCW and (b) – SHS channels. Fuel: UC_2.

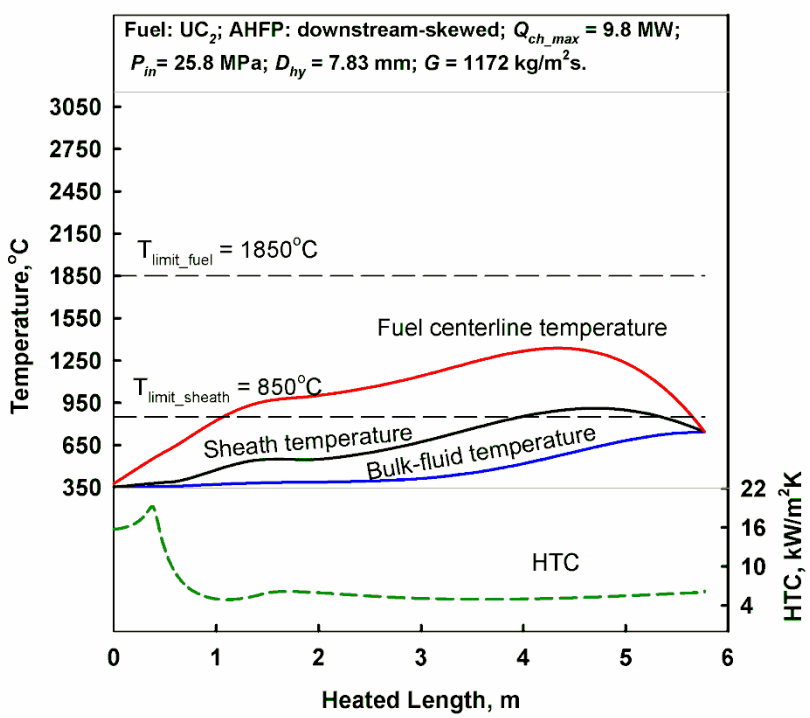

(a)

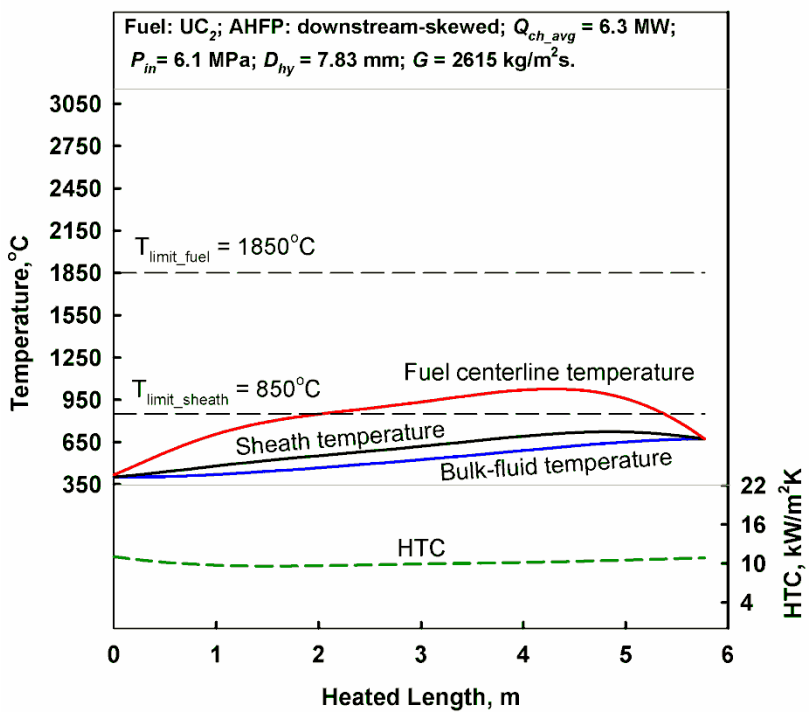

(b)

Figure C.22. Temperature profiles at maximum power and downstream-skewed AHFP. (a) – SCW and (b) – SHS channels. Fuel: UC_2.

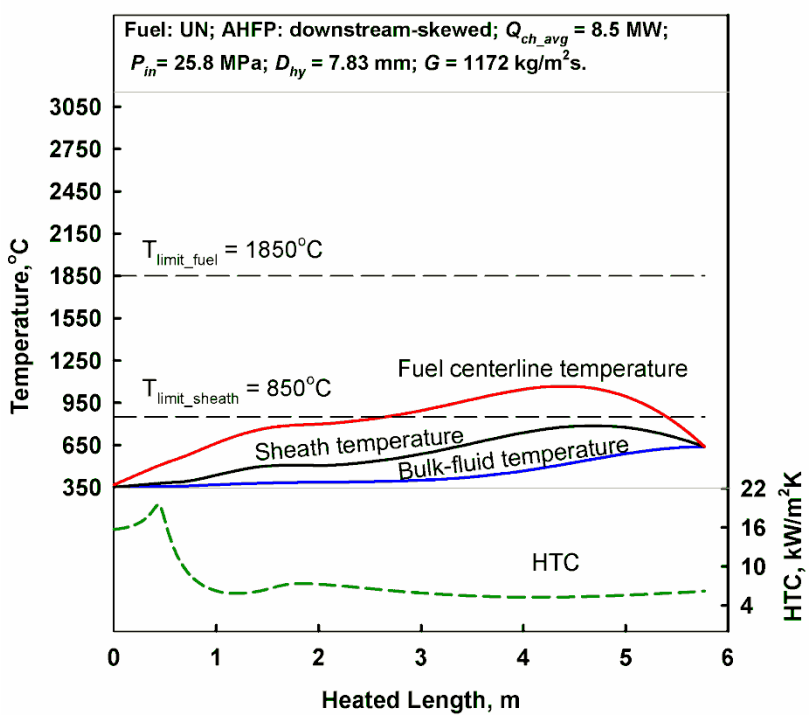

(a)

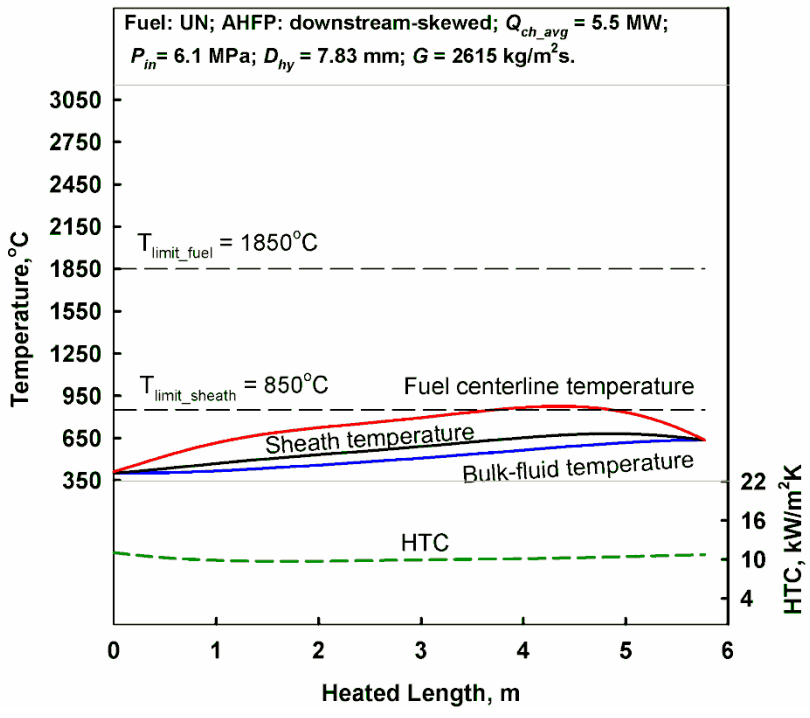

(b)

Figure C.23. Temperature profiles at average power and downstream-skewed AHFP. (a) – SCW and (b) – SHS channels. Fuel: UN.

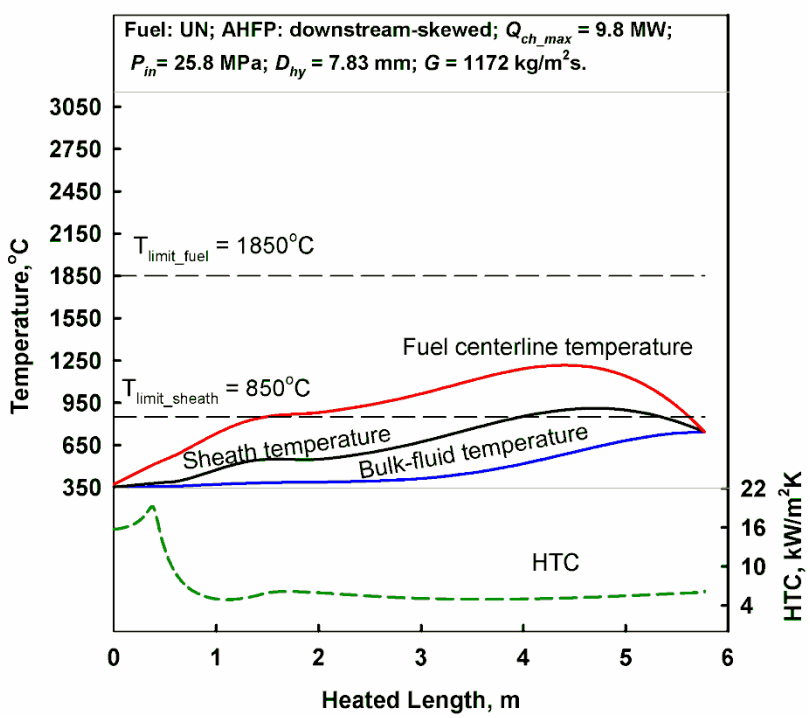

(a)

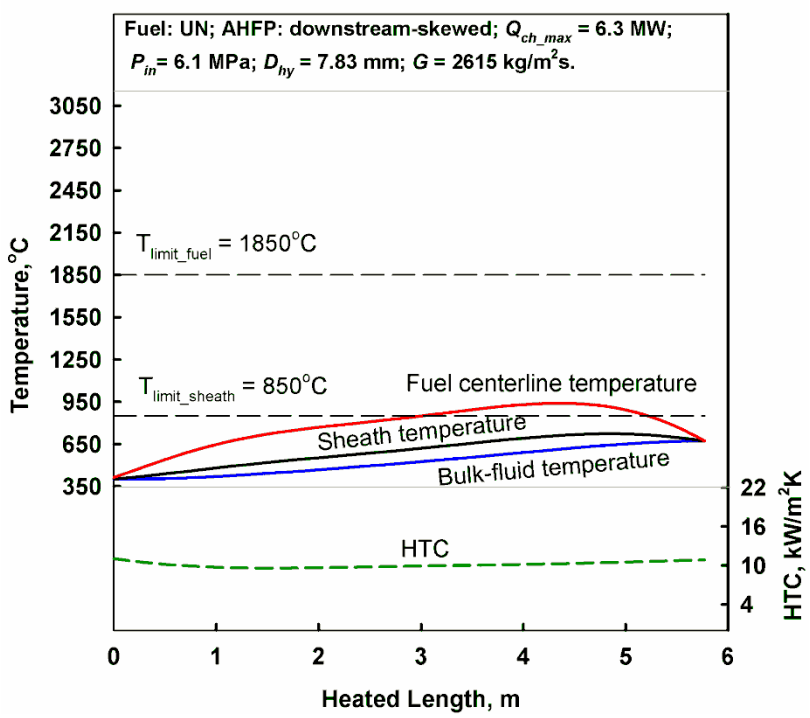

(b)

Figure C.24. Temperature profiles at maximum power and downstream-skewed AHFP. (a) – SCW and (b) – SHS channels. Fuel: UN.

APPENDIX D

NUMERICAL VALUES OF TEMPERATURES AT 12 POINTS ALONG THE CHANNEL AT AVERAGE POWER

Table D.1. Values of bulk-fluid, wall, inner-sheath and UO_2 fuel centerline temperatures at 12 points of SCW channel at average power.

Axial position, m	AHFP	q' per pin, W/m	T_{bf},°C	T_w,°C	$T_{sh,id}$,°C	T_f,°C
0	Uniform	35063	350	564	596	1625
	Downstr.-sk.	1797	350	354	356	386
0.481	Uniform	35063	370	577	610	1647
	Downstr.-sk.	16160	385	661	404	725
0.962	Uniform	35063	382	562	595	1620
	Downstr.-sk.	28185	369	480	509	1226
1.443	Uniform	35063	386	528	562	1557
	Downstr.-sk.	35698	380	583	616	1699
1.924	Uniform	35063	389	523	557	1547
	Downstr.-sk.	39574	386	587	623	**1863**
2.405	Uniform	35063	393	543	576	1585
	Downstr.-sk.	41770	389	594	634	**1963**
2.886	Uniform	35063	403	574	607	1641
	Downstr.-sk.	43927	396	644	683	**2131**
3.367	Uniform	35063	420	613	644	1710
	Downstr.-sk.	46515	413	719	756	**2334**
3.848	Uniform	35063	445	657	687	1785
	Downstr.-sk.	48411	446	796	832	**2497**
4.329	Uniform	35063	479	704	733	**1863**
	Downstr.-sk.	47249	496	843	878	**2516**
4.810	Uniform	35063	521	753	781	**1941**
	Downstr.-sk.	39985	555	834	863	**2258**
5.291	Uniform	35063	571	804	830	**2018**
	Downstr.-sk.	24226	605	757	776	1530
5.772	Uniform	1997	625	857	882	**2092**
	Downstr.-sk.	0	625	625	625	625

Temperature values in red are those exceeding the industry accepted limit for UO_2 of 1850°C

Table D.2. Values of bulk-fluid, wall, inner-sheath and UO_2 fuel centerline temperatures at 12 points of SHS channel at average power.

Axial position, m	AHFP	q' per pin, W/m	T_{bf},°C	T_w,°C	$T_{sh,id}$,°C	T_f,°C
0	Uniform	22688	400	477	500	1031
	Downstr.-sk.	1163	400	404	405	425
0.481	Uniform	22688	481	497	518	1059
	Downstr.-sk.	10456	404	434	450	657
0.962	Uniform	22688	437	515	537	1088
	Downstr.-sk.	18237	416	478	497	908
1.443	Uniform	22688	456	534	556	1117
	Downstr.-sk.	23099	434	514	537	1109
1.924	Uniform	22688	475	553	574	1147
	Downstr.-sk.	25607	454	544	569	1242
2.405	Uniform	22688	494	572	593	1177
	Downstr.-sk.	27028	477	572	597	1339
2.886	Uniform	22688	514	591	612	1207
	Downstr.-sk.	28423	501	601	627	1441
3.367	Uniform	22688	534	611	631	1237
	Downstr.-sk.	30098	527	632	659	1559
3.848	Uniform	22688	554	630	650	1266
	Downstr.-sk.	31325	554	663	690	1661
4.329	Uniform	22688	573	650	669	1296
	Downstr.-sk.	30573	582	687	713	1670
4.810	Uniform	22688	594	669	688	1326
	Downstr.-sk.	25873	608	695	716	1496
5.291	Uniform	22688	614	689	708	1356
	Downstr.-sk.	15676	627	678	691	1107
5.772	Uniform	22688	634	708	727	1389
	Downstr.-sk.	0	634	634	634	634

APPENDIX E

PUBLISHED PAPERS, CONFERENCES ATTENDED AND AWARDS

In total: papers in refereed proceedings of international/national conferences/symposiums – 7; major technical reports – 1;

Papers in refereed proceedings of international/national conferences/symposiums

1. Pioro, I., Mokry, S., Peiman, W., Grande, L. and Saltanov, Eu., 2010. Supercritical Water-Cooled Nuclear Reactors: NPP Layouts and Thermal Design Options of Pressure Channels, Proceedings of the 17th Pacific Basin Nuclear Conference (PBNC-2010), Cancun, Mexico, October 24-30, 31 pages.
2. Saltanov, Eu., Peiman, W., Farah, A., King, K., Naidin, M. and Pioro, I., 2010. Steam-Reheat Options for Pressure-Tube SCWRs, Proceedings of the 18th International Conference On Nuclear Engineering (ICONE-18), Xi'an, China, May 17-21, Paper 29972, 12 pages.
3. Peiman, W., Saltanov, Eu., Gabriel, K. and Pioro, I., 2010. Heat-Loss Calculations in a SCWR Fuel-Channel, Proceedings of the 18th International Conference On Nuclear Engineering (ICONE-18), Xi'an, China, May 17-21, Paper 30069, 9 pages.
4. Pioro, I., Naidin, M., Mokry, S., Saltanov, Eu., Peiman, W., King, K., Farah, A. and Thind, H., 2010. General Layouts of Supercritical-Water NPPs, Proceedings of the 18th International Conference On Nuclear Engineering (ICONE-18), Xi'an, China, May 17-21, Paper 29993, 9 pages.
5. Saltanov, E., King, K., Farah, A., and Pioro, I., 2010. Nuclear Steam-Reheat Options: Russian Experience, Proceedings of The 2nd Canada-China Joint Workshop on Supercritical Water-Cooled Reactors (CCSC-2010) Toronto, Ontario, Canada, April 25-28, 2010, Paper 72, 8 pages.
6. Saltanov, E., King, K., Farah, A., and Pioro, I., 2010. Nuclear Steam-Reheat Options: World Experience, Proceedings of the 31st Canadian Nuclear Society

(CNS) and 34th Student Conference of the CNS and CNA, Montreal, Canada, May 24-27, 9 pages.

7. Saltanov, E., Monichan, R., Tchernyavskaya, E. and Pioro, I., 2009. Steam-Reheat Option for SCWRs, Proceedings of the 17th International Conference On Nuclear Engineering (ICONE-17), Brussels, Belgium, July 12-16, Paper 76061, 10 pages.

Major technical reports

1. Pioro, I., Saltanov, Eu., Naidin, M., King, K., Farah, A., Peiman, W., Mokry, S., Grande, L., Thind, H., Samuel, J. and Harvel, G., 2010. Steam-Reheat Option in SCWRs and Experimental BWRs, Report for NSERC/NRCan/AECL Generation IV Energy Technologies Program (NNAPJ) entitled "Alternative Fuel-Channel Design for SCWR" with Atomic Energy of Canada Ltd., Version 1, UOIT, Oshawa, ON, Canada, March, 128 pages.

Conferences attended with paper presentation:

1. 17th International Conference On Nuclear Engineering (ICONE-17), Brussels, Belgium, July 12-16, 2009.
2. 2nd Canada-China Joint Workshop on Supercritical Water-Cooled Reactors (CCSC-2010) Toronto, Ontario, Canada, April 25-28
3. 18th International Conference On Nuclear Engineering (ICONE-18), Xi'an, China, May 17-21, 2010.
4. 31st Canadian Nuclear Society (CNS) and 34th Student Conference of the CNS and CNA, Montreal, Canada, May 24-27.

Awards and honors:

1. Winner in the ICONE-18 (International Conference On Nuclear Engineering) Student Best Poster Competition for the paper/poster "Steam-Reheat Options for Pressure-Tube SCWRs";
2. Winner in the ICONE-18 North America Student Best Poster Competition for the paper/poster "Heat-Loss Calculations in a SCWR Fuel-Channel".